Multiple molecular adaptation strategies of *Clostridioides difficile* to respond to various stresses in the gut environment during infection

Von der Fakultät für Lebenswissenschaften

der Technischen Universität Carolo-Wilhelmina zu Braunschweig

zur Erlangung des Grades

einer Doktorin der Naturwissenschaften

(Dr. rer. nat.)

genehmigte

D i s s e r t a t i o n

von Annika-Marisa Dorothee Michel

aus Braunschweig

1. Referent: Prof. Dr. Dieter Jahn
2. Referent: Prof. Dr. Michael Steinert
eingereicht am: 11.01.2021
mündliche Prüfung (Disputation) am: 12.03.2021

Druckjahr 2021

Vorveröffentlichungen der Dissertation

Teilergebnisse aus dieser Arbeit wurden mit Genehmigung der Fakultät für Lebenswissenschaften, vertreten durch den Mentor der Arbeit, in folgenden Beiträgen vorab veröffentlicht:

Publikationen

Berges M.*, Michel A.-M.*, Lassek C.,Nuss A.M., Beckstette M., Dersch P.,Riedel K., Sievers S., Becher D., Otto A.,Maaß S., Rohde M., Eckweiler D.,Borrero-de Acuña J.M., Jahn M.,Neumann-Schaal M. and Jahn D. (2018) Iron regulation in *Clostridioides difficile*. Front. Microbiol. 9:3183 (* equally contributed).

Hofmann J.D., Otto A., Berges M., Biedendieck R., Michel A.-M., Becher D., Jahn D. and Neumann-Schaal M. (2018) Metabolic Reprogramming of *Clostridioides difficile* during the stationary phase with the induction of toxin production. Front. Microbiol. 9:1970.

Bernal I., Hofmann J.D., Bulitta B., Klawonn F., Michel A.-M., Jahn D., Neumann-Schaal M., Bruder D. and Jänsch L. (2018) *Clostridioides difficile* activates human mucosal-associated invariant T cells. Front. Microbiol. 9:2532.

Boekhoud I.M., Michel A.-M., Corver J., Jahn D., Smits W.K. 2020. Redefining the *Clostridioides difficile* σB regulon: σB activates genes involved in detoxifying radicals that can result from the exposure to antimicrobials and hydrogen peroxide. mSphere 5:e00728-20.

Tagungsbeiträge

Michel, A.-M., Berges, M., and Jahn, D.: PerR-mediated response of *Clostridium difficile* (Poster), Vereinigung für Allgemeine und Angewandte Mikrobiologie (VAAM) und Deutsche Gesellschaft für Hygiene und Mikrobiologie (DGHM) – Jahrestagung, Würzburg, Germany (2017).

Michel, A.-M., Berges, M., Neumann-Schaal M., and Jahn, D.: PerR is starvation regulator in *Clostridium difficile* (Poster), ClostPath, Ann Arbor, Michigan, USA – 10th International Conference (2017).

Michel, A.-M., Hoffmann T., Bremer E., Borréro de Acuña J. M., and Jahn, D.: Adaption of *Clostridioides difficile* to osmotic stress (Poster), Vereinigung für Allgemeine und Angewandte Mikrobiologie (VAAM) – Jahrestagung, Wolfsburg, Germany (2018).

Michel, A.-M., Hoffmann T., Bremer E., Borréro de Acuña J. M., and Jahn, D.: Adaptation of *Clostridioides difficile* to osmotic stress (Poster), 6th International *C. difficile* Symposium (ICDS) – Bled, Slowenien (2018).

Michel, A.-M., Hoffmann T., Bremer E., Borréro de Acuña J. M., and Jahn, D.: Adaptation of *Clostridioides difficile* to osmotic stress (Poster), Vereinigung für Allgemeine und Angewandte Mikrobiologie (VAAM) – Jahrestagung, Mainz, Germany (2019).

Meinen Eltern

TABLE OF CONTENT

1. INTRODUCTION

1.1 *Clostridioides difficile*

The genus *Clostridium* was first proposed by A. Prazmowski in 1880 and constitutes today, with 168 species, one of the most species-rich groups of the prokaryotes (1, 2). The genus is characterized by a high phylogenetic diversity, which is reflected in the definition of 19 clusters based on 16S rDNA sequencing. This also allowed the reclassification of some genera (2, 3), including *Clostridioides difficile*. *C. difficile* was first isolated in 1935. Due to its difficult cultivation it was given the name *Bacillus difficilis* (4) before it was assigned to the genus *Clostridium* in 1980 and reclassified as *Clostridium difficile* (5). After a further renaming to *Peptoclostridium difficile* (6), the classification into the new genus *Clostridioides* followed, in compliance with the description for *Clostridium difficile* (Figure 1) (7). Features such as rod-shaped cell morphology, Gram-positive behavior, motility, peritrichous flagellation and size specifications of 0.5 - 1.9 µm x 3.0 - 16.9 µm are still valid (1, 7). Species of the genus *Clostridioides* are also strictly anaerobic endospore producers, capable of colonizing ecological niches and withstand adverse environmental conditions (1, 7, 8).

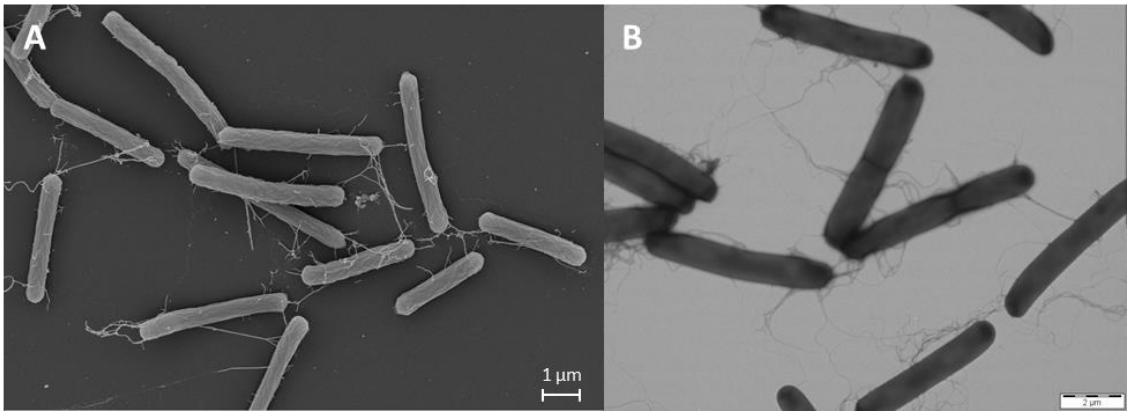

Figure 1 Scanning (A) and transmission (B) electron microscopy of *C. difficile* 630Δ*erm*. Images were taken by Prof. Dr. Manfred Rohde, HZI, Braunschweig.

1.1.1 Pathogenesis of *C. difficile* infections

In addition to environmentally associated habitats such as soil, lakes, rivers, sewage, or plant and animal products, possible habitats of the genus *Clostridioides* include wounds and the gastrointestinal (GI) tract of humans or animals, especially for pathogenic representatives like *C. difficile* (9). Although the first isolation from the stool of a healthy newborn child suggested a commensal presence in the intestinal microbiome, in the late 1970s the organism was identified as a pathogen causing antibiotic-associated pseudomembranous colitis (9, 10, 11), indicating that a *C. difficile* infection (CDI) can be both asymptomatic or symptomatic (12). Furthermore, *C. difficile*-associated disease (CDAD) varies from mild diarrhea to toxic megacolon and can lead to death (11, 12, 13). In 2011, 29,000 of almost a half million infected people in the United States died as a result of CDI (14). Over the past decades, *C. difficile* has become the most common cause of healthcare-associated infections worldwide, replacing methicillin-resistant *Staphylococcus aureus* (MRSA) (15). Risk-factors like increasing age, prolonged hospital stay and immunosuppression favor the acquisition of CDI. The pathogen is transmitted via the fecal-oral route in form of spores (12), which can survive for several months on surfaces due to their high resistance to oxygen, disinfectants including alcohols and acids, and extreme temperatures (8). Once ingested into the human body, their resistance to acids allows them to pass through the stomach and consequently colonize the intestine and colon. Along the GI tract, the germination of spores is stimulated by primary bile acids (16, 17). The administration of antibiotics and the associated suppression of the intestinal microbiota, which acts normally as defense barrier, additionally promotes the proliferation of vegetative cells that can produce the exotoxins TcdA and TcdB (11, 16, 18, 19). On the luminal side of the colonic epithelium both proteins bind to specific receptors before they are transported into the cytoplasm. Inside the cell, the toxins catalyze the transfer of glycosyl residues to small Rho GTPases leading to an inactivation of Rho and subsequently to cell rounding, inhibition of cell division and eventually cell death. Due to their biological activity as enterotoxin (TcdA) and cytotoxin (TcdB), the proteins stimulate the disruption of the cytoskeleton of the intestinal mucosa and the release of pro-inflammatory cytokines (11, 20). The toxin production is regulated by toxin-encoding genes located in a pathogenicity locus, termed

PaLoc, of 19.6 kb which consists five genes (Figure 2). The genes *tcdA* and *tcdB,* coding for corresponding glycosylating toxins TcdB and TcdA, are embedded between the regulatory genes *tcdR* and *tcdC*. While *tcdR* codes for an RNA polymerase sigma factor that positively regulates its own and the toxin expression, *tcdC* codes for an anti-sigma factor that interferes with TcdR resulting in the repression of toxin production. An additional gene, *tcdE*, is located between *tcdB* and *tcdA.* The encoded holin-like protein is involved in the secretion of toxins (19, 21). In non-toxigenic strains, a 115-bp non-coding sequence usually replaces the PaLoc region. However, it has been shown that a non-toxic strain can receive the PaLoc of a toxic strain via horizontal gene transfer and thus acquire its pathogenicity (19, 21, 22).

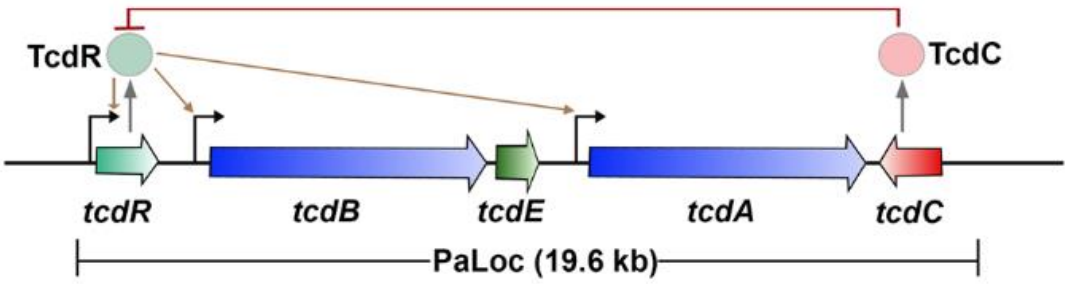

Figure 2 Organization of the pathogenicity locus (PaLoc).

Blue arrows indicating toxin-encoding genes *tcdA* and *tcdB*, separated by the holin-encoding gene *tcdE* colored in dark green. The light green arrow represents the gene *tcdR* regulating its own expression as well as the expression of *tcdA* and *tcdB* positively (indicated by brown arrows). The negative regulatory gene *tcdC* is shown in red. The transcription direction is given by direction of arrows.The anti-sigma factor TcdC regulates the toxin expression negatively by inhibition of TcdR (21).

Mortality rates are exacerbated by so-called hypervirulent strains, many of which produce a third toxin named *C. difficile* transferase (CDT). CDT is part of the binary toxins consisting two components, where the N-terminus is responsible for receptor binding as well as toxin uptake and the C-terminus harbors actin-specific ADP-ribosyl transferase activity (19, 21). Toxin production can not only vary dramatically between different strains but it is also associated with central carbon metabolism and nutrient availability, especially the access to amino acids occurrence. An efficient expression of the toxins is normally detectable in the late exponential or stationary phase depending on the media composition (23, 24, 25, 26, 27). It could be shown that biotin-limited conditions increase the toxin production (28), while the presence of certain amino acids such as cysteine and

proline reduces toxin production (29). Carbohydrates as glucose can lead to a reduction of toxin formation in complex medium (24, 30), whereas in minimal medium an increase could be measured (30).

1.1.2 Metabolism and energy production of *C. difficile*

The metabolism of bacteria encompasses a complex network of biochemical reactions catalyzed by a variety of enzymes for the generation of energy conserved in high-energy compounds such as adenosine diphosphate (ADP) and adenosine triphosphate (ATP). The heterotrophic metabolism, which sustains all pathogens vital functioning, is characterized by the oxidation of organic compounds like carbohydrate, lipids and proteins. While aerobic organisms completely oxidize organic components to carbon dioxide and water during the process of respiration using oxygen as a terminal electron acceptor (31), anaerobic organisms like *C. difficile* have developed alternative systems for energy production such as fermentations using various organic compounds as electron acceptors (32). During these processes, however, only an incomplete decomposition of the substrates to carbon dioxide takes place, whereby simple organic compounds in the form of alcohol and acids are secreted into the medium as waste products (31). As many other bacteria, *C. difficile* utilize different sugars e.g. glucose as carbon source. However, the primary source of ATP generation is the fermentation of amino acids via the Stickland reaction (Figure 3) (2, 33, 34, 35, 36). The Stickland reaction involves the coupling of oxidation and reduction of amino acid pairs with simultaneous formation of their corresponding organic acid, in which both processes are preceded by the transamination of an amino acid to its corresponding 2-oxo acid, which in turn yields NADH (27, 32, 37). While amino acids such as isoleucine, valine or alanine serve as effective electron donors in the oxidative pathway, the amino acids proline, glycine or methionine act as electron acceptors in the reductive pathway. Leucine, phenylalanine and tyrosine can function both as electron acceptors and donors, resulting in different pathway-dependent products (32, 34, 36, 38). Thus, leucine is converted to isovalerate in the oxidative pathway, while isocaproate is derived from the reductive pathway. Of the amino acids used in the Stickland reaction, seven essential amino acids for *C. difficile* were identified. For growth in minimal defined

medium (MDM) the amino acids proline, cysteine, methionine, leucine, isoleucine, valine and tryptophan are indispensable. The consumption of these amino acids is strongly associated with the media composition, which is reflected in a different metabolite spectrum. In MDM, cysteine and methionine are utilized right from the beginning of growth, whereas proline and leucine are consumed later. In contrast, proline and leucine are the preferred carbon and energy sources in the more complex *C. difficile* minimal medium (CDMM) containing casamino acids. Here, the amino acids glutamate and lysine were hardly used (27). Fermentation processes are used to generate a sodium/proton gradient with the aid of a membrane-spanning Rnf complex, which in turn is used to generate energy in the form of ATP (32, 39).

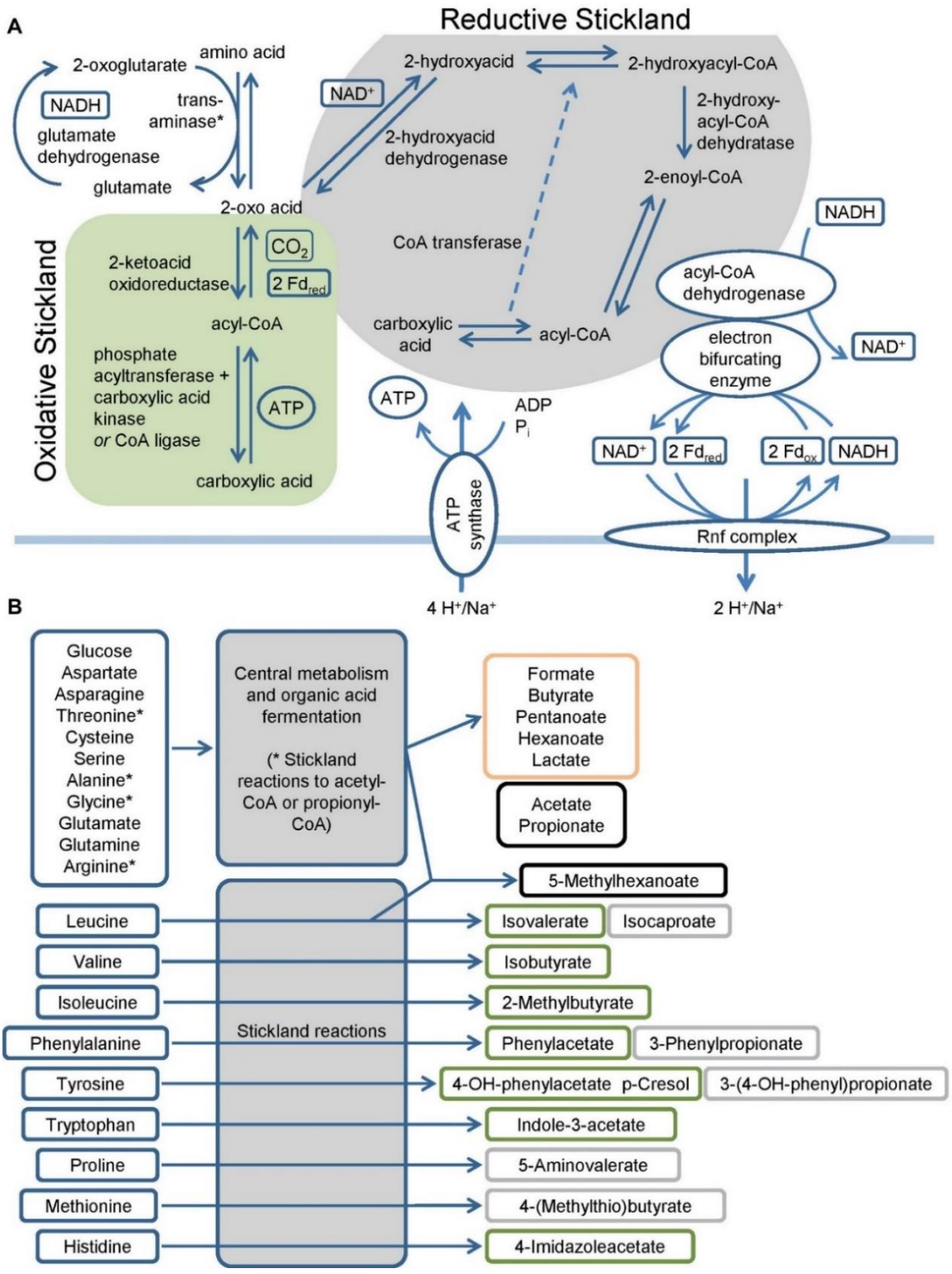

Figure 3 Schematic overview of Stickland reactions and fermentation products.

A) Steps of Stickland reactions containing oxidative and reductive pathways are shown in connection to the ion pumping Rnf complex supplied by electron bifurcating enzymes.
B) Fermentation products of amino acid and glucose utilization.
Green: oxidative Stickland reactions and their products, grey: reductive Stickland reactions and their products, orange: central carbon metabolism-associated fermentation products, black: oxidative and/or reductive Stickland products and central carbon metabolism-associated fermentation products (32).

1.2 Adaptation to osmotic stress

Bacteria are ubiquitous organisms able to survive widely varying environmental stimuli such as temperature, pH value, nutrient availability and osmolarity (40). Osmotic fluctuations are present in various habitats. Soil-living bacteria have adapted to the constant change between drought and rainfall, while pathogens of the urinary or gastrointestinal tract are exposed to concentrated and diluted urine (41) or osmotic fluctuations during food digestion (42). The adaptation process for Gram-positive and Gram-negative bacteria is similar and is accompanied by changes in cell structure, organization as well as composition as a consequence of the water-flow across the cytoplasmic membrane (41). Latter is permeable for water, but an effective barrier for solutes in the surrounding medium or for metabolites in the cytoplasm (43, 44). Due to the generally lower osmolarity of the environment compared to the cytoplasm, an influx of water occurs with a simultaneous build-up of hydrostatic pressure, the turgor, which gives the cell its shape. Furthermore, regulating function in the cell division rate are attributed to the turgor (43, 45, 46).

A further increase in turgor is generated when the bacteria are exposed to a sudden shift to hypoosmotic conditions, such as during the exposure to distilled water by rain. The osmotic adaptation of their intracellular solute concentration to an equal level of that in the environment results in a rapid influx of water. This leads to an increasing tension of the membrane and potentially to cell lysis. In order to prevent cell lysis and reduce the membrane tension, mechanosensitive channels (Msc) located in the cytoplasmic membrane are activated to allow the diffusion of nonspecific osmolytes out of the cell (47, 48, 49).

In contrast, high osmolarity conditions like in dried out soil lead to a rapid efflux of water from the cytoplasm followed by the loss of the turgor and an increasing concentration of ions and macromolecules that inhibit DNA replication and protein biosynthesis. To prevent dehydration and cell death, bacteria developed an adaptive mechanism to sense and react to osmotic changes (50). Two strategies, known as “*salt-in*”- and “*salt out*”-strategy, are elicited by microorganisms depending on their environment. The “salt-in” strategy is generally used by halophilic organisms, such as members of Halobacteriaceae (Archaea), *Salinibacter* (Bacteria), and the anaerobic Halanaerobiales (Bacteria), living in

e.g. hypersaline lakes. The strategy involves the intracellular accumulation of molar concentrations of chloride ions (Cl^-) and potassium ions (K^+), causing a high ionic strength of the cytoplasm (51). Life under these extreme conditions requires a comprehensive adaptation of the enzymatic machinery. Thus, proteins are subjected to amino acid substitution, so that they are enriched with acidic amino acids with weakly hydrophobic residues, aiming at enhancing hydrophobic interactions and stabilizing the folded conformation of proteins. Consequently, several studies have shown that halophilic proteins differ significantly from their non-halophilic homologues as they display an instability under low salt conditions that can lead to denaturation (52, 53).

Even in halotolerant bacteria, potassium ions are accumulated in the first instance in response to high osmotic conditions. But in these organisms, high ion concentrations are detrimental for intracellular processes. The long-term response involves the partial but essential replacement of K^+ through organic osmolytes and is accordingly termed as “salt-out”, “low-salt in” or “compatible solute”-strategy (50, 51, 54, 55).

For *C. difficile*, little is known about general adaptation strategies to high osmolar conditions, the occurrence, involvement and function of various transporters, gene regulation or metabolic changes.

1.2.1 Initial phase of osmoadaptation: K^+ uptake

The initial phase of osmoadaptation in halotolerant bacteria involves the stimulation of potassium (K^+) uptake through specific transport systems (52, 55, 56). In *Escherichia coli*, four constitutive transporters with low affinity to K^+, including Trk, and a high-affinity Kdp system are involved in the uptake of the ion. The inducible *kdp* regulon comprises a *kdpFABC* operon coding for membrane-bound subunits of the Kdp-ATPases (*kdpA, kdpB, kdpC*) and an open reading frame of unknown function (*kdpF*). This operon is regulated by the membrane-bound protein KdpD as well as by KdpE, a soluble cytoplasmic protein, belonging to a two-component system (52, 56, 57). Studies on the responsible stimulus that initiates the expression of *kdpD* revealed contradictory results. Based on their results, in which increasing gene expression under high osmolarity was observed, Epstein and colleagues concluded that KdpD is a turgor sensor (58).

Other studies support the hypothesis that the gene expression might be coupled to the external K^+ concentration accompanied by changes in rate of K^+ fluxes (59, 60).

In contrast to the Kdp system of *E. coli*, the transcription level of the K^+ transporter in *B. subtilis*, termed KtrAB and KtrCD, is not affected by changes in K^+ concentration in the medium or increasing osmolarity, suggesting that it is a constitutive transport system. KtrB and KtrD are membrane-embedded proteins probably regulated by the membrane-associated protein KtrA or KtrC, which are able to bind NAD^+ and NADH, using a ligand-mediated conformational switch mechanism. Although the subunits of KtrAB and KtrCD are pairwise similar, they differ in their affinity to take up K^+ (55).

1.2.2 Secondary phase of osmoadaptation: accumulation of compatible solutes

The rapid accumulation of high intracellular K^+ concentrations protects the cell from excessive water efflux, but is also detrimental to DNA-protein interactions, protein biosynthesis, protein functionality and other physiological processes. To avoid this damage, it is essential to replace a part of the enriched potassium by synthesis or absorption of so-called compatible solutes (50, 55).

1.3 Compatible solutes

Compatible solutes belong to a special group of organic osmolytes protecting cells against the crucial effect of different stress conditions (61) including high osmolarities, cold and heat (62, 63, 64).

They are polar, highly soluble molecules that do not carry a net charge at physiological pH (46, 61). This property gives them the benefit of being accumulated intracellularly in high concentrations without affecting physiological processes of the cell (46, 50, 61). Under high osmotic conditions, compatible solutes are not only used by microorganisms to adjust the osmotic potential of their cytoplasm, which prevents dehydration (65), they also act as protein stabilizer and assistant in refolding of unfolded polypeptides giving them the name “chemical chaperones” (66).

Compatible solutes can be grouped into the following chemical categories: free amino acids (e.g. proline and glutamate), derivatives thereof (e.g. proline betaine and ectoine), sugars (e.g. trehalose), polyols (e.g. glycerol and glucosylglycerol), quaternary amines and their sulfonium analogues (e.g. glycine betaine, carnitine and dimethylsulfoniopropionate [DMSP]), sulfate esters (e.g. choline-O-sulfate), and N-acetylated diamino acids as well as small peptides (67, 68).

1.3.1 Providing and acquiring compatible solute

The strategy to accumulate compatible solutes in response to osmotic stress is not only common in bacteria or archaea (40), but also in plants, fungal, animal and even human cells (67, 69, 70, 71, 72). The list of preferred osmo protectants vary from organism to organism and depends on the stress timespan as well as the availability of substrates in the environment (72). The decay of eukaryotic cells and excretion of mammals provides a diversity of natural solutes (67). Two options for the accumulation of compatible solutes are known: endogenous *de novo* synthesis or exogenous uptake via specific transporters (67, 72).

The *de novo* synthesis is mainly limited to a few selected molecules and is usually carried out when no other osmolytes are present in the environment. The predominant synthesized endogenous solute for *E. coli* and *S. typhimurium* is trehalose while *B. subtilis* and other Gram-positive bacteria synthesize proline in the first instance after sudden increase in osmolarity (65, 67, 73). The most common compatible solute is glycine betaine, which is used in the prokaryotic as well as in eukaryotic kingdom. Those prokaryotes, that are capable of its synthesis, catalyze the reaction by methylation of glycine or by oxidation of exogenous choline (40). The accumulation of choline serves solely for the conversion to glycine betaine. Choline itself has no osmo-protective function (44, 74). The synthesis of glycine betaine from choline requires an electron acceptor, whose role is usually played by oxygen. Considering this aspect, it is impossible for anaerobes to use choline as a precursor (46, 75). Another way to generate glycine betaine is the metabolism of the quaternary amine compound carnitine that is widely distributed in nature, especially in muscle tissues (76). In eukaryotic cells, carnitine is best studied for its contribution to the transport of fatty acids into the mitochondria, whereas in bacteria it is used as a final electron acceptor and

carbon-, nitrogen, and energy source. Carnitine also acts as a compatible solute, that is transported into the cell or is generated directly from γ-butyrobetaine as precursor or via crotonobetaine (77, 78).

The uptake of precursor molecules for synthesis and ready-to-use osmolytes from the environment is mediated by specific osmotically inducible transport systems. In the Gram-positive model organism *B. subtilis* five high-affinity so-called Opu-transporter exist for the osmo protectant uptake. The primary transporters OpuA, OpuB and OpuC are multi-component systems that contain an ATP-binding cassette subunit and are therefore also known as ABC transporters (79, 80, 81, 82). In contrast, OpuE and OpuD belong to the family of secondary transporters, which comprise a single-component system (83, 84). The substrate specificity is strongly transporter-dependent and shows partial overlaps (Figure 4) (65, 85).

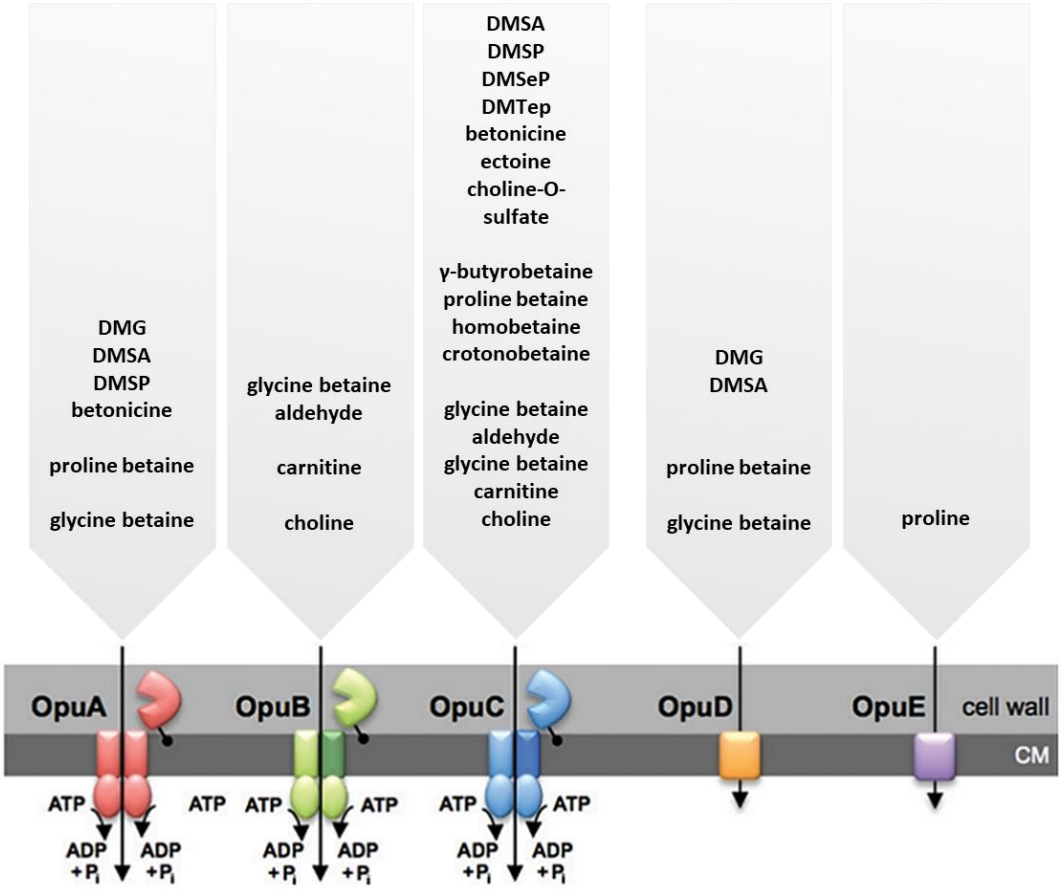

Figure 4 Substrate spectra of the osmo protectant uptake (Opu) systems of *B. subtilis*.
Schematic overview is modified after (65) and (81).

Thus, OpuE is only capable of transporting proline into the cell, whereas OpuC can be considered a universal transporter for a range of 15 osmolytes used e.g. glycine betaine, choline, γ-butyrobetaine, carnitine (65, 79, 81, 83). Another structurally related ABC transporter, OpuF, is present in many members of the large genus *Bacillus*, except *B. subtilis*, as well as in *C. acetobutylicum.* Compared to OpuC, OpuF is characterized by a lower substrate spectrum with glycine betaine, proline betaine, homobetaine and DMSP (86). In *C. difficile* nothing is known about the osmo protectant uptake system and their substrate specifity.

1.4 The diversity of the ABC transporter family

ATP-binding cassette (ABC) transporters form one of the largest superfamily of ATP-dependent protein complexes that are present in all three domains of life, bacteria, archaea and eukarya (87, 88, 89, 90, 91, 92). Classified as importers or exporters, ABC transporter mediate the translocation of a wide variety of molecules across the membrane. While importers have been identified predominantly in prokaryotes, archaea and more recently in plants, exporters are found in all organisms (87, 88, 89, 92, 93). The spectrum of transported substrates including ions, sugars, amino acids, vitamins, lipids, antibiotics, drugs and more (94, 95), reflects the diversity of their functional roles ranging from nutrient uptake to clinical relevance (87, 88, 94). In eukaryotes, they are directly involved in tumor resistance to chemotherapeutics due to the increased supply of multidrug resistance (MDR) proteins and the coupled export of medicine compounds (94, 96, 97). Another specific ABC transporter associated with antigen processing (TAP) plays an important role in the cellular immune response of vertebrates by identifying infected or malignantly transformed cells. TAP transporters, localized to the membrane of the endoplasmic reticulum (ER), mediate the transport of cytosolic peptides of proteasomal degradation into the ER lumen, where the peptides are loaded onto MHC class I molecules. This complex is translocated from the ER to the cell surface where it is presented to cytotoxic T-lymphocytes (98, 99, 100). On the other hand, a dysfunction of the ABC transporter causes several human diseases such as the most commonly known cystic fibrosis. This genetic disorder is caused by mutations in the gene

for the transmembrane conductivity regulator (CFTR) of cystic fibrosis, which acts as Cl^- channel (95, 101, 102).

1.4.1 Structure and general mechanism of ABC transporters

ABC transporters are classified into exporters and importers, whereby importers can be further divided into Type I, Type II and ECF (energy coupling factor; Type III) transporters (Figure 5) (87, 92).

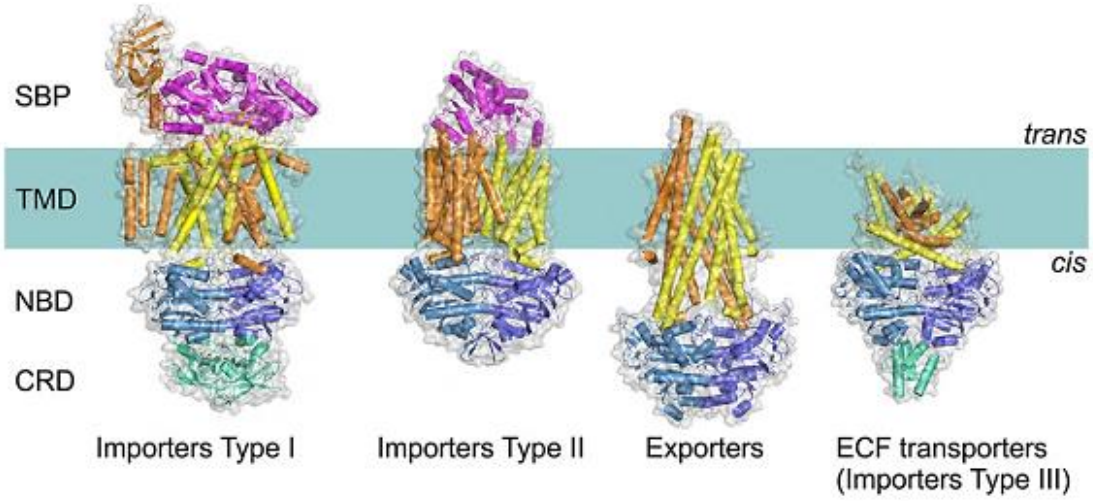

Figure 5 Structure of four ABC transporter subgroups.

All ABC transporters share a common modular architecture consisting of two hydrophobic trans membrane domains (TMDs; orange and yellow) and two water-soluble nucleotide binding domains (NBDs; blue) bound to the cytosolic surface of the TMDs. Additional domains (green) are present in some transporters acting as regulatory domains. Type I and II importers are dependent on a substrate binding protein (SBP; magenta) for the translocation of substrates. SBDs of Gram-negative bacteria are located in the periplasm. SBD of Gram-positives or archaea are fused to the TMD (modified after (92)).

Regardless of the transport direction (uptake or secretion), the type of substrate transported or the physiological function, all ABC transporters share a common modular architecture consisting of two hydrophobic trans membrane domains (TMDs) and two water-soluble nucleotide binding domains (NBDs) bound to the cytosolic surface of the TMDs (87, 91, 92, 93, 95, 100, 103, 104, 105). While for exporters the TMD and NBD can be fused (87, 92, 106, 107), importers have core TMD and NDB subunits that form individual chains. These can be merged to form homo- or heterodimeric TMDs bound to typically homodimeric NBDs (87, 92, 95). NBDs consist of highly conserved motifs including the Walker A (P-loop), Walker

B (87, 91, 92, 108), ABC signature motif as well as additional conserved NBD regions (H-loop/switch region, Q-loop) (87, 91, 92, 109). The domain interface typically contains two binding sites for ATP molecules that are located between the conserved Walker A motif of one monomer and the ABC signature motif (the LSGGQ motif) of the other monomer. Thus, the ATP-bound NBD provides the energy for translocation of substrates by ATP-hydrolysis (92, 110, 111, 112). TMDs are two hydrophobic proteins spanning the membrane as a bundle of α-helices that form a channel for substrate translocation (95, 113). In contrast to the highly conserved NBDs, TMDs share little or no sequence similarity among ABC transporters, reflecting the widely diversity of substrates that can be transported (93, 112). While ABC exporters are characterized by a conserved TMD core containing six transmembrane (TM) helices per subunit, the number of helices per TM segment of ABC importers range from 5 to 10 (87, 92, 113). Type I transporters have fewer helices than Type II importers (87). Furthermore, the TMD subunits of the importers may differ in their structure. While Type II TMDs always appear as homodimers, this does not always apply to Type I importers. In this case, the subunits may also only show structural similarities. In contrast, ECF TMDs are structurally and functionally unrelated (92).

A significant structural distinction between Type I-II importers and exporters, but also from ECF transporters, is the dependence of a substrate binding protein (SBP) for the translocation of substrates. Due to their simpler mechanism, exporters do not depend on substrate binding protein to function (92, 95). ECF transporters use one of the two TMDs, called S-component, for high-affinity substrate binding, so that no additional protein is required (92, 114, 115). SBD allows importers the recognition and binding of substrates in micromolar or even nanomolar concentrations for subsequent transfer to TMD (87, 93, 116, 117). In Gram-negative bacteria, SBDs are located in the periplasm, whereas in Gram-positive bacteria as well as archaea they are anchored to the membrane by a lipid chain and a hydrophobic helix. In some cases, the SBD of Gram-positives is fused to the TMD. Although SBPs have a highly conserved general architecture with two domains that form a substrate binding pocket, they can vary considerably in sequence and size, resulting in different substrate specificities (92, 118, 119). The structure-based differentiation allows SBDs to be categorized into six different clusters A to F, including several subclasses depending on the binding

ligand (119). SBD are often able to bind several, mostly similar, substrates like the SBP of the multi-sugar transporter Msm of *Streptococcus mutans*, which has affinity to carbohydrates such as melibiose, sucrose, raffinose, isomaltotriose, and isomaltotetraose (92, 120). This aspect could explain the partly broad substrate spectrum of transporters. A further explanation can be the interaction between transporters and different SBPs represented by the His/ Lys/ Arg transport system in Enterobacteriacea (92, 121).

It is still not clear why three types of importers have evolved, as they share overlapping substrate specificities. The combination of capacity and affinity of/to substrates could play a role in this context. Type I importers are known to transport compounds required in large quantities (such as sugars and amino acids). This may suggest that they are more suitable for high capacity transport (92). One of the most intensively studied Type I system is the maltose transporter $MalEFGK_2$ of enterobacteria, such as *E. coli* and *S. typhimurium* (Figure 6) (92, 122).

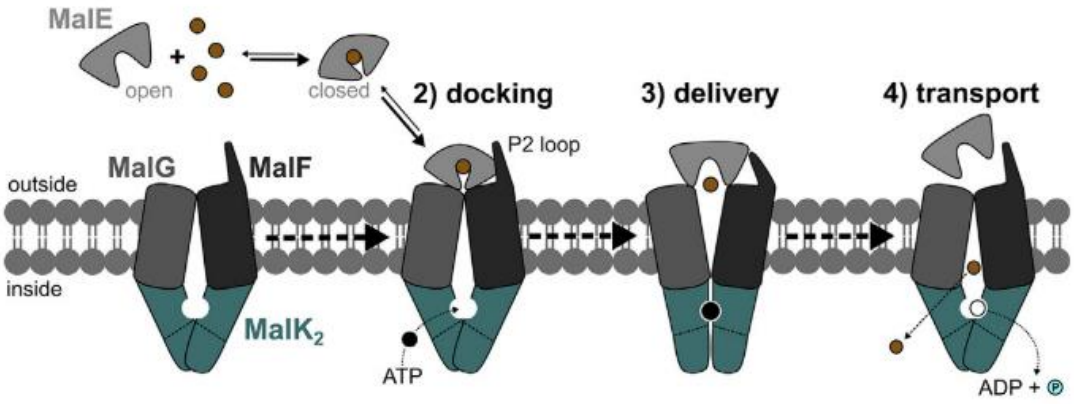

Figure 6 Transport mechanism of type I importer using the example of the maltose transporter $MalEFGK_2$.

The transporter complex $MalEFGK_2$ consists of two TMDs, MalF and MalG, two copies of an ATPase subunit, MalK, and the SBP, MalE. MalE recognizes and binds the substrate. The loaded SBD interacts with the TMD leading to a conformation change of TMDs and NBDs. NBDs dimerize upon ATP-binding resulting in an outward opened TMD that allows the delivery of substrate into the translocation channel. ATP-hydrolysis interrupts the dimerization and leads to an inward opened channel for the transport into the cytoplasm (modified after (123)).

This complex consists of two TMDs, MalF and MalG, two copies of an ATPase subunit, MalK, and the SBP, MalE, that is typically localized in the periplasm of Gram-negative bacteria. However, the transporter has an additional, rare feature that is characterized by a second binding site in one of the TMDs (92, 122, 124, 125, 126, 127). In contrast, Type II and Type III transporters are more often specific for compounds that are needed in small quantities (metal chelates, vitamins) and may therefore be better suited for high affinity, low capacity transports. The vitamin B_{12} importer $BtuC_2D_2F$ from *E. coli* constitutes the best investigated type II transporter (92, 128, 129).

Loaded SBDs stimulate the translocation cycle of substrates. After recognition and binding of ligands, they undergo a conformational change, known as Venus flytrap mechanism, followed by the interaction with the TMDs (123, 130). This in turn leads to a conformational change in TMDs and NBDs. NPDs dimerize by ATP-binding, while TMDs alternate, depending on the transporter type, from inward- to outward-facing (Type I;Figure 6) or from outward- to inward- facing (Type II) (131, 132). ATP-binding results in an opened TMD releasing the substrate from the SBD in the translocation channel. When ATP is hydrolyzed to ADP plus phosphate, the dimerization of NBDs is interrupted and TMDs open their channel to the cytoplasmatic site, releasing the substrate (88, 123, 131, 132, 133).

1.4.2 The ABC transporter OpuC and OpuF of *Bacillus species*

The primary ABC transporters OpuA, OpuB and OpuC of the model organism *B. subtilis* are multi-component systems playing an important role during the osmotic stress response. Due to their ability to translocate compatible solutes across the membrane, the transporters contribute to the protection against dehydration of the bacteria (65, 79, 80, 81, 82).

For *C. difficile* an ABC transporter OpuC, which is postulated to transport glycine betaine, carnitine and choline, is annotated. However, little is known about the complete spectrum of solutes and their function as an osmoprotective agent. The OpuC transporter of *B. subtilis* is very well characterized displaying a broad spectrum of 15 compatible solutes transported e.g. glycine betaine, carnitine, choline, ectoine or DMSP and its derivatives (Figure 4) (65, 67, 134). The OpuC system consists of two cytoplasmic membrane-associated ATPases, OpuCA, two membrane-spanning domains, OpuCB/OpuCD, and an extracellular SBP, OpuCC, that is tethered to the cytoplasmic membrane (Figure 7B). All five proteins are coded by corresponding genes organized in an operon (Figure 7A) (79, 86, 135).

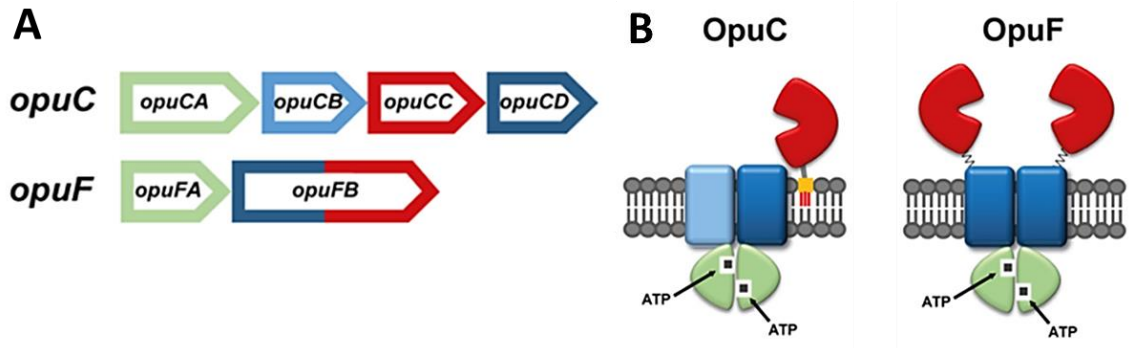

Figure 7 Structural gene (A) and protein (B) organization of the OpuC and OpuF transporters.

(A) Operon organization of the *B. subtilis* OpuC ABC transporter including corresponding genes *opuCA-opuCB-opuCC-opuCD* and of the OpuF ABC transporter from *B. infantis* consisting of *opuFA-opuFB*. (B) Illustration of the predicted subunit composition of the OpuC system from *B. subtilis* and of the OpuF ABC transport system from *B. infantis* (86).

The structure of the substrate binding pocket of OpuCC was elucidated by Du and colleagues (136). They showed that similar to other SBDs, OpuCC is constructed like an "aromatic cage" consisting of four tyrosine residues, Tyr^{91}, Tyr^{137}, Tyr^{217} and Tyr^{241} in combination with the residue Asn^{135} at the bottom as well as the residues Gln^{39}, Ser^{71}, Asn^{72} and Thr^{94} at the top. Crystallization of OpuCC both in the apo-form and in complex with several substrates revealed that carnitine, choline or glycine betaine share a common head group with trimethylammonium that interacts with the four tyrosine residues of the binding pocket, while the other residues above mentioned are responsible for the different binding affinities due to their interaction with different polar functions and the fit of lengths of the main chain of the substrates. It has been shown that carnitine, due to its long carbon chain, fits almost completely into the binding pocket and is therefore stabilized via three hydrogen bonds with Gln^{39}, Ser^{71} and Asn^{72}, resulting in a high binding affinity. Although glycine betaine also forms three hydrogen bonds, the binding affinity to OpuCC is only similar to carnitine, but not identical. This is due to the truncated carbon chain of glycine betaine, which does not allow binding via Ser^{71} and Asn^{72}. Instead, hydrogen bonds are formed via the amino acids Thr^{94} and Gln^{39}, as well as via a water molecule Wat^{27}. The influence of the hydrogen bond to specific amino acids of the substrate binding pocket is most evident in the example of choline. As a result of the very short carbon chain of choline, polar parts cannot form hydrogen bonds with the usual amino acid residues of the substrate pocket. This forces the trimethyl group of choline to shift, which leads to the formation of a hydrogen bond with Asn^{135} and consequently to an attenuated binding affinity compared to carnitine or glycine (136). The ability of OpuCC to bind multiple substrates is probably the result of a single evolutionary amino acid exchange within the substrate binding pocket (79, 136). Comparative sequence analyses with the ABC transporter OpuB showed a high degree of relationship with 83 % amino acid identity for the two NBDs (OpuBA/OpuCA), 85 % for the TMD pairs (OpuBB/OpuCB, OpuBD/OpuCD) and 69 % for the mature SBPs (OpuBC/OpuCC). Furthermore, the proximity of the two operons to each other and the high identities of the sequences in between suggest that the structural genes of one transporter were developed by an event of gene duplication (79). Nevertheless, the OpuB transporter has a much lower substrate spectrum compared to OpuCC. Thus, OpuB has only a very high affinity

to choline and a very low affinity to carnitine (81). Responsible for the loss of glycine betaine/ ectoine and weak carnitine binding is the replacement of Thr^{94}, present in OpuC, with Asp^{96}, present in OpuB. The exchange leads to electrostatic repulsion between the negatively charged carboxy group of Asp^{96} and the adjacent negatively charged carboxy group of carnitine, glycine betaine or ectoine (81, 136, 137).

Recently, an additional ABC transporter, OpuF, was described by Teichmann and colleagues (86) to be one of the most predominant osmolyte transporter in the genus *Bacillus*, exclusive *B. subtilis*. Interestingly, phylogenetic analysis displayed homologous transporter in *C. kluyveri* and *C. acetobutylicum*. In comparison to the intensively studied OpuC and OpuB transporters of *B. subtilis*, the genetic structure of OpuF is organized in an operon of two genes instead of four (Figure 7A). While the NBD is still encoded by a separate gene, *opuFA*, the TMD and SBD are encoded by a common gene, *opuFB*. This implies a fusion of the two proteins and thus a differentiation regarding the subunit composition compared to the other primary ABC transporters (Figure 7B). *In silico* model analysis predicted a TMD consisting of typically six helices and a SBD carrying an aromatic cage that is formed by the side chains of three tyrosine and one phenylalanine residue. At the amino acid position, which marks the difference between the transporters OpuC and OpuB, a threonine residue is located, as in OpuC. The amino acid sequence identity to OpuC is 34 % and 33 % to OpuB. The substrate spectrum of OpuF is wider than that of OpuB, but narrower than that of OpuC. Transportable substrates are limited to glycine betaine, proline betaine, homobetaine and DMSP (86).

1.5 The role of Fur-family regulators in adaptation processes

Ever since the earth's atmosphere initiated its change from anaerobic to aerobic conditions, bacteria have been struggling with iron starvation and oxidative stress in the form of molecular oxygen and reactive oxygen species (ROS) (138). For pathogens the circumvention of iron limitation as well as the fight against ROS play important role. During infection, the host initiates an antimicrobial response that includes the restriction of iron by producing siderophore- and iron-chelating proteins, by the export of iron from intracellular pathogen-containing compartments, by limiting the absorption of dietary iron, and by the production of ROS generated by cells of the host's immune system to reduce the growth of pathogenic invaders (13, 139). Especially intestinal microorganisms have to deal with the stress of iron restriction. Although the intestinal lumen contains high amounts of dietary iron, the freely available "unbound" iron is probably limited due to the environmental conditions of the colonic lumen (13, 140).

Iron is an essential metal for the growth and metabolism of bacteria. Nevertheless, free iron can cause the formation of hydroxyl radicals via the Fenton reaction, in which iron is reduced by H_2O_2. In order to avoid ROS-mediated cell damage, bacteria evolved strategies to tightly regulate the transcription of genes involved in iron uptake and homeostasis as well as in response to oxidative stress (138, 139, 140). The Fur-family regulators Fur (ferric uptake regulator) and PerR (peroxide-sensing regulator) are very well studied transcription factors in this context. Both are characterized as dimeric metal-dependent regulators binding conserved DNA sequences, the PerR or Fur boxes, usually suppressing the transcription of PerR- and Fur-regulated genes, respectively. Changes in environmental conditions lead to a conformational change which results in the release of the repressor and the transcription of target genes (138, 139, 141, 142).

1.5.1 Structure and function of PerR in the oxidative stress response

During the oxidative stress response of aerobic or facultatively anaerobic bacteria such as *Bacillus*, as well as strictly anaerobic organisms such as Clostridia, PerR takes on the role of a peroxide sensor (141, 143). The regulator is organized as a dimer in which each monomer has two binding sites. While one binding site serves for binding zinc (Zn^{2+}) and thus contributes to protein stability, the second is characterized as a regulatory metal binding site for iron (Fe^{2+}) or manganese (Mn^{2+}), which stabilizes the DNA binding domain (2, 138, 141, 142). Due to the higher affinity of Fe^{2+} to PerR, it is postulated that this metal is employed for to the detection of H_2O_2 (2, 144, 145).

In its active form, PerR is bound to the PerR DNA-boxes, suppressing the transcription of PerR-regulated genes (2, 141, 145, 146). At this stage the repressor forms a pyramid-like conformation whose regulatory side is coordinated by three histidine (H^{37}, H^{91}, H^{93}) and two aspartate residues (D^{104}, D^{85}) (2, 144, 145, 147, 148). The presence of H_2O_2 is detected via PerR-Zn^{2+}-Fe^{2+}, which leads to a metal-catalyzed Fenton reaction (2, 145). By oxidation of H^{37} and H^{91} to 2 oxo-histidine, hydroxyl radicals trigger the degradation of the iron coordination and thus a conformational change. This leads to destabilization of the binding domain, release of the repressor and transcription of target genes (2, 144, 145, 148).

In many bacteria, PerR mainly regulates the transcription of genes involved in the response to oxidative stress, such as *katA* (vegetative catalase) and *ahpCF* (alkylhydroxoperoxide reductase) in *B. subtilis* (2, 141, 142, 149, 150) or *rd* (rubredoxin), *tpx* (thiolperoxidase) and *bcp* (alkylhydroperoxidase) in *C. acetobutylicum* (151). But also genes of other metabolic processes can be regulated by PerR. In *B. subtilis*, PerR has been linked to the regulation of metal homeostasis genes such as *fur* (iron uptake regulator), *zosA* (zinc uptake) and *hemAXCDBL* (heme biosynthesis) (2, 142, 149, 150). Transcriptome analyses of *perR* deletion mutants in *C. acetobutylicum* led to a strong repression of *bsaA2* (glutathione peroxidase) as well as two genes that play a putative role in the biosynthesis and transport of siderophores (2, 151). In addition, PerR autoregulates itself by repression its own expression (145, 150). Based on transcriptional analysis, preliminary data of our laboratory investigations have

shown both H_2O_2-dependent and H_2O_2-independent PerR regulation in *C. difficile* (2). Thus, genes of general defense, fatty acid biosynthesis, PTS, arginine or proline biosynthesis as well as nucleotide metabolism and flagella assembly are under the control of PerR if the organism is exposed to oxidative stress. In contrast, genes, especially those of the detoxification system, redox balance and energy conversion are also regulated by PerR, even when no stress conditions exist. Particularly noteworthy are the genes repressed in the *perR* mutant, which code for rubrerythrin (*rbr*; CD630DERM_08250), rubredoxin oxidoreductase (*rbo*; CD630ERM_08270) as well as for an oxidative stress glutamate synthase (CD630ERM_08280), since they are located in an operon with *perR* and indicate an autoregulation of the operon. On the other hand, the *perR* mutation also led to the induction of genes belonging to the detoxification system and redox balance (CD630DERM_16230: oxidoreductase, CD630DERM_17770: arsenate reductase, CD630DERM_18220: thiol peroxidase; *bcp*) as well as being involved in energy conversion in leucine fermentation and butanoate metabolism (2).

1.5.2 Structure and function of Fur in low iron response

In many bacteria, the Fur (ferric uptake regulator) protein is known to act as global regulator of iron homeostasis. As repressor, Fur mainly controls the transcription of genes involved in iron uptake and iron storage (13, 138, 152). Studies in several organisms describe a broad spectrum of genes regulated by Fur. Thus, the synthesis and uptake of siderophores (153) are under the control of the Fur regulon as well as genes that are involved in oxidative stress response (154, 155), acid tolerance (156), quorum sensing (157), virulence (155, 158) and general energy metabolism (13, 155).

The regulator consists of two monomers with a structural Zn^{2+} binding site and two metal-binding sites for Fe^{2+}. Under high iron conditions, Fur binds Fe^{2+} and forms a dimeric structure bound to Fur boxes, thereby suppressing the transcription of Fur-regulated genes. Depression of these genes is induced when Fur is released from the DNA by conformational changes due to low iron levels (138, 158).

1.6 Aim of the study

During infection, the strictly anaerobic and spore-forming human pathogen *C. difficile* is exposed to ever-changing osmolarities, oxygen concentrations and iron availability. Consequently, the organism must diploy diverse adaption strategies to thrieve on these challenging conditions. In particular, its adaptation process in response to high osmolarity conditions remains largely elusive. In this study, the characterization of involved transporters and their substrate spectrum for compatible solutions using a heterologous *Bacillus* system and in *C. difficile* itself will be pursued. Investigations on *C. difficile* and the corresponding mutants should provide a view on the phenotypic and metabolic changes under salt stress and upon addition of compatible solutes. Furthermore, the aim of this work is to define a more precise characterization of the PerR regulation, a peroxide sensor involved in the oxidative stress response using a combined systems biology approach encompassing transcriptome and metabolome analyses. Additionally, earlier observations regarding Fur-dependent iron regulation will be followed up by conducting complementary phenotypical profiling aiming at expanding our understanding of the adaptive response of *C. difficile* during infection.

2. MATERIALS UND METHODS

2.1 Equipment

All equipment used in this work are listed in Table 1 with name of model and supplier.

Table 1 List of equipment including name of model and supplier

Equipment	Model	Supplier
Agarose gel electrophoresis	PowerPac™ Basic	BioRad, München, Germany
Agarose gel documentation	Intas Gel IX-20 Imager	Intas Science Imaging, Göttingen, Germany
Anaerobic chamber	Type B flexible vinyl chamber	Coy Laboratory Products, Grass Lake, USA
Anaerobic culture tubes (Hungates)	18 x 150 mm, Hals N20	Glasgerätebau Ochs, Bovenden/Lenglern, Germany
Anaerobic bottles	150 mL Afnor Typ 1	Zscheile Klinger GmbH, Hannover, Germany
Autoclave	V-150	Systec, Linden, Germany
	LABOKLAV MSLV160	SHP, Neckarwestheim, Germany
	ELV 2450	Tuttnauer, Breda, Netherland
Bioanalyzer	Bioanalyzer 2100	Agilent Technologies, Santa Clara, USA
Centrifuges	Mini Spin	Eppendorf, Hamburg, Germany
	Megafuge 1.0R	Heraeus, Hanau, Germany
	Biofuge PrimoR Centrifuge	
	Multifuge X1R Centrifuge	
	Avanti J-E	Beckmann Coulter, Krefeld, Germany
	Optima™L-90K Ultracentrifuge	
Flower plate	MTP-48-B — without optodes + biomass, fluorescences	m2p-labs GmbH, Baesweiler, Germany
Homogenizer	FastPrep®24 Instruments	MP Biomedicals, Eschwege, Germany
Microbioreactor system	BioLector®	m2p-labs GmbH, Baesweiler, Germany

Equipment	**Model**	**Supplier**
Microplate Reader	Infinite® 200Pro	Tecan Trading AG, Switzerland
Pipettes	Research® plus	Eppendorf, Hamburg, Germany
pH determination	766 Calimatic	Knick, Berlin, Germany
Real-time PCR cycler	CFX96™	BioRad, Hercules, USA
Spectrophotometer	NanoDropTM1000	Peqlab, Erlangen, Germany
	WPA spectrophotometer C08000	Biochrom, Berlin, Germany
	Libra S11visible spectrophotometer	
	Genesys 10S UV-Vis spectrophotometer	Thermo Fisher Scientific, Waltham, USA
Thermocycler	T personal	Biometra, Göttingen, Germany
Thermomixer	Thermomixer comfort	Eppendorf, Hamburg, Germany
Vortex	Vortex Genie 2	Scientific Industries, New York, USA
Water purification	Milli-Q system	Millipore, Billerica, USA

2.2 Plasmids, synthesized DNA fragments and strains

2.2.1 Plasmids and synthesized DNA-fragments

All plasmids used and/or constructed in this work are listed in Table 2 to Table 4. Features and origin are named.

Table 2 List of plasmids used for ClosTron mutagenesis

Plasmid	Features	Description	Origin
pMTL007C-E2	*catP*, *erm*RAM, RepH, Ori_pBR, *traJ*, P_fdx, LtrA, Term_rrnBT1T2	ClosTron plasmid	(159)
pMTL007C-E2::Cdi_*opuCC*-936 l 937s	*catP*, *erm*RAM, RepH, Ori_pBR, *traJ*, P_fdx, LtrA, Term_rrnBT1T2	ClosTron plasmid pMTL007C-E2 retargeted to *C. difficile* 630Δ*erm*-*opuCC*936l937s::intron *ermB*	This work
pMTL007C-E2::Cdi_*putP*-1005 l 1006s	*catP*, *erm*RAM, RepH, Ori_pBR, *traJ*, P_fdx, LtrA, Term_rrnBT1T2	ClosTron plasmid pMTL007C-E2 retargeted to *C. difficile* 630Δ*erm*-*putP*1005l1006s::intron *ermB*	This work
pMTL007C-E2::Cdi_*ribBA*-285 l 286s	*catP*, *erm*RAM, RepH, Ori_pBR, *traJ*, P_fdx, LtrA, Term_rrnBT1T2	ClosTron plasmid pMTL007C-E2 retargeted to *C. difficile* 630Δ*erm*-*ribBA*285l286s::intron *ermB*	This work
pMTL007C-E2::Cdi_*ribU*-374 l 375a	*catP*, *erm*RAM, RepH, Ori_pBR, *traJ*, P_fdx, LtrA, Term_rrnBT1T2	ClosTron plasmid pMTL007C-E2 retargeted to *C. difficile* 630Δ*erm*-*ribU374*l375a::intron *ermB*	This work
pMTL007C-E2::Cdi_*perR*-187a::intron	*catP*, *erm*RAM, RepH, Ori_pBR, *traJ*, P_fdx, LtrA, Term_rrnBT1T2	ClosTron plasmid pMTL007C-E2 retargeted to *C. difficile* 630Δ*erm*-*perR187*l188a::intron *ermB*	(13)

Plasmid	Features	Description	Origin
pMTL007C-E2::Cdi_*rbr1*-297 I 298s	*catP*, *erm*RAM, RepH, Ori_pBR, *traJ*, P_fdx, LtrA, Term_rrnBT1T2	ClosTron plasmid pMTL007C-E2 retargeted to *C. difficile* 630Δ*erm-rbr1-297I298s*::intron *ermB*	This work
pMTL007C-E2::Cdi_dsr-186 I 187s	*catP*, *erm*RAM, RepH, Ori_pBR, *traJ*, P_fdx, LtrA, Term_rrnBT1T2	ClosTron plasmid pMTL007C-E2 retargeted to *C. difficile* 630Δ*erm-dsr-186I187s*::intron *ermB*	This work
pMTL007C-E2::Cdi_oxstressglutdehy-171 I 172s	*catP*, *erm*RAM, RepH, Ori_pBR, *traJ*, P_fdx, LtrA, Term_rrnBT1T2	ClosTron plasmid pMTL007C-E2 retargeted to *C. difficile* 630Δ*erm-CDIF630_00947-171I172s*::intron *ermB*	This work
pMTL007C-E2::Cdi_*fur*-274 I 275a	*catP*, *erm*RAM, RepH, Ori_pBR, *traJ*, P_fdx, LtrA, Term_rrnBT1T2	ClosTron plasmid pMTL007C-E2 retargeted to *C. difficile* 630Δ*erm-fur274I275a*::intron *ermB*	(13)

Table 3 List of plasmids used for complementation experiments

Plasmid	Features	Description	Origin
pMTL82151	pMTL8000 back bone, pBP1, *catP*, ColE1 + tra, MCS, *lacZ* alpha region	*E. coli - C. difficile* shuttle vector	(160)
pRPF185	pMTL960 back bone Term(fdx)-P_{tet}-*gusA*-Term(slpA)	*E. coli - C. difficile* shuttle vector	(161)
pJet1.2	rep(pMB1), *bla* (Ap^R), *eco47IR*,P_{lacUV5},T7 promotor, MCS, blunt DNA ends for ligation with insert	blunt end cloning vector	Thermo Fisher Scientific, Waltham, USA
pAMCDX	pMTL82151 back boneΔ*lacZ* alpha region, *catP*	control vector for pAMCD03 to pAMCD06	(162) supervised in this work
pAMCDY	pRPF185 back boneΔ*gusA*,P_{tet}	control vector for pAMCD01 and pAMCD02	(162) supervised in this work

Plasmid	Features	Description	Origin
pAMCD01	pRPF185 back bone Δ*gusA*::*perR*(*C.difficile* 630Δ*erm*), *catP,* P_{tet}	complementation vector	(163) supervised in this work
pAMCD02	pRPF185 back bone Δ*gusA*::*perR*(*C.difficile* 630), *catP,* P_{tet}	complementation vector	(163) supervised in this work
pAMCD03	pMTL82151 back bone Δ*lacZ* alpha region::350nt upstream *perR*::*perR*(*C.difficile* 630Δ*erm*), *catP*	complementation vector	(163) supervised in this work
pAMCD04	pMTL82151 back bone Δ*lacZ* alpha region::350nt upstream *perR*::*perR*(*C.difficile* 630), *catP*	complementation vector	(163) supervised in this work
pAMCD05	pMTL82151 back bone Δ*lacZ* alpha region::350nt upstream *rbr1*::*perR*(*C.difficile* 630Δ*erm*), *catP*	complementation vector	(163) supervised in this work
pAMCD06	pMTL82151 back bone Δ*lacZ* alpha region::350nt upstream *rbr1*::*perR*(*C.difficile* 630), *catP*	complementation vector	(163) supervised in this work

Table 4 List of plasmids and synthesized DNA fragments used for *B. subtilis* experiments

Plasmid/DNA fragment	Features	Description	Origin/ Reference
pX	*xyl*R, Cm^R, Amp^R *amyE* front/back	Vector for integration of genes into the *amyE* gene	Gift from Dr. T.Hoffmann, University of Marburg (164)
pMA-RQ-*opuC*$_{C.\ difficile\ 630\Delta erm}$	Amp^R, Col E1 origin, optimized *CDIF630erm_01020:: CDIF630erm_01021* operon, *B. subtilis* promotor region	Gene Art cloning vector	This work synthezied by Thermo Fisher
pMA-RQ-unkn.transporter$_{C.\ difficile\ 630\Delta erm}$	Amp^R, Col E1 origin, optimized *CDIF630erm_03510:: CDIF630erm_03509* operon, *B. subtilis* promotor region	Gene Art cloning vector	This work synthezied by Thermo Fisher

Plasmid/DNA fragment	**Features**	**Description**	**Origin/ Reference**
pJet1.2	rep(pMB1), *bla* (Ap^R), *eco47IR*,P_{lacUV5},T7 promotor, MCS, blunt DNA ends for ligation with insert	blunt end cloning vector	Thermo Fisher Scientific, Waltham, USA
pXΔ*xylR*::*opuC*$_{C.\ difficile\ 630\Delta erm}$	Cm^R, Amp^R, Δ*xylR*, optimized *opuC*$_{C.\ difficile\ 630\Delta erm}$ (*CDIF630erm_01020:: CDIF630erm_01021*) inserted	Vector for integration of the gene *opuC*$_{C.\ difficile\ 630\Delta erm}$ optimized for *B. subtilis* into the *amyE* gene	This work
pXΔ*xylR*:: unkn.transporter$_{C.\ difficile\ 630\Delta erm}$	Cm^R, Amp^R, Δ*xylR*, optimized *CDIF630erm_03510:: CDIF630erm_03509*$_{C.\ difficile\ 630\Delta erm}$ inserted	Vector for integration of the gene *opuC*$_{C.\ difficile\ 630\Delta erm}$ optimized for *B. subtilis* into the *amyE* gene	This work

2.2.2 Strains

All strains used and/or generated in this work are listed in Table 5 to Table 7. Features and references are named.

Table 5 List of *E. coli* strains

Strain	Features	Reference
E. coli DH10B	F- *mcrA Δ(mrr-hsdRMS-mcrBC) φ80lacZΔM15 ΔlacZX74 recA1 endA1 araD139 Δ (ara-leu)7697 galU galK λ-rpsL(Str^R) nupG*	Thermo Fisher Scientific, Waltham, USA
E. coli CA434	*E. coli* HB101 carrying the Incβ conjugative plasmid R702 (F-, *thi*-1,hsdS20(r_B-m_B-), *sup*E44, *recA1*3, ara-14, *rps*L20(str^r), *leu*B6,*gal*K2,*xyl*-5,*mtl*-1)	(165)

Table 6 List of *B. subtilis* strains

Strain	Features	Reference
B. subtilis JH642	wild type *trp*C2, *phe*A1	(166)
B. subtilis TMB118	Δ(*opuA*::*tet*)3 Δ(*opuC*::*spc*)3 Δ*opuD*::*kan*)2 Δ*opuB*::*erm*)1	(81)
B. subtilis AM01	TMB118 *amyE*:: *opuC*$_{C.\ difficile\ 630\Delta erm}$ (*CDIF630erm_01020:: CDIF630erm_01021*)	This work
B. subtilis AM02	TMB118 *amyE*::*CDIF630erm_03510:: CDIFerm630_03509*$_{C.\ difficile\ 630\Delta erm}$	This work

Table 7 List of *C. difficile* strains

Strain	Features	Origin
Clostridium difficile 630Δ*erm* (DSM28645)	Erythromycin sensitive mutant of *C. difficile* 630, thi^r	(167); DSMZ Braunschweig, Germany
Cdi630Δ*erm-opuCC*-936I937s::intron *ermB* (CD630DERM_09010)	*opuCC* insertional mutant of *C. difficile* 630Δ*erm,* target site 936I937 sense, thi^r, erm^r	(168) supervised in this work
Cdi630Δ*erm-putP*-1005I1006s::intron *ermB* (CDIF630erm_03896)	*putP* insertional mutant of *C. difficile* 630Δ*erm,* target site 1005I1006 sense, thi^r, erm^r	This work
Cdi630Δ*erm-perR*187a::intron *ermB* (CD630_08260)	*perR* insertional mutant of *C. difficile* 630Δ*erm,* target site 187I188 antisense, thi^r, erm^r	(13)
Cdi630Δ*erm-ribBA*-285I286s::intron *ermB* (CD630DERM_01883)	*ribBA* insertional mutant of *C. difficile* 630Δ*erm,* target site 285I286 sense, thi^r, erm^r	This work
Cdi630Δ*erm-ribU*-374I375a::intron *ermB* (CD630DERM_00266)	*ribU* insertional mutant of *C. difficile* 630Δ*erm,* target site 374I375 antisense, thi^r, erm^r	This work
Cdi630Δ*erm-fur*-274I275a::intron *ermB* (CD630_12870)	*fur* insertional mutant of *C. difficile* 630Δ*erm,* target site 274I275 antisense, thi^r, erm^r	(13)

2.3 Oligonucleotides and DNA fragments

All oligonucleotides used in this work are listed in Table 8 and Table 9.

Table 8 List of primers used for ClosTron mutagenesis

Name	Sequence 5´ to 3´	Product optained	Annealing temperature [°C]	Origin
Cdiff16S_Fw	GTG AGC CAG TAC AGG	744 bp	48	DSMZ
Cdiff16S_Rv	TTA AGG AGA TGT CAT TGG			
EBS_universal	CGA AAT TAG AAA CTT GC G TTC AGT AAA C	-	55	(169)

Name	Sequence 5´ to 3´	Product optained	Annealing temperature [°C]	Origin
ErmRAM_Fw	ACG CGT TAT ATT GAT AA A AAT AAT AGT GGG	spliced: 900 bp unspliced: 1300 bp	59	(169)
ErmRAM_Rv	ACG CGT GCG ACT CAT AGA ATT ATT TCC TCC CG			
Cdi_opuCC_Fw2	GTA AAA TTG AAG TTG CAG TTA C	wild type: 898 bp mutant: 2798 bp	58	This work
Cdi_opuCC_Rv1	CCA AGT TCA TCC ACT TGA TAG T			
Cdi_putP_Fw1	ATG TTA ACA TTT TGG GAA AAT GG	wild type: 1395 bp mutant: 3195 bp	58	This work
Cdi_putP_Rv1	TTA TAG ATT ATT TTG TGT ATT TAA ATT TTC ACC			
Cdi_perR_Fw1	GTT CAT CCT ACT GCG GAT TAC	wild type: 332 bp mutant: 2132 bp	59	(13)
Cdi_perR_Rv1	CCT ACT TGG CTA CAC CTT TTA C			
Cdi_fur_Fw1	CTG GTT TTA AGA TTA CGC CAC	wild type: 394 bp mutant: 2194 bp	59	(13)
Cdi_fur_Rv1	CCA TTA CAC TCG TCA CAT AGT C			
Cdi_ribBA_Fw1	ATG TTT AAT ACT ATT GAA GAA GC	wild type: 1194 bp mutant: 2994 bp	53	This work
Cdi_ribBA_Rv1	TTA TAT AAT ATC TAA AA G ATG TCC			
Cdi_ribU_Fw1	ATG CAA AAC ACA GCA AAA AGA GGC	wild type: 606 bp mutant: 2406 bp	62	This work
Cdi_ribU_Rv1	TTA TTT CTT TAT TAT ATT TCC CAT TTT TTT ATA AAG TGG C			

Table 9 List of primers used for complementation experiments

Name	Sequence 5´ to 3´	Description	Annealing temperature [°C]	Origin
perR_compl_Fw	ATC AGA GCT CCT GCA GTA AAG GAG AAA ATT TTA TGA AAT TTT CTA AAC AAC G	Amplification of *perR* including the restriction side SacI for cloning in pRPF185	55	This work
perR_compl_Rv	ATC AGG ATC CCT AAC CTA CTT GGC TAC ACC	Amplification of *perR* including the restriction side BamHI for cloning in pRPF185	55	This work
350nt_up_perR_Fw	ATC AGC GGC CGC TTT AAA GGA TGC AGC AGC AGG	Amplification of *perR* including 350 nt upstream and the restriction side NotI for cloning in pMTL82151	68	This work
perR_compl_Rv2	ATC AGC TAG CCT AAC CTA CTT GGC TAC ACC	Amplification of *perR* including 350 nt upstream and the restriction side NheI for cloning in pMTL82151	61	This work
350nt_up_rbr1_Fw	ATC AGC GGC CGC TTG CTA GAC AGT GAA AAG AAA AAA TCT GTC G	Amplification of 350 nt upstream *rbr1* and the restriction side NotI for fusion with *perR* and cloning in pMTL82151	61	This work

Name	Sequence 5´ to 3´	Description	Annealing temperature [°C]	Origin
perR_Fw_MERG_up_rbr1_Rv	CTA TTA TTA AAA AGG GAG GAA TTA ATT ATG AAA TTT TCT AAA CAA CG	Forward primer for fusion of 350 nt upstream *rbr1* with *perR*	61	This work
Up_rbr1_Rv_MERG_perR_Fw	CGT TGT TTA GAA AAT TTC ATA ATT AAT TCC TCC CTT TTT AAT AAT AG	Reverse primer for fusion of 350 nt upstream *rbr1* with *perR*	61	This work

Table 10 List of primers used for control of *C. difficile* complementation vectors

Name	Sequence 5´ to 3´	Annealing temperature [°C]	Origin
Seq_pMTL82151-lacZ_F	GAT TGC CAA GCA CGT CCC CAT GCG	69	This work
Seq_pMTL82151-lacZ_R	CGT CTT CAT TAA ATG CCT TAG AAT CCA TTA C	69	This work
Seq_pMTL82151_F	CAG GAA ACA GCT ATG ACC GCG G	65	This work
Seq_pMTL82151_R	GAA GCC TGC AAA TGC AGG CTT C	65	This work
Seq_pMTL82151_R3	GCT AAG GAT TCA GAA CGG CGC G	69	This work
Seq_univ_pRPF185_F	CTT GAT CGT AGC GTT AAC AG	58	This work
Seq_univ_pRPF185_R	CCT TTT TCT ATT TAA AGT TTT ATT AAA AC	58	This work
Seq_pRPF185_TetR_F	GGC GAG TTT ACG GGT TGT TA	64.5	This work
Seq_pRPF185_traJ_R	GCT TGG CAA GGT CAT GAT GGG C	66	This work

Name	Sequence 5´ to 3´	Annealing temperature [°C]	Origin
Seq_pRPF185-traJ_R2	GCG GAT GGC TGA TGA AAC CAA GCC	64.5	This work

Table 11 List of primers used for control of *B. subtilis* complementation vectors

Name	Sequence 5´ to 3´	Annealing temperature [°C]	Origin
pX_universal_Fw	GGC GCT CAG GAT CTG TTA AGA TC	65	This work
pX_universal_Rv	CGA TAA GCT TCT AGG ATC TCG AGC	65	This work
Bsub_Promotor_Fw	AGC TGA TCA TCC CTT CAA ATG GC	63	This work
OpuCA_opt_Fw1	ATG ATT GAA ATT AGA AAT GTC ACG AAA AAA ATC	64	This work
OpuCC_opt-Fw2	GCA CGG AAT GGC AAA CTT TTT TAA C	63	This work
OpuCA_opt_Fw3	GGT TGA AAT CCT GAA TGT CAT GAA TAG AAA TAG	68	This work
OpuCA_opt_Rv1	GTT TAG CCC AGG ACT GAA ACT TC	63	This work
OpuCC_opt_Rv2	CCA GGC CTT CTT TAA CCA GAA ATG	64	This work
unkn.Transp_opt_F2	GAA TGA CAC CGA TTA TTC AGT TCA AG	63	This work
unkn_Transp_Fw3	CGC AAC AAA GCC GAT GAC AG	30	This work

2.4 Commercial kits, buffer and enzymes

All kits used for DNA- and RNA-isolation, cloning procedures, array analysis and toxin quantification are listed in Table 12.

Commercial buffer and enzymes are shown in Table 13.

Restriction enzymes used in this work were sourced from New England BioLabs® and are listed in Table 14 with specific recognition sequence.

Table 12 List of used kits

Name	Supplier
DNA- and RNA isolation kits	
FastDNA™Spin Kit for Soil	MP Biomedical, Eschwege, Germany
Qiagen RNeasy® Mini (50)	Qiagen, Hilden, Germany
Plasmid preparation and purification kits	
NucleoSpin® Plasmid (NoLid)	Macherey-Nagel, Düren, Germany
NucleoSpin® Gel and PCR Clean up	
QIAprep® Spin Miniprep Kit	Qiagen, Hilden, Germany
QIAquick® Gel Extraction Kit	
QIAquick® PCR Purification Kit	
Cloning kits	
CloneJet PCR Cloning Kit	Thermo Fisher Scientific, Waltham, USA
Kits for array analysis	
Agilent RNA 6000 Nano Kit	Agilent Technologies, Santa Clara, USA
Gene Expression Hybridization Kit	
Hybridization Gasket Slide Kit (5)	
ULS labeling kit with Cy3 and Cy5 for Agilent® gene expression arrays	KREATECH Biotechnology, Amsterdam, Netherland
Clostridium difficile Toxin A or B quanti	tgc Biomics, Bingen am Rhein, Germany

Table 13 List of commercial buffer and enzymes

Name	Supplier
Enzymes, buffer and other components for DNA amplification	
Q5® High-Fidelity DNA polymerase	New England BioLabs®, Frankfurt am Main, Germany
5 x Q5® Reaction buffer	
dNTP Solution Mix	
Enzymes and buffer for ligation reaction	
T4 DNA Ligase	New England BioLabs®, Frankfurt am Main, Germany
1 x T4 Ligase reaction buffer	
Enzymes for RNA isolation	
Lysozym from chicken egg white (10,0000 U/mg)	Sigma Aldrich, St. Louis, USA
RNase free DNase Set (50)	Qiagen, Hilden, Germany
Buffer for array analysis	
Gene Expression Washpuffer 1	Agilent Technologies, Santa Clara, USA
Gene Expression Washpuffer 2	
Enzyme for protein protection	
cOMPLETE™, Mini, EDTA-free Protease Inhibitor Cocktail	Sigma Aldrich, St. Louis, USA

Table 14 List of used restriction enzymes obtained from New England BioLabs®

Name	Recognition sequence	Reaction buffer
BamHI-HF™	G↓GATC↑C	Cut Smart
BsrGI-HF™	T↓GTAC↑A	
HindIII-HF™	A↓AGCT↑T	
NheI-HF™	G↓CTAG↑C	
NotI-HF™	GC↓GGCC↑GC	
PvuI- HF™	CGAT↓CG	
SacI-HF™	G↓AGCT↑C	
XbaI™	T↓CTAG↑A	

2.5 Media and media supplements

All media, compounds and supplements were purchased from Applichem, BD Becton Dickinson, Merck, MP Biomedicals, Roth, Serva, Fluka and Sigma-Aldrich unless otherwise stated.

2.5.1 Growth media for cultivation of *E. coli*

E. coli cells were cultivated aerobically at 37 °C in lysogenic broth (LB) supplemented with ampicillin (100 µg/ml) or chloramphenicol (20 µg/ml) if required for plasmid maintenance (see 2.2.1). Antibiotics were added after sterilization.

Lysogenic broth (LB)

Yeast extract	5	g/l
NaCl	5	g/l
Tryptone/Peptone	10	g/l

For cultivation on agar plates 15 g/l agar-agar was added before autoclaving.

Table 15 Supplemented antibiotics for *E. coli* cultivation

Supplement	Concentration of stock solution	End concentration
Ampicillin (Ap)	100 mg/ml in MQ-H_2O	100 µg/ml
Chloramphenicol (Cm)	20 mg/ml in 70 % EtOH	20 µg/ml

2.5.2 Growth media for cultivation of *B. subtilis*

B. subtilis cells were cultivated routinely at 37 °C in LB medium (see 2.5.1) under aerobic conditions. Ampicillin (100 µg/ml) or chloramphenicol (5 µg/ml) were added if required for plasmid maintenance (see 2.2.1). Transport studies were performed in a defined Spizizen´s minimal medium (SMM) supplemented with trace element solution and 0.5 % glucose as carbon source. L-tryptophan (20 µg/ml) and L-phenylalanine (18 µg/ml) were added to complement the auxotrophic strain *B. subtilis* JH642.

Table 16 Compounds of 5 x Spizizen´s minimal medium (SMM) in 950 ml MQ-H_2O

Compound	Concentration of stock solution [g]	End concentration [g/l]
$(NH_4)_2SO_4$	10	2
K_2HPO_4	70	14
KH_2PO_4	30	7
Na_3Citrate x 2 H_2O	5	1
$MgSO_4$ x 7 H_2O	1	0.2

Table 17 Compounds of 100 x trace element solution

Compound	Concentration of stock solution [g/l]	End concentration [g/l]
$CaCl_2$ x 2 H_2O	0.7283	0.0073
$FeCl_3$	0.8101	0.0081
$MnCl_2$ x 4 H_2O	0.10	0.0010
$ZnCl_2$	0.17	0.0017
$CuCl_2$ x 6 H_2O	0.05	0.0005
$CoCl_2$ x 6 H_2O	0.06	0.0006
Na_2MoO_4 x 2 H_2O	0.06	0.0006

2.5.3 Growth media for cultivation of *C. difficile*

C. difficile cells were cultivated anaerobically without shaking at 37 °C in Brain-Heart-Infusion (BHI) broth (37 g/l) or on BHI agar plates (52 g/l) supplemented with 0.1 % L-cysteine and 5 g/l yeast extract (BHIS) if needed. To promote germination process 0.1 % taurocholate was added (BHIST).

During mutagenesis and complementation experiments *C. difficile* Supplement (Sigma Aldrich, Taufkirchen, Germany), containing D-cycloserine (500 µg/ml) as well as cefoxitin (16 µg/ml), and thiamphenicol (15 µg/ml) were used. Erythromycin (2.5 µg/ml) was added for selection of potential ClosTron mutants.

For short-time storage *C. difficile* was cultivated on CHROMID® *C. difficile* agar plates (bioMérieux, Nürtingen, Germany).

Table 18 Supplemented antibiotics for *C. difficile* cultivation

Supplement	Concentration of stock solution	End concentration
C. difficile Supplement in MQ-H_2O (CC) - D-cycloserine - Cefoxitin	 125 mg/ml 4 mg/ml	 500 µg/ml 16 µg/ml
Thiamphenicol (thi)	15 mg/ml in MeOH	15 µg/ml
Erythromycin (erm)	2.5 mg/ml in MQ-H_2O	2.5 µg/ml

2.5.4 Media for growth experiments and systems biology approaches

Growth experiments and systems biology approaches with *C. difficile* were performed in a modified *Clostridium difficile* minimal medium (CDMM) after Cartman and Minton 2010 (170) (see Table 19) and/or in a modified minimal defined medium (MDM) after Karlsson *et al.* 1999 (171). Instead of the casamino mix of the CDMM, the MDM was prepared with a mixture of amino acids containing only essential amino acids for *C. difficile* (see Table 20).

Table 19 Compounds of *Clostridium difficile* minimal medium (CDMM)

Stock solution	Concentration of stock solution [g/l]	End concentration [g/l]	Volume per liter [ml]
10 x salt mix			100
Na_2HPO_4 NaH_2PO_4 x H_2O KH_2PO_4 NaCl	50 20 9 9	5 2 0.9 0.9	
5 x casamino mix			200
Casamino acids (BD) L-cysteine L-tryptophan	50 2.5 0.5	10 0.5 0.1	

Stock solution	**Concentration of stock solution [g/l]**	**End concentration [g/l]**	**Volume per liter [ml]**
100 x trace salts			10
$(NH_4)_2SO_4$ $CaCl_2$ x 2 H_2O $MgCl_2$ x 6 H_2O $MnCl_2$ x 4 H_2O $CoCl_2$ x 6 H_2O $NaHSeO_3$	4 2.6 2 1 0.1 0.015	0.04 0.026 0.02 0.01 0.001 0.00015	
500 x iron			2
$FeSO_4$ x 7 H_2O	2	0.004	
200 x vitamine			5
D-biotin Ca-D-pantothenate pyridoxin	0.06 0.2 0.2	0.003 0.001 0.001	
20 x glucose			50
D-glucose	200	10	
MQ-H_2O			633

Table 20 Compounds of amino acid mix used in the minimal defined medium (MDM)

Stock solution	**Concentration of stock solution [g/l]**	**End concentration [g/l]**	**Volume per liter [ml]**
5 x amino acid mix			200
L-tryptophan L-leucine L-valine L-proline L-isoleucine L-methionine L-cysteine L-threonine	0.5 2.0 1.5 10.0 1.5 1.0 2.5 2.815	0.1 0.4 0.3 2.0 0.3 0.2 0.5 0.563	

2.5.5 Media supplements

For investigations under high osmotic conditions MDM and SMM were treated with increasing sodium chloride concentrations. For this purpose, a 5 M NaCl stock solution was prepared.

Several compatible solutes have been added to determine their potential protective function (Table 21).

Table 21 List of compatible solutes used in MDM and SMM

Supplement	Concentration of stock solution	End concentration
Carnitine	100 mM	1 mM
Choline	100 mM	1 mM
Crotonobetaine	100 mM	1 mM
DMSP (dimethylsufoniopropionate)	100 mM	1 mM
Ectoine	100 mM	1 mM
γ-Butyrobetaine	100 mM	1 mM
Glycine betaine	100 mM	1 mM
Homobetaine	100 mM	1 mM
Proline betaine	100 mM	1 mM

Cationic antimicrobial peptides (CAMPs) were tested in CDMM (Table 22).

Table 22 List of CAMPs used in CDMM

Supplement	Concentration of stock solution [mg/ml]	End concentration [µg/ml]
Nisin	40	20
		50
Polymyxin B	50	75
		150
Vancomycin	50	0.30
		0.75

2.6 Microbiological methods

2.6.1 Sterilization

All media, buffer and materials were vapor sterilized at 121 °C and 1 bar overpressure for 20 min. Heat-sensitive media like vitamine solutions were sterilized by filtration using pore width with 0.2 µm (Sarstedt, Nümbrecht, Germany). Materials and solutions for RNA preparation were double autoclaved.

2.6.2 Anaerobic work

Liquid media of 150 ml were anaerobized in anaerobic bottles by fumigation of nitrogen for 20 min. Before use, agar plates were stored at least 12 h in the anaerobic chamber (Coy Laboratory Products, Grass Lake, USA).

Anaerobic procedures were performed in an anaerobic chamber containing a gas mix of 95 % nitrogen and 5 % hydrogen. The hydrogen concentration was adjusted to 2.7 to 3.0 %.

2.6.3 Cultivation of bacteria

E. coli and *B. subtilis* cells were routinely cultivated aerobically at 37 °C on LB agar plates and in LB broth (see 2.5.1) supplemented with antibiotics if required for plasmid maintenance (see 2.2.1) over-night. Liquid cultures were shaken at 180 rpm.

Bacillus subtilis

For *B. subtilis* growth experiments a 5 ml LB pre-culture was inoculated with a single colony. After 4-5 h incubation, a 20 ml SMM pre-culture containing required amino acids (2.5.2) was prepared by transferring of 5 µl LB cell culture. The SMM pre-culture was grown up to an OD_{578} of appr. 1.5. Main cultures with increasing osmolarities and various compatible solutes were inoculated to OD_{578} 0.1 by adding the pre-culture. Growth experiments with three biological replicates were performed in a volume of 1 ml each in a microbioreactor system at 37 °C and 1,400 rpm under humidity control.

C. difficile

The cultivation of *C. difficile* was carried out under strict anaerobic conditions using an anaerobic chamber (Coy Laboratory Products, Grass Lake, USA). Cells were routinely grown in BHI broth without shaking or on BHI agar plates containing required additives (see 2.5.3).

Growth experiments and systems biology approaches of *C. difficile* were performed in CDMM and MDM main cultures with four biological replicates (see 2.5.4). To reduce spore yields in the main culture two CDMM pre-cultures were prepared. The first pre-culture was inoculated with *C. difficile* colonies grown on ChromID agar plates. The culture was incubated for 20 h. The second pre-culture was inoculated proportionally 1:100 using the first pre-culture. Main cultures were inoculated to OD_{600} 0.01 by transferring the second pre-culture. Growth experiments were performed in a volume of 10 ml. For systems biology approaches up to 1 l cell culture per replicate was prepared.

High osmolarities were reached by increasing NaCl concentrations. Various compatible solutes were added for transport assays (see 2.5.5).

The cationic antimicrobial peptides (CAMP) vancomycin and polymyxin B (see 2.5.5) were added to CDMM for growth experiments of *C. difficile* wild type and the corresponding *fur* mutant.

2.6.4 Preparation of *C. difficile* spores

Spores of *C. difficile* were generated for immunological mice infection experiments in a procedure modified after Sorg and Sonenshein 2010 (16). *C. difficile* 630Δ*erm* wild type strain and corresponding mutants were cultivated over-night in 10 ml BHIS broth. A volume of 100 µl culture was transferred onto oxygen reduced BHIS agar medium and incubated anaerobically for 7 to 10 days at 37 °C. After an aerobically incubation period of three days, the cell mass was scraped off avoiding the edge and resuspended in 1 ml sterile MQ-H_2O. To support the release of spores from mother cells, the suspension was incubated over-night at 4 °C followed by three washing steps involving centrifugation at 4,000 x g for 40 min at 4 °C, resuspension and mixture of the sediment with 3 ml ice-cold MQ-H_2O. For separation of spores from cells and debris a gravity

centrifugation was performed. For this purpose, a 15-ml centrifugation tube with 10 ml of 50 % saccharose (w/v) solution was prepared and over-laid with 3 ml spore suspension. During centrifugation for 20 min at 3,000 x g and 4 °C, vegetative cells and debris remained in the interface. Whereas spores build a sediment after passage the saccharose solution. Then the sediment was washed five times with 1 ml sterile MQ-H_2O by centrifugation for 10 min at 3,000 x g and 4 °C. Purity and number of spores were determined by microscopy. The storage of spores was carried out in 1 ml sterile MQ-H_2O at 4 °C.

2.6.5 Motility assay

Motility assays were performed in test tubes with 10 ml CDMM each containing 0.175 % agar. For high iron conditions 15 µM iron sulfate was added. Single colonies of corresponding strains were taken up with a cannula and transferred into the medium by a straight stitch. Incubation was performed for 24 h at 37 °C.

2.6.6 Sample collection for ribosome characterization

The sample collection of *C. difficile* 630Δ*erm* for ribosome characterization was performed and handed over to the cooperation partners Prof. Dr. Thomas Marlovits and Dr. Oliver Vesper from the Institute of Structural and Systems Biology at the UKE Hamburg, Germany. For the characterization of ribosomes, 2 to 3 mg biomass were needed. For this purpose, 3 l of *C. difficile*, split in 4 x 750 ml, were cultivated anaerobically in BHI broth at 37 °C to the mid-exponential phase. Cells were harvested by centrifugation at 3,000 x g and 4 °C for 20 min (Avanti J-E, Rotor JLA 10.500, Beckmann Coulter, Krefeld, Germany). The supernatant was discarded. The sediment was washed with 20 ml 1 x PBS and transferred in gas tight tubes. After centrifugation at 3,000 x g and 4 °C for 15 min (Megafuge 1.0R, Heraeus, Hanau, Germany), 10 ml of resuspension buffer was added to the first cell sediment. Then, the resuspended cells were transferred to the second cell sediment. This step was repeated until all sediments were united. The suspension was divided into four 15 ml-tubes. The mixture was homogenized using the FastPrep® instrument for 30 s at 6.5 m/s, twice. After 5 min incubation in the ultrasonic, glass beads, insoluble matrix and cell debris

were sedimented by centrifugation at 2,000 x g and 4 °C for 20 min (Megafuge 1.0R, Heraeus, Hanau, Germany). The supernatant was transferred to clean ultra-centrifuge tubes. To conduct separation of membrane and cytosolic fraction, the samples were ultra-centrifuged at 18,000 rpm and 4 °C for 65 min (Optima™L-90K Ultracentrifuge, Rotor type 70.1, Beckmann Coulter, Krefeld, Germany). The supernatant was separated from the cell sediment. Both fractions were stored at -80 °C.

10 x PBS buffer

NaCl	1.37	M
KCl	27.00	mM
Na_2HPO_4	100.00	mM
KH_2PO_4	20.00	mM

Resuspension buffer

Tris/HCl (pH 7.4)	100.0	mM
EDTA	1.0	mM
CH_3CO_2K	100.0	mM
$Mg(CH_3COO)_2$	10.0	mM
DTT	5	mM

One tablet of protease inhibitor (see Table 13) was added to 10 ml resuspension buffer.

2.6.7 Determination of cell densitiy

The cell density of bacterial solutions was determined by measuring the optical density (OD). The OD of *C. difficile* cultures was determined at 600 nm wavelength using a WPA spectrophotometer C08000. For biomass correlation, the OD was measured in parallel in the spectrophotometer Genesys 10S UV VIS. The OD of *B. subtilis* cultures was determined at 578 nm wavelength using the spectrophotometer Libra S11.

Biomass measurements, detected by scattered light with λ=620 nm at gain=10, of *B. subtilis* main cultures were determined in flower plates MTP-48-B using the BioLector as microbioreactor system (m2p-labs GmbH, Baesweiler, Germany).

Dilutions were prepared for cell densities with an OD ≥ 1.

2.6.8 Storage of bacterial strains

Short term storage of *E. coli* and *B. subtilis* cells was carried out on agar plates for approximately four weeks at 4 °C. For long term storage glycerol stocks were prepared by mixing 1 ml cell culture with 500 µl of sterile 86 % glycerol. Glycerol stocks were pre-cooled for 30 min on ice and stored at -80 °C.

C. difficile cultures were stored anaerobically in hungate tubes at 4 °C.

Selected *C. difficile* strains were also deposited at the Deutsche Sammlung für Mikroorganismen (DSMZ), Braunschweig, Germany.

2.7 Molecular biological methods

2.7.1 Preparation of plasmid DNA

A clean preparation of plasmid DNA was carried out with 2 x 2 ml over-night bacterial culture using the QIAprep® Spin Miniprep Kit (Qiagen, Hilden, Germany) in accordance to manufacturer´s guidelines. Plasmid DNA was eluted with 32 µl 70 °C pre-warmed MQ-H_2O. Purity and concentration were determined with the NanoDrop™1000 spectrophotometer. Plasmid DNA was stored at 4 °C.

2.7.2 Preparation of genomic DNA

Preparation of genomic DNA was carried out with the FastDNA™Spin Kit for Soil (MP Biomedical, Eschwege, Germany) according to manufacturer´s guidelines. A volume of 200 µl over-night cell culture was added to a Lysing Matrix E Tube containing 978 µl sodium phosphate buffer and 122 µl MT buffer. The mixture was homogenized in the FastPrep® instrument for 40 s at 6.0 m/s. Insoluble matrix and cell debris were sedimented by centrifugation at 13,400 rpm for 7 min. The supernatant was transferred to a clean 2 ml microcentrifuge tube. A volume of 250 µl PPS was added and mixed by inverting the tube 10 times. Precipitates were spin down at 13,400 rpm for 5 min. In a new reaction tube the supernatant was mixed with 1 ml of resuspended binding matrix by inverting for 2 min. To allow settling of silica matrix the tube was placed in a rack for 3 min. A volume of 500 µl supernatant was removed and discarded. Settled binding matrix was gently resuspended with the remaining supernatant and transferred by two steps to a Spin™ filter. After each centrifugation step of 1 min at 13,400 rpm the catch tube was emptied. The sedimented binding matrix was gently resuspended using 500 µl of prepared SEWS-M and centrifuged at previous conditions. For drying the Spin™ filter was incubated for 5 min at room temperature. The bounded DNA was eluted by resuspension of binding matrix with 75 µl DES and centrifugation at 13,400 rpm for 1 min. Concentration of eluted DNA was determined with the NanoDrop™1000 spectrophotometer. Genomic DNA was stored at 4 °C.

2.7.3 Preparation of RNA

Total-RNA of *C. difficile* was isolated using the Qiagen RNeasy Kit Mini (Hilden, Germany). Preparation steps included enzymatical and mechanical lysis, RNA isolation, DNA degradation and elution of total-RNA.

I. Enzymatical and mechanical lysis

Prepared cell sediment (see 2.9.1) was resuspended in 200 µl TE-buffer including freshly added lysozyme (15 mg/ml) to achieve enzymatical cell lysis. After 30 min incubation at room temperature and vortexing every 2 min for 10 s, 700 µl RLT-buffer (Qiagen, Hilden, Germany) was added. The mechanical lysis was achieved by adding a spatula point of soda lime and mixing for 3 min. The separation of glass beads was carried out by centrifugation at 4,000 x g for 3 min. The supernatant of 800 µl was transferred into a new 2 ml reaction tube mixed with 470 µl 100 % ethanol.

TE-buffer

Tris/HCl	10.0	mM
EDTA	1.0	mM
pH	8.0	

II. Isolation of total-RNA

The isolation of total-RNA was performed by binding of RNA to the RNeasy Mini Spin column membrane (Qiagen, Hilden, Germany). For this purpose, a sample volume of 700 µl was placed on the column and centrifuged at 10,000 rpm for 30 s. Subsequently, the flow-through was discarded. This step was repeated with the remaining sample volume.

III. DNA-degradation and elution

Remaining DNA was subjected to 2 cycles of degradation by RNase-free DNaseI (Qiagen, Hilden, Germany). RNase-free DNase I was resuspended with RNase-free H_2O in accordance to manufacturer´s guidelines. A working solution of 10 µl DNase I and 70 µl RDD-buffer was prepared and stored until use at -20 °C.

Prior to the first DNA degradation, the column was washed previously with 350 µl RW1-buffer (Qiagen, Hilden, Germany). After centrifugation at 10,000 rpm for 30 s, 80 µl of the DNase working solution was added onto the column and incubated 15 min at room temperature. A second washing step, performed as described before, followed with an incubation period of 5 min after adding of 350 µl RW1-buffer. Then, the column was placed in a new reaction tube and was washed with 500 µl RPE-buffer twice. The flow-through was discarded after 30 s and 2 min centrifugation. Remaining liquid excess was removed by additional 1 min centrifugation at 10,000 rpm. The column was transferred in a new catch tube. RNA was eluted with 2 x 45 µl RNase-free H_2O followed by 1 min centrifugation at 10,000 rpm.

The second DNA degradation was carried out directly into the RNA catch tube by adding a DNase I working-solution of 2.5 µl DNase I and 10 µl RDD-buffer. After 30 min incubation, 350 µl RLT-buffer and 250 µl 100 % ethanol (v/v) were added. The sample volume of 700 µl was transferred onto a new RNeasy Mini spin column and further centrifuged at 10,000 rpm for 30 s to separate unwanted constituents. Then, the column was placed in a new reaction tube and was washed with 500 µl RPE-buffer twice. The flow-through was discarded after 30 s and 2 min centrifugation, respectively. Remained liquid was removed by additional 1 min centrifugation at 10,000 rpm. The column was transferred in a new catch tube. RNA was eluted with 25 µl RNase-free H_2O (Qiagen, Hilden, Germany) followed by 1 min centrifugation at 10,000 rpm. The elution was repeated with the obtained eluate. The storage of RNA occurred at -80 °C.

The RNA-concentration was determined using the NanoDrop™1000 spectrophotometer. For micro array analysis the quality of isolated RNA was checked using the bioanalyzer.

2.7.4 Quality control of RNA by bioanalyzer

The quality-control of total-RNA was performed using the bioanalyzer 2100 (Agilent Technologies, Santa Clara, USA) and RNA Nano chips (Agilent Technologies, Santa Clara, USA) in accordance to manufacturer´s guidelines. Based on the principle of capillary electrophoresis, results are presented as electropherograms as well as gel images. Thereby RNA degradations can be

made visible. The RNA integrity number (RIN) served as a measure of RNA quality. The total-RNA was classified by an algorithm of the RIN software from RIN=1 to RIN=10. A RIN of 1 implied degraded RNA, whereas a RIN of 10 indicated intact RNA. For array analysis, RNA with a RIN of ≥7 was used.

2.7.5 Determination of DNA and RNA concentration

Purity and concentration of DNA and RNA were determined with the NanoDrop™1000 spectrophotometer by measuring the absorbance at 260 nm and 280 nm. A ratio of 260 nm/280 nm of 1.8 - 2.0 indicated pure DNA and RNA, respectively.

2.7.6 Amplification of DNA fragments by polymerase chain reaction

For cloning purposes, DNA fragments were amplified using the polymerase chain reaction (PCR). Modifications of DNA fragments like fusion of single sequence parts were also performed with PCR. Gradient PCR was carried out to define the annealing temperature of primers. The following PCR composition was used for all PCR programs.

PCR composition

Template DNA	<1.0	µg
5 x Q5 reaction buffer	5.0	µl
10 µM forward primer	1.25	µl
10 µM reverse primer	1.25	µl
10 mM dNTPs	0.5	µl
Q5 polymerase	0.25	µl
MQ-H_2O add to	25.0	µl

The following PCR program (Table 23) was performed, unless otherwise stated.

Table 23 General thermocycling conditions

Step	Reaction	Temperature [°C]	Time	Cycle
1	Initial denaturation	98	4 min	1
2	Denaturation	98	30 s	30
3	Annealing	variable	30 s	
4	Elongation	72	30 s/kb	
5	Final elongation	72	2 min	1
6	hold	10	for ever	

Gradient PCR

PCR was used to determine the optimal annealing temperature of primer pairs whose melting temperatures were widely apart. For this purpose, the real-time PCR cycler CFX96™ (Biorad, Hercules, USA) was used which allowed several reaction set-ups to be carried out in parallel with the same program, but at eight different temperatures. In general, a temperature gradient from 57 °C to 71 °C was used.

PCR conditions for ClosTron mutant verification

Gene specific PCR was performed using general thermocycling conditions (Table 23). The validation of group II intron insertion and ErmRAM presence was carried out with the following thermocycling program (Table 24):

Table 24 Thermocycling conditions used for ClosTron mutant verification

Step	Reaction	Temperature [°C]	Time	Cycle
1	Initial denaturation	98	30s	1
2	Denaturation	98	10 s	30
3	Annealing	variable	20 s	
4	Elongation	72	30 s	
5	Final elongation	72	10 min	1
6	hold	10	for ever	

2.7.7 Digestion of plasmid DNA and PCR products by restriction enzymes

Double stranded plasmid DNA or PCR products were digested by restriction enzymes recognizing specific palindromic sequences. The cleavage of DNA was performed for preparative and analytical purposes.

Restriction enzymes and buffer were obtained from New England BioLabs® (see Table 14). All enzymes were diluted in Cut Smart buffer.

Cleavage composition

Template DNA	1.0	µg
10 x Cut Smart buffer	3.0	µl
Enzyme 1	0.5	µl
Enzyme 2	0.5	µl
MQ-H_2O add to	30.0	µl

The reaction was incubated for 30 min at 37 °C followed by an agarose gel electrophoresis for verification or isolation via gel extraction, if needed.

2.7.8 Generation of complementation vectors

Vectors for complementation of *C. difficile* 630Δ*erm perR* mutants were based on the backbone of the ClosTron vectors pMTL82151 and pRPF185.

I. Generation of the control vectors pAMCDX and pAMCDY

The control plasmids pAMCDX and pAMCDY rely on the backbone of the vectors pMTL82151 and pRPF185.

The vector pRPF185 was linearized using the restriction enzymes BamHI and SacI resulting in excision of the *gusA* sequence (see 2.7.7). The vector pMTL82151 was linearized with the restriction enzymes NotI and NheI resulting in excision of the *lacZ alpha* sequence. Both vector backbones were purified by gel extraction (see 2.7.9) followed by modification of sticky-ends to blunt ends and ligation using the CloneJet PCR Cloning Kit according to manufacturer´s

guidelines. The ligation of pMTL82151Δ*lacZ alpha* resulted in the control vector pAMCDX, whereas the construct pRPF185Δ*gusA* resulted in pAMCDY.

II. Generation of the vectors pAMCD01 and pAMCD02

For the generation of the complementation vectors pAMCD01 and pAMCD02, the ClosTron vector pRPF185 containing a tetracycline inducible promotor was used. The vector pRPF185 was linearized using the restriction enzymes BamHI and SacI resulting in excision of the *gusA* sequence (see 2.7.7). The pRPF185 backbone was purified by gel extraction (see 2.7.9) and ligated to *perR* codons of the strain *C. difficile* 630Δ*erm* or of the parental strain *C. difficile* 630 (see 2.7.10). Corresponding sequences were previously amplified via PCR (see 2.7.6) using the primer pairs perR_compl_Fw and perR_compl_Rv (see 2.3), which allowed the amplification including necessary restriction sites. Sticky ends were generated by digestion followed by PCR purification (see 2.7.9). The construct pRPF185Δ*gusA*::$perR_{C.\ difficile\ 630\Delta erm}$ resulted in the new complementation vector pAMCD01, whereas the construct pRPF185Δ*gusA*::$perR_{C.\ difficile\ 630}$ resulted in pAMCD02.

III. Generation of the vectors pAMCD03 and pAMCD04

For the generation of the complementation vectors pAMCD03 and pAMCD04, the ClosTron vector pMTL82151 was modified. Here, the potentially natural promotor of the *perR* gene was used.

The vector pMTL82151 was linearized using the restriction enzymes NotI and NheI resulting in excision of the *lacZ alpha* sequence (see 2.7.7). The pMTL82151 backbone was purified by gel extraction (see 2.7.9) and ligated to *perR* codons including 350 nt upstream of the strain *C. difficile* 630Δ*erm* or of the parental strain *C. difficile* 630 (see 2.7.10). Corresponding sequences were previously amplified via PCR (see 2.7.6) using the primer pairs 350nt_up_perR_Fw and perR_compl_Rv2 (see 2.3), which allowed the amplification including necessary restriction sites. Sticky ends were obtained by digestion followed by PCR purification (see 2.7.9). The construct pMTL82151Δ*lacZ alpha*::350 nt up *perR*-$perR_{C.\ difficile\ 630\Delta erm}$ resulted in the new complementation vector pAMCD03, whereas the construct pMTL82151Δ*lacZ alpha*::350 nt up *perR*-$perR_{C.\ difficile\ 630}$ resulted in pAMCD04.

IV. Generation of the vectors pAMCD05 and pAMCD06

For the generation of the complementation vectors pAMCD05 and pAMCD06, the ClosTron vector pMTL82151 was modified. Here, the putative natural promotor of the *perR* gene was used.

The vector pMTL82151 was linearized using the restriction enzymes NotI and NheI resulting in excision of the *lacZ alpha* sequence (see 2.7.7). The pMTL82151 backbone was purified by gel extraction (see 2.7.9) and was ligated with the fusion product of the *perR* sequence and 350 nt upstream of the gene *rbr1* within the *perR* operon of the strain *C. difficile* 630Δ*erm* or of the parental strain *C. difficile* 630.

Single fragments were amplified at first via the following PCR using the primer pairs 350nt_up_rbr1_Fw and Up_rbr1_Rv_MERG_perR_Fw for sequence 350 nt upstream *rbr1* as well as perR_Fw_MERG_up_rbr1_Rv and perR_compl_Rv2 for the *perR* sequence (see 2.3), which allowed the amplification of necessary restriction sites. For each fragment, four reactions were prepared. Successful amplification was confirmed by agarose gel electrophoresis (see 2.7.11) and products were purified using the NucleoSpin® Gel and PCR Clean up (see 2.7.9).

PCR composition

Template DNA	2.0	µl
5 x Q5 reaction buffer	4.0	µl
10 µM forward primer	1.0	µl
10 µM reverse primer	1.0	µl
10 mM dNTPs	0.4	µl
Q5 polymerase	0.2	µl
MQ-H_2O add to	20.0	µl

The following PCR program (Table 25) was performed.

Table 25 Thermocycling conditions for fusion of complementary overhangs

Step	Reaction	Temperature [°C]	Time	Cycle
1	Initial denaturation	98	30	1
2	Denaturation	98	10 s	30
3	Annealing	61	20 s	
4	Elongation	72	60 s	
5	Final elongation	72	10 min	1
6	hold	10	for ever	

Both single fragments were used as template for fusion over complementary overhangs. Two reactions were performed as followed using the PCR program as before.

Fusion PCR composition

Template DNA 1	2.0	µl
Template DNA 2	2.0	µl
5 x Q5 reaction buffer	4.0	µl
10 mM dNTPs	0.4	µl
Q5 polymerase	0.2	µl
MQ-H_2O add to	20.0	µl

During the elongation phase (step 4) within the third cycle, 2 µl of a primer mix consisting the primers 350nt_up_rbr1_Fw and perR_compl_Rv2 was added.

Primer Mix

350nt_up_rbr1_Fw	6.0	µl
perR_compl_Rv2	6.0	µl

Both reactions were united and resolved by gel electrophoresis (see 2.7.11) using 100 V for 5 min followed by 60 V for 95 min. Desired fragments were purified via gel extraction (see 2.7.9) and amplified again in four reaction with the

following composition. The primer pair 350nt_up_rbr1_Fw and perR_compl_Rv2 was used.

PCR composition

Template DNA	1.0	µl
5 x Q5 reaction buffer	4.0	µl
10 µM forward primer	1.0	µl
10 µM reverse primer	1.0	µl
10 mM dNTPs	0.4	µl
Q5 polymerase	0.2	µl
MQ-H_2O add to	20.0	µl

Both reactions were combined and the reaction products were purified using the PCR purification protocol (see 2.7.9). Sticky ends were generated by digestion followed by PCR purification. The construct pMTL82151Δ*lacZ alpha*::350 nt up *rbr1-perR*$_{C.\ difficile\ 630\Delta erm}$ resulted in the new complementation vector pAMCD05, whereas the construct pMTL82151Δ*lacZ alpha*::350 nt up *rbr1-perR*$_{C.\ difficile\ 630}$ resulted in pAMCD06.

2.7.9 Purification of DNA: PCR product purification and gel extraction

For quality control an aliquot of amplified DNA by PCR or restriction reaction was analyzed by gel electrophoresis (see 2.7.11).

Purification of DNA fragments via PCR purification

PCR products were purified using the QIAquick® PCR Purification Kit (Qiagen, Hilden, Germany) or NucleoSpin® Gel and PCR Clean up (Macherey-Nagel, Düren, Germany) if only one amplicon was present after the gel electrophoresis. Restriction reactions were purified likewise if a gel extraction of fragments of interest was no feasible. The purification was performed in accordance to manufacturer´s guidelines. To increase the concentration of DNA MQ-H_2O was heated to 70 °C before 32 µl was used for elution.

Purification of DNA fragments via gel extraction

DNA fragments amplified by PCR or generated by restriction reaction were purified via gel extraction if more than one product was present after gel electrophoresis as control. In accordance to manufacturer´s guidelines the QIAquick® PCR Purification Kit (Qiagen, Hilden, Germany) or NucleoSpin® Gel and PCR Clean up (Macherey-Nagel, Düren, Germany) was used. To increase the concentration of DNA MQ-H_2O was heated to 70 °C before 32 µl was used for elution.

2.7.10 Ligation of DNA

Double-stranded DNA fragments were ligated using the T4 ligase from New England BioLabs® (see Table 13). The preparation of DNA included the digestion of vector and insert using identical restriction enzymes. The ratio of vector and insert was calculated using the NEBioCalculator™ or was set to 7:1.

Ligation composition

Vector	50 - 200	ng
Insert	100 - 500	ng
10 x ligase buffer	1.0	µl
MQ-H_2O add to	10.0	µl

The ligation reaction was incubated at room temperature for 20 min followed by transformation of *E. coli* DH10B cells.

Ligation of pJET1.2/blunt vector

Purified PCR products or synthetical DNA fragments were cloned into the pJET1.2/blunt vector using the CloneJet PCR Cloning kit from New England BioLabs® (see Table 12) in accordance to manufacturer´s guidelines.

Ligation composition for pJET1.2

pJET1.2 (50 ng/µl)	0.5	µl
PCR product	1.0	µl
2 x ligase buffer	5.0	µl
T4 ligase	0.5	µl
MQ-H_2O	3.0	µl

The ligation reaction was incubated at 22 °C for 20 min followed by the inactivation at 65 °C for 10 min. The new constructed vector was transferred in *E. coli* DH10B cells (see 2.7.15).

2.7.11 Agarose gel electrophoresis

The agarose gel electrophoresis was performed for separation of DNA fragments according to their molecular weight. Agarose gels containing 1 % agarose (w/v) dissolved in 1 x TAE buffer were used. For visualization the samples, 6 x loading dye (New England Biolabs, Frankfurt, Germany) was mixed with the DNA before loading the gel. The GeneRuler™ DNA Ladder Mix (Thermo Fisher Scientific, Waltham, USA) was used as size standard. The separation of DNA was performed in 1 x TAE running buffer using an electric current of 80 V for 45 min. DNA was visualized by staining in an 0.001 % ethidium bromide solution for 20 min followed by stimulation under UV light.

2.7.12 Sequencing of DNA fragments

Sanger sequencing of DNA amplicons was conducted to verify the accuracy amplification of PCR products, successful cloning and exclusion of occurring mutations. The samples were prepared according to the specifications of the executing company Eurofins Genomics (Ebersberg, Germany).

2.7.13 Preparation of competent *E. coli* cells

The preparation of competent *E. coli* cells occurred chemically with rubidium chloride. For this purpose, a pre-culture of 20 ml LB was inoculated with *E. coli* cells of a glycerol stock and was incubated over-night at 200 rpm and 37 °C. The 50 ml main culture was inoculated proportionally 1:100 using the pre-culture and incubated for 2.5 h. After reaching an $OD_{578} = 0.6 – 0.8$, the cells were sedimented at 4,000 rpm for 5 min at 4 °C (Megafuge 1.0R). The supernatant was discarded, and the cells were resuspended with 20 ml ice-cold TBF1 (0.4 Vol.%). After 5 min on ice, the culture was centrifuged as described before. The buffer was removed and 2 ml ice-cold TBF2 was added. The cells were resuspended and incubated on ice for 60 min before they were aliquoted to 50 µl in 1.5 ml reaction tubes. The competent cells were stored at -80 °C.

Table 26 Compounds of TBF1 and TBF2

Buffer solution	Compound	Concentration
TBF1 pH 5.8	$CaCl_2$	10 mM
	Glycerol	15 % (v/v)
	KCH_3CO_2	30 mM
	$MnCl_2$	50 mM
	$RbCl_2$	100 mM
TBF2 pH 6.5	$CaCl_2$	75 mM
	Glycerol	15 % (v/v)
	MOPS pH 6.5	10 mM
	$RbCl_2$	10 mM

2.7.14 Preparation of competent *B. subtilis* cells

The organism *B. subtilis* belongs to the group of natural competent bacteria which is able to take up free DNA from the environment without chemical or mechanical pre-treatment. For the preparation of competent *B. subtilis* cells, 3 ml of 1 x SMM (see Table 16) was inoculated with strains who has to be transformed. The cultures were incubated as before described at 200 rpm. The main culture of 20 ml pre-warmed low-salt (LS) medium was inoculated with 1 ml of the pre-culture. After 3 h incubation at 37 °C and 200 rpm *B. subtilis* reached the stationary phase and was able to take up free DNA.

Table 27 Composition of low-salt (LS) medium

Compound	Volume for 20 ml	End concentration
5 x SMM (incl. trace element solution)	2 ml	
20 % D-glucose	200 µl	2.0 g/l
10 % yeast extract	200 µl	1.0 g/l
2 % casamino acids	100 µl	0.1 g/l
50 mM spermine	200 µl	0.5 mM
1 M $MgCl_2$	50 µl	2.5 mM
Trp (4 g/l),Phe (3.6 g/l)	50 µl	Trp 0.01g/l, Phe 0.009 g/l

2.7.15 Transformation of *E. coli* cells

Competent *E. coli* cells were thawed on ice and mixed with 1 to 10 ng plasmid DNA or 5 µl of ligation reaction. The transformation reaction was incubated on ice for 20 min followed by a heat shock at 42 °C for 45 s. The cells were cooled down for 2 min on ice before 250 µl LB medium were added. After 1 h incubation at 37 °C and 300 rpm, 50 µl and 100 µl of the mixture was plated onto LB agar medium containing corresponding selection marker (Table 2 and Table 3).

2.7.16 Transformation of *B. subtilis* cells

In order to transform *B. subtilis*, cells were prepared as described in chapter 2.7.14. A volume of 1 ml *B. subtilis* cultured in LS medium was mixed with 3 - 5 µg plasmid DNA and was incubated for 2 h at 37 °C and 300 rpm. The mixture was streaked out onto LB agar plates containing corresponding selection marker (Table 4).

2.7.17 Optimization of DNA sequences for *B. subtilis* mutagenesis

For the expression of homologous *C. difficile* transporter genes in *B. subtilis*, DNA sequences were fused with natural promotor regions of *B. subtilis* and were optimized for *B. subtilis´* codon usage.

For optimization the GeneArt Gene Synthesis tool of Thermo Fisher Scientific was used. Sequences for the transporters OpuC (*CDIF630erm_01020-01021*) and “unknown” (*CDIF630erm_03509-03510*) were ordered as shuttle vector pMA-RQ-opuC$_{C.\ difficile\ 630\Delta erm}$ and pMA-RQ-unknownTransporter$_{C.\ difficile\ 630\Delta erm}$. The sequence for the PutP transporter was ordered as a string fragment.

2.7.18 Expression of chromosomally integrated genes in *B. subtilis*

Gene expression experiments in *B. subtilis* were based on the double homologous recombination-based integration of genes to be investigated into the *amyE* locus of the genome of *B. subtilis*.

Genes of interest were isolated by gel extraction after digestion of pMA-RQ-opuC$_{C.\ difficile\ 630\Delta erm}$ and pMA-RQ-unknownTransporter$_{C.\ difficile\ 630\Delta erm}$ with XbaI and PvuI, if required. After that, the sequences were cloned between recombinantly 5´- and 3´-flanked regions for *amyE* into the integration vector pX (see Table 4) after excision of *xylR* by digestion using the restriction enzyme XbaI (see 2.7.7). Corresponding *B. subtilis* strains were transformed with desired pX vectors as described before in chapter 2.7.16. Transformed cells were selected due to the chloramphenicol (Cm) resistance cassette on pX by strikeout the transformation reaction onto LB-Cm agar plates and incubation at 37 °C over-night. Integration success of the gene of interest into the genome-located

amyE was detected by missing amylase-activity of the corresponding strain (see 2.8.1).

2.7.19 Mutagenesis of *C. difficile* – mutant generation

Mutagenesis experiments of *C. difficile* 630Δ*erm* were performed via conjugation with the ClosTron technology according to Heap *et. al.* 2009 (160, 169, 172). This technology profits from the insertion of a group II intron consisting an erythromycin cassette as selection marker. For transferring the group II intron into the gene of interest, the shuttle vector pMTL007C_E2 was designed with a specific intron targeting region using the Perutka algorithm (173) implemented at the ClosTron website (http://www.clostron.com). Customized vectors were synthesized by ATUM (Newark, California, USA).

I. Mating procedure of *E. coli* CA434 and *C. difficile* 630Δ*erm*

The isolation of plasmid DNA from GF/C filter was performed in accordance to manufacturer´s guidelines followed by transformation of the donor strain *E. coli* CA434 (see 2.7.15). Transformed cells were incubated in 5 ml LB broth supplemented with 20 µg/ml chloramphenicol at 37 °C and 200 rpm over-night. Simultaneously, *C. difficile* 630Δ*erm* was anaerobically cultivated in 2 ml BHIS broth at 37 °C for 24 h. After incubation, *E. coli* cells were centrifuged 1 min at 13,400 rpm. The supernatant was discarded and the sediment was washed with 500 µl sterile 1 x PBS (see 2.6.6) twice. Under anaerobic conditions, a conjugation mixture of 200 µl *C. difficile* culture and *E. coli* sediment was prepared. The mixture was spotted onto BHI agar plates without additives. After incubation at 37 °C for 6 h, spots were rinsed with 500 µl 1 x PBS. A volume of 50 µl conjugation mixture was streaked out onto BHI agar plates supplemented with 500 µg/ml D-cycloserine and 16 µg/ml cefoxitin (*C. difficile* supplement, Sigma Aldrich) for enterobacteria inhibition, and 15 µg/ml thiamphenicol for selection of colonies carrying the plasmid. Plates were incubated anaerobically at 37 °C for 72 h before single colonies were transferred onto fresh BHI agar plates supplemented with D-cycloserine and cefoxitin as well as 2.5 µg/ml erythromycin for selection of potential mutants. For verification of successfully mutant generation, a volume of 2 ml BHI broth with erythromycin was inoculated

with a single colony. After incubation over-night, genomic DNA was isolated (see 2.7.2) and the insertion of the group II intron was checked by different PCR procedures.

II. Verification of insertional mutant generation

The verification of insertional mutants was carried out by independent PCRs (see 2.7.6). Strain specific primer pairs were used to confirm the desired *C. difficile* strain and to exclude contamination with *E. coli*. The insertion of the group II intron into the gene of interest was confirmed with gene specific primers resulting in an appropriate 1,800 bp larger amplicon in comparison to the wild type gene fragment (gene specific PCR). The second confirmation of the existing intron was performed with a primer pair of the EBS universal primer (169) and the gene specific forward/reverse primer depending on the target region (Intron/Exon PCR). The ErmRAM primer pair was used to validate the RAM state (ErmRAM PCR). A spliced RAM results in a PCR product of 900 bp, whereas an unspliced marker gives a product of 1,300 bp.

2.7.20 Complementation of *C. difficile* 630Δ*erm perR* mutants

Complementation experiments were performed according to the described ClosTron technology. *E. coli* CA434 cells carrying modified pMTL82151 or pRPF185 vectors (see 2.7.8) were used as donor strains. Conjugation processes were carried out as described before with minor modifications (see 2.7.19).

After anaerobic incubation at 37 °C for 72 h, single colonies were transferred onto fresh BHI agar plates supplemented with D-cycloserine and cefoxitin as well as 15 µg/ml thiamphenicol. Newly grown colonies were used for inoculation of 10 ml BHI broth supplemented with thiamphenicol. For verification of successful vector-uptake and -stability, 2 ml culture was used for plasmid isolation via quick and dirty protocol (see 2.7.1) followed by a corroboration via PCR (see 2.7.6).

2.8 Biochemical methods

2.8.1 Toxin quantification

The extracellular toxin A and B production of *C. difficile* was quantified from the supernatant of 58 h cultures in quadruplicates. Samples were centrifuged at 8,000 rpm for 10 min (Centrifuge 5424, Eppendorf, Hamburg, Deutschland). The supernatant was sterile filtered and stored for max. three days at 4 °C.

For toxin A quantification, samples were diluted in dilution buffer in a ratio of 1:20. Toxin B was determined with undiluted samples.

The quantification of both toxins was performed using the "*Clostridium difficile* Toxin A or B quanti Kit" (tgc Biomics, Bingen am Rhein, Germany) according to manufacturer´s guidelines using the two-step-protocol.

2.8.2 Detection of amylase-activity

The integration of genes into the genome of *B. subtilis* took place by double homologous recombination into the gene *amyE* (see 2.7.18). The gene a*myE* encodes the enzyme amylase which allows the organism to degrade starch. The detection of amylase-activity was performed by over-inoculation of potential clones on LB-starch agar plates (10 g/l) incubated at 37 °C over-night. A functional *amyE* gene lead to a degradation of starch resulting in a visible zone after overcoating with potassium iodine solution (Lugol´sche Lösung, Morphisto, Frankfurt am Main, Germany). The successfully integration resulted in the loss of enzyme amylase activity and no zone formation.

2.9 Systems biology approach

Samples for systems biology approach were collected from five independent biological replicates cultivated in CDMM or MDM and their modified variants.

Samples for transcriptome and metabolome analysis were collected during the mid-exponential phase, unless otherwise stated. Cultures were harvested under anaerobic conditions and transferred into gas-tight polypropylene tubes.

2.9.1 Transcriptome analysis by micro array

For transcriptome analysis a volume of 45 ml was centrifuged at 4 °C for 10 min and 4,000 x g (Megafuge 1.0R, Heraeus, Hanau, Germany). The supernatant was discarded. The cell sediments were immediately frozen in liquid nitrogen and stored at -80 °C until further processing. RNA was isolated after chapter 2.7.3. The quality control was performed as described before (see 2.7.4).

DNA micro array analysis were performed in quadruple determination using micro arrays 8x15K (Agilent Technologies, Santa Clara, USA). The design was carried out by Dr. Rebekka Biedendieck/AK Jahn and is based on the genome of *C. difficile* 630Δ*erm* (Genbank: LN614756.1).

I. RNA labelling

RNA was labeled after the two-color-principle using "ULS Labeling Kit with Cy3 and Cy5 for Agilent Gene Expression Arrays" (KREATECH Technology, Amsterdam, Netherland). A concentration of 1.5 µg RNA of the consistently chosen sample was labeled with 1.5 µl cyanine 5-ULS-labelling agent (Cy5). Per µg RNA of the to be studied sample was labeled with 1 µl cyanine 3-ULS-labelling agent (Cy3) resulting in a RNA concentration of 50 µg/µl.

Labelling composition

RNA (1 µg or 1.5 µg)	x	µl
RNase-free H_2O	x	µl
10 x labelling solution	2	µl
Cy3- or Cy5- ULS-labelling dye	1	µl resp. 1,5 µl
final volume	20	µl

After an incubation of 15 min at 85 °C with the exclusion of light, the samples were cooled down on ice. KREApure columns were prepared by mixing and dissolving the filter material. In accordance to manufacturer´s guidelines, the material was washed with 300 µl RNase-free H_2O before the sample was transferred onto the column. Redundant dye has been removed by centrifugation at 10,000 rpm for 1 min (Biofuge pico, Heraeus, Hanau, Germany).

The concentration and degree of labelling of the corresponding dye was determined using the NanoDrop TM 1000.

II. Determination of degree of labelling (DOL)

The determination of RNA concentration in ng/µl and incorporation rate of fluorescent dyes Cy5 resp. Cy3 in pmol/µl was performed using the microarray measurement protocol RNA-40 at the NanoDrop TM 1000.

The efficiency of the *degree of labeling* (DOL) in [%] was determined as followed:

$$\text{Labelling [\%]} = \frac{340 \bullet \text{pmol dye} \bullet 100\,\%}{\text{ng RNA} \bullet 1000}$$

An efficiency of 1.0 to 3.6 % was aimed at. Deviations resulted in a repetition of the labelling procedure.

III. Fragmentation and hybridization of RNA

For fragmentation and hybridization of labelled RNA the Gene Expression Microarrays Hybridization Kit was used (Agilent Technologies, Santa Clara, USA).

Fragmentation composition

Cy3-labeled RNA (300 ng)	x	µl
Cy5-labeled RNA (300 ng)	x	µl
1 x blocking agent	5	µl
RNase-free H_2O	x	µl
final volume	24	µl

The fragmentation composition was mixed by vortexing followed by a brief centrifugation step before 1 µl of 25 x fragmentation buffer was added. After exactly 30 min incubation at 60 °C block- and 70 °C lid-temperature in a thermocycler (Biometra, Göttingen, Germany), the reaction was quenched by adding 25 µl 2 x HI-RPM hybridization buffer avoiding air bubbles. Samples were stored on ice until the array slides were loaded.

IV. Loading and analysis of array slides

DNA micro array analysis were performed in quadruple determination using micro arrays 8x15K (Agilent Technologies, Santa Clara, USA) based on the genome of *C. difficile* 630Δ*erm* (Genbank: LN614756.1). Gasket slides including eight microarrays per slide (Agilent Technologies, Santa Clara, USA) were used for hybridization. A sample volume of 40 µl was placed onto each microarray field avoiding air bubbles. Prepared gasket slides were fixated with the Agilent microarray slide using a hybridization chamber (Agilent Technologies, Santa Clara, USA). The hybridization was performed at 65 °C at 10 rpm for 17 h.

After hybridization the slides were washed and stored in buffer 1 (Agilent Technologies, Santa Clara, USA) until all slides were separated, followed by a 1 min washing step in a 37 °C pre-warmed buffer 2 (Agilent Technologies, Santa Clara, USA).

The array scan was conducted with High-Resolution Microarray Scanner (Agilent Technologies, Santa Clara, USA).

2.9.2 Metabolome analyses

Metabolome analyses were performed in cooperation with Dr. Sabine Will and Dr. Meina Neumann-Schaal from the group Bacterial Metabolomics at the Leibniz Institute DSMZ-German Collection of Microorganisms and Cell Cultures GmbH (Braunschweig, Germany) supervised by Dr. Meina Neumann-Schaal.

I. Sample collection for metabolome analysis

Sample collection for intracellular metabolome analysis

For metabolome analyses a volume of 45 ml was centrifuged with a pre-cooled rotor at -20 °C and 10,000 rpm for 10 min. The supernatant was discarded. The cell sediments were immediately resuspended with 15 ml of -32 °C pre-cooled quenching solution consisting of 0.9% sodium chloride/methanol [50 % (v/v)]. After a repeated centrifugation under the same conditions, the supernatants were discarded and the sediments were frozen in liquid nitrogen. Samples were stored at -80 °C until further processing.

Sample collection for extracellular metabolome and CoA analysis

For extracellular metabolome analyses and CoA derivatives measurements a volume of 45 ml was centrifuged with a pre-cooled rotor at 4 °C and 10,000 rpm for 10 min. A volume of 2 ml supernatant, used for extracellular metabolome analysis, was transferred in duplicates in cryo tubes. To determine the fermentation profile, samples were harvest at OD_{max}. A volume of 1 ml supernatant was collected. The remaining supernatant was discarded. The cell sediments were used for CoA derivatives measurements.

All samples were immediately frozen in liquid nitrogen and stored at -80 °C.

Sample collection for uptake profile determination

Samples to determine the uptake of osmolytes were harvested at different time points including lag-, exponential- and stationary phase, depending on the media and strain employed, by centrifugation at 8,000 rpm for 10 min at 4 °C. A volume of 100 µl was transferred in cryo tubes and immediately frozen in liquid nitrogen and stored at -80 °C.

II. Analysis of intra- and extracellular as well as volatile compounds by gas chromatography/mass spectrometry

Intra- and extracellular as well as volatile compounds were analyzed by gas chromatography/mass spectrometry (GC-MS) measurements. The preparation and extraction were carried out as previously described in Hofmann *et al.* 2018 (26) with minor modifications.

For intra- and extracellular compounds analysis a volume of 150 µl of the polar phase was transferred in glass vials. Gas chromatography/mass spectrometry measurement was performed. An Agilent GC-MSD system (7890B coupled to a 5977 GC) equipped with a high-efficiency source (HES) and a PAL RTC system was used as described before (174).

Volatile compounds were measured on an Agilent VF-WAXms column (0.25 mm 30 m, Agilent, Santa Clara, CA, United States). An Agilent GC-MSD system (7890B coupled to a 5977 GC) equipped with a high-efficiency source (HES) and a PAL RTC system was used. A volume of 1 µl was injected in pulsed split mode

with a split ratio of 10:1 (split flow of 12 ml/min). Separation and measurement were conducted as described before (27).

III. Analysis of coenzyme A derivatives by liquid chromatography/mass spectrometry

Coenzyme A derivatives were analyzed by liquid chromatography/mass spectrometry (LC-MS) measurements.

For this purpose, frozen precipitated cells were resuspended in 700 µl methanol per 1 mg cell dry weight. A volume of 1 ml cell suspension was transferred into 2 ml screw-cap tubes containing 600 mg glass beads (70 - 110 µM diameter). As internal standard 250 ng of $^{13}C_3$-malonyl-CoA was added followed by lysation of cells using a FastPrep-24 classic instrument equipped with a CoolPrep adapter (MP Biomedicals). The lysate was mixed with 10 mL ice cold ammonium acetate (25 mM, pH 6) and centrifuged (5 min, 10,000 rpm, 4 °C). The extraction of CoA derivatives was performed using a Strata XL-AW solid phase column (Phenomenex, Aschaffenburg, Germany) as described previously (175). The measurement was carried out on an Agilent LC-QTOF system (6545 coupled to a 1290 Infinity II UHPLC) equipped with an electrospray interface. The separation was performed on a C_{18} analytical column (Gemini 2.0 x 150 mm, particle size 3 mm; Phenomenex) followed by data analysis as described previously (175).

IV. Analysis of amino acids by high performance liquid chromatography/mass spectrometry

Amino acids were analyzed by high performance liquid chromatography/mass spectrometry (LC-MS) measurements on a 1260 Infinity II HPLC system as described previously (26).

2.10 Field emission scanning microscopy (FESEM) and transmission electron microscopy (TEM)

The field emission scanning microscopy (FESEM) and transmission electron microscopy (TEM) measurements were performed by Prof. Dr. Manfred Rohde at the Helmholtz Zentrum für Infektionsforschung (HZI) (Braunschweig, Germany). *C. difficile* 630Δ*erm* cells were grown anaerobically in MDM as reference medium, under salt stressed conditions induced by additional 350 mM NaCl as well as under salt stressed conditions supplemented with 1 mM carnitine as compatible solute. A volume of 20 ml cell culture was harvested at the mid-exponential phase and pre-fixated with 1 % formaldehyde. The samples were stored at 4 °C until further processing by Prof. Dr. Manfred Rohde.

I. Field emission scanning microscopy (FESEM)

After fixation with 5 % formaldehyde and 2 % glutaraldehyde in HEPES buffer on ice, samples were washed twice with TE buffer (20 mM TRIS, 2 mM EDTA, pH 6.9). Bacteria were attached for 15 min onto cover slips (12 mm in diameter) coated with poly-L-lysine. After fixation with 1 % glutaraldehyde in TE buffer and washing with TE buffer, cells were dehydrated with a graded series of acetone (10, 30, 50, 70, 90, 100 %) on ice for 15 min for each step. In the 100 % acetone step samples were allowed to reach room temperature before another change in 100 % acetone was followed. Samples were then subjected to critical-point drying with liquid CO_2 (CPD 300, Leica). Dried samples were covered with an appr. 8 nm thick gold-palladium film by sputter coating (SCD 500 Bal-Tec, Liechtenstein). It followed the examination in a field emission scanning electron microscope Zeiss Merlin (Oberkochen, Germany) using the Everhart-Thornley SE-detector and the Inlens SE-detector in a 75:25 ratio with an acceleration voltage of 5 kV.

II. Transmission electron microscopy (TEM)

For transmission electron microscopy (TEM), samples were embedded in LRWhite resin. For this purpose, the sediment of aldehyde fixed bacteria (see above) was mixed with an equal volume of 1.75 % water agar. After solidification, the agar was cut into small cubes and samples were incubated in 1 % aqueous osmiumtetroxide for 1 h at room temperature. Then, samples were washed with TE buffer followed by dehydration with a graded series of ethanol (10, 30, 50%) with an incubation time of 15 min for each step.

After dehydration, performed with 4 % uranylaceate in 70 % ethanol over-night, samples were further dehydrated with 90 % and 100 % ethanol. Here, the last step with 100 % ethanol was repeated twice. It followed an infiltration with one part 100 % ethanol and one part LRWhite resin for overnight as well as an infiltration with 1 part 100 % ethanol and 2 parts LRWhite resin for 24 h hours and subsequently an infiltration with pure LRWhite resin with two changes over two days. A volume of 10 ml LRWhite resin was mixed with 1 µl starter and was put into 0.5 ml gelatin capsules, the tip of which was filled with the samples. The polymerization was carried out for 2 days at 50 °C before ultrathin sections were cut using a diamond knife. Sections were counter-stained with 4 % aqueous uranyl acetate for 1 min. The examination of samples was performed with a Zeiss TEM 910 at an acceleration voltage of 80 kV and at calibrated magnifications. For digitally recording of images a Slow-Scan CCD-Camera (ProScan, 1024x1024, Scheuring, Germany) was used with ITEM-Software (Olympus Soft Imaging Solutions, Münster, Germany).

2.11 *In vivo* experiments using mice

For immunological investigations, spores of *C. difficile 630Δerm* as wild type strain and corresponding insertion mutants were used in mouse infection models.

Immunological investigations were performed in cooperation with Friederike Kruse under the supervising of Dr. Matthias Lochner from the TWINCORE, Hannover, Germany as described previously (176). All animal experiments were performed in compliance with the German animal protection law, Tierschutzgesetz (TierSchG, BGBl. I S. 626, 2017/03/29), and were approved by the Lower Saxony Committee on the Ethics of Animal Experiments as well as the responsible state office (Lower Saxony State Office of Consumer Protection and Food Safety) under the permit number 33.9-42502-04-16/2329. Mice housing and handling occurred in accordance with good animal practice as defined by FELASA (Federation of European Laboratory Animal Science Associations) and the national animal welfare body GV-SOLAS (Gesellschaft für Versuchstierkunde/Society for Laboratory Animal Science).

I. Mice infection with *C. difficile*

All experiments were performed with 15- to 30-week old mice of C57BL/6 genetic background and were bred as well as maintained under specific pathogen-free conditions in animal facilities at the TWINCORE, Hannover, Germany or the Helmholtz Center for Infection Research Braunschweig, Germany. For infection, spores of *C. difficile* were prepared as described before (see 2.6.4). After 24 h of an intraperitoneally (i.p.) treatment with 10 mg/kg of clindamycin hypochloride (Sigma Aldrich), 1 x 10^4 spores of *C. difficile* in a total volume of 100 µl PBS (see 2.6.6) were administered orally to the mice.

After washing the cecum with PBS and collecting the content, the feces was homogenized and titrated. For colony counting, serial dilutions of feces were plated on *Clostridium difficile* selective agar (BioMérieux) and incubated under anaerobic conditions at 37 °C for 3 - 5 days.

II. Isolation of colonic lamina propria cells

For isolation of colonic lamina propria cells, the colon was prepared from the mice and physically emptied. The longitudinally opened colon was cut into 2 - 3 cm pieces followed by incubation in 30 mM EDTA contained PBS. To remove remaining mucus and epithelial cells, the tissue pieces were vigorously washed. After further cutting, the tissue was digested in pre-warmed Iscove's modified Dulbecco's medium (Life Technologies/Gibco) containing 1 mg/ml collagenase D (Roche) and 100 µg/ml DNaseI (Roche). The supernatant was filtered. The remaining tissue was passed through a 100 µm mesh. For cell separation, a Percoll solution gradient of 40 %/80 % (GE Healthcare; 900 g, 20 min, 20 °C, no break) was used. Washed cells, used for flow cytometry analysis, were harvested from the interphase.

III. Flow cytometry

Cells for flow cytometry analysis were harvested from the interphase as described before and incubated with PBS containing 0.2 % bovine serum albumin and 1 % anti-mouse CD16/CD32 antibody (BioXcell) for 5 min on ice. For live/dead staining in PBS, the LIVE/DEAD Fixable Dead Cell Stain Kit (Life Technologies/Thermo Fisher Scientific) was used according to the manufacturer's guidelines. Surface staining was performed in PBS containing 0.25 % BSA (Roche), 0.02 % NaN3 (Roth) and 2 mM EDTA (Roth) for 30 min on ice. The acquirement of cells for cytometry analysis occurred on an LSR II (BD) or Cyan ADP (Beckman Coulter) followed by data analysis using FlowJo software (Tree Star). "Monoclonal antibodies specific to the following mouse antigens and labeled with the indicated fluorescent markers were used: CD11c-APC-eFluor780 (N418), CD11b-eFluor450 (M1/70), MHC Class II (I-A/I-E)-FITC (M5/114.15), Streptavidin-PE from eBiosciences/Thermo Fisher Scientific, Ly-6C-PE-Cy7 (HK1.4), Ly-6G-Biotin (1A8), CD64(FcγRI)-PE (X54-5/7.1) from Biolegend and CD45-PE-TexasRed (30-F11) from Invitrogen/ Thermo Fisher Scientific" (176).

2.12 Bioinformatical analysis

2.12.1 Sequence and structure analysis

DNA and protein sequence alignments, pairwise and multiple, were performed using Clustal Omega (177).

Topology predictions were made using Phyre^2 (178) in the first instance as well as TMHMM Server v. 2.0 (179, 180) and Topcons (181). The visualization of the topology was optimized using the webservice Protter (http://wlab.ethz.ch/protter).

2.12.2 Processing of microarray data

Microarray data were analyzed using the statistical software “R” as described in Hofmann *et al.* 2018 (26). The R-script was optimized by Dr. Alexander Dudek. Here, the library packages “gplots” (182) and bioconductor “limma” (183, 184) were integrated. Background correction was performed by subtraction using the “normexp” method (185). Each array was normalized by loess normalization (186). Same empirical distributions across arrays and channels were ensured by “quantile” normalization (187). P-values, adjusted by the method described in Benjamini and Hochberg 1995 (188), of <0.05 and $\log_2$ fold changes < -1 and > 1 implicated significant differently expressed genes.

2.12.3 Processing of metabolomic data

Data processing was performed as described previously (26) by Dr. Meina Neumann-Schaal and Dr. Sabine Will from the group Bacterial Metabolomics at the Leibniz Institute DSMZ-German Collection of Microorganisms and Cell Cultures GmbH (Braunschweig, Germany).

2.12.4 Searching and prediction of binding motifs

Motif prediction was performed with the standalone version of MEME (189) using the upstream sequences [-250,0]nt of genes differentially regulated by PerR (|logFC|≥1, Pval≤0.05). Differentially regulated genes were used from at least two out of three different experimental setups. Set up 1 (wild type stressed with H_2O_2 vs *perR* mutant) is described in Michel, 2016 (2). Set up 2 (wild type vs *perR* mutant in the exponential growth phase) and 3 (wild type vs *perR* mutant in the exponential growth phase) are part of this work. MEME was run with options zero or one motif occurrence per sequence, the motif length was constrained between 10 and 25 nucleotides, and a first order Hidden Markov Model was provided. Motif prediction was carried out by Dr. Denitsa Eckweiler.

3. RESULTS AND DISCUSSION

During the last decades, *C. difficile* has become the most common cause of healthcare-associated infections worldwide (14, 15). The anaerobic, spore-forming pathogen colonizes the human gastrointestinal tract (GI) via the fecal-oral route, which may result in infections ranging from mild diarrhea to pseudomembranous colitis and death (12). Along the GI tract and finally in the gut, *C. difficile* must adapt to changing conditions. In a balanced intestinal ecosystem osmolarities of 310 mosM, low oxygen tension and low concentration of free iron prevail (190). The nutrition and immune response of the host as well as the administration of antibiotics for therapeutic purposes can disturb this balance (42, 190, 191), which requires a rapid adaptation strategy by *C. difficile*. The adaptive response of this pathogen to stress during infection is poorly understood (192). In this thesis the influence of osmotic stress on *C. difficile* and the role of the Fur-family regulators PerR and Fur in further adaptation processes were investigated.

3.1 Adaptation of *Clostridium difficile* to osmotic stress

Osmotic shifts occur in different habitats. In the soil, the constant alternation between drought and rainfall causes osmotic up- and down shifts, while in the urinal and gastrointestinal tract, the concentration and dilution of urine (41) and food digestion (42) have an influence. Soil-dwelling bacteria as well as pathogens have evolved strategies for adaptation in order to survive under these varying conditions. Adaptation processes to increasing salt concentrations are very well characterized in certain species such as *Bacillus* or *Escherichia* (67), but not in *C. difficile.* They are accompanied by changes in cell structure and cytoplasmic composition (193). Furthermore, ABC transporters, which are able to take up compatible solutes play a crucial role in the prevention of threatening cell dehydration (65). In contrast, adaptation strategies to osmotic shock in *C. difficile* have been poorly characterized.

In order to elucidate adaptation mechanisms of *C. difficile* to osmotic stress, the identification and characterization of potentially related transport systems were pursued. Comparative structural analysis with already investigated transporters of other organisms on the gene as well as on the protein level shall provide these

insights. The characterization was performed in the heterologous *Bacillus* system and in *C. difficile* itself. Investigations in *C. difficile* and corresponding mutants were presumed to reveal phenotypic and metabolic changes under salt stress as well as further information regarding possible protection strategies by compatible solutes.

3.1.1 Structural comparison of *C. difficile* transport systems

During the adaptation process to low or high osmolarity conditions, different transport systems take on specific roles. In order to prevent cell lysis and reduce the membrane tension under hypoosmotic conditions, mechanosensitive channels (Msc) located in the cytoplasmic membrane are activated to allow the trafficking of nonspecific osmolytes out of the cell (48, 65). In the genome of *C. difficile* a small-conductance mechanosensitive channel encoded by the gene *mscS (*CDIF630erm_00022*)* is annotated, which could potentially take over this function. The structural comparison using the Phyres[2] tool resulted in a homology of a 36 % sequence identity to *E. coli* MscS. On the other hand, the increasing osmolarity makes the rapid influx of K^+ ions and compatible solutes essential. The translocation of K^+ ions is facilitated by transport systems, that could be inducible like the Kdp-transporter in *E. coli* or constitutive like the Ktr-system in *B. subtilis* (55, 57). Browsing the genome annotation of *C. difficile* 630Δ*erm* (GenBank: CP016318.1) both potassium uptake systems were encountered based on sequence homology by blast. The *kdp* operon consisting of three ATPase chains encoded by *kdpABC* (CDIF630erm_01764/ 01765/01766)*,* a two-component sensor histidine kinase as well a two-component regulator that are encoded by the *kdpDE* operon (CDIF630erm_02031/02032)*.* The histidine kinase KdpE shows 44 % sequence identity (s.id.) to the corresponding protein in *E. coli*, whereas the regulator KdpD presents higher homology to *Pseudomonas syringae* (55 % s.id.). The second potassium system is homologous to the *B. subtilis* transporter Ktr and it is encoded by *ktrB* (CDIF630erm_00810), a membrane-embedded protein (GenBank: ARE61598.1), and *ktrC* (CDIF630erm_00811), a predicted NAD -binding component (GenBank: ARE61599.1). $KtrB_{Cdiff}$ resulted in a sequence identity of 43% to $KtrB_{Bsub}$. $KtrC_{Cdiff}$ shows 47 % s.id. to $KtrC_{Bsub}$. To partially counteract the

detrimental excess of potassium absorption the transport of the so-called compatible solutes is guaranteed by specific osmo protectant uptake (Opu) transporters (55, 65). Potential osmolyte uptake transporters in *C. difficile* were studied in the following.

I. Genetic organization of *C. difficile* potential Opu transport systems

Protein blast searches using *B. subtilis* OpuC SBD sequence as template and manual searches in the genome annotation of *C. difficile* 630Δ*erm* (GenBank: CP016318.1) yielded two proteins that are predicted as “ABC-type transport system, glycine betaine/ carnitine/ choline permease” (CDIF630erm_01021) and "ABC-type transport system, glycine betaine/ carnitine/ choline-like permease" (CDIF630erm_03510). While the first one is already annotated as OpuC transporter, the second one is still without name. Therefore, as an abbreviation standing for “unknown transporter” we will hereafter name it “UtS” (unknown transport system). Genetic inspection displayed that each system is organized in an operon consisting of two genes (Figure 8).

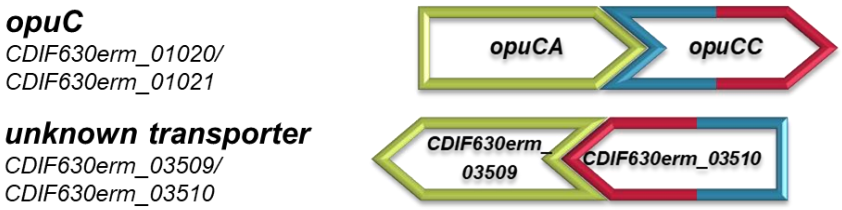

Figure 8 Operon organization of *C. difficile* transport systems.

The OpuC and UtS of *C. difficile* are both organized in an operon consisting of two genes coding for a permease (blue/red) and an ATP-binding protein (green).

One gene encodes for a permease and the other for an ATP-binding protein. The first gene of the *opuC* operon is annotated as *opuCA* (CDIF630erm_01020*)* and encodes for the ATP-binding protein. The second gene is annotated as *opuCC* (CDIF630erm_01021) and encodes the permease. The operon of the “UtS” is organized in reversed gene order. The gene CDIF630erm_03510, coding for the permease, is in the first position, while the gene CDIF630erm_03509, coding for the ATP-binding protein, is located downstream. For both transport systems, a separate gene encoding for a substrate binding domain (SBD) is missing.

Although the blast search led to the identification of a transport system for *C. difficile*, annotated as OpuC, the operon structure obviously differs from the very well characterized OpuC of *B. subtilis.* In contrast to the results of this study, the *Bacillus* operon consisting of four genes, where in addition to *opuCA* and *opuCC,* two genes called *opuCB* and *opuCD,* exist (Figure 7). In this operon, *opuCA* encodes also for the ATP-binding protein. The genes *opuCB*, and *opuCD* code for the permease subunits and *opuCC* encode a separate substrate binding domain, which is tethered to the membrane (79, 86) like in manifold of Gram-positive bacteria or Archaea (118). A similar operon structure to the OpuC of *B. subtilis* was discovered for the carnitine-uptake transporter OpuC in *L. monocytogenes,* in which the SBD is predicted to be fused to the TMD (194, 195). Besides the $OpuC_{Lmo}$ transporter, encoded also by four genes, in *L. monocytogenes* another transporter, the BilE, exists, which is encoded by the genes *bilEA* (lmo1421*)* and *bilEB* (lmo1422) (195). A similar genetic arrangement to BilE is also present for the very well characterized glycine-betaine uptake system OpuA of *Lactococcus lactis* (196) and has recently been described as an ABC transporter OpuF, which is widely distributed across *Bacillus species*, with the exception of *B. subtilis* (86). For these transport systems, consisting of a two-gene operon, it was proposed that the permease-encoding gene additionally encodes for a substrate binding protein (SBP), which is anchored to the TMD (86, 195, 196). Translocator-bound SBDs were discovered in several families of low-GC Gram-positive bacteria such as Clostridiaceae, Listeriacea, Streptococcaceae (118).

Previous findings in other organisms, also showing an operon organization with two genes like *C. difficile*, suggest that $OpuCC_{Cdiff}$ encodes not only for a permease but also for a SBP, that may also be fused with TMD, resulting in a protein with dual function (TMD/SBD). The same structure would be conceivable for the unknown transporter. In order to obtain a more precise prediction of the protein structure and function of OpuC and UtS, the TMD/SBD sequences were compared with different protein structures formerly resolved.

II. Protein structure of *C. difficile* transport systems

The genetic organization of *C. difficile* transport systems OpuC and UtS comprise an operon consisting of two genes, which encodes for an ATP-binding protein and a permease. This permease is suggested to include a substrate-binding domain for compatible solutes (3.1.1I). In order to obtain a more reliable prediction of the protein structure and function of OpuC and UtS, the corresponding amino acid sequences comprising the TMD/SBDs were analyzed in the database Phyre^2 (178). The tool allows the prediction, modeling and analysis of protein structure based on already crystallized proteins. Sequence alignments and structural homologies with already described SBDs may potentially provide with relevant information about binding capacity of solutes, which is dependent upon the conserved amino acids in the aromatic cage.

Structural comparisons using the Phyre^2 database yielded the soluble binding domain BilEB (*lmo1422*) of the *L. monocytogenes* BilE transporter as the top hit for both *C. difficile* TMD/SBDs. For OpuCC$_{Cdiff}$, a sequence identity of 41 % was reached deriving in a high-confidence homology model. The TMD/SBDs of the UtS showed a sequence identity of 33 % to BilEB dealing with a remote homology. The following top matches included the SBDs OpuCC and OpuBC of *B. subtilis*, for which OpuCC has an identity of 39 % and 35 % respectively. On the other hand, the TMD/SBD of the UtS revealed an identity of 35 % for both SBDs. Based on these results, a multiple sequence alignment was performed using the program Clustal Omega (Figure 9). Protein sequences of *C. difficile* TMD/SBDs were compared to BilEB (*lmo1422*) of *L. monocytogenes* and OpuCC as well as OpuBC of *B. subtilis* to determine their resemblance in more detail. Additionally, OpuFB of *B. infantis* was compared due to the similarity in terms of genetic organization. Special attention was paid to the presence and, if applicable, composition of the aromatic cage, which in OpuCC$_{Bsub}$ and OpuBC$_{Bsub}$ typically consists of four preserved tyrosines (136, 137).

A

Percent Identity Matrix - created by Clustal2.1

1: C.difficile630deltaerm_OpuCC	100.00	35.63	35.33	31.13	37.77	39.04
2: C.difficile630deltaerm_unknownTransporter	35.63	100.00	31.97	33.45	35.60	36.07
3: B.subtilis_OpuCC	35.33	31.97	100.00	69.31	32.30	32.76
4: B.subtilis_OpuBC	31.13	33.45	69.31	100.00	33.33	33.45
5: B.infantis_OpuFB	37.77	35.60	32.30	33.33	100.00	67.66
6: L.monocytogenes_lmo1422	39.04	36.07	32.76	33.45	67.66	100.00

B

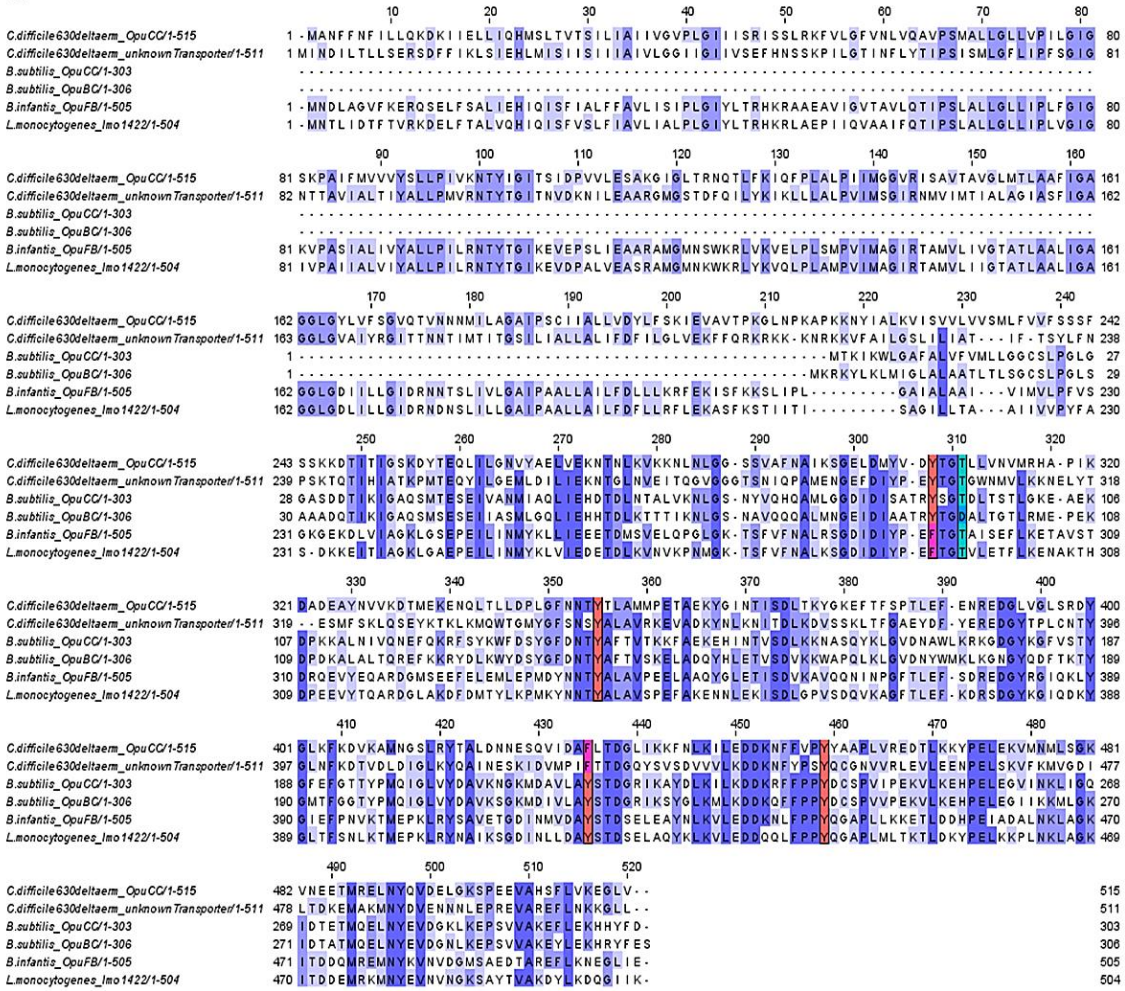

Figure 9 Amino acid alignment of substrate binding domains between *C. difficile* 630Δ*erm*, *B. subtilis*, *B. infantis* and *L. monocytogenes*.

TMD/SBD sequences of *C. difficile* OpuCC (CDIF630erm_01021) and UtS (CDIF630erm_03510) were compared with SBD sequences of *B. subtilis* OpuCC (BSU_33810), OpuBC (*BSU_ 33710*), *B. infantis* OpuFB (N288_21525) and BilEB (lmo1422) of *L. monocytogenes*. A) Percentage identities between all amino acid sequences created by Clustal Omega 2.1 are shown. B) The aromatic cage of *C. difficile* OpuCC and unknown transporter TMD/SBD is defined by three tyrosines (Y; red) at position 308, 355 and 459, and by one phenylalanine (F; magenta) at position 435, where the compared SBD display an additional tyrosine. At position 310 the binding site is characterized by a threonine (T; cyan). Percentage identities between all sequences based on Clustal Omega are marked in blue.

Multiple alignments with the Clustal Omega program resulted in similar, but not identical sequence percentage identities (SPIs) to those displayed by Phyre[2] (Figure 9A), which is not unusual since SPIs are calculated and reported in a different manner depending on the program´s presetting. For OpuCC$_{Cdiff}$ the highest percentage identity was reached for *L. monocytogenes* lmo1422 (39 %) followed by OpuFB$_{Binf}$ (37 %), OpuCC$_{Bsub}$ (35 %) and OpuBC$_{Bsub}$ (31 %). Almost identical resemblance but showing lower sequence identities was achieved when aligning the UtS: *L. monocytogenes* BilEB (36 %) followed by OpuFB$_{Binf}$ (35 %), OpuBC$_{Bsub}$ (33 %) and OpuCC$_{Bsub}$ (31.9 %). The alignment also showed that the *C. difficile* OpuCC and the TMD/SPD of the UtS shared only 35 % amino acid sequence, which could be a hint for different functions. A more detailed comparison showed that both sequences of *C. difficile* (OpuCC: 515 aa; UtS: 511 aa) were larger than those of the SBD of OpuCC$_{Bsub}$ (303 aa) or OpuBC$_{Bsub}$ (306 aa) and have a similar length to that of OpuFB$_{Binf}$ (505 aa) or BilEB$_{Lmo}$ (lmo1422; 504 aa) (Figure 9B). While OpuCC$_{Bsub}$ and OpuBC$_{Bsub}$ are known to be SBDs anchored to the membrane as well as encoded in separate genes, OpuFB$_{Binf}$ and BilEB$_{Lmo}$ are merged products of permease and SBD, which are coded by a single gene. The additional N-terminus (1 - 214 aa) of *B. infantis* and *L. monocytogenes* in front of the aligned SBD represents the TMD. Due to the fact that *C. difficile* protein consist of a N-terminal domain, it can be assumed that a fused product of TMD and SBD is also present in this organism. The TMDs of OpuCC$_{Cdiff}$ (Figure 10A based on Phyre[2]) consists of six predicted, membrane spanning helices (yellow), which is within the typical range of 5 to 10 helices per TM segment for ABC importers (113). Both, the N- (aa 1 - 21) and C- termini (aa 242 - 515) of OpuCC$_{Cdiff}$ are predicted to be located extracellularly. The latter represents the SBP of this dual-functional protein. Similar structures were obtained with the tool TMHMM and Topcons. The prediction for the TMD/SBP hybrid protein of the UtS yielded a similar protein structure using Phyre[2] (Figure 10B) and Topcons. In contrast the TMHMM server generated a model including an intracellular N-terminus and five transmembrane helices. Despite these differences, all tools delivered a predicted extracellular SBD that is a hallmark to importers independently of the number of TMH.

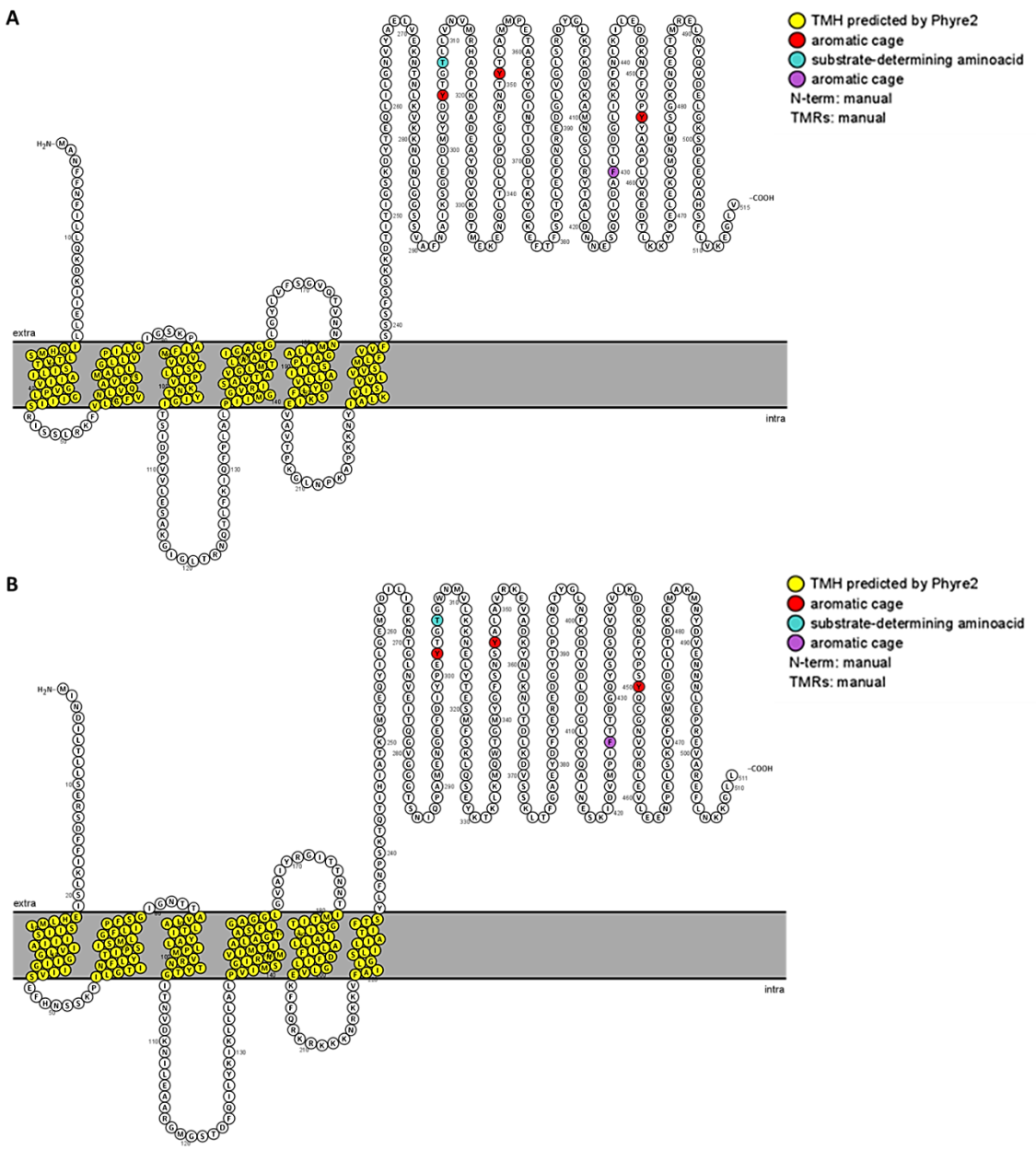

Figure 10 Prediction of transmembrane helix organization *C. difficile* transport systems.

The organization of TMHs of OpuCC (A) and the unknown transporter UtS (B) was predicted by Phyre[2]. The visualization was optimized using the webservice Protter (http://wlab.ethz.ch/protter). Transmembrane helices are colored in yellow. The aromatic cage consists of three tyrosine (red) and one phenylalanine (purple). The cyan-labeled threonine displays the substrate-determining amino acid in $OpuCC_{Bsub}$.

In conclusion, it was shown that OpuCC of *C. difficile* exhibited the highest protein sequence similarity to $OpuFB_{Binf}$ and $BilEB_{Lmo}$, followed by $OpuCC_{Bsub}$ and $OpuBC_{Bsub}$. The TMD/SBP hybrid protein of the unknown transporter also showed homologies to these transporters, although less pronounced. While all Opu transporters are involved in the osmostress response acting as importers,

the classification of BilEB$_{Lmo}$ is still discussed. Due to significant similarities to known compatible solute transporters, it was first suggested that BilE was preferentially involved in the acquisition of osmo protectant substrates (betaine, carnitine or choline). Sleator and colleagues demonstrated that BilE is not involved in the osmostress response. Instead the authors defined BilE as an exclusion system playing an important role in bile tolerance (197). However, intensive crystal structure analyses of BilE SBD, have revealed that the C-terminus has a distinctive SBP fold that allows the classification as a type I transporter (195). A significant structural distinction between importers and exporters is the dependence on an extracellular SBP translocating substrates from the environment into the cell. Due to their simpler mechanism, exporters do not depend on substrate binding protein to function (92, 95). The previous structural analyses implied that *C. difficile* harbors two import systems.

Focusing merely on the SBD, it became obvious that the SBD of both *C. difficile* transporters contained an aromatic cage (marked in red/purple), which is responsible for binding compatible solutes in other ABC transporters. In contrast to the binding pocket of *B. subtilis*, which is characterized by four tyrosines^{308,355,435,459} (Y; red), the SBD of both *C. difficile* transporters as well as OpuFB$_{Binf}$ and BilEB$_{Lmo}$ are defined by a binding site consisting of three tyrosines and one phenylalanine (F; magenta). While in *B. infantis* and *L. monocytogenes* the tyrosine at position 308 is replaced by phenylalanine, in *C. difficile* position 435 differs. Nevertheless, the SBD of *C. difficile* seems to form an aromatic pocket, implicating the ability to bind compatible solutes. A claim on the possible substrate spectrum of the respective transporter was beforehand difficult to provide with certainty on the basis of structural comparisons. Only for the evolutionary related transporters OpuC$_{Bsub}$ and OpuB$_{Bsub}$ it was shown that the replacement of one amino acid (Figure 9; aa 311; cyan), threonine, present in OpuC, with aspartate, present in OpuB, led to a reduced spectrum (81, 136, 137). At this position both *C. difficile* SBDs possess a threonine, which could indicate a broader spectrum similar to OpuC$_{Bsub}$. The predicted substrate binding pocket of OpuCC$_{Cdiff}$ and the already structure-wise resolved pocket of OpuCC$_{Bsub}$ are illustrated in Figure 11. Due to the extensive transporter studies in the model organism *B. subtilis*, the substrate spectrum of both *C. difficile* transporters was heterologously investigated in *Bacillus*.

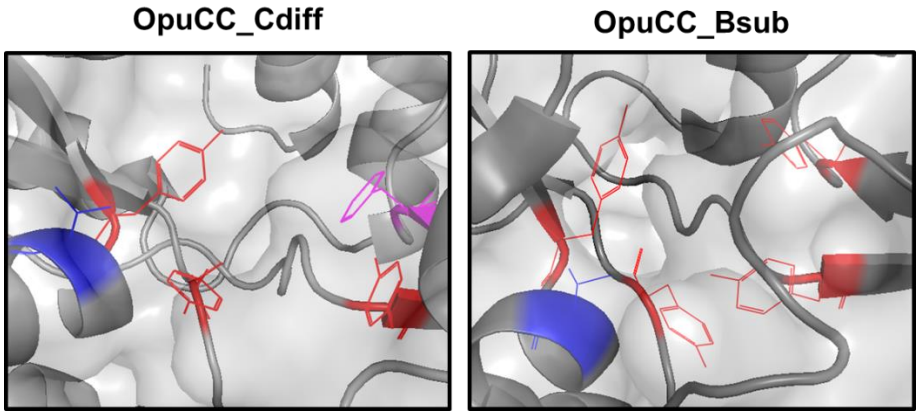

Figure 11 Predicted substrate binding pocket of OpuCC$_{Cdiff}$ and OpuCC$_{Bsub}$.

The prediction of OpuCC$_{Cdiff}$ by Phyre^2 is based on the crystal structure of OpuCC$_{Bsub}$ and was generated using the software Pymol 2.4. The aromatic cage consisting of tyrosine (red) or phenylalanine (purple) is shown. The substrate-determining threonine is marked in blue. The illustration was developed in collaboration with Dr. José M. Borrero de Acuña.

3.1.2 Characterization of *C. difficile* transporters by homologous recombination of *B. subtilis* TMB118

The adaptation systems triggered by high salinity conditions are very well characterized in *B. subtilis*. Five osmo protectant uptake (Opu) transporters, OpuA/B/C/D/E, with specific substrate spectra are known to be involved during the stress response (65). Conversely, very little is known about the transporters and compatible solutes orchestrate the response in *C. difficile* when the organism is exposed to increasing salt concentrations. Blast searches using *B. subtilis* OpuC SBD sequence as template and manual searches in the genome annotation of *C. difficile* 630Δ*erm* (GenBank: CP016318.1) revealed two transport systems predicted to be “ABC-type transport system, glycine betaine/ carnitine/ choline permease” (CDIF630erm_01021) and "ABC-type transport system, glycine betaine/ carnitine/ choline-like permease" (CDIF630erm_03510) (see 3.1.1). While the first one is already annotated as OpuC transporter, the second one is still unannotated and will therefore be called “unknown transporter” and abbreviated as “UtS” in the following. It could be shown that the SBDs of both transporters are homologous to SBDs of partial well characterized bacterial domains. Furthermore, structural analysis revealed a TMB-fused SBD containing an aromatic cage defined by three tyrosines and one phenylalanine. To define the substrate spectrum of each single system, the integration of corresponding operon structures into the OpuA/B/C/D-deficient *B. subtilis* strain TMB118 was aimed followed by osmostress protection growth assays.

I. Homologous recombination of *B. subtilis* TMB118

The OpuA/B/C/D-deficient *B. subtilis* strain TMB118 (81) was employed to independently characterize the substrate spectrum of two *C. difficile* transport systems which are predicted to transport compatible solutes into the cell probably under hyperosmotic conditions. For the expression of homologous *C. difficile* transporter genes in *B. subtilis*, DNA sequences were optimized for *B. subtilis´* codon usage and were fused with the natural *opuC* promotor regions of *B. subtilis* (Suppl. Figure 1). Synthesized inserts were cloned in between the 5´- and 3´-flanking regions of the *amyE* and ligated into the integration vector pX (164) yielding pXΔ*xylR*::*opuC*$_{Cdiff}$ and pXΔ*xylR*::unkn.transporter$_{Cdiff}$, respectively. Afterwards, transformation of *B. subtilis* TMB118 was performed to allow the

integration of the optimized operon sequences from pX into the chromosomal *amyE* locus of *B. subtilis* TMB118 yielding the strains *B. subtilis* AM01 containing OpuC and AM02 containing the UtS, respectively. Potential recombinants were tested for their amylase activity by cultivation on starch containing medium and subsequent overcoating with potassium iodine solution (Figure 12). For *B. subtilis* AM01 27 (Figure 12A) and for *B. subtilis* AM02 9 (Figure 12B) positive clones were screened. *B. subtilis* TMB118 with functional amylase was used as control strain (Figure 12B; +).

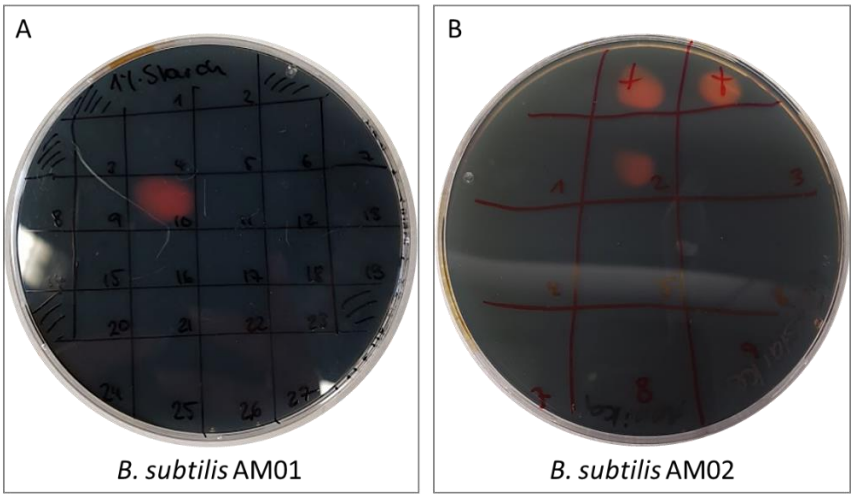

Figure 12 Amylase-activity screening of potential recombinant strains *B. subtilis* AM01 and *B. subtilis* AM02.

Amylase-activity was performed by cultivation of potential clones on starch-containing medium and overcoating with potassium iodine solution. A) Screening of *B. subtilis* AM01 containing $OpuC_{Cdiff.}$ All of the tested clones, except no. 10, showed no amylase activity. B) Screening of *B. subtilis* TMB118 (+) and *B. subtilis* AM02 containing $UtS_{Cdiff.}$ All of the tested clones, except no. 2, and TMB118, showed no amylase activity indicating proper integration.

After overcoating with potassium iodine solution, *B. subtilis* TMB118 (Figure 12B; +) displayed a hydrolyzed zone around the bacterial colony. Consequently, the strain contained the functional *amyE* gene encoding for the enzyme α-amylase, which catalyzes the hydrolysis of starch (164, 198) resulting in a visible zone. One of 27 tested *B. subtilis* AM01 (no. 10) and one of nine screened *B. subtilis* AM02 (no. 2) recombinants showed also a hydrolyzed halo around the bacterial colony, indicating amylase activity and consequently no successful integration of desired operon structures. Successful homologous recombination led to a disruption of *amyE* resulting in the deactivation of its function and no halo formation, which was visible for all other screened integrants. Selected integrants

were grown in an osmostress protection assays in order to define the substrate spectrum of OpuC and the UtS of *C. difficile* under high salinity conditions.

II. Characterization of osmolyte transport

The characterization of the substrate spectrum of both *C. difficile* transport systems, OpuC and UtS, in the heterologous *B. subtilis* system was pursued by performing an osmostress protection growth assay. For this purpose, the recombinant *B. subtilis* strain AM01 expressing the *C. difficile* 630Δ*erm opuC* operon and the *B. subtilis* strain AM02 expressing the operon of the UtS were generated by homologous recombination (see 3.1.2 I). The expression of both operons relied on the *B. subtilis* promotor shown in Suppl. Figure 1. These strains are based on *B. subtilis* TMB118 (81), a derivative of JH642 (199), being deficient for the transporter OpuA, OpuB, OpuC and OpuD, but still functional for the proline transporter OpuE (81). Consequently, it was used as negative control strain. The *B. subtilis* strain JH642 expresses all functional Opu transporters and thus served as a positive control strain. The assay was performed in SMM as reference medium as well as under salt stressed conditions triggered by 1.0 M NaCl in the absence or presence of various compatible solutes using a final concentration of 1 mM for each. Cultures were grown aerobically for 25 h measuring biomass by scattered light intensity (SLI) using a BioLector system (see 2.6.7). Figure 13 displays the observed substrate profile for all tested strains by measuring the biomass after 12 h cultivation.

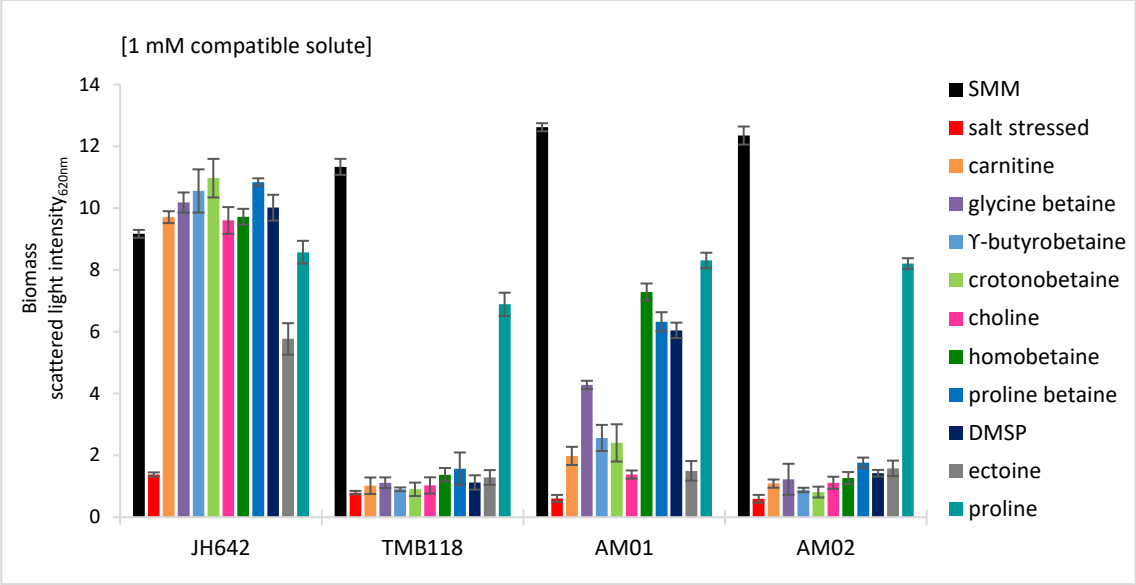

Figure 13 Substrate profile of *C. difficile* 630Δ*erm* transport systems tested in *B. subtilis* within an osmostress protection growth assay.

B. subtilis strains were cultivated in SMM as reference medium and under salt stressed conditions induced by 1.0 M NaCl in the absence or presence of various compatible solutes using of each a concentration of 1 mM. Cultures were grown in three biological replicates in 48-well FlowerPlates in a BioLector system for 25 h at 37 °C, 1,400 rpm under humidity control. The mean and standard deviation value of biomass measured by scattered light at 620nm after 12 h cultivation is shown. The *B. subtilis* strain JH642 was include as positive control strain as it expresses all functional Opu transporter (166). The strain TMB118 was taken as negative control strain lacking the OpuA, OpuB, OpuC, and OpuD compatible solute transport systems (81). The strains AM01 and AM02 are based on TMB118 expressing the *C. difficile* 630Δ*erm opuC* operon and *unknown transporter* operon integrated into the chromosomal *amyE* gene.

The growth behavior of all tested strains cultivated in the reference medium SMM showed a similar phenotype. The exponential phase was entered after an average of 4 h of incubation to reach the maximum measured SLI of 11.1 to 14.6 after 9 to 10 h, before the cells switch to the stationary phase (Suppl. Figure 2 to Suppl. Figure 5; black). Salt stressed conditions revealed delayed and partly reduced growth. While *B. subtilis* JH642, *B. subtilis* TMB118 and AM02 initiated the exponential phase after 13 h, AM01 started to grow with a delay of 1 h. In the presence of each single tested compatible solute, the strain JH642 showed a reversible growth phenotype. In contrast, with the exception of proline, the supplementation had no osmoprotective effect on TMB118. Due to the availability of five Opu transporters, OpuA/B/C/D/E, the strain JH642 is able to transport different solutes into the cytoplasm in order to protect the cell against dehydration when the osmolarity in the environment increases. However, *B. subtilis* TMB118, a derivative of JH642, is lacking the transporters OpuA/B/C/D but is still functional

for the proline transporter OpuE. The Opu-system is characterized by the wide range of transferable solutes and a partially overlapping spectrum, with OpuC acting as universal importer (65, 81). Consequently, the deficiency renders the transport as well as the protection against hyperosmolarity unfeasible. For the recombinant strain AM01, the supplementation with all compatible solutes promoted growth when it was exposed to salt stress conditions (Figure 13), indicating a functionally expressed and translated $OpuC_{Cdiff}$ in *B. subtilis*. Recording of growth showed that the addition of homobetaine, proline betaine, DMSP, glycine betaine, γ-butyrobetaine, crotonobetaine, carnitine, ectoine, and choline led to an earlier onset into the exponential phase in descending order (Suppl. Figure 2). The time of entry was restricted for the above mentioned osmolytes to 9 h to 12 h after incubation start, achieving an improvement of 50 %, in contrast to the positive control JH642, which conversely achieved up to 78 %. Furthermore, differences were observed regarding the maximum SLI's reached. While in the control strain biomasses identical to that in the reference medium were achieved after addition of all tested solutes, this was not the case for the AM01 strain (SLI_{SMM}=14.3) with each osmolyte. The highest SLI´s were observed for ectoine (SLI=10.0), carnitine (SLI=9.7), proline betaine (SLI=9.7), homobetaine (SLI=9.6), γ-butyrobetaine (SLI=9.4), glycine betaine (SLI=9.1) and choline (SLI=9.1). Interestingly, DMSP (SLI=8.7) and crotonobetaine (SLI=8.7) led to lower biomasses, but still stimulated the growth of the recombinant strain exposed to salt stress.

These data proved that the homologous recombination resulted in a functional $OpuC_{Cdiff}$ in the heterologous *B. subtilis* system, able to transport different compatible solutes, namely homobetaine, proline betaine, DMSP, glycine betaine, γ-butyrobetaine, crotonobetaine, carnitine, ectoine, and choline. All substrates are also part of the OpuC transport system of *B. subtilis*, while the OpuF system of *B. infantis* only exhibits affinity to glycine betaine, proline betaine, homobetaine and DMSP (86). Accordingly, the substrate spectrum of the OpuC system of *C. difficile* showed more similarities to the *B. subtilis* OpuC, although the operon structure is more closely related to OpuF. A possible explanation could be the different amino acid composition within the conserved aromatic box (Figure 9). While OpuF contains a phenylalanine at position 308 of the alignment, OpuC of *B. subtilis* and *C. difficile* contained a tyrosine. Moreover, although the

heterologous system *B. subtilis* AM01 was able to transport different compatible solutes, the second system *B. subtilis* AM02 (harboring UtS) did not present stimulated growth under salt stress conditions when compatible solutes were added (Suppl. Figure 3). For all cultures supplemented with the various compatible solutes, an identical growth phenotype was observed as in the salt-stressed *B. subtilis* AM02 strain (Suppl. Figure 3) and the control strain TMB118 (Suppl. Figure 4), respectively. These results indicated that the UtS either transfers osmolytes others than those tested or it is not activated by NaCl, which was outlined by Scaria and colleagues, who determined differential expressed genes in response to osmotic shock. During these experiments, genes of the secondly predicted ABC transport system (CD3215/CD3216), which corresponds to the operon CDIF630erm_03509/03510 of the unknown transporter, were not listed as differently expressed (200).

3.1.3 Generation of an insertional *opuCC* mutant in *C. difficile* 630Δ*erm*

The generation of insertional mutants in the laboratory strain *C. difficile* 630Δ*erm* was based on the ClosTron technology established in 2007 by Minton and co-workers. This technique allows a stable and specific integration of a plasmid-borne group II intron, containing an retrotransposition-activated marker (RAM) for erythromycin resistance, into the chromosomal target gene resulting in its disruption and subsequent inactivation of its function (159, 169). In this section, the generation of a mutant lacking the substrate binding domain of the osmo protectant uptake transport system (*opuCC;* CD630DERM_09010) was addressed. The intron specifity to a target sequence was evaluated by determining distinct integration sites for the re-targeting intron using the Perutka algorithm (173). The intron targeting region was synthesized and cloned into the ClosTron shuttle vector pMTL007C-E2 by ATUM (Newark, USA) resulting in pMTL007C-E2::Cdi_*opuCC*-936l937s. The plasmid pMTL007C-E2 is one of the typical suitable plasmids used for mutagenesis in *C. difficile* 630Δ*erm,* containing the plasmid marker *catP* as well as the FRT-flanked intron marker *ermB* RAM for selection. The transfer into *C. difficile* was driven by conjugation (159). In this work, the *E. coli* strain CA434 was transformed with the newly generated pMTL007C-E2::Cdi_*opuCC*-936l937s and served as donor strain. The plasmid-borne *ColE1* allows a high copy replication mechanism in Gram-negative hosts while the Gram-positive replicon *pCB102* is sustains replication in *C. difficile* (159, 160). Mating gave rise to colonies that were re-streaked onto agar plates containing appropriate selection marker for the detection of putative mutants. Erythromycin-resistant colonies were isolated, and the DNA extracted. Different PCR screenings were performed to confirm the desired insertion (Figure 15). A schematic overview of the integration of the group II intron into the target gene with corresponding PCR product sizes is shown in Figure 14.

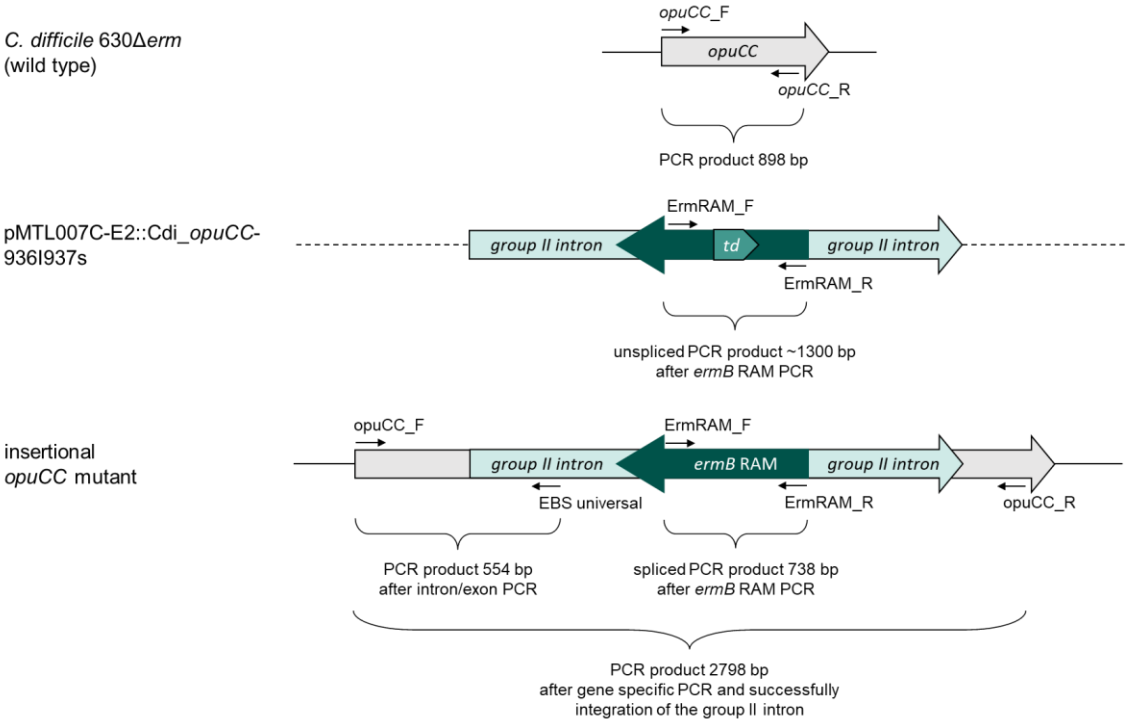

Figure 14 Schematic overview of the integration mechanism of the group II intron into the target gene *opuCC* with corresponding PCR product sizes.

C. difficile 630Δ*erm* was used as wild type control strain. Gene specific primers were designed to confirm the insertional event. The ClosTron plasmid pMTL007C-E2::Cdi_*opuCC*-936I937s containing the *ermB* RAM including a phage *td* group I intron was synthesized by ATUM (Newark, USA). The chromosome *C. difficile* 630Δ*erm opuCC* mutant carried a group II intron with a *td*-spliced *ermB* RAM. Illustration is modified after Berges *et al*. 2018 (201).

A preliminary validation of the successful generation of an *opuCC* mutant was conducted via PCR using primers aligning to flanking regions of the wild type gene. Genomic DNA of *C. difficile* 630Δ*erm* was used as wild type control and resulted in a PCR product of 898 bp while a product of 2,789 bp suggested the insertion of the group II intron in our gene of interest (Figure 15, Lane A).

Furthermore, the insertion was confirmed by an intron-exon PCR with selected primers that bind to the intron and the *opuCC* gene, resulting in a product of 554 bp (Lane B). A final PCR using *ermB* RAM specific primers was performed to verify the spliced and thus activated *ermB* RAM. Within the ClosTron plasmid, the marker is present in an inactive form through the insertion of a phage *td* group I intron. During mutagenesis, the *td* intron is capable to catalyzing its own orientation dependent splicing from RNA transcripts (159, 169, 202). A non-spliced *ermB* RAM yields a PCR product of ~1,300 bp while, a spliced and activated marker results in a 738 bp product (Lane C). A successful insertional

mutation event into the gene *opuCC* in *C. difficile* 630Δ*erm* was verified by different PCRs as represented in Figure 15.

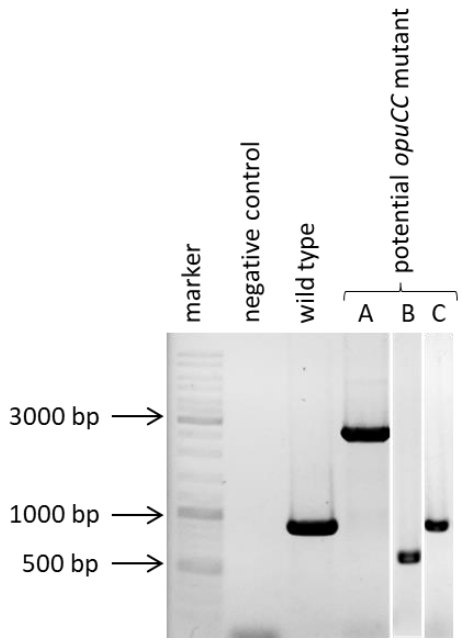

Figure 15 Agarose gel electrophoresis for the confirmation of potential an *opuCC* mutant in *C. difficile* 630Δ*erm*.

The wild type DNA was used as control and showed a product of 898 bp after performing the gene specific PCR. Lane A displayed a product of 2,789 bp after the gene specific PCR indicating the insertion of the group II intron. The intron exon PCR resulted in a product of 554 bp shown in Lane B. Lane C shows a product of 738 bp indicating a spliced *ermB* RAM after corresponding PCR. The negative control contained no DNA. The GeneRuler™ DNA Ladder Mix (Thermo Fisher Scientific, Waltham, USA) served as marker. Lane B and C belonging to separate gels. Experiments were performed in cooperation with Elisabeth Derksen 2018 (168).

3.1.4 Evaluation of the osmotic tolerance of *C. difficile* wild type and an the corresponding *opuCC*-deficient mutant

The soil as habitat of *C. difficile*, but also the preferred intestinal tract of humans as habitat, requires adaptation to osmotic changes. In the soil, organisms are exposed to the everchanging of dryness and moisture (41). During the human infection, *C. difficile* must adapt to increasing osmolarity resulting from uptake to successfully colonize the intestine (42). In order to evaluate the osmotic tolerance, the growth behavior of the wild type and an *opuCC* destructed mutant (see 3.1.3) was monitored after exposing the strains to increasing osmolarity induced by NaCl. Growth experiments were performed in minimal defined medium (MDM contained 15.5 mM NaCl) supplemented with NaCl increasing concentrations ranging from 100 mM to 400 mM (Figure 16) (168). In all tested conditions up to 300 mM additional NaCl, the *opuCC*-deficient mutant showed a restricted growth in comparison to the wild type, which was more pronounced with increasing salt concentration (A - D). In the reference medium MDM and those supplemented with 100 mM NaCl, both strains showed a characteristic growth behavior encompassing the four phases: lag, exponential (log), stationary, and death (A and B), while the strains remained in the stationary phase when NaCl was added over 200 mM NaCl (C - E). The maximum optical density (OD_{max}) of the wild type is up to a salt concentration of 300 mM on average 0.85 (A - D), which is also (A - C) or may also (D) achieved by the mutant. Osmotic stress evoked with a concentration of 350 mM NaCl exhibits a reduced growth for the wild type with an OD of 0.52 after 26 h incubation and already no growth for the mutant (E). Concentrations higher than 400 mM NaCl led to no detectable growth for both strains (F).

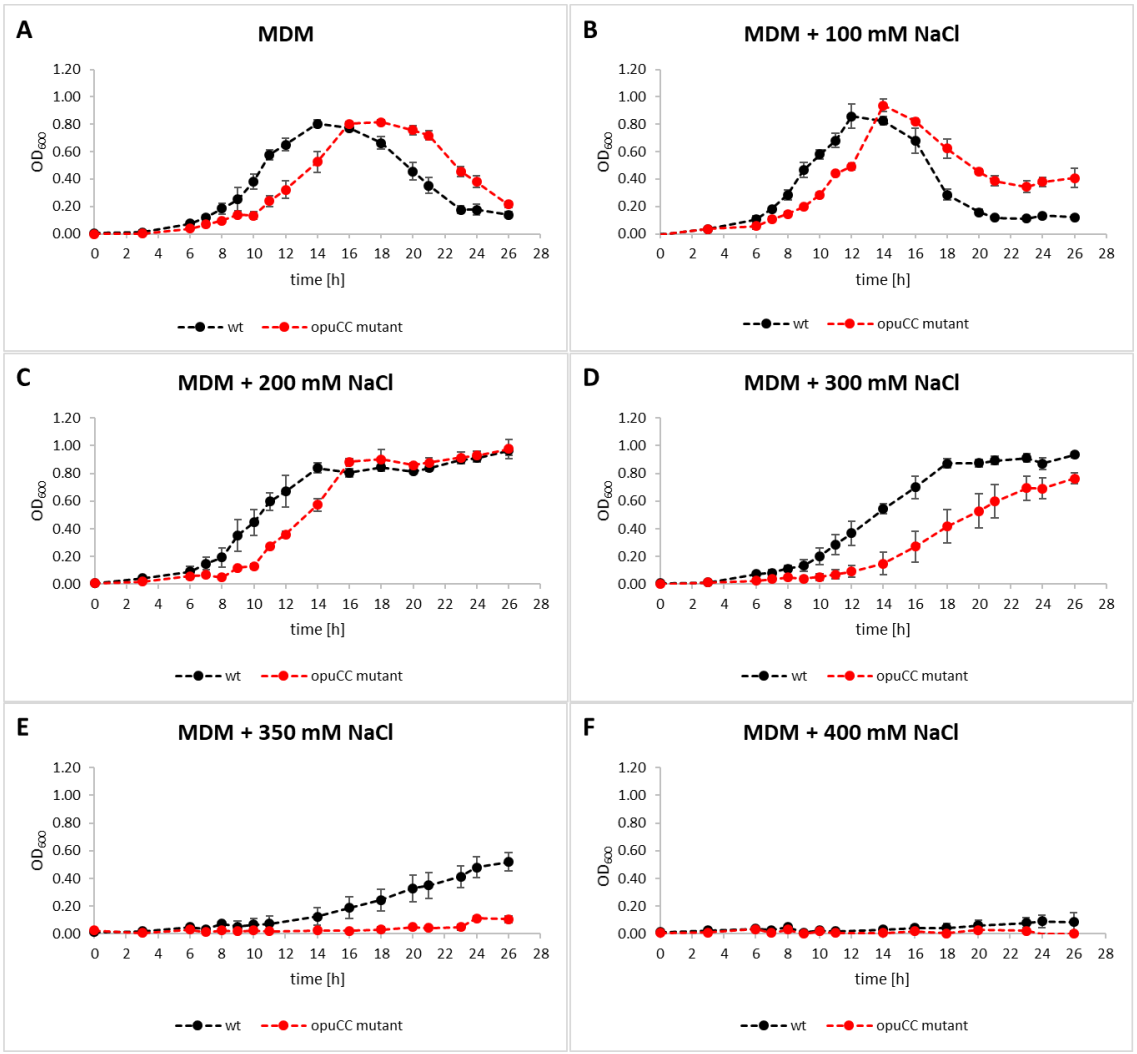

Figure 16 Growth behavior of *C. difficile* 630Δ*erm* (wt) and *opuCC* mutant under increasing salt stress conditions.

Comparative growth experiments were carried out in MDM in four biological replicates. Standard deviations are indicated. Osmotic strength was increased by supplementation of NaCl. Figure (A) displays *C. difficile* 630Δ*erm* (●) and *opuCC* mutant (●) grown in MDM as reference medium. The *opuCC* mutant shows a delayed growth to the wild type. Figures B - F display the growth behavior of both strains under increasing NaCl concentrations. Up to 300 mM NaCl the mutant shows a delayed growth in comparison to the wild type (B - D). Osmotic stress elicited with a concentration of 350 mM NaCl promoted reduced growth for the wild type and no growth for the mutant (E). Concentrations higher than 400 mM NaCl led to no detectable growth for both strains (F). Experiments were performed in cooperation with Elisabeth Derksen 2018 (168).

These data showed that the range of osmotic tolerance for *C. difficile* is up 350 mM additional NaCl. Dapa and colleagues also showed in 2013 that the critical value of NaCl was 300 mM, which led to biofilm inhibition (203). Higher osmolarities than 400 mM lead to no detectable growth while other soil-living bacteria like the model organism *B. subtilis* and *B. licheniformis* can easily withstand concentrations of 1.2 M NaCl (45, 204).

Even compared to other pathogens like *S. aureus*, which only shows a reduced growth under high salinity conditions containing 2.5 M NaCl (205), or opportunistic pathogens of the gastrointestinal tract like *Klebsiella pneumoniae* and *E. coli*, whose growth is inhibited at 0.8 M (206), *C. difficile* appears to be more sensitive to salt stressed conditions. The preferred habitat of this pathogen is the intestinal tract of humans and animals, where an osmotic concentration of 350 mM NaCl is feasible (42, 207) dependent upon the ingested food (208). Consequently, *C. difficile* inhabits the intestine at its osmotic limit, which requires a saline-responsive underlying protein machinery.

3.1.5 Characterization of osmo protective osmolytes in *C. difficile*

The ABC transporter OpuC is known in many bacteria to take up a wide spectrum of compatible solutes to preserve the organisms from dehydration under high salinity conditions. The characterization of the *C. difficile* OpuC transporter system, expressed in the recombinant *B. subtilis* strain AM01, resulted in a substrate spectrum containing 9 of 9 tested solutes, namely carnitine, glycine betaine, γ-butyrobetaine, crotonobetaine, homobetaine, proline betaine, choline, DMSP and ectoine (see 3.1.2). To define the osmotically protective substrate profile for *C. difficile*, the range of osmotic tolerance for the wild type and the corresponding *opuCC* mutant was first evaluated (see 3.1.4). Osmotic stress elicited by a concentration of 350 mM NaCl resulted in reduced growth for the wild type and no detectable growth for the corresponding OpuC lacking mutant (Figure 16E). Consequently, 350 mM NaCl was added to the growth medium MDM in the following transport assays to evoke high salt stress conditions. Compatible solutes were added in a concentration of 1 mM to NaCl-supplemented MDM to determine their potential osmoprotective function. Stimulating growth from osmolytes alone was tested by adding the compatible solutes to the reference medium. MDM served as reference medium. All cultures were grown anaerobically for 23 h. The growth behavior of *C. difficile* wild type and the corresponding *opuCC* mutant under all tested conditions over time is shown in Suppl. Figure 6. Cell densities of all strains and compatible solutes after 15 h cultivation are summarized in Figure 17.

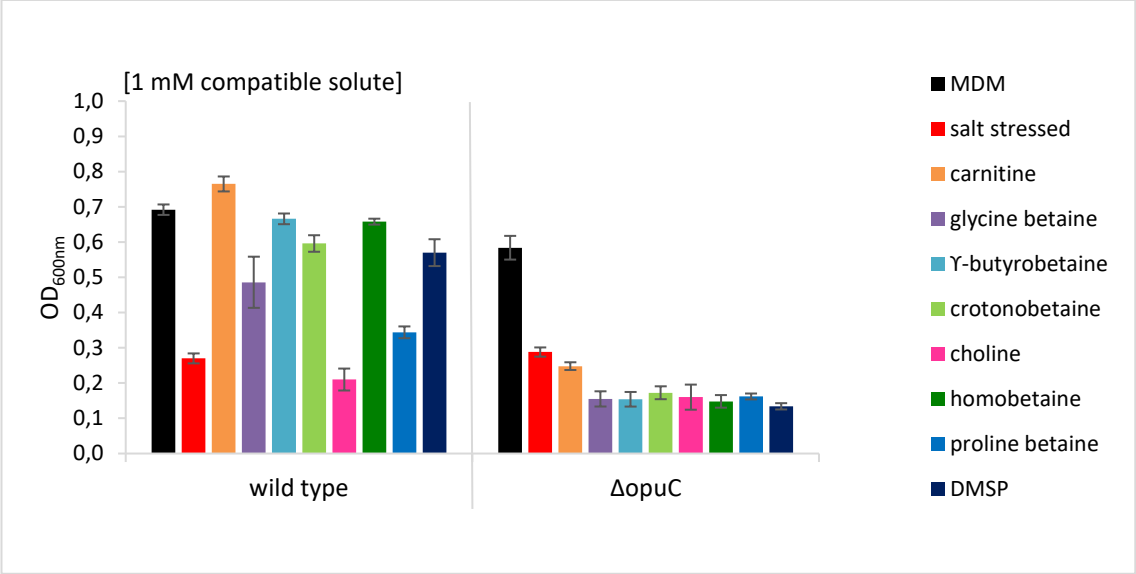

Figure 17 Saltstress growth assays assessing the osmo protective substrate profile of the OpuC transport system in *C. difficile* 630Δ*erm*.

C. difficile 630Δ*erm* (wt) and the corresponding *opuCC* mutant (Δ*opuC*) were grown in MDM as reference medium and under salt stress conditions induced by 350 mM NaCl addition in the absence or presence of various compatible solutes using a concentration of 1 mM. All measurements were made in quintuplicates. The mean and standard deviation of the growth yields measured at OD_{600nm} after 15 h cultivation are indicated.

The documentation of the growth behavior for the *C. difficile* wild type under salt stress showed that the presence of some compatible solutes promoted enhanced growth traits (Figure 17). While salt stress conditions led to a diminished growth (Suppl. Figure 6B; black), supplementation with carnitine (Suppl. Figure 6D; black) resulted in a growth behavior identical to that of the reference medium (Suppl. Figure 6A; black). Similar protective effects on growth, although slightly decreased, were observed when adding the solutes γ-butyrobetaine, homobetaine, crotonobetaine, DMSP (Suppl. Figure 6L ,N ,J ,R), and glycine betaine (Suppl. Figure 6F; black) in descending order, implying an osmotic protective function in *C. difficile*. Supplementation with proline betaine resulted in a growth improvement only after 17 hours of incubation (Suppl. Figure 6P; black). Choline, on the other hand, was the only one among the tested solutes that was unable to achieve a positive effect on growth under high salinity conditions (Suppl. Figure 6H; black). That prompted us to conclude that choline did not act as an osmoprotective agent in this pathogen. To verify whether the compatible solutes only improve growth under salt stress or possibly also stimulate growth under unstressed conditions, the wild type and *opuCC* mutant were cultivated

only with the addition of osmolytes. For both strains, none of the tested compatible solutes led to an enhanced growth in comparison to the reference medium (Suppl. Figure 6A, C, E, G, I, K, M, O, Q) suggesting that the function of these solutions is limited only to osmoprotection and that they do not serve as an energy source.

As shown above, in addition to the annotated OpuC transporter, *C. difficile* possesses a further putative permease, predicted to be a glycine betaine/carnitine/choline ABC transport system (CDIF630erm_03509/03510) (see 3.1.2). To determine whether osmolytes are transported in *C. difficile* by OpuC and not by this or a further unknown transporter, the growth behavior of the corresponding *C. difficile opuCC* mutant was analyzed in parallel. In contrast to the wild type, whose transporters are all functional, the specific insertion of a group II intron into the gene *opuCC*, led to the expression of a dysfunctional protein unable to bind substrates with the usual affinity and specificity. Accordingly, potential osmoprotection could only be the result of the action of the second, still active transporter. In this assessment no improvement in terms of growth was achieved by adding compatible solutes to the salt-stressed mutant (Figure 17; for details Suppl. Figure 6), thus confirming that the transport of osmolytes occurred by means of OpuC. The expression of the OpuC transporter under high osmolarity conditions was confirmed in transcriptomic studies in the strain *C. difficile* 630 by Scaria and colleagues (200). Furthermore, genes of a second predicted ABC transport system (CD3215/CD3216), which corresponds to the operon CDIF630erm_03509/ 03510, were not registered as differentially expressed during the osmotic shock (200), underlining that OpuC alone is responsible for the osmolyte transport during osmotic stress.

In previous experiments, the general transportability of choline via the $OpuC_{Cdiff}$ transporter was demonstrated (see 3.1.2). The examination was carried out in *B. subtilis*, which is known to be indirectly protected by this osmolyte (45, 74, 81). Choline itself has no osmo-protective function, but is accumulated by bacteria to serve as a precursor for one of the commonest osmolytes, glycine betaine (45, 74). In *C. difficile*, choline displayed no osmoprotective effect, whereas such a function was demonstrated for glycine betaine, indicating that choline is not converted to glycine betaine in this pathogen. In aerobic or facultatively anaerobic

bacteria, this conversion is coupled to the availability of oxygen, which is used as electron acceptor (75). Given the anaerobic nature of *C. difficile*, oxygen is an inaccessible electron acceptor being thereby alternative electron acceptors required. However, even for *E. coli* under anaerobic conditions, including fermentative growth and nitrate as the external electron acceptor, a conversion was so far undocumented (75). Nevertheless, should a conversion for *C. difficile* be possible, this would require the corresponding enzymes. In *B. subtilis,* this process involves two oxidation steps. The first step is catalyzed by the type III alcohol dehydrogenase GbsB resulting in the intermediate glycine betaine aldehyde, while the second oxidation to glycine betaine is catalyzed by glycine betaine aldehyde dehydrogenase GbsA (74, 209). Pathway analyses on the database KEGG (Kyoto Encyclopedia of Genes and Genomes, updated in April 2020) showed that neither GbsA nor GbsB homologous proteins are present in the genome of *C. difficile*. This fact combined with the results of the growth phenotypic studies support the thesis that *C. difficile* is not able to use choline as an osmo protectant by its conversion into glycine betaine after its uptake into the cell by OpuC. This raises the question, which benefit results from the energy-consuming transport of choline for *C. difficile*. Conceivably, it might be used as a carbon source, as has been previously demonstrated for the gut microbe *Proteus mirabilis*. Jameson and colleagues showed that choline was utilized anaerobically, fostering the growth rate and biomass yield in liquid culture as well as enhanced swarming motility on solid medium (210). In this study, no stimulated growth was observed in *C. difficile* when choline or another compatible solute was added to the reference medium, indicating that none of the tested compounds is used as additional carbon and/or energy sources in minimal defined medium. These findings were consistent with results from *C. difficile* (DSM1296^T) from Möller *et al*. (211). Investigations conducted in this working group on the degradation of amine compounds by clostridia proved a strain-specific use of choline as energy and/or carbon source. While the growth of the strains *C. histolyticum* (DSM2158^T), *C. sporogenes* (DSM795^T) or *C. formicoacetieum* (DSM93) was not affected, *C. carnis* (DSM1293^T), *C. formicoaceticum* (DSM94) or *C. sporogenes* (DSM633) showed a stimulated growth. Furthermore, it has been shown that choline, regardless of its use as an energy/carbon source, can be degraded by most strains to form trimethylamine

(TMA). In other strains such as *C. difficile* (DSM1296^T), *C. perfringens* (DSM756^T) and *C. sordellii* (DSM2141^T) TMA production was not confirmed (211). The gene cluster responsible for the anaerobic choline metabolism was first characterized in *Desulfovibrio desulfuricans* in 2012 (212), although the anaerobic degradation of choline to acetaldehyde and TMA was already described in the early 1960s (213). Studies in *Desulfovibrio* identified the choline TMA-lyase CutC and the activating protein CutD to be responsible for catalyzing the reaction (212). A proposed model involves further catabolizing steps from acetaldehyde either to ethanol by the alcohol dehydrogenase CutO or to acetyl-CoA via CutF, an aldehyde dehydrogenase. Acetyl-CoA is then either available for further biosynthesis or it is converted to acetate and ATP via an intermediate product using the phophotransacylase CutH (214). Transcriptomics studies in *P. mirabilis* displayed induced expression of genes coding for choline utilization (*cut*) operon and shell proteins involved in the formation of microcompartments (210). It was shown by Martínez-del Campo and co-workers that the *cut* operon is widely distributed across facultative and strict anaerobic human gut microbes, including members of *Anaerococcus*, *Klebsiella* or *Clostridium* (214). The genome annotation of *C. difficile* 630Δ*erm* (GenBank: CP016318.1) also contains genes encoding the choline TMA lyase (CDIF630erm_01264) and the glycyl radical enzyme activase (CDIF630erm_01265), implying that *C. difficile* 630Δ*erm* (DSM 28645) is capable of generating TMA and acetaldehyde in contrast to the strain *C. difficile* (DSM1296^T) tested by Möller and colleagues. In humans, TMA is absorbed by the liver, where it is further metabolized to trimethylamine-N-oxide (TMAO) which is known to trigger cardiovascular disease (CVD) and colon cancer (214, 215, 216).

Similar to choline, carnitine is known to serve as a compatible solute, final electron acceptor, carbon, nitrogen or energy source in both Gram-negative and Gram-positive bacteria in aerobic and anaerobic environments (76). In *C. difficile*, the osmoprotective function of carnitine was confirmed by its supplementation under high salt stress conditions resulting in an enhanced growth, conversely to choline. Experiments under unstressed conditions with additional carnitine showed no stimulated growth emphasizing on the phenotypic level that carnitine is only used as osmoprotective agent and not as energy source. In order to confirm the hypothesis, the volatile fermentation profile of the *C. difficile* wild type

and the corresponding *opuCC* mutant, grown in the reference medium MDM and MDM supplemented with 1 mM carnitine (Figure 18), was analyzed from samples after reaching OD_{max} (Suppl. Figure 6A & C). Metabolites surpassing the cut-off of $-0.6 \geq \log_2 FC \geq 0.6$ were considered as strongly increased or decreased.

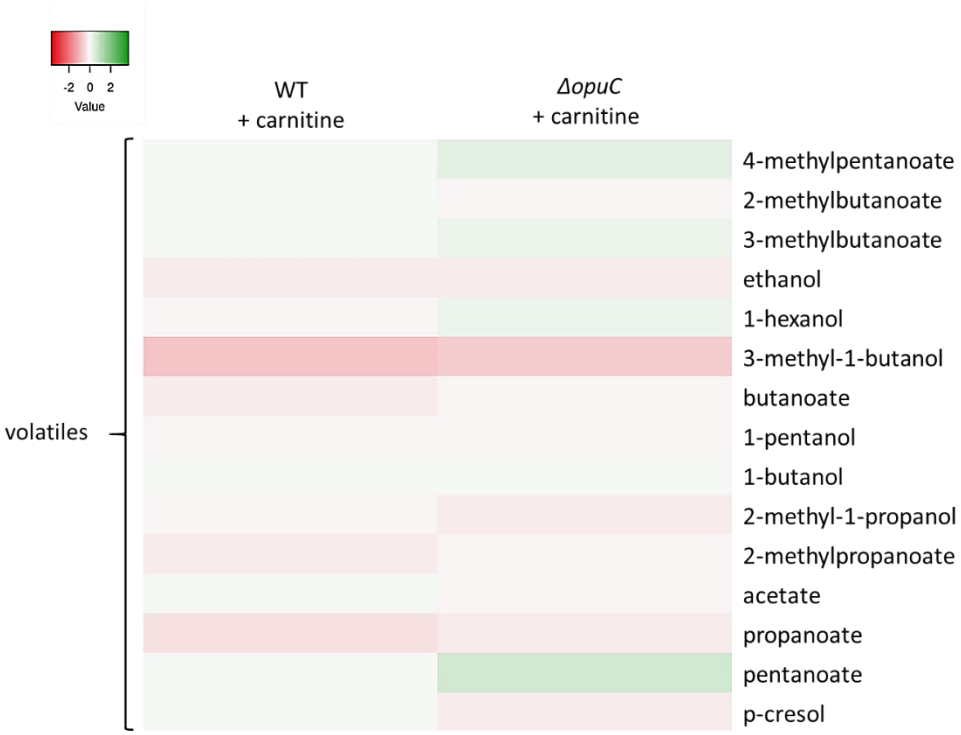

Figure 18 Volatile metabolite profile of *C. difficile* in carnitine supplemented medium.

The relative ratio of volatiles as $\log_2 FC$ is shown. Peak areas of volatiles from cultures grown under salt stress conditions or in high osmolar medium supplemented with carnitine were compared with peak areas of volatiles from untreated cultures. Samples were taken at the mid-exponential growth phase. All measurements were made in quintuplicates. Experiments were performed in cooperation with Dr. Meina Neumann-Schaal.

The analysis showed that $\log_2$fold changes ($\log_2 FC$) of fermentation products produced by both wild type *C. difficile* (wt) and *opuCC* mutant (Δ*opuC*) in the carnitine-supplemented minimal medium did not differ significantly from that of the reference medium (Figure 18; for more details Suppl. Table 1) when a cut-off of $-0.6 \geq \log_2 FC \geq 0.6$ was set. In the wild type none of the analyzed product, except for 3-methyl-1-butanol, was secreted into the medium to higher or lower extents if carnitine was present, indicating that related pathways were not or only weakly affected and therefore carnitine was not used as an energy source. 3-methyl-1-butanol was secreted in the mutant in lower amounts compared to the wild type, while pentanoate accumulated slightly more extracellularly.

Supplementation of carnitine as a carbon or nitrogen source implies in many bacteria, as for choline, the production of TMA. Moreover, in case of carnitine, malic acid is also produced, which enters the TCA cycle (76, 78). However, TMA production could be identified in some members of the human microbiota (217), several *Clostridium* strains are not able to form TMA (218). The reaction is catalyzed by a carnitine oxygenase (217), which is missing in the genome annotation of *C. difficile* 630Δ*erm* (GenBank: CP016318.1), implying that *C. difficile* 630Δ*erm* (DSM 28645) is not able to generate TMA and malic acid from carnitine. Another possible pathway to use carnitine as carbon source involves the conversion to glycine betaine and subsequently to glycine, which is set available to the central metabolism. The reaction to glycine betaine occurs via the intermediate product dehydrocarnitine, catalyzed by L-carnitine dehydrogenase (76, 78). The enzyme search annotated *C. difficile* genome did not project any hits indicating that this pathway is not available for this organism. Another indication for the unlikely performance of both pathways is that they are only described under aerobic conditions (78). Under anoxygenic conditions and in presence of alternative carbon and nitrogen sources, enterobacteria such as *E. coli, Salmonella typhimurium or Proteus vulgaris* use carnitine as alternative electron acceptor if the common acceptor is not available. For this purpose carnitine is utilized via crotonobetaine to γ-butyrobetaine which is catalyzed by the enzymes L-carnitine dehydratase and crotonobetaine reductase (76, 78, 219, 220, 221). The corresponding enzymes could not be identified in *C. difficile* either by searches in the KEGG database or by browsing its genome annotation, indicating that *C. difficile* is unable to convert carnitine into its related compounds, each of which shows an osmoprotective function when the organism is exposed to salt stress.

3.1.6 Morphological adaptation of *C. difficile* 630Δ*erm* to osmotic changes

Growth experiments of *C. difficile* 630Δ*erm* under increasing salt stress conditions showed that a concentration of 350 mM NaCl led to a drastically inhibited growth behavior of this pathogen (see 3.1.4 and Figure 20). But the supplementation of different compatible solutes protects the cells resulting in a reversible growth phenotype comparable to the reference medium wheraeas the corresponding *opuCC* mutant remained inhibited in its growth (Suppl. Figure 6). In this study, one of the first evaluated osmo protective substrates for the wild type was carnitine. To investigate the morphological phenotype of the wild type strain *C. difficile* 630Δ*erm* and the *opuCC* mutant to osmotic changes, field emission scanning microscopy (FESEM) and transmission electron microscopy (TEM) imaging was performed in cooperation with Prof. Dr. Manfred Rohde (HZI, Braunschweig, Germany). Cells were grown anaerobically in MDM as reference medium (Figure 19A), in presence of 1 mM carnitine (Figure 20D), under salt stressed conditions induced by additional 350 mM NaCl (Figure 19B) as well as under salt stressed conditions supplemented with 1 mM carnitine as compatible solute (Figure 19C). Images were taken at the mid-exponential growth phase for each condition.

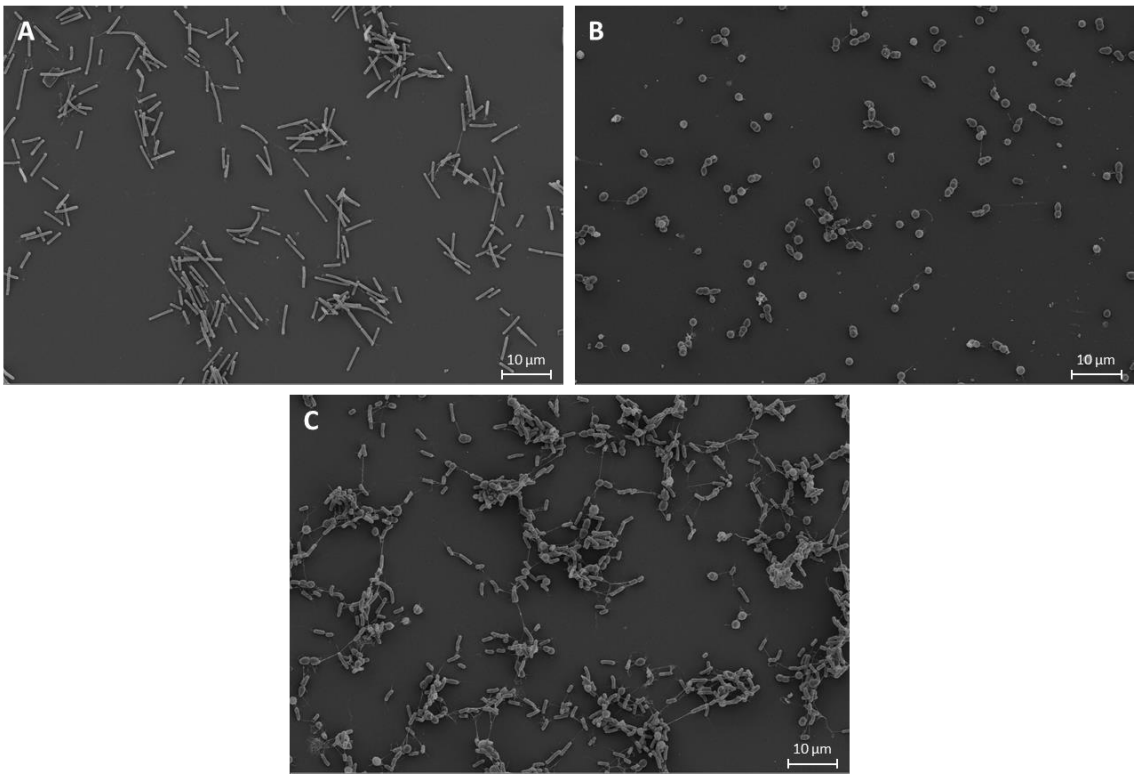

Figure 19 Electron microscopy analyses of *C. difficile* wild type displaying morphological changes as a consequence of its adaptation to high osmolarity.

Cells were grown in MDM as reference medium (A) and under salt stress conditions induced by 350 mM NaCl in the absence (B) or presence of 1 mM carnitine (C) as osmo protectant. For microscopy analysis, cells were harvested during the mid-exponential phase in triplicates. Electron microscopic images were taken by Prof. Dr. Manfred Rohde, HZI, Braunschweig.

Changes of the phenotypical growth behavior in response to osmotic stress correlated with morphological changes. While under unstressed conditions *C. difficile* wild type and mutant showed typical rod-shaped cells with a length of 2 - 10 µm and formation of flagella and pili was observed (Figure 20A and D), salt stress effects reduced growth and a significantly impacted on the cellular shape. Cells were oval to coccoid with a diameter of 1 - 1.5 µm and presented smooth or rough surfaces (Figure 20B). Cell lysis resulting in releasing intracellular content was visible by TEM (Suppl. Figure 7).

Similar observations were made by Waligora and colleagues (222). Cell shrinkage and cell death imply the loss of hydrostatic pressure resulting in dehydration caused by the outflow of water in response to high osmolarity. At the same time, the rounded shape leads to a reduction in surface area and thereby to likely energy savings. Other studies revealed that also cell attachment and biofilm formation are affected by salt stress. Waligora and colleagues showed an

increased adherence, presuming that physico-chemical changes, such as hydrophobicity are induced in the bacterial surface and promote colonization (222). Biofilm formation can also be influenced in different ways. While biofilm formation in high salinity is inhibited for the hypervirulent *C. difficile* strain R20921 and not or only slightly influenced in *C. difficile* 630 (203) its formation is induced in other Clostridia such as the industrial strain *C. ljungdahlii* (223). Morphological changes in response to salt-induced stress were also shown for other bacteria. Thus, in contrast to *C. difficile,* cells of *B. megaterium* or *S. aureus* swell and become larger, and the addition of glycine betaine reverses the cell shape of *S. aureus* to its regular (193, 205). In *C. difficile* wild type, the presence of carnitine led not only to a growth behavior identical to that of the reference medium, but also to the reversion of its cell morphology. Electron microscopy images evidenced that stress-induced coccoid cells were re-formed to rod-shaped bacteria by the supplementation of protective osmolytes (Figure 20C). However, the rods under protective conditions were shorter (1.5 - 3 µm) than those under regular conditions. A lower number of round cells was still present indicating that the organism was still affected. The mutant, on the other hand, remained in the coccoid form despite osmoprotection (Figure 20C). In contrast to unstressed and stressed conditions cells grown in carnitine-contained medium were strongly intertwined to each other forming clusters (Figure 19). These data showed that high salinity and the protection by compatible solutes profoundly affects the cell morphology as well as the growth behavior of *C. difficile* 630Δ*erm.* The supplementation of carnitine to the medium induces no morphological changes (Figure 20D). The influence of salt stress to the metabolism remains unclear and was further investigated.

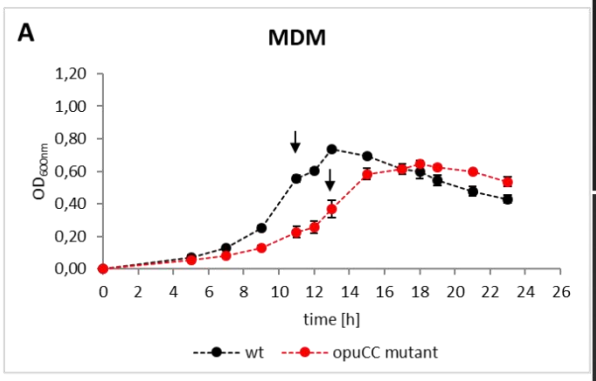
A
MDM
1,20
1,00
0,80
0,60
0,40
0,20
0,00
OD600nm
0 2 4 6 8 10 12 14 16 18 20 22 24 26
time [h]
wt
opuCC mutant

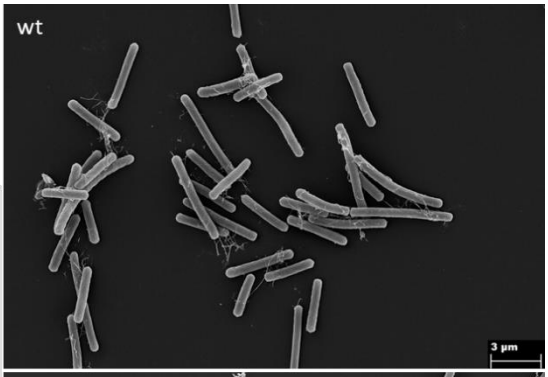
wt
3 µm

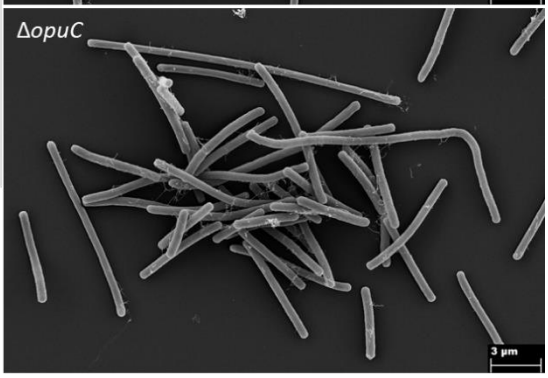
ΔopuC
3 µm

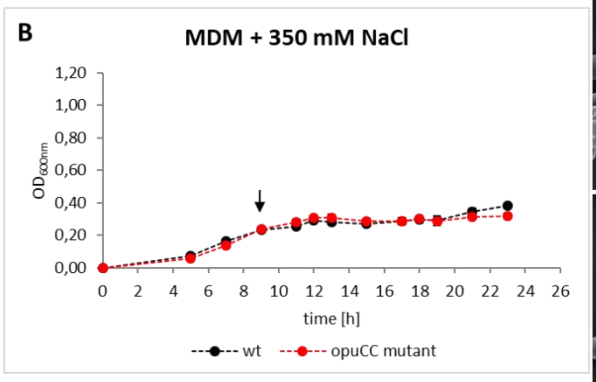
B
MDM + 350 mM NaCl
1,20
1,00
0,80
0,60
0,40
0,20
0,00
OD600nm
0 2 4 6 8 10 12 14 16 18 20 22 24 26
time [h]
wt
opuCC mutant

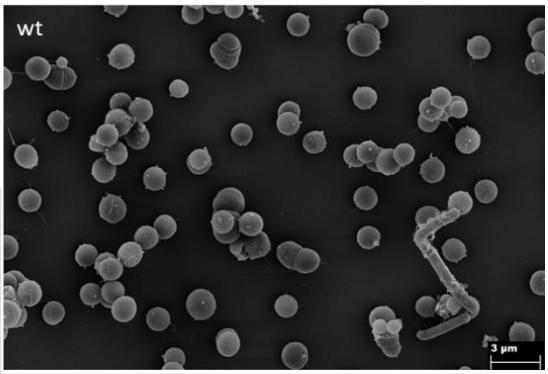
wt
3 µm

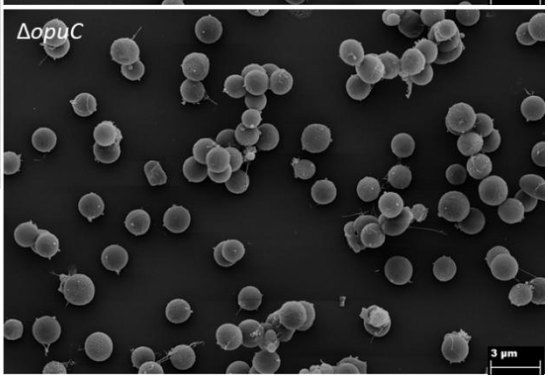
ΔopuC
3 µm

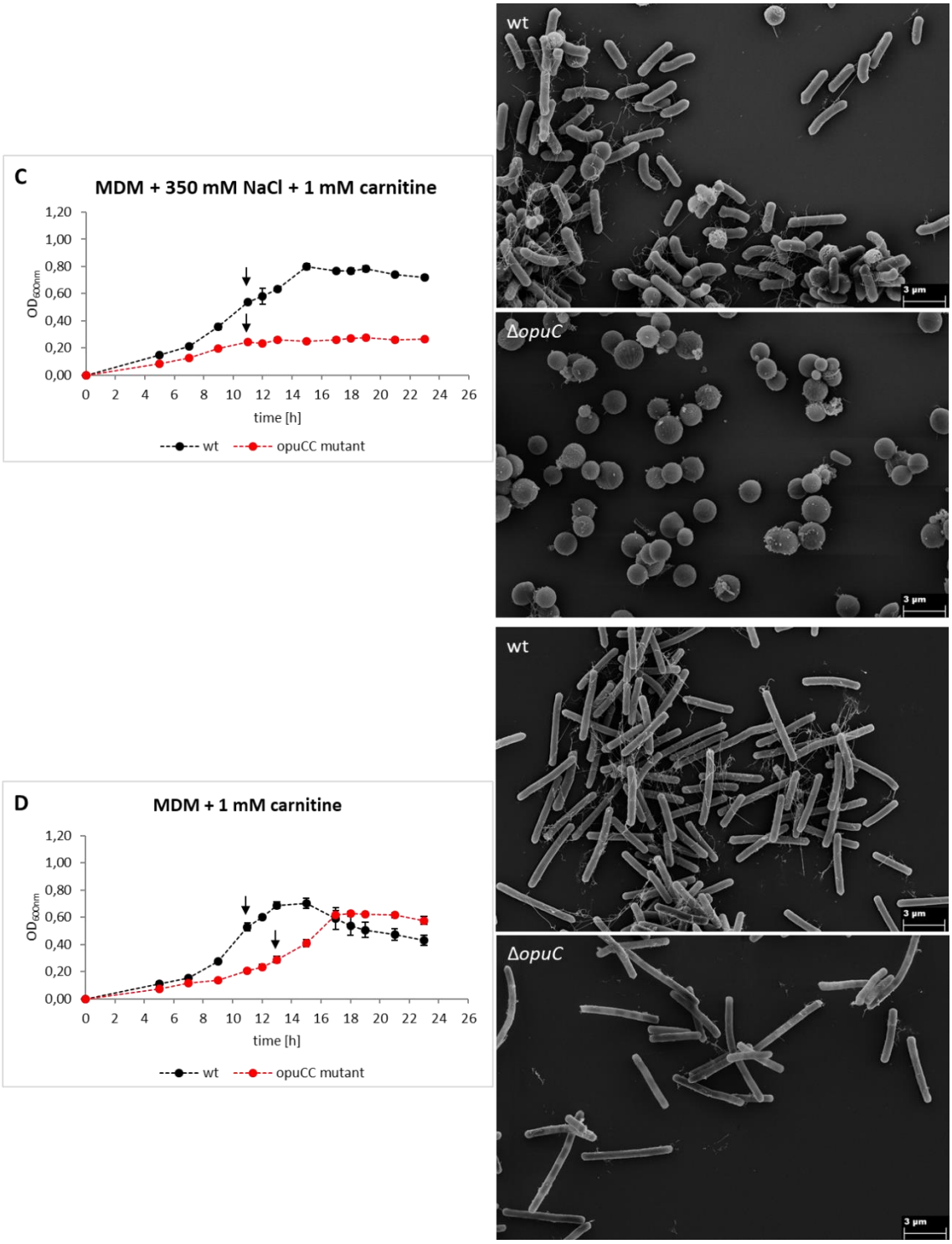

Figure 20 Morphological changes of *C. difficile* 630Δ*erm* and the *opuCC* mutant under conditions of salt stress with and without the osmo protectant carnitine.

C. difficile 630Δ*erm* (wt) and the corresponding *opuCC* mutant (Δ*opuC*) were grown in MDM as reference medium (A), under salt stress conditions induced by 350 mM NaCl in the absence (B) or presence of 1 mM carnitine (C) as osmo protectant and in MDM in presence of 1 mM carnitine (D). For microscopy analysis cells were harvested during the mid-exponential phase in triplicates. Arrows indicate sample collection timepoints. Electron microscopic images were taken by Prof. Dr. Manfred Rohde, HZI, Braunschweig.

3.1.7 Metabolic changes in response to osmotic stress

Previous results of this work display that salt stress elicited by addition of 350 mM NaCl led to impaired growth behavior of *C. difficile* 630Δ*erm* (see 3.1.4 and Figure 20). In contrast, the supplementation of different compatible solutes protects the pathogen resulting in a stimulated growth phenotype (Suppl. Figure 6). Changes of the phenotypical growth behavior in response to osmotic stress correlated also with morphological changes. While under unstressed conditions *C. difficile* shows typical rod-shaped cells, high osmolarity derived in oval to coccoid shaped cells. The additions of the osmo protectant carnitine led to a reversion into unstressed cell morphology (Figure 20). In order to characterize the metabolic consequences of salt stress, changes in the metabolite osmosis patterns and other components involved in the overall metabolism were investigated. For this purpose, *C. difficile* 630Δ*erm* wild type was grown in MDM as reference medium, under high osmolarity conditions induced (350 mM NaCl) in the presence or absence of 1 mM carnitine as osmo protectant. Cells were harvested during the mid-exponential growth phase.

I. Metabolic consequences of salt stress in *C. difficile* wild type strain

A holistic view on metabolic changes was obtained by analyzing the pool of substrates, metabolites, products and co-enzymes both intra- and extracellularly (Figure 27). *C. difficile* was cultivated in a minimal defined medium (MDM) containing the amino acids proline, threonine, leucine, isoleucine, valine, methionine, tryptophan, and cysteine. As in other Clostridia, *C. difficile* ferments these amino acids via the Stickland reactions to generate energy in the form of ATP (34). Inhibited growth under salt stressed conditions implies a downregulated metabolism, while the improvement of growth by adding carnitine indicates a restored metabolism. In order to determine whether this is indeed associated with an altered substrate uptake rate or if it only affects later passages of the metabolism, extracellular amino acid concentrations were determined in pure medium (filled bars) and in the supernatant of *C. difficile* cultures (hatched bars) (Figure 21).

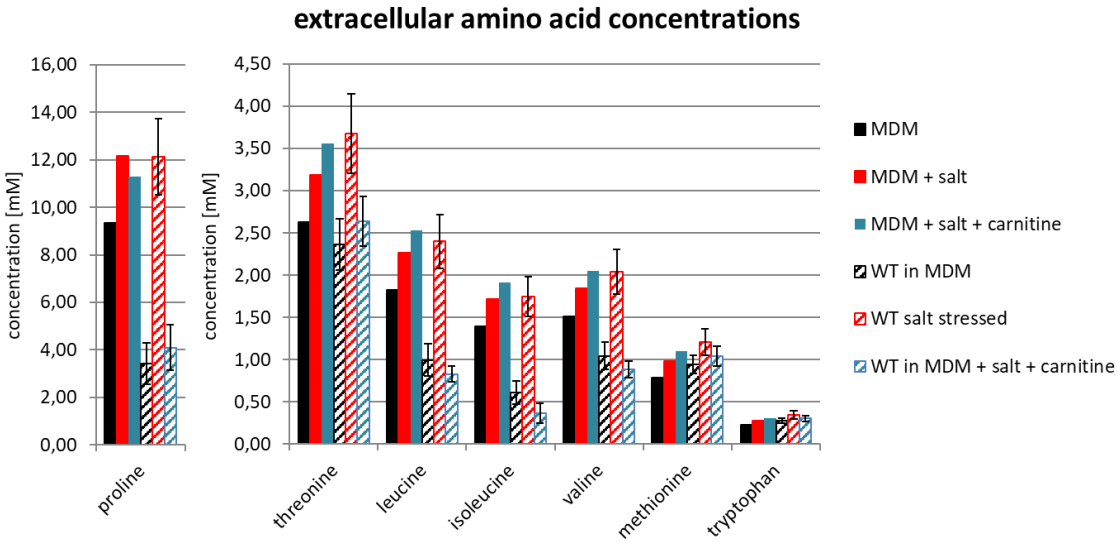

Figure 21 Extracellular accumulation of amino acids.

Amino acids´ concentration in mM contained in pure medium (filled bars; MDM: black; MDM with 350 mM NaCl: red; MDM with salt and 1 mM carnitine: blue) are shown. Concentrations measured in the supernatant of *C. difficile* wild type (wt) cultures are represented by hatched bars. Cells were grown under unstressed (black) and salt stressed conditions (red) as well as supplemented with 1 mM carnitine (blue). Samples were taken at the mid-exponential growth phase. All measurements were made in quintuplicates. Experiments were performed in cooperation with Dr. Meina Neumann-Schaal.

Measurements of the extracellular amino acid concentration revealed drastically reduced amounts of several amino acids, when *C. difficile* was grown in MDM (Figure 21; black). Especially, proline, leucine and isoleucine were highly taken up in agreement with previous observations where proline and leucine were declared as preferred amino acids (27). A moderate uptake of threonine and valine was detected. In contrast, under salt stressed conditions (red) similar concentrations compared to pure medium were registered. In the presence of carnitine, the wild type resumed amino acid intake, which was deduced from low extracellular detection (blue). Similar observations were made for cysteine, which is normally consumed from the beginning of growth by degradation to pyruvate and thus being also part of the central carbon metabolism (27). In conclusion, the extracellular accumulation of amino acids as result of hyperosmolarity suggested a decreased uptake. Similar observations were made in transcriptomics studies of salt stressed *C. ljungdahlii* in which genes involved in amino acid transport and metabolism were significantly down-regulated (223). As a consequence of reduced amino acid uptake, a reduced Stickland fermentation as well as a decreased carbon metabolism was presumed.

In order to identify which pathways are potentially affected by salt stress and the impact that carnitine brought about, further analyses were performed by closely inspecting intracellular metabolites and co-enzymes as well as exported metabolites and volatile compounds in comparison to unstressed conditions. Initial measurements showed that amino acid uptake was reduced when cells were exposed to salt stress conditions. Nevertheless, higher intracellular amino acid concentrations, especially for proline, leucine, isoleucine valine and threonine, were detected under salt stress in comparison to the untreated control (Figure 22; for more details Suppl. Table 2A) suggesting that subsequent Stickland reactions for energy production were inhibited.

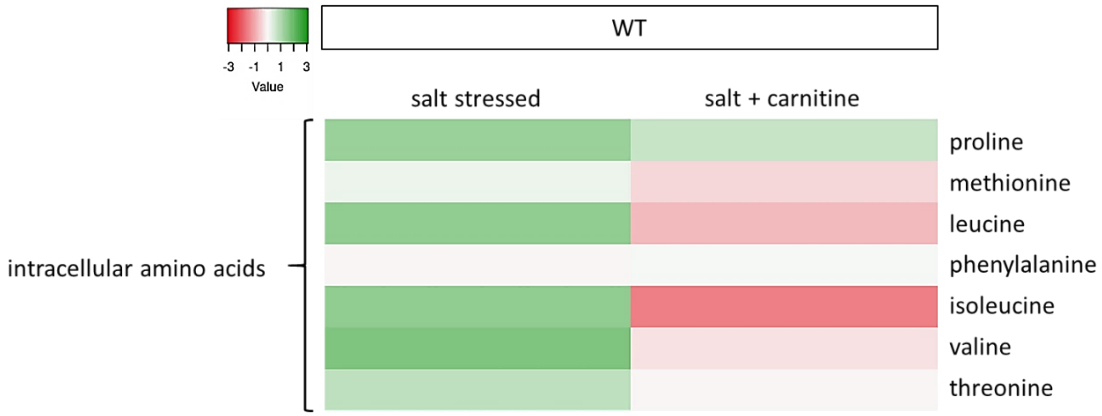

Figure 22 Intracellular accumulation amino acids.

Shown is the relative ratio of intracellular amino acids as log_2FC. Peak areas of amino acids from *C. difficile* wild type (wt) cultures grown under salt stress conditions or in high osmolar medium supplemented with carnitine were compared with peak areas of amino acids from untreated cultures. Samples were taken at the mid-exponential growth phase. All measurements were made in quintuplicates. Experiments were performed in cooperation with Dr. Meina Neumann-Schaal.

The Stickland reactions are characterized as the coupling of oxidation and reduction of amino acid pairs with simultaneous formation of their corresponding organic acids involving several co-enzymes. Energy is mainly conserved in form of ATP by substrate level phosphorylation (27). While amino acids such as isoleucine, valine or alanine serve as effective electron donors in the oxidative pathway, the amino acids proline, glycine or methionine act as electron acceptors in the reductive pathway. Leucine, phenylalanine and tyrosine can function both as electron acceptors and donors, resulting in different pathway-dependent products (32, 34, 36, 38). Thus, leucine is converted into isovalerate in the oxidative pathway, while isocaproate is derived from the reductive pathway (32).

Salt stress conditions led to an accumulation of intermediates and Stickland fermentation products in the cell (Figure 23; for more details Suppl. Table 2B and C) and therefore they were not fully metabolized or exported.

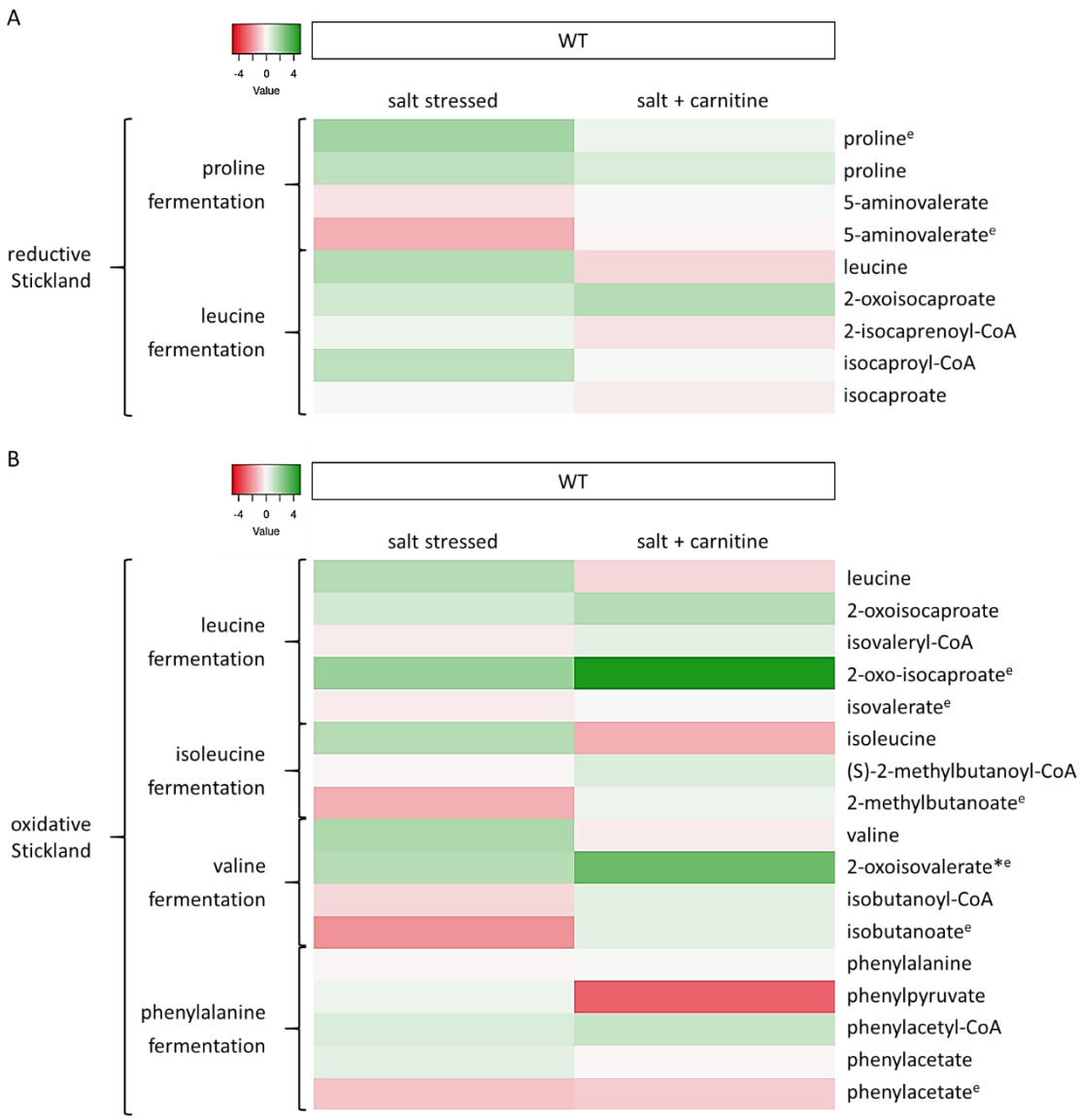

Figure 23 The effect of high salinity on various Stickland fermentation reactions.

The relative ratio of intracellular Stickland reaction partners as log_2FC is shown. A) Metabolites involved in the reductive Stickland reactions are displayed. B) Metabolites of the oxidative Stickland pathway are shown. Peak areas of intermediates and products from *C. difficile* wild type (wt) cultures grown under salt stress conditions or in high osmolar medium supplemented with carnitine were compared with peak areas of compounds from untreated cultures. Extracellular detected metabolites are indicated by "e". "*" indicates intermediates, which were not detected in MDM grown cultures. Samples were taken at the mid-exponential growth phase. All measurements were made in quintuplicates. Experiments were performed in cooperation with Dr. Meina Neumann-Schaal.

This implies that enzymes of the lower part of the pathway may be more affected by high salt concentrations than early enzymes. Even proline as highly preferred amino acid is consumed to a lower extent as indicated by reduced amounts of its corresponding fermentation product 5-aminovalerate in the culture supernatant. Lower concentrations of 5-aminovalerate may the result of salt stress-related inhibition of the proline reductase, although these considerations are in conflict with RNAseq data from Scaria *et al.* (200). In these studies, no differential gene expression for proline reductase was found for 3 of 4 strains of *Clostridium*, including *C. difficile 630*. However, the fourth strain QCD_32g58 showed an increased expression (200). As our considerations are in conflict with Scaria´s observations, further *in vitro* activity assessments must be performed to evaluate proline reduction. *C. difficile* requires proline for optimal growth (27, 224), while other bacteria use it not only as a nutrient but also as an osmo-protective agent, such as *B. subtilis*. In this case, proline is taken up by an osmotically inducible transporter OpuE or can be synthesized from its precursor glutamate, which is another compatible solute (225). The transfer of proline by OpuC was not confirmed in *B. subtilis*. OpuE shows marked similarities to another proline transporter PutP, whose occurrence was registered in *E. coli*, *S. typhimurium* and *S. aureus* (83), but the latter remains inactive under salt stress (226). PutP serves exclusively the purpose of acquiring proline as carbon and nitrogen source (226). The genome annotation of *C. difficile* contains also genes which encode for PutP, but not for OpuE, which may point to a non-usage of proline as osmolyte supported by the reduced uptake of amino acids. Due to the addition of carnitine, equal concentrations of extracellular fermentation products could be detected as in the unaffected conditions. Furthermore, the intracellular amino acid concentrations displayed similar or lower values (Figure 22), implying improved energy production via Stickland reactions. Nevertheless, intracellular proline and intermediates of the oxidative Stickland pathway remained still increased.

Like the other amino acids involved in the oxidative Stickland reaction, threonine was accumulated both extracellularly and intracellularly (Figure 24; for more details Suppl. Table 2D).

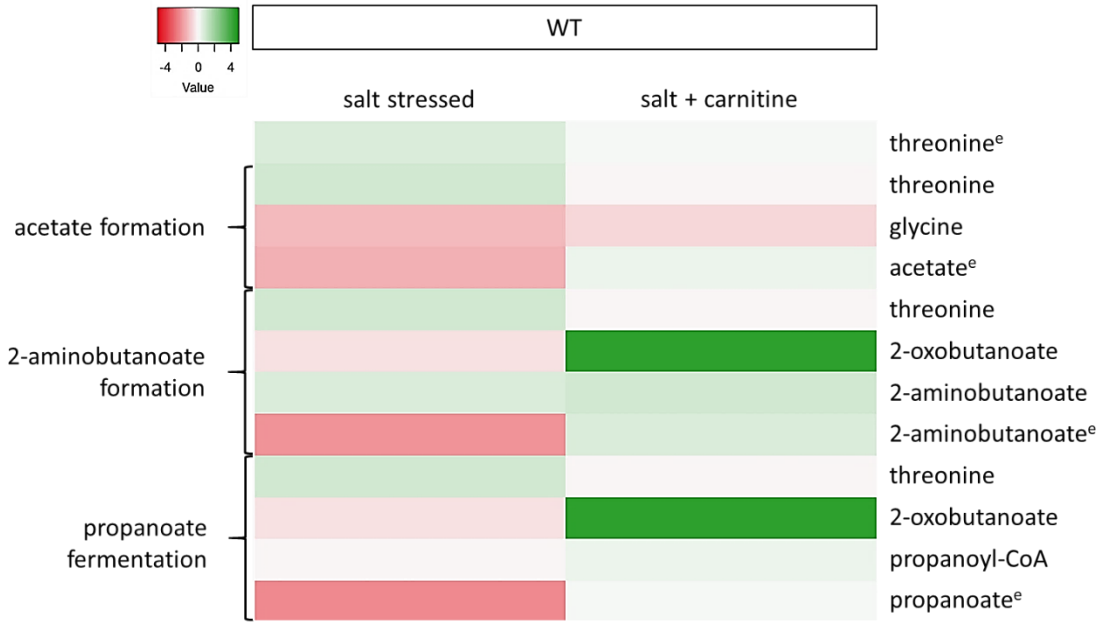

Figure 24 Threonine-associated metabolic pathways decreased under salt stress.

The relative ratio of intracellular metabolites as log_2FC is shown. Peak areas of metabolites related to threonine degradation from *C. difficile* wild type (wt) cultures grown under salt stress conditions or in high osmolar medium supplemented with carnitine were compared with peak areas of compounds from untreated cultures. Extracellularly detected metabolites are indicated by “e”. Samples were taken at the mid-exponential growth phase. All measurements were made in quintuplicates. Experiments were performed in cooperation with Dr. Meina Neumann-Schaal.

In general, threonine can be used to form acetate via glycine and 2-aminobutanoate via 2-oxobutanoate (227). While glycine and acetate were less abundant under salt stress, intracellularly higher amounts of 2-aminobutanoate were detected. However, only minor amounts were detected extracellularly, indicating that the export was limited. Another reaction that starts with 2-oxobutanoate is the production of propanoate involving the co-enzyme propanoyl-CoA (227). Like 2-aminobutanoate, reduced amounts of propanoate were detected as a volatile compound. The addition of carnitine resulted in improved uptake and metabolism of threonine with increasing amounts of 2-oxobutanoate, 2-aminobutanoate and propanoate. While the latter one showed equal concentrations such as the unstressed control, the other intermediates reached even higher concentrations.

In contrast to the Stickland reactions, the glycolysis was not affected by hypoosmotic stress (Figure 25A; for more details Suppl. Table 2E) resulting in similar amounts of pyruvate.

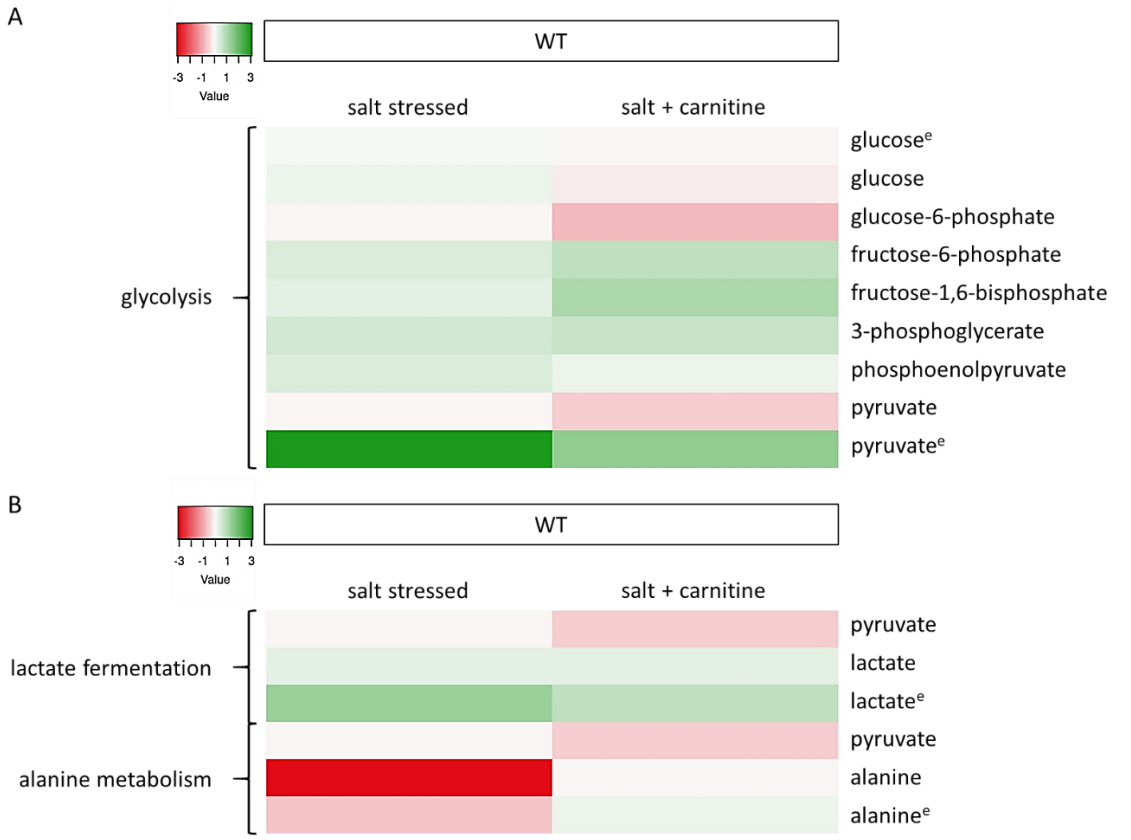

Figure 25 The effect of high salinity to glycolysis and pyruvate related pathways.

The relative ratio of intracellular metabolites as log_2FC is shown. Peak areas of metabolites related to glycolysis (A) and pyruvate degradation (B) from *C. difficile* wild type (wt) cultures grown under salt stress conditions or in high osmolar medium supplemented with carnitine were compared with peak areas of compounds from untreated cultures. Extracellularly detected metabolites are indicated by "e". Samples were taken at the mid-exponential growth phase. All measurements were made in quintuplicates. Experiments were performed in cooperation with Dr. Meina Neumann-Schaal.

Global metabolic analysis of 15 different species performed by Sévin and colleagues resulted in lower glycolysis endeavor due to the accumulation of intermediates of the lower part (228). With the addition of carnitine, intermediate products such as fructose-6-phosphate and fructose-1,6-bisphosphate were accumulated. Nevertheless, more pyruvate was exported under both conditions in contrast to the unstressed control. The degradation of the key metabolite pyruvate may be conducted through diverse metabolic wires. On the one hand pyruvate can be converted to lactate (229), which accumulates extracellularly as the only fermentation product under both tested conditions (Figure 25B; for more details Suppl. Table 2F). On the other hand, starting from pyruvate, L-alanine can be synthesized or acetyl-CoA can be generated via oxidative decarboxylation

(229). Both processes were hindered under salt stress but again compensated by the addition of carnitine (Figure 25B and Figure 26).

The reduced abundance of the second key metabolite acetyl-CoA had especially a negative impact on the following formation of acetate as a volatile compound which was encountered strongly reduced under salt stress. Another pathway involving acetyl-CoA is the tricarboxylic acid (TCA) cycle, which begins with the synthesis of citric acid by transferring this co-enzyme to oxaloacetate (229). The visibly reduced amount of acetyl-CoA resulted in a slightly increase (still below the cut-off $log_2FC \geq 0.6$) of oxaloacetate, as the conversion to citrate can no longer take place at a sufficient pace. Citrate and the following intermediates were not detected, resulting a drop in 2-oxoglutarate (Figure 26; for more details Suppl. Table 2G).

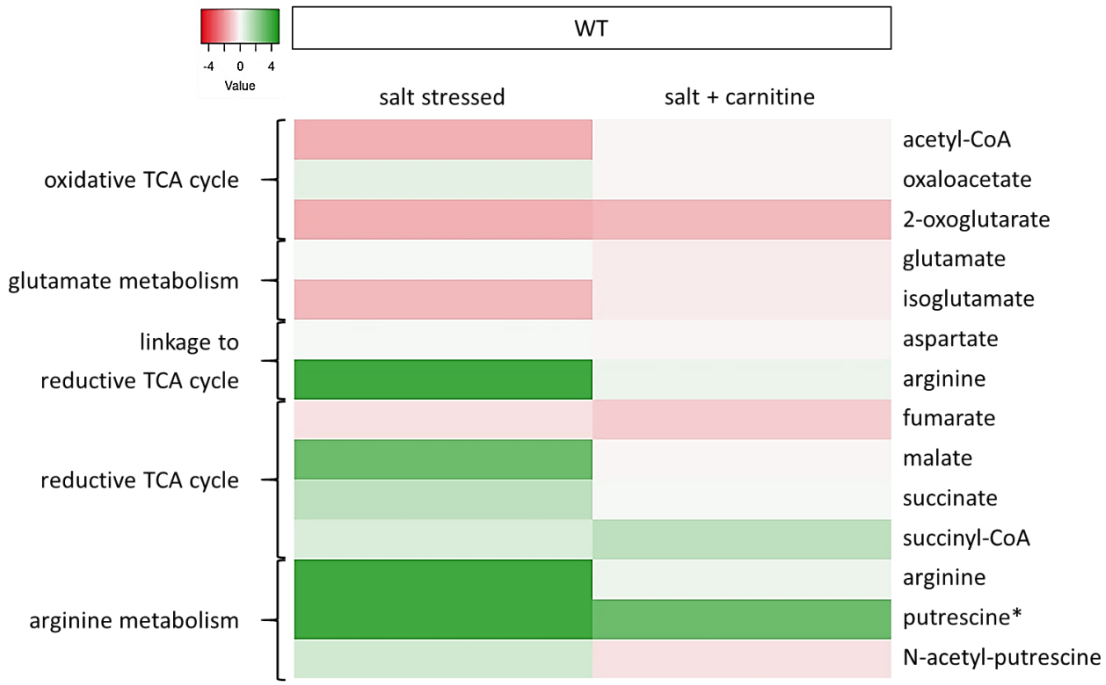

Figure 26 Salt stress lead to accumulation of intermediates involved in the TCA cycle.

The relative ratio of intracellular metabolites as log_2FC is shown. Peak areas of intermediates involved in the TCA cycle from *C. difficile* wild type (wt) cultures grown under salt stress conditions or in high osmolar medium supplemented with carnitine were compared with peak areas of compounds from untreated cultures. Intermediates which were not detected in the untreated control are indicated by "*". Samples were taken at the mid-exponential growth phase. All measurements were made in quintuplicates. Experiments were performed in cooperation with Dr. Meina Neumann-Schaal.

Since the metabolic interplay between 2-oxoglutarate and succinyl-CoA is absent in *C. difficile* 630Δ*erm*, 2-oxoglutarate forms the final product of the oxidative TCA cycle and it is subsequently delivered into the glutamate metabolism (229). Here, 2-oxoglutarate is usually converted via glutamate into iso-glutamate. In *E. coli* glutamate is accumulated as compatible solute (228), however in *C. difficile* the concentrations of glutamate did not differ significantly in the tested conditions, in contrast to its related compound isoglutamate, which was most frequently detected in *C. difficile* under non-stress growth conditions, but it was present to lower extents under highly saline conditions. While intermediates of the oxidative TCA cycle were decreased or not detected, intermediates of the reductive TCA cycle, ranging from malate to succinyl-CoA, were accumulated with the exception of fumarate (Figure 26; for more details Suppl. Table 2G). The formed succinyl-CoA is further used for the synthesis of methionine or in the formation butanoate via crotonyl-CoA (229). The latter pathway remained unaffected despite high salt concentration (Figure 27; for more details Suppl. Table 2H). In contrast to the TCA cycle of other microorganisms, the direct linkage between malate and oxaloacetate does not exist in *C. difficile*. Instead, the connection between the oxidative and reductive part is maintained via aspartate or via pyruvate and malate (229). The abundance of aspartate under salt stress conditions was equal to that of unstressed conditions indicating that production and degradation was still balanced. Aspartate is converted to fumarate via arginine or IMP (inosinmonophosphat) biosynthesis (229). Increasing amounts of arginine, which were also previously found in *E. coli* (228) and its metabolic products putrescine as well as N-acetylputrescine indicated its increased biosynthesis and metabolism. On the other hand, the fumarate content was slightly decreased, which can be attributed to reduced fumarate formation and/or increased conversion of fumarate to malate or succinate as these were significantly accumulated. Metabolic changes within the TCA cycle, arginine biosynthesis and catabolism, and acetate formation are recovered by carnitine addition with a few exceptions such as putrescine and 2-oxoglutarate.

These data outlined the global metabolic response of *C. difficile* to osmotic stress, which is reflected in a decreased uptake of amino acids, an accumulation of Stickland intermediates coupled with a reduced export of fermentation products. The only increased and secreted fermentation product was lactate under salt

stress in presence or absence of carnitine. Even strongly preferred amino acids such as cysteine and proline were consumed to a lower extent. Furthermore, intermediates of the reductive TCA cycle were more abundant (Figure 27A). The compatible solute carnitine mostly restored the original metabolism and thus it seems to act as an osmotic protectant. Only few metabolites remained altered involved in the oxidative Stickland pathways and the glycolysis (Figure 27B).

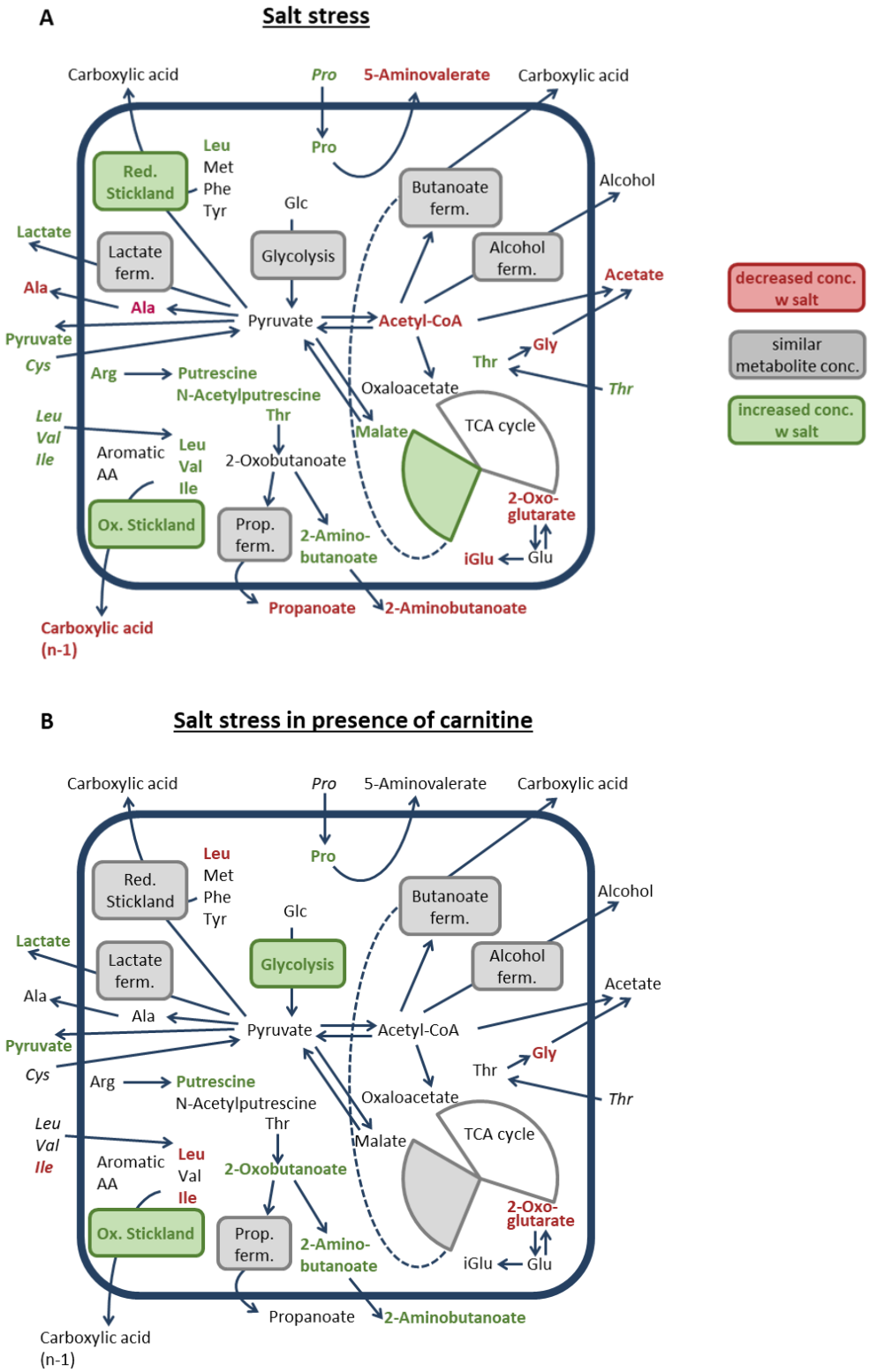

Figure 27 Schematic overview of metabolic changes in *C. difficile* during salt stress and osmo-protection by carnitine.

A) Schematic overview of salt stress affected metabolic pathways. B) Schematic overview of metabolic pathways changed in presence of 1 mM carnitine. An increase in metabolic compounds compared to the unaffected wild type control is displayed in green, while a decrease is shown in red and no significant change in grey. The illustration was developed by our collaborator Dr. Meina Neumann-Schaal.

II. The metabolic profile is not restored by carnitine in the *opuCC* mutant

A shown above, *C. difficile* possesses an OpuC transporter, which is able to traffic several compatible solutes into the cell. Furthermore, it was shown, that almost all of them have an osmotic protection function. Carnitine presented the most beneficial effect on growth phenotypic level and it was able to restore the metabolism with minor exceptions of the wild type. A corresponding mutant confirmed that OpuC is responsible for the osmolyte transport. Whether the phenotypic results were also reflected on the metabolomic level was further investigated. For this purpose a volatile fermentation profile of the wild type and the *opuCC* mutant was characterized under salt stress conditions in presence or absence of carnitine in comparison to the unstressed control (Figure 28; for more details Suppl. Table 3). Sample were taken after reaching the maximum OD, at the early stationary phase.

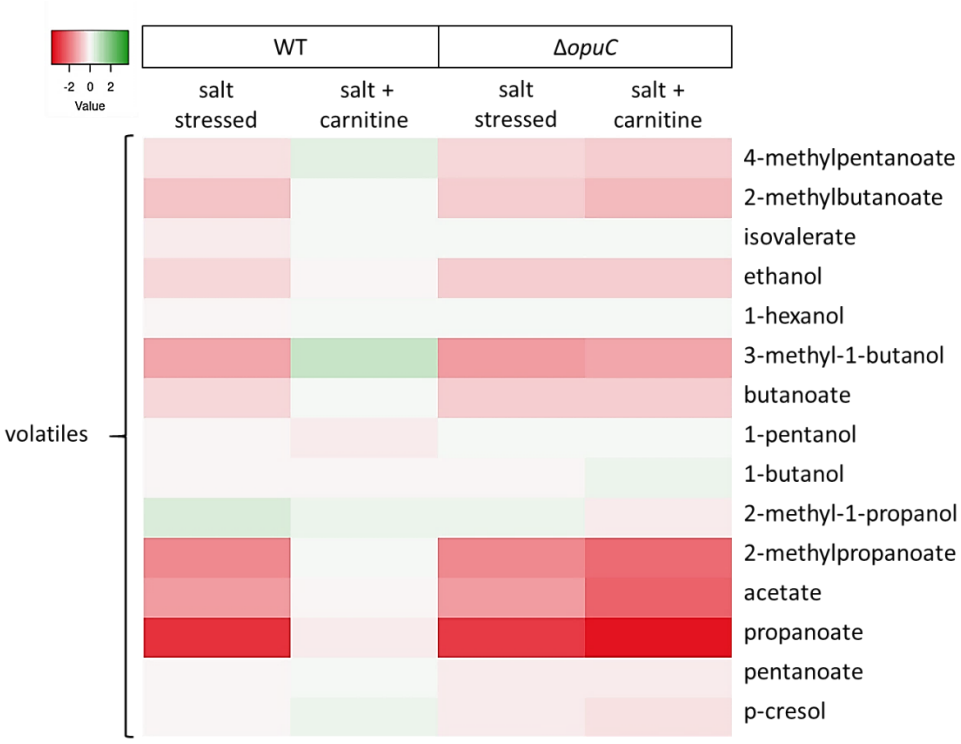

Figure 28 Fermentation profile of *C. difficile* and the *opuCC* mutant under salt stressed and osmo-protected conditions by carnitine.

C. difficile wild type (wt) and the corresponding *opuCC* mutant (Δ*opuC*) were grown in the reference medium MDM, under salt stressed conditions as well as supplemented with 1 mM carnitine. Samples were taken after reaching OD_{max}. All measurements were made in quintuplicates. Indicated is the log_2FC to the unstressed reference. Metabolites outside the cut-off $-0.6 \geq log_2FC \geq 0.6$ were assessed as strongly increased or strongly decreased. Experiments were performed in cooperation with Dr. Meina Neumann-Schaal.

In both strains osmotic stress led to decreased amounts of typical fermentation products involved in the oxidative and reductive Stickland pathway such as butanoate as well as isocaproate. While acetate, propanoate and isobutanoate were reduced very significantly, alcohol fermentation products remained unaffected. As previously shown, the addition of carnitine restores almost completely the metabolism of the wild type to the level of the unaffected control. The metabolic profile of the mutant was not rescued upon addition of carnitine confirming thereby that carnitine transport is dependent on the assembly of a functional OpuC transporter.

3.1.8 Toxin production

The pathogenicity of *C. difficile* is known to be strongly associated to the formation the enterotoxin A (TcdA), cytotoxin B (TcdB) and the binary toxin CDT, which represent the major virulence factors. An efficient production of these toxins is normally detectable in the late exponential or stationary phase, which correlates with cultures from 48 - 72 h incubation. Additionally, the toxin production can vary dependent on the central carbon metabolism and nutrient availability, especially amino acids occurrence (26, 27). In order to determine the influence of salt stress and carnitine as major osmoprotectant to the toxin formation in *C. difficile* wild type and its isogenic *opuCC* mutant, cultures were grown anaerobically for 58 h in MDM as reference medium, under salt stress conditions (350 mM NaCl) as well as in the presence or absence of 1 mM carnitine. The extracellular TcdA concentration was determined by an ELISA assay (Figure 29).

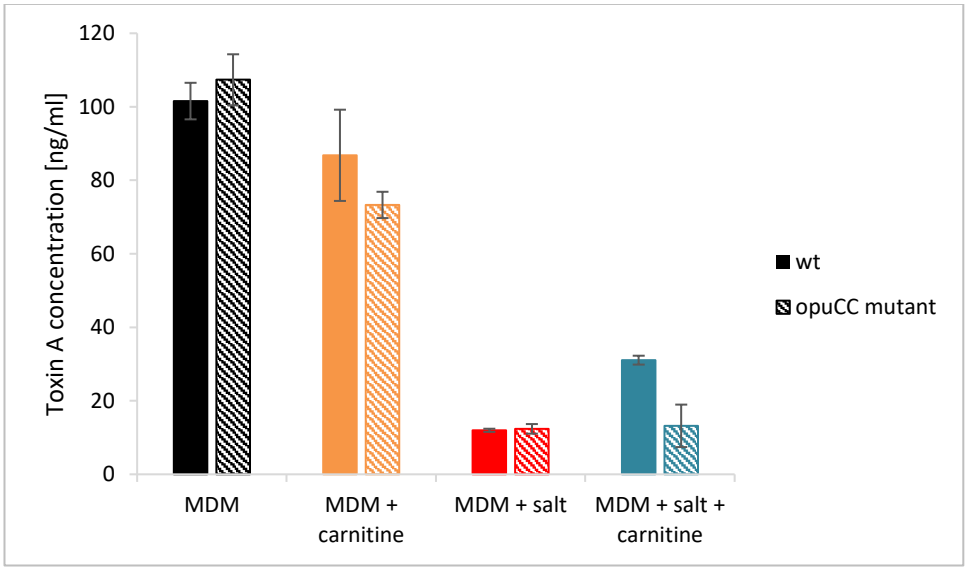

Figure 29 Extracellular Toxin A concentration of *C. difficile* 630Δ*erm* (wt) and the corresponding *opuCC* mutant grown in MDM, under salt stress conditions and supplemented with the osmo-protectant carnitine.

Salt stress was induced by 350 mM NaCl. Carnitine was supplemented in a concentration of 1 mM. Cells were harvested after 52 h cultivation. The Toxin A quantification was performed in triplicates using the "*Clostridium difficile* Toxin A or B quanti Kit" (tgc Biomics, Bingen am Rhein, Germany). Standard deviations are given.

Both strains, *C. difficile* wild type and its isogenic *opuCC* mutant presented no extracellular TcdB or its concentration was below the detection limit. Hence, TcdB production is not represented in the graph above. In contrast, TcdA formation was detectable in all tested conditions (Figure 29). In the reference medium MDM (black) a TcdA concentration of 101.55 ng/ml for the wild type (filled bars) and 107.35 ng/ml for the *opuCC* mutant (hatched bars) was quantified. Considering and including the standard deviation, an inactivation of the OpuC transporter did not appear to have an influence on the toxin secretion levels. The supplementation of carnitine (blue) resulted in slightly reduced TcdA concentration, which was quantified to 86.79 ng/ml for the wild type and 73.29 ng/ml for the *opuCC* mutant. A drastic reduction of toxin formation was detected when both strains were exposed to salt stress (red). Here 11.97 ng/ml and 12.35 ng/ml TcdA in the wild type and the mutant were produced, respectively. The supplementation of carnitine to high osmolarity (orange) resulted in slightly increased TcdA concentration for the wild type (31.06 ng/ml), whereas the mutant´s production remained unaffected (13.18 ng/ml).

As shown above (see 3.1.5 and 3.1.6), high salinity led to an inhibited growth behavior of *C. difficile* and no detectable growth for the corresponding *opuCC*-deficient mutant. Moreover, high osmolarity causes cell lysis and cell death. Accordingly, the significant decrease in TcdA concentration can be attributed to reduced cell density or impaired metabolism. Furthermore, it was shown that the availability of carnitine to rescue the phenotypic growth behavior in the wild type was completely dependent on the production of a functional OpuC transporter. In contrast, toxin production was not restored to the same extent. Even if a slight increase in the toxin concentration was detected, it remained reduced by 2/3. In this case, cell density and toxin formation do not correlate. This is inconsistent with other observations where virulence factors of other pathogens are more effective at high cell densities due to quorum sensing. Darkoh and colleagues demonstrated also for *C. difficile* that toxin production is controlled by cell-cell communication and suggested that the toxin-inducible signal is a novel thiolactone (25). Probably this signal is blocked by high salt concentrations and thus disrupts cell communication to induce toxin production despite high cell densities. Furthermore, changes in metabolism may have led to reduced toxin production. The influence of various amino acids, carbohydrates and the central metabolism on toxin production has been described multiple ways (26, 27, 29, 30, 230). Karlsson and colleagues (29) demonstrated that all essential amino acids for *C. difficile* especially cysteine and proline reduced toxin formation, which was confirmed by Dubois and colleagues 2016 (231). Other studies suggested that the process leading to toxin reduction is more complex than the abundance of individual amino acids. It is rather presumed that multiple metabolic pathways of the central metabolism influence toxin production (26). In this study, metabolomic analysis of *C. difficile* wild type under salt stress displayed an accumulation of several amino acids, especially of cysteine, proline, threonine, Stickland reaction partners as well as products of the central carbon metabolism such as pyruvate (see 3.1.7). This observation could be a further explanation for the toxin reduction besides the reduced cell density, although it should be noted here that metabolome analyses were generated from the exponential growth phase and cannot be directly extrapolated to the stationary phase without caution. Upon addition of carnitine the fermentation of amino acids was restored as well as parts of the central carbon metabolism (e.g. TCA cycle). However, there are

still limitations, e.g. in the oxidative Stickland fermentation and the existing extracellular accumulation of pyruvate. Dubois *et al.* concluded that pyruvate could probably act as metabolic signal mediating the repression of toxin formation (231). These results may explain the still strongly impaired toxin production despite high cell density. Furthermore, a direct inhibition of the toxin biosynthesis and of the toxin export by salt is conceivable.

3.2 Transcriptional and metabolic network of PerR-dependent metabolism

The regulator PerR is described as repressor protein that is capable sensing hydrogen peroxide and regulating the response to oxidative stress in various bacteria (141, 142, 143). In its dimeric active form, PerR is bound to the PerR DNA-boxes, suppressing the transcription of PerR-regulated genes (141, 145, 146). In the presence of H_2O_2 PerR undergoes a conformational change leading to the dissociation of the protein from DNA and the de-repression of PerR-regulated genes (141, 144, 146, 148). Recent studies on *C. difficile* 630Δ*erm* revealed a constitutive de-repression of PerR-regulated genes involved in the oxidative stress response in contrast to its parental strain *C. difficile* 630. DNA-*perR*-sequence alignments of both strains, *C. difficile* 630 and *C. difficile* 630Δ*erm*, unveiled an amino acid exchange from threonine to alanine at position 41 within the helix-turn-helix motif of the DNA binding domain (232). These studies were based on band shift assays which are reliant on DNA-protein concentration. It was observed that within a specific protein concentration range the PerR protein from *C. difficile* 630Δ*erm* did not associate with its promotor-localized binding box. Nevertheless, previous analysis of our laboratory comparing transcriptomics changes between *C. difficile* 630Δ*erm* and the corresponding *perR* mutant showed pronounced PerR-dependent regulation of genes involved in amino acid metabolism and energy conversion (2). This indicates that PerR repression is likely dependent on protein concentration as a factor of affinity. The aim of this work was to define a more precise characterization of H_2O_2-independent PerR regulation using a combined systems biology approach encompassing transcriptome and metabolome analyses.

3.2.1 Growth phenotype of the *perR* mutant

First, the anaerobic growth behavior of the wild type and a corresponding *perR* mutant in the nutrient richer CDM medium (CDMM) as well as in the minimal defined medium MDM was documented over a period of 26 hours (Figure 30).

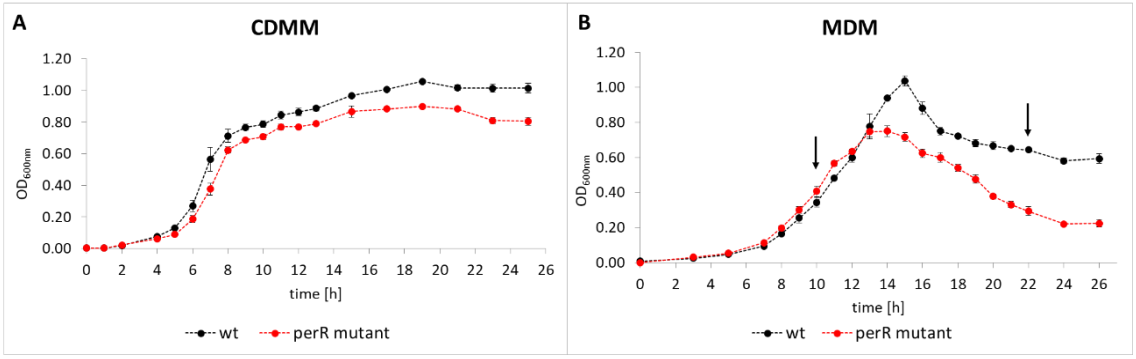

Figure 30 Growth behavior of *C. difficile* wild type and *perR* mutant under nutrient limited conditions.

A) *C. difficile* 630Δerm (●; wt) and *perR* mutant (●) were grown in CDMM containing casamino acids. The *perR* mutant shows no significant growth phenotype compared to wild type. B) In minimal defined medium (MDM) containing the essential amino acids for *C. difficile* a significant growth impairment is exhibited by the *perR* mutant (●) compared to the wild type (●) in the stationary phase. Arrows indicate the timepoints selected to withdraw samples for further transcriptomic and metabolomic studies.

The phenotypic growth behavior of the *perR* mutant (red) did not differ significantly from that of the wild type (black) when the cells were cultured in CDMM (Figure 30A). However, a slightly reduced growth was observed in the mutant at the beginning of the stationary growth phase. This observation became clearer when the organism was cultivated in MDM (Figure 30B), indicating that PerR plays a role in the stationary growth phase, in which a large number of nutrients are already consumed. That this effect is more pronounced in the nutrient-poorer MDM could also be an indication of a nutrient-dependent regulation of PerR. While CDMM is a minimal medium containing a mix of casamino acids, MDM is a defined medium consisting of only the essential amino acids (cysteine, isoleucine, leucine, tryptophan, methionine, proline, valine) and threonine, which are the primary source of energy produced via Stickland fermentation in *C. difficile* (27).

3.2.2 Growth phase dependent PerR-regulation

Destruction of *perR* in *C. difficile* resulted in a significantly inhibited growth phenotype during the stationary phase compared to the wild type, when the cells were cultivated in minimally defined medium. This suggested that *perR* regulation is mostly triggered during this growth phase. To define the transcriptional and metabolic network of the PerR-dependent metabolism, a combined systems biology approach was performed from MDM-grown samples collected in the exponential and stationary phase (Figure 30). The transcriptome or metabolome level of the *perR* mutant was compared to that of the wild type in the respective phase (*perR* mutant vs. wt). A cut-off of $-0.6 \geq \log_2 FC \geq 0.6$ was determined for metabolites with different frequencies. Genes with a cut-off of $-1 \geq \log_2 FC \geq 1$ were considered as differentially expressed.

I. Predicted PerR DNA binding motif

Based on previous transcriptomic data (2) as well as transcriptomic data generated in this work, a PerR binding sequence was defined with the software MEME (189) using DNA sequences located 250 nucleotides (nt) upstream of differentially regulated genes.

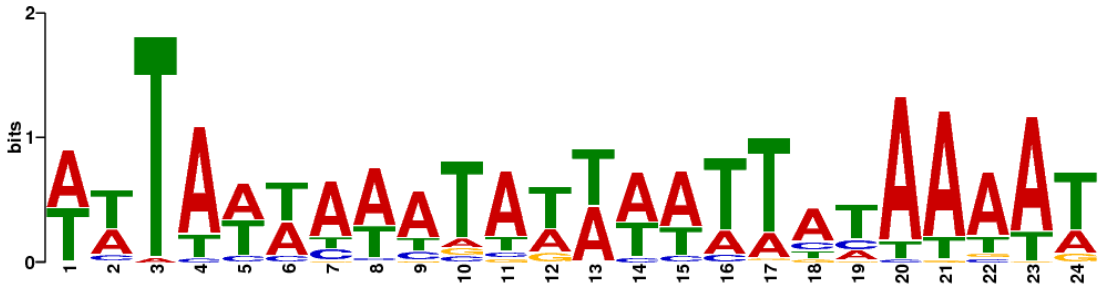

Figure 31 Predicted PerR binding motif using MEME software.

Differentially regulated genes by PerR of three different experimental setups (wild type stressed with H_2O_2 vs. *perR* mutant; wt vs. *perR* mutant during exponential growth phase; wt vs. *perR* mutant during stationary growth phase) were used to predict the DNA binding motif (www.meme-suite.org/tools/meme). Bioinformatical analysis was carried out by Dr. Denitsa Eckweiler.

The predicted motif resulted in a sequence of 24 nucleotides with a high content of adenine (A) and tyrosine (T) and equally low frequency of conserved nucleotides. Only T at position 3 and probably A at positions 20, 21 and 23 might be conserved. Due to the generally high AT frequency in the genome of *C. difficile* in combination with the non-conserved motif, the prediction of a PerR binding site

upstream of genes is less significant. Nevertheless, this motif was used to predict direct PerR-dependent regulation, insofar as the alignment of 250 nt upstream of the regulated genes led to an agreement, even if only partial, with T at position 3 and A conserved at positions 20 to 23.

II. Regulation of the *perR* encoding operon by PerR

In the first instance the gene expression profile of the *perR* operon was analyzed (Table 28).

Table 28 Repressed gene expression of the *perR* operon

++: Probability is very high. Base T at position 3 and base A at position 23-23 of the predicted binding motif are conserved.

-: No binding motif detected.

locus tag	gene name	function	log_2FC Δ*perR* vs wt exp. phase	log_2FC Δ*perR* vs wt stat. phase	putative PerR-box
perR operon					
CD630DERM_08250	*rbr*	Rubrerythrin	-1.81*	-0.02	-
CD630DERM_08260	*perR*	putative ferric-uptake regulator	-2.75*	-0.87	++
CD630DERM_08270	*rbo*	Rubredoxin oxidoreductase (desulfoferrodoxin)	-3.75*	-1.62*	-
CD630DERM_08280		putative oxidative stress glutamate synthase	-2.79*	-0.96*	-
CD630DERM_12870	*fur*	Transcriptional regulator, Fur family	-1.92	1.84*	++

During both growth stages the entire *perR* operon was downregulated by the *perR* mutation in comparison to the wild type. The operon consists of four genes encoding the rubrerythrin (*rbr*; CD630DERM_08250), rubredoxin oxidoreductase (*rbo*; CD630ERM_08270), the peroxide sensing regulator PerR itself (CD630DERM_08260) as well as an oxidative stress glutamate synthase (CD630ERM_08280). The suppression of this operon elicited by the absence of the regulator implies the requirement of the protein and suggests an autoregulation as already postulated in other organisms such as *B. subtilis* and *Campylobacter jejuni* (150, 233). In contrast to our study results, the *perR* mutation in *C. jejuni* led to a de-repression of *perR* transcription (233), which is consistent with the function as repressor. In *C. difficile* 630Δ*erm* a constitutive de-repression of PerR-regulated genes including the *perR* operon itself is postulated due to an amino acids exchange of threonine to alanine at position 41 within the helix-turn-helix motif of the DNA binding domain (232). Nevertheless, this phenomenon might be dependent on PerR protein levels, which entails repression to a certain degree. Interestingly, a predicted PerR binding site was

detected upstream of *perR* gene itself but not upstream of *rbr*, the first gene of this operon. The repression of the *C. difficile* 630Δ*erm* operon, when PerR is not present at all, could be the result of another co-repressor. In *Desulfovibrio vulgaris* the *rbr* gene is co-transcribed with an upstream *fur*-like gene. It is assumed that the product regulates the oxidative stress response in *D. vulgaris* (234, 235). A sequence alignment of the predicted Fur binding motif with 250 nucleotides upstream of rbr_{Cdiff} resulted in a well fitted comparison (Suppl. Figure 8). On the other hand, the predicted PerR binding site was detected upstream of the *fur* gene indicating a reciprocal co-regulation.

The absence of PerR led also to a repression of the related iron uptake-regulator Fur during the exponential phase. In *B. subtilis* a regulation of Fur by PerR was already described, where PerR acts as a repressor of the *fur* gene (150), which is in disagreement with our results. At this point, activator function of PerR in *C. difficile* regarding Fur cannot be excluded. But interestingly, in the stationary phase a de-repression of the *fur* gene was detected in the *perR* mutant, which aligns with the observations for *Bacillus*. Alternation of amino acid fermentation via Stickland reactions by the loss of PerR was analyzed in the following.

III. Amino acid uptake: Leucine is highly consumed by the *perR* mutant

The minimal defined medium (MDM) contains the amino acids proline, threonine, leucine, isoleucine, valine, methionine, tryptophan, and cysteine. Additionally, glucose is present as carbon source. Nevertheless, *C. difficile* primarily utilizes amino acids to generate energy in the form of ATP through the Stickland reactions (33, 34, 35, 36). The comparison of intracellular and extracellular nutrient abundance in the exponential and stationary phase provided information about altered nutrient uptake (Figure 32).

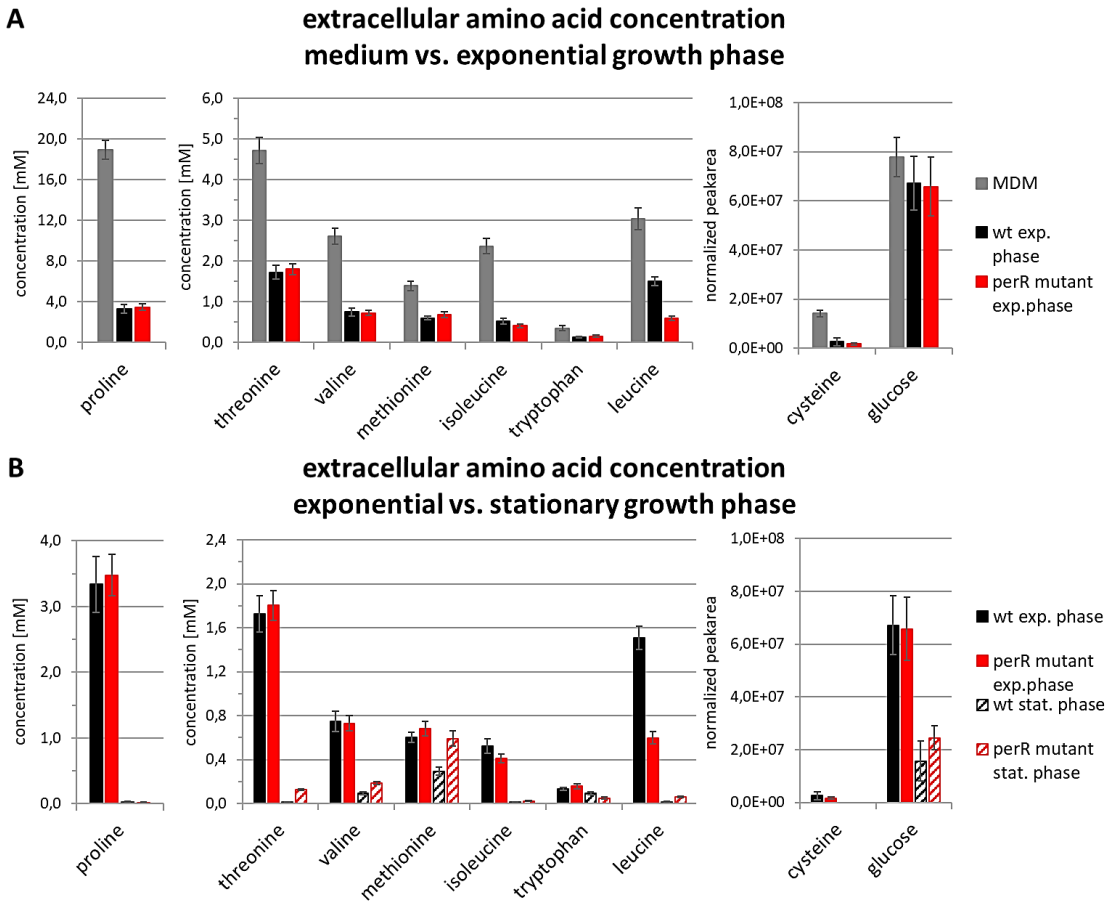

Figure 32 Extracellular metabolite profile of the *perR* mutant in comparison with the wild type.

Extracellular amino acid and glucose abundance in mM or as normalized peak area is shown. A) Grey bars: concentration in pure medium. Black bars: concentration of wild type (wt) cultures sampled in the exponential phase. Red bars: concentration of *perR* mutant cultures sampled in the exponential phase. B) Black filled bars: concentration of wild type cultures sampled in the exponential phase. Black hatched bars: concentration of wild type cultures sampled in the stationary phase. Red bars: concentration of *perR* mutant cultures sampled in the exponential phase. Red hatched bars: concentration of *perR* mutant cultures sampled in the stationary phase. Experiments were performed in cooperation with Dr. Meina Neumann-Schaal.

Extracellular metabolite concentrations of the exponential growth phase (filled bars) showed similar values for the wild type (black bars) and the *perR* mutant (red bars) indicating an equal uptake rate (Figure 32A). Leucine was the only amino acid, whose concentration was reduced in culture supernatants of the *perR* mutant, which implies an increased uptake and higher consumption of this amino acid. In the stationary phase (hatched bars) almost all nutrients were completely consumed (Figure 32B), whereby the wild type showed a higher uptake rate for glucose, methionine, isoleucine, valine, leucine and threonine. Threonine was no longer be present in the supernatant of wild type cultures. The higher uptake rate

of the nutrients by the wild type in the stationary phase could be explained by the inhibited growth of the *perR* mutant, which was previously observed (Figure 30). Due to the reduced uptake, the mutant lacks the necessary substrates to generate energy via the Stickland reaction, which results in reduced growth. Cysteine could no longer be detected in both strains, which is due to complete utilization. Interestingly, the extracellular methionine concentration of *perR* mutant cultures showed equal values in the stationary phase and in the exponential growth phase, indicating no further uptake. In order to verify which Stickland reactions are differentially regulated by the *perR* mutant, first the intracellular amino acid concentration was determined (Figure 33; for more details Suppl. Table 4) followed by transcriptomic and metabolomic analyses.

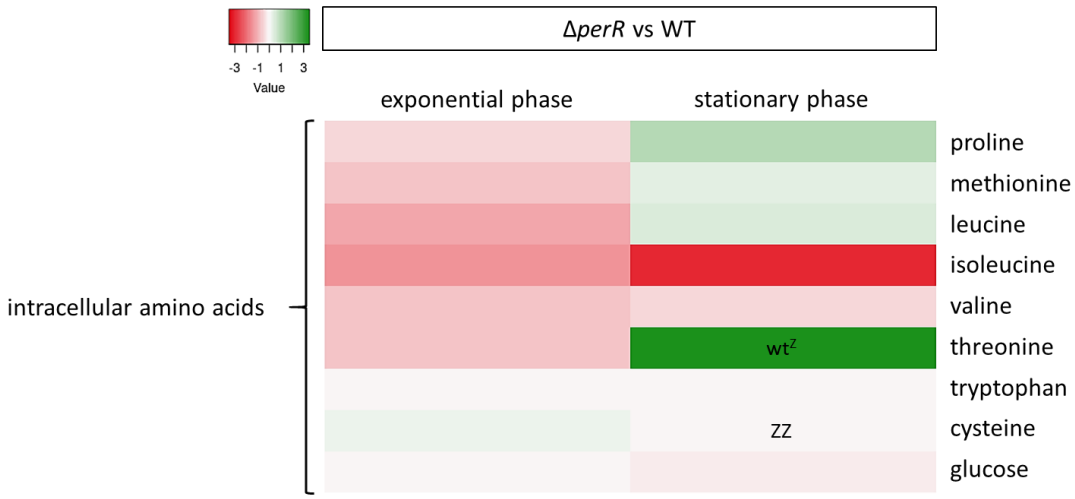

Figure 33 Differences in intracellular amino acid concentrations between the *perR* mutant and the wild type.

The relative ratio of intracellular amino acids and glucose in the exponential and stationary phase is shown as log_2FC. Nutrient abundance from *perR* mutant (Δ*perR*) cultures was compared to wild type (wt) cultures. Samples were taken at the mid-exponential growth phase and stationary growth phase. All measurements were made in quintuplicates. Completely consumed nutrients in the wild type are indicated by "wt^Z", in both strains by "zz". "Z" stands for "zero". Log_2FC<0 (red) indicates decreased abundance in the *perR* mutant in comparison to the wild type. Increased abundance is indicated by log_2FC>0 (green). Experiments were performed in cooperation with Dr. Meina Neumann-Schaal.

Measurements of the intracellular amino acid concentration revealed reduced amounts of several amino acids in the *perR* mutant, when the organism was in the exponential growth phase. Due to the equal uptake rate in comparison to the wild type, with the exception of leucine, a reduced intracellular abundance may have been caused by an increased Stickland fermentation. In the stationary phase, the level of intracellular nutrients is similar for both strains except for

isoleucine and threonine. The latter is only present in the *perR* mutant and thus not completely utilized, while isoleucine is more metabolized than in the wild type.

IV. Amino acid fermentation under stress conditions is controlled by PerR

Amino acid fermentation via Stickland reactions is the primary process in *C. difficile* to generate energy, which is mainly conserved in form of ATP by substrate level phosphorylation. The Stickland reactions involve the coupling of oxidation and reduction of amino acid pairs with simultaneous formation of their corresponding organic acid involving several co-enzymes (27). While amino acids such as isoleucine, valine or alanine serve as effective electron donors in the oxidative pathway, the amino acids proline, glycine or methionine act as electron acceptors in the reductive pathway. Leucine, phenylalanine and tyrosine can function both as electron acceptors and donors, resulting in different pathway-dependent products. (32, 34, 36, 38). Thus, leucine is converted to isovalerate in the oxidative pathway, while isocaproate is derived from the reductive pathway (32). The comparison of intracellular amino acid concentrations during the exponential phase showed among others an abundance reduction for leucine, isoleucine, valine in the *perR* mutant in comparison to the wild type (Figure 33), indicating an enhanced utilization. In the next step, a detailed analysis of single reductive and oxidative Stickland pathways were performed with regard to the produced intermediates and end products and the associated gene regulation in the exponential and stationary phase (Figure 34).

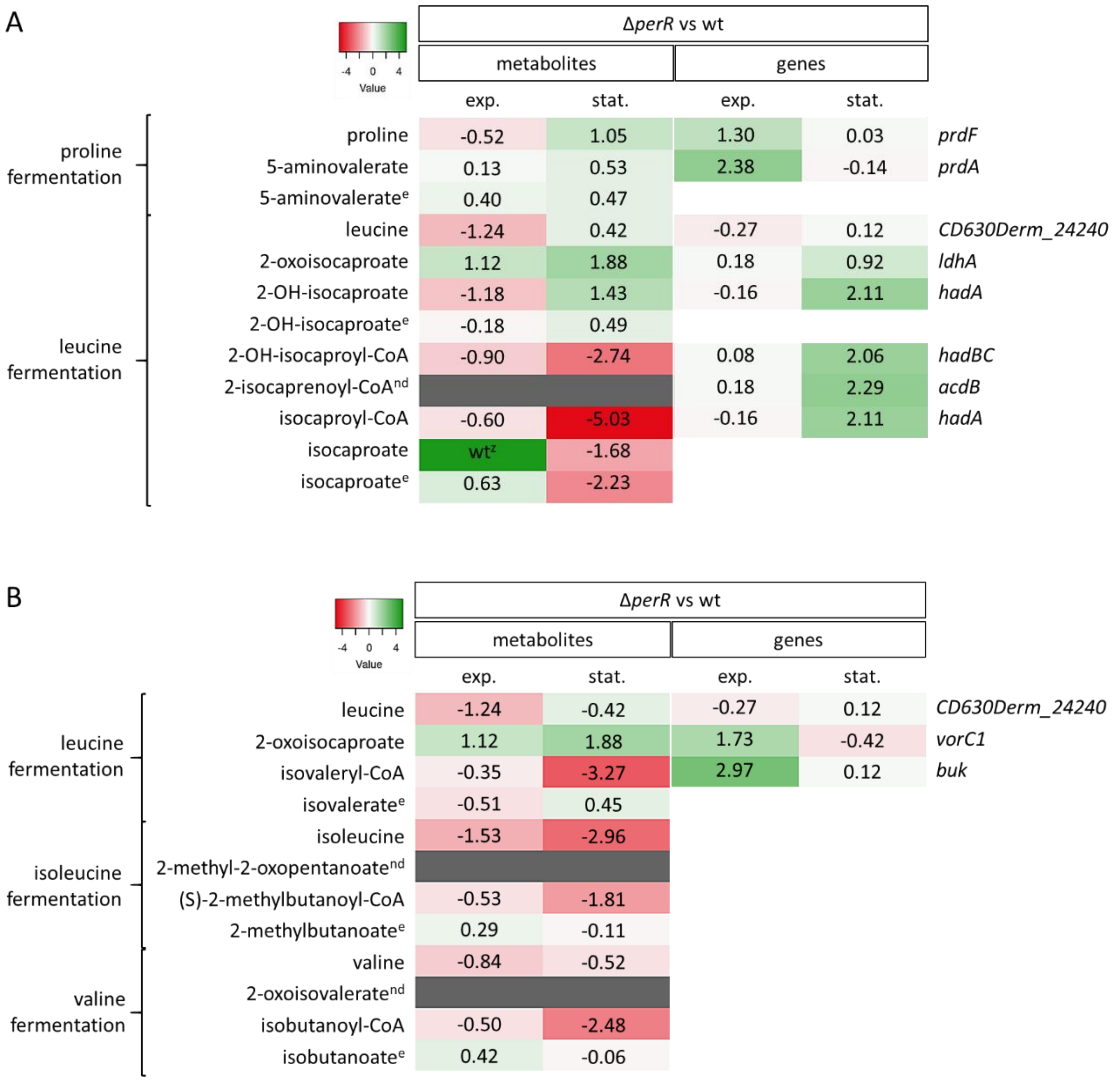

Figure 34 Metabolite and corresponding gene expression profiles associated with Stickland fermentation reactions of the *C. difficile perR* mutant in comparison to the wild type.

The relative ratios of the intracellular Stickland reaction metabolites and gene expression values as log_2FC are shown. Peak areas of intermediates and products as well as gene expression from *perR* mutant (Δ*perR*) cultures grown in MDM were compared with that of the wild type (wt). Extracellular detected metabolites are indicated by "e". "nd" indicates intermediates, which were not detected. Not detected nutrients in the wild type are indicated by "wt^Z" A) Metabolites and genes involved in the reductive Stickland reactions are displayed. B) Metabolites and genes involved in the oxidative Stickland pathway are shown. Leucine, isoleucine and valine fermentation are regulated by the same genes. Samples were taken at the mid-exponential and stationary growth phase. All measurements were made in quintuplicates. Experiments were performed in cooperation with Dr. Meina Neumann-Schaal.

During the exponential growth phase genes involved in the reductive proline fermentation (Figure 34A and Suppl. Table 5), *prdF* (CD630DERM_32370) and *prdA* (CD630DERM_32440), as well as genes involved in the oxidative leucine, isoleucine and valine fermentation (Figure 34B), *vorC1* (CD630DERM_01150) and *buk* (CD630DERM_01130), were strongly upregulated in the *perR* mutant.

Upregulated genes indicate an increased utilization followed by decreased substrate concentrations, which was observed for all substrates. However, in the case of proline, the abundance was found slightly above the threshold of $log_2FC \leq -0.6$. Due to the reduced amount of proline and the upregulation of *prdA* coding for the proline reductase, an increase of the end product 5-aminovalerate was expected. This was not detected both intra- and extracellularly. Similar observations were made for the oxidative Stickland reactions of isoleucine and valine with the end products 2-methylbutanoate and isobutanoate, respectively. This discrepancy could be a result of different parameters, including insufficient spatial proximity of enzyme and the corresponding substrate and a missing or inefficient translation of the enzymes despite existent transcription (transcriptome does not equal proteome). This explanation may also argue other discrepancies herein found. Within the leucine fermentation an accumulation of the intermediate 2-oxoiscaproate was detected followed by the decreased abundance of its end product isovalerate, indicating an incomplete utilization of leucine, although this amino acid is a preferred substrate for energy generation (27). The transcriptome analyses showed that in the *perR* mutant a progressive switch from oxidative leucine fermentation to reductive fermentation takes place during the growth process up to the stationary phase as indicated by the upregulation of the genes *ldhA* (CD630DERM_03940), *hadABC* (CD630DERM_03950/-70/-80) and *acdB* (CD630DERM_03990). These observations were made before by Neumann-Schaal and colleagues for *C. difficile* 630Δ*erm* at the metabolomic level (27). In the *perR* mutant this phenomenon is induced at the transcriptomic level. In accordance with the upregulated *ldhA* and *hadA*, also the intermediates 2-oxoisocaproate and 2-hydroxyisocaproate were more abundant. The latter could be detected extracellularly and was thus secreted prematurely. Despite increased expression of the genes of the lower metabolic pathway, subsequent intermediates were detected in the *perR* mutant in significantly reduced amounts, which again suggests incomplete utilization.

Phenylalanine and tyrosine are amino acids, which were not initial constituents of the medium. Nevertheless, phenylalanine and fermentation products of tyrosine were detected in both strains *C. difficile* wild type and *perR* mutant in both growth stages (Figure 35).

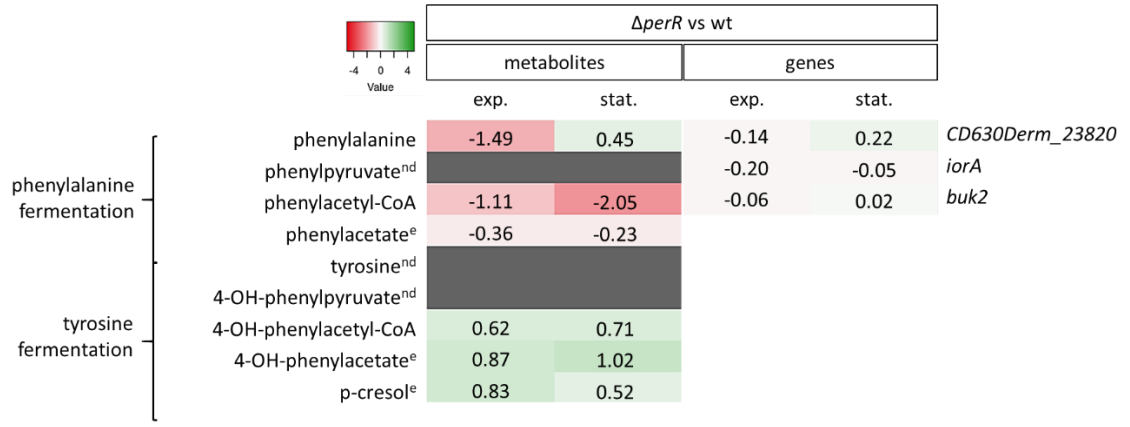

Figure 35 Compared metabolite and gene expression profiles associated with the reductive phenylalanine and tyrosine Stickland fermentation reactions.

The relative ratios of intracellular Stickland reaction metabolites as log_2FC are shown. Peak areas of intermediates and products as well as gene expression from *perR* mutant (Δ*perR*) cultures grown in MDM were compared with that of the wild type (wt). Extracellular detected metabolites are indicated by "e". "nd" indicates intermediates, which were not detected. Phenylalanine and tyrosine fermentation are regulated by the same genes. Samples were taken at the mid-exponential and stationary growth phase. All measurements were made in quintuplicates. Experiments were performed in cooperation with Dr. Meina Neumann-Schaal.

Transcription analysis revealed that the operon involved in the biosynthesis of phenylalanine and tyrosine was upregulated in the *perR* mutant during the exponential growth phase but not in the stationary phase (Table 29). Although genes, which are involved in phenylalanine or tyrosine utilization are not differently expressed, the fermentation products 4-hydroxy-phenylpyruvate and p-cresol, derived from tyrosine were produced to a higher extent in the mutant in both growth stages.

Table 29 Upregulated phenylalanine and tyrosine biosynthesis in the *perR* mutant.

locus tag	gene name	function	log_2FC Δ*perR* vs wt exp. phase	log_2FC Δ*perR* vs wt stat. phase
Phenylalanine and tyrosine biosynthesis				
CD630DERM_18320	*aroF1*	3-Deoxy-D-arabino-heptulosonate 7-phosphatesynthase	0.91*	0.39
CD630DERM_18330	*aroB*	3-Dehydroquinate synthase	1.04*	0.52
CD630DERM_18340	*aroA*	3-Phosphoshikimate 1-carboxyvinyltransferase	1.07*	0.30
CD630DERM_18350	*aroC*	Chorismate synthase(5-enolpyruvylshikimate-3-phosphate phospholyase)	1.20*	0.38
CD630DERM_18360	*pheA*	Bifunctional P-protein, chorismatemutase/prephenate dehydratase	1.43*	0.20
CD630DERM_18370	*aroE1*	Shikimate dehydrogenase 1 [Clostridioides difficile]	1.59*	0.31
CD630DERM_18380	*aroK*	Shikimate kinase (SK)	1.70*	-0.19
CD630DERM_18390	*tyrC*	Prephenate dehydrogenase	1.75*	0.11
CD630DERM_13390	*aspB*	Aspartate aminotransferase (AspAT) (TransaminaseA)	1.25*	-0.50*

Threonine is not essential for *C. difficile* growth but improves the biomass formation (27). Threonine can be degraded to acetate via glycine and 2-aminobutanoate via 2-oxobutanoate. In the following, 2-oxobutanoate is converted in 2-aminobutanoate or propionate involving the co-enzyme propanoyl-CoA.

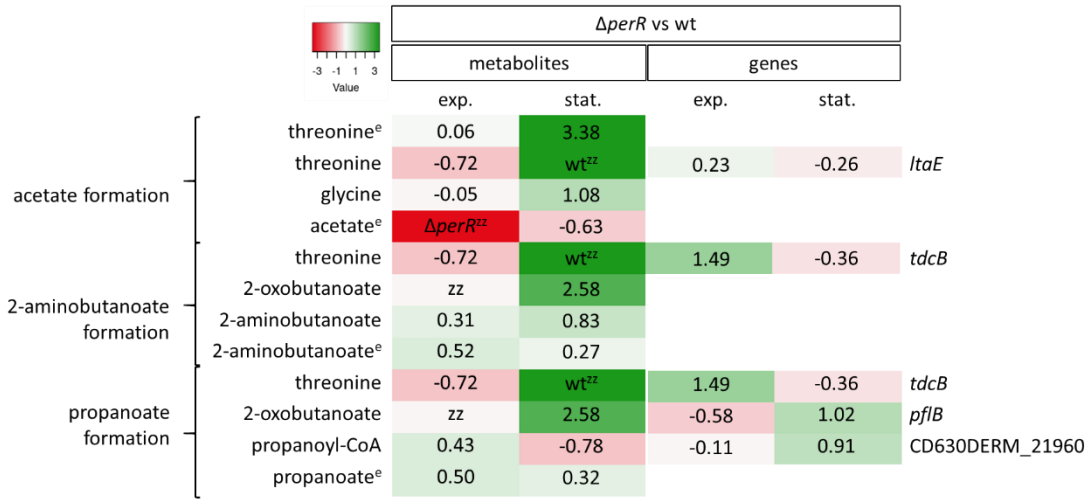

Figure 36 Threonine-associated metabolic pathways in the wild type and the *perR* mutant.

The relative ratios of intracellular metabolites and gene expression values as log_2FC are shown. Peak areas of intermediates and products as well as gene expression from *perR* mutant (Δ*perR*) cultures grown in MDM were compared with that of the wild type (wt). Extracellularly detected metabolites are indicated by "e". Completely consumed nutrients in both strains by "zz", only in the wild type by "wt^{ZZ}" and only in the *perR* mutant by "Δ$perR^{ZZ}$". Samples were taken at the mid-exponential and stationary growth phase. All measurements were performed in quintuplicates. Experiments were performed in cooperation with Dr. Meina Neumann-Schaal.

During the exponential growth phase, the production of acetate was only detected in the wild type, while the intermediate 2-oxobutanoate was not detected in any of the strains. The end products 2-aminobutanoate and propanoate were abundant to equal levels as in the wild type indicating no influence by the *perR* mutation on the metabolomic level. Nevertheless, the gene *tdcB* (CD630DERM_25140), which encodes for a threonine dehydratase and mediated the conversion of threonine to 2-oxobutanoate, was upregulated. During the stationary phase intracellular threonine was not detected in the wild type probably due its utter utilization. Subsequently, the intermediates glycine and 2-oxobutanoate were found more abundant in the *perR*-mutant while the end products showed similar amounts in comparison to the wild type, although the

genes *pflB* and CD630DERM_21960 involved in the propanoate formation were slightly upregulated.

V. Glycolysis: wild type versus *perR* mutant

In addition to amino acid fermentation, *C. difficile* produces energy in the form of ATP via glycolysis in which glucose is degraded to pyruvate (26). During the exponential growth phase, several genes, e.g. *pfkA* (CD630DERM_33950)*, gabA* (CD630DERM_31740)*, pgk* (CD630DERM_31730) and *pyk* (CD630DERM_33940) involved in glycolysis were upregulated in the *perR* mutant compared to the wild type (Figure 37A). In accordance, intermediates such as fructose-1,6-bisphosphate and phosphoenolpyruvate were reduced, which indicated an increased glucose utilization. Nevertheless, higher abundance of pyruvate was not detected neither intracellularly nor extracellularly indicating its subsequent degradation. The degradation of the key metabolite pyruvate might undertake different routes. On the one hand pyruvate can be converted to lactate, which is exported in the following process. On the other hand, starting from pyruvate, L-alanine can be synthesized or acetyl-CoA can be generated via oxidative decarboxylation (229). The conversion to lactate is mediated by lactate-dehydrogenase, encoded by *ldh* (CD630DERM_21640), which is downregulated in the *perR* mutant (Figure 37B). In accordance, lactate levels as end product were strongly decreased. In contrast, the gene *asb* (CD630DERM_13390) encoding for a transaminase A was upregulated leading to an accumulation of intracellular alanine.

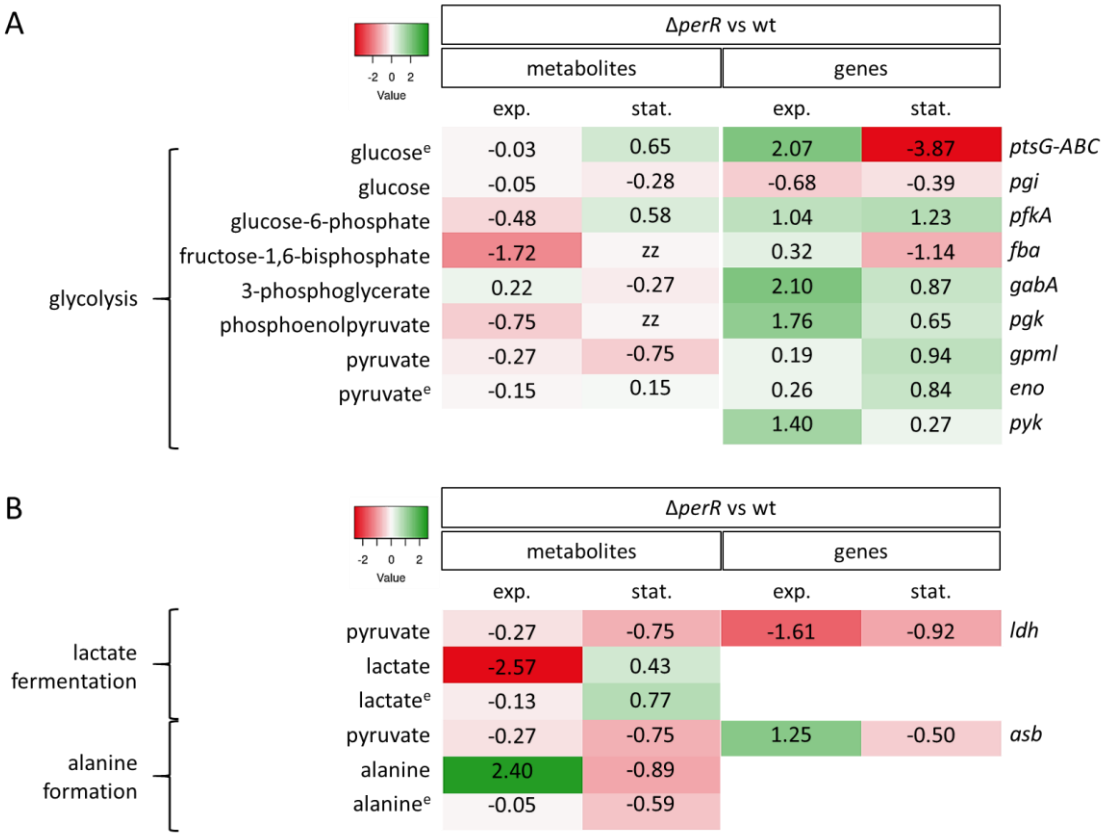

Figure 37 Metabolite and gene expression profiles associated with changes in glycolysis and pyruvate degradation between wild type and *perR* mutant.

The relative ratios of intracellular metabolites and gene expression values as log_2FC are shown. Peak areas of intermediates and products as well as gene expression from *perR* mutant (Δ*perR*) cultures grown in MDM were compared with that of the wild type (wt). Extracellular detected metabolites are indicated by "e". Completely consumed nutrients in both strains by "zz". Samples were taken at the mid-exponential and stationary growth phase. All measurements were conducted in quintuplicates. Experiments were performed in cooperation with Dr. Meina Neumann-Schaal.

During the stationary phase the uptake of glucose by the *perR* mutant was reduced (Figure 32) in accordance with the downregulated glucose-specific phosphotransferase system PTS, encoded by the genes *ptsG-A* (CD630DERM_26660) and *ptsG-BC* (CD630DERM_26670). In this line, most of the genes involved in glucose degradation were found just slightly upregulated in the mutant or expressed at similar levels as in the wild type with the exception of *fba* (CD630DERM_04030), which was downregulated. The gene *fba* encodes for fructose-1,6-bisphosphate aldolase, which mediates the conversion of fructose-1,6-bisphosphate to glyceraldeyde-3-phosphate. At the metabolic level, fructose 1,6-bisphosphate and phosphoenolpyruvate were not detected in any of the strains wild type and mutant, indicating complete degradation. Nevertheless, the

final product of the glycolysis pyruvate was found drastically reduced in the *perR* mutant, which implies further consumption. Interestingly, in contrast to the exponential growth phase, more lactate is produced in the stationary phase.

VI. TCA cycle: wild type versus *perR* mutant

The degradation of glucose resulted in the formation of pyruvate followed by the formation of acetyl-CoA a key enzyme involved in multiple pathways but importantly in the TCA cycle. In *C. difficile* the TCA cycle is truncated into the reductive and oxidative part (32, 229).

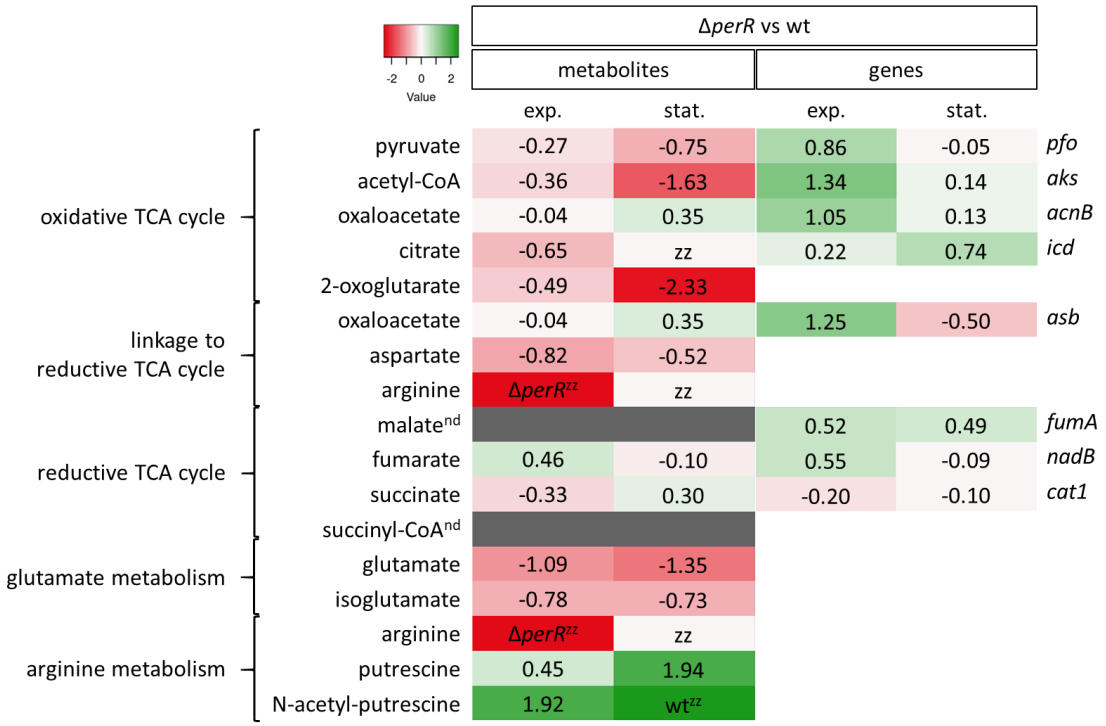

Figure 38 Metabolite and gene expression profiles associated with changes in the TCA cycle and related pathways between wild type and *perR* mutant.

The relative ratios of intracellular metabolites and gene expression values as log_2FC are shown. Peak areas of intermediates and products as well as gene expression from *perR* mutant (Δ*perR*) cultures grown in MDM were compared with that of the wild type (wt). Not detected metabolites are indicated by "nd". Completely consumed nutrients in both strains are indicated by "zz", only in the wild type by "wt^{ZZ}" and only in the *perR* mutant by "Δ*perR*^{ZZ}". Samples were taken at the mid-exponential and stationary growth phase. All measurements were made in quintuplicates. Experiments were performed in cooperation with Dr. Meina Neumann-Schaal.

The latter starts with the conversion of oxaloacetate to citrate and results in 2-oxoglutarate (32, 229). Genes involved in this part of the TCA cycle, *acnB* CD630DERM_08330 and *icd* CD630DERM_08340, encoding for aconitate hydratase (citrate hydrolyase) or isocitrate dehydrogenase, respectively, were

only slightly upregulated or not differentially regulated in the *perR* mutant in comparison to the wild type (Figure 38). On the metabolomic level citrate and 2-oxoglutarate amounts were not significantly decreased. In the stationary phase citrate was no longer detected in either strain. Moreover, the production of 2-oxoglutarate was strongly reduced in the *perR* mutant. Due to the missing link between 2-oxoglutarate and succinyl-CoA in *C. difficile* 630Δ*erm*, 2-oxoglutarate forms the final product of the oxidative TCA cycle and it is subsequently released into the glutamate metabolism (229). Involved metabolites namely glutamate and isoglutamate were less abundant in the mutant in both growth stages. The regulation of the reductive part of the TCA cycle did not differ between the *perR* mutant and the wild type at both growth stages neither on the metabolome nor the transcriptome level. In contrast to the TCA cycle of other microorganisms, the direct linkage between malate and oxaloacetate does not exist in *C. difficile*. Instead, the connection between the oxidative and reductive part is maintained via aspartate or via pyruvate and malate. Aspartate is converted to fumarate through the arginine biosynthesis route (229). Both metabolites were strongly reduced in the *perR* mutant. Moreover, in the exponential growth phase arginine was not detected at all in the mutant and at the stationary phase in any strain. This was consistent with the strongly downregulated arginine biosynthesis (Table 30). The downregulation of genes involved in the arginine biosynthesis was also observed for the Δ*perR* mutant in *C. acetobutylicum* (151). Small amounts of synthesized arginine appeared to be further converted to putrescine or N-acetyl-putrescine, which was significantly more abundant in the *perR* mutant especially at the stationary phase (Figure 38).

Table 30 Gene expression profiles associated with changes in arginine biosynthesis between wild type and *perR* mutant.

The relative ratios of gene expression values as log_2FC are shown.

(+): Probability is moderate. Base T at position 3 and base A at position 23-23 of the predicted binding motif are not conserved.

-: No binding motif detected.

locus tag	gene name	function	log_2FC Δ*perR* vs wt exp. phase	log_2FC Δ*perR* vs wt stat. phase	putative PerR-box
Arginine biosynthesis					
CD630DERM_20300	*argF*	Ornithine carbamoyltransferase (OTCase)	-6.93	-2.66	(+)
CD630DERM_20310	*argM*	Succinylornithine transaminase (ACOAT)	-6.84	-2.82	-
CD630DERM_20320	*argB*	Acetylglutamate kinase	-7.06	-3.32	(+)
CD630DERM_20330	*argJ*	Amino-acidacetyltransferase]; Arginine biosynthesis bifunctional protein ArgJ[Includes: Glutamate N-acetyltransferase	-7.08	-3.32	-
CD630DERM_20340	*argC*	N-Acetyl-gamma-glutamyl-phosphate reductase	-6.29	-2.79	(+)
CD630DERM_17850	*argG*	Argininosuccinate synthase(Citrulline--aspartate ligase)	-3.63	-2.56	-
CD630DERM_25000	*argH*	Argininosuccinate lyase (Arginosuccinase)(ASAL)	-2.09	-0.86	-

VII. Butanoate production is strongly reduced in the *perR* mutant

In *C. difficile*, energy can be generated in the course of butanoate/butyrate production (229, 236). On the metabolic level both butanoate metabolism intermediates and the final butanoate were less abundant in the *perR* mutant at both growth stages, exponential and stationary (Figure 39). During the exponential growth butanoate was not produced at all, although the genes *ptb* (CD630DERM_01120) and *buk* (CD630DERM_01120) were highly upregulated. This was also detected for the *perR* mutant of *C. acetobutylicum* (151). During the stationary phase the gene expression was in agreement with detected metabolite amounts.

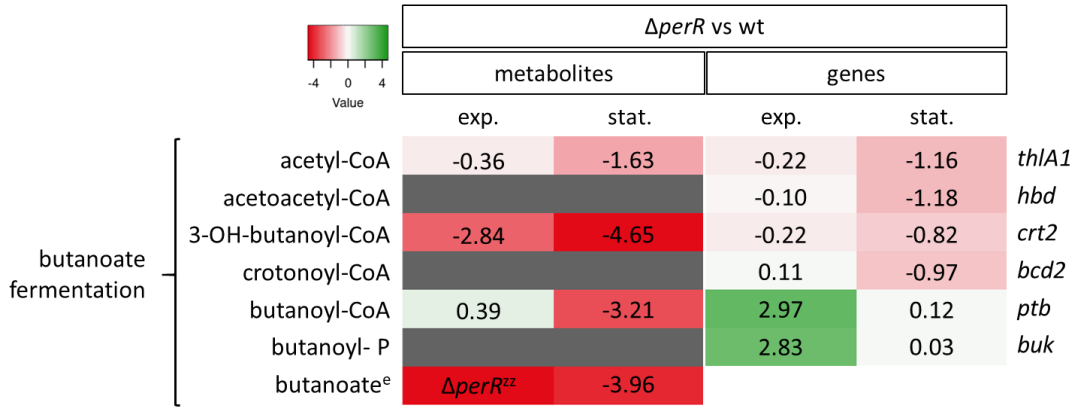

Figure 39 Metabolite and gene expression profiles associated with changes in the butanoate metabolism between wild type and *perR* mutant.

The relative ratios of intracellular metabolites and gene expression values as log_2FC are shown. Peak areas of intermediates and products as well as gene expression from *perR* mutant (Δ*perR*) cultures grown in MDM were compared with that of the wild type (wt). Extracellularly detected metabolites are indicated by "e". Completely consumed nutrients in the *perR* mutant are indicated by "Δ*perR*^{ZZ}". Samples were taken at the mid-exponential and stationary growth phase. All measurements were carried out in quintuplicates. Experiments were performed in cooperation with Dr. Meina Neumann-Schaal.

Butanoate does not play only a role in energy formation in *C. difficile* or other Gram-positives of the human gut microbiota but it is also an energy source of the colonic mucosa and acts as regulator of gene expression, inflammation, differentiation and apoptosis in host cells (236, 237). Increasing concentrations of short-chain fatty acids (SCFAs), which include butyrate, acetate and propionate, improve the inflammatory host response and reduce tissue damage. It was shown, that the restoration of intestinal concentrations of butyrate attenuated CDI in mice (238). Consequently, the *perR* mutation may affect infectivity, which might be reflected in a decreased inflammatory response and more pronounced CDI symptoms.

VIII. Fatty acid biosynthesis is differentially regulated in the wild type and the *perR* mutant

The loss of PerR led at the exponential growth phase to a highly upregulation of genes involved the biosynthesis of fatty acids (CD630DERM_11770-11840), while during the stationary phase a strong downregulation was detected (Table 31).

Table 31 Gene expression profiles associated with changes in fatty acid biosynthesis between wild type and *perR* mutant.

The relative ratios of gene expression values as log_2FC are shown.

(+): Probability is moderate. Base T at position 3 and base A at position 23-23 of the predicted binding motif are not conserved.

-: No binding motif detected.

locus tag	gene name	function	log_2FC Δ*perR* vs wt exp. phase	log_2FC Δ*perR* vs wt stat. phase	putative PerR-box
Fatty acid biosynthesis					
CD630DERM_19360	*accA*	Acetyl-coenzyme A carboxylase carboxyltransferase subunit alpha	0.55*	-1.27*	
CD630DERM_19370	*accD*	Acetyl-CoA carboxylase subunit beta	0.70*	-1.33*	
CD630DERM_19380	*accC*	Acetyl-CoA carboxylase subunit	0.55*	-1.33*	
CD630DERM_19390	*accB*	Acetyl-CoA carboxylase subunit	0.17	-1.33*	
CD630DERM_11770	*fabR*	Transcriptional regulator, DeoR family (Fattyacid and phospholipid biosynthesis regulator)	1.49*	-1.37*	-
CD630DERM_11780	*plsX*	Fatty acid/phospholipid synthesis protein PlsX	1.54*	-1.15*	(+)
CD630DERM_11790	*fabH*	3-Oxoacyl-[acyl-carrier-protein] synthase 3	1.91*	-1.19*	-
CD630DERM_11800	*fabK*	Enoyl-(Acyl-carrier-protein) reductase II	1.89*	-1.13*	-
CD630DERM_11810	*fabD*	Malonyl CoA-acyl carrier protein transacylase(MCT)	1.79*	-1.21*	-
CD630DERM_11820	*fabG*	3-Oxoacyl-[acyl-carrier protein] reductase(3-ketoacyl-acyl carrier protein reductase)	1.71*	-1.26*	-
CD630DERM_11830	*acpP1*	Acyl carrier protein (ACP)	1.88*	-1.59*	(+)
CD630DERM_11840	*fabF*	3-Oxoacyl-[acyl-carrier-protein] synthase 2	1.84*	-1.24*	-

In previous studies an upregulation of the fatty acid biosynthesis was also shown for the *C. difficile fur* mutant in comparison to the wild type. This is likewise found when comparing iron limited conditions with high iron levels. A predicted Fur binding box was identified upstream of *fabH*, but not of *fabR*, which encodes for the transcriptional regulator of this operon leading to the presumption of an indirect regulation by Fur (13, 201). Due to the downregulation of the *fur* gene in the exponential growth phase caused by the *perR* mutation (Table 28) an indirect regulation of PerR is likely. A direct regulation is rather improbable due the absence of a PerR binding box. In agreement with the upregulation of *fur* in the stationary phase, the fatty acid biosynthesis is downregulated. In *C. acetobutylicum* a slight downregulation of the *fab* operon was detected in the *perR* mutant (151) indicating a *C. difficile* specific regulation. Since fatty acids play a central role in cellular processes such as in the biosynthesis of essential

cellular structural components, cofactors, energy storage reservoirs and diffusible secondary metabolites such as quorum-sensing signal molecules or siderophores (239) the downregulation at the stationary phase explain the reduced growth of the *perR* mutant.

IX. Genes of riboflavin and thiamine biosynthesis are differentially regulated between the wild type and the *perR* mutant

During the exponential growth phase genes organized in an operon (CD630DERM_16970-17000) encoding for the riboflavin biosynthesis were upregulated, whereas these genes were downregulated in the *perR* mutant at the stationary phase (Table 32).

Table 32 Gene expression profiles associated with changes in riboflavin biosynthesis between wild type and *perR* mutant.

The relative ratios of gene expression values as log_2FC are shown.

(+): Probability is moderate. Base T at position 3 and base A at position 23-23 of the predicted binding motif are not conserved.

-: No binding motif detected.

locus tag	gene name	function	log_2FC Δ*perR* vs wt exp. phase	log_2FC Δ*perR* vs wt stat. phase	putative PerR-box
Riboflavin biosynthesis					
CD630DERM_16970	*ribH*	6,7-Dimethyl-8-ribityllumazine synthase	2.10	-2.51	-
CD630DERM_16980	*ribBA*	GTPcyclohydrolase-2; Riboflavin biosynthesis protein ribBA; 3,4-dihydroxy-2-butanone 4-phosphate synthase	2.33	-2.41	(+)
CD630DERM_16990	*ribE*	Riboflavin synthase alpha subunit	1.91	-2.13	-
CD630DERM_17000	*ribD*	Riboflavin biosynthesis protein ribD; Diaminohydroxyphosphoribosylaminopyrimidine deaminase; 5-amino-6-(5-phosphoribosylamino)uracil reductase	2.11	-2.17	(+)

An upregulation of the riboflavin operon was also described previously for the *C. difficile fur* mutant in comparison to the wild type. This was also observed when comparing iron limited conditions with high iron levels. Furthermore, the operon shows upstream of *ribH* a predicted Fur binding box, indicating a direct regulation by Fur (13, 201). Due to the downregulation of the *fur* gene in the exponential growth phase caused by the *perR* mutation (Table 28) it may be presumed that the PerR-dependent regulation of the riboflavin biosynthesis is rather indirect. This presumption arises from the observation of the likely absence or a moderate probability of having a PerR binding box. In agreement with the upregulation of *fur* in the stationary phase, the riboflavin biosynthesis is downregulated, which supports the direct interplay between Fur in this pathway and the indirect regulation by PerR. In *C. acetobutylicum* no differential regulation for the *rib*

operon was detected in the *perR* mutant (151) indicating a *C. difficile* specific regulation. Riboflavin, also known as vitamin B_2, acts as precursor of flavin mononucleotides (FMN) and flavin adenine dinucleotides (FAD), which are cofactors for several redox enzymes (240, 241). The negative regulation of riboflavin genes by Fur or iron was also described for *Caulobacter crescentus* and *C. acetobutylicum* (242).

A similar expression profile was observed for genes involved in the thiamine biosynthesis (CD630DERM_17020-17060) or metabolism (CD630DERM_15990 - 16010) (Table 33).

Table 33 Gene expression profiles associated with changes in thiamine biosynthesis between wild type and *perR* mutant.

The relative ratios of gene expression values as log_2FC are shown.

++: Probability is very high. Base T at position 3 and base A at position 23-23 of the predicted binding motif are conserved.

(+): Probability is moderate. Base T at position 3 and base A at position 23-23 of the predicted binding motif are not conserved.

-: No binding motif detected.

locus tag	gene name	function	log_2FC Δ*perR* vs wt exp. phase	log_2FC Δ*perR* vs wt stat. phase	putative PerR-box
Thiamine biosynthesis/ metabolism					
CD630DERM_17020	*thiC*	Thiamine biosynthesis protein ThiC	2.83*	-4.53*	(+)
CD630DERM_17021	*thiS*	Thiamine biosynthesis protein ThiS	2.22*	-5.28*	(+)
CD630DERM_17030	*thiF*	Thiamine biosynthesis protein ThiF	2.25*	-5.11*	(+)
CD630DERM_17040	*thiG*	Thiazole biosynthesis protein ThiG	1.80*	-4.33*	-
CD630DERM_17050	*thiH*	Thiamine biosynthesis protein ThiH	1.53*	-5.20*	-
CD630DERM_17060	*thiE2*	Thiamine-phosphate pyrophosphorylase ThiE2	1.18*	-4.85*	-
CD630DERM_15990	*thiD*	Phosphomethylpyrimidine kinase	1.50*	-0.75*	-
CD630DERM_16000	*thiM*	Hydroxyethylthiazole kinase	1.71*	-1.78*	++
CD630DERM_16010	*thiE*	Thiamine-phosphate pyrophosphorylase	1.25*	-1.94*	(+)

Herein, a putative PerR binding site was detected for the upstream region of *thiM* and probably of *thiC, thiS* and *thiF* indicating a PerR-dependent regulation. Thiamine, also known as vitamin B_1, is in its active form thiamine diphosphate (ThDP) an essential cofactor for enzymes involved in carbohydrate and branched-chain amino acid metabolism (243). The coupling of oxidation and reduction of amino acid pairs via Stickland reactions is a preferred process of *C. difficile* to generate energy (27). The upregulation of the riboflavin biosynthesis combined with an upregulation of that for thiamine might be a reaction to generate energy by an alternative way to compensate alterations caused by *perR*-mutation

in the Stickland fermentation, glycolysis and TCA cycle, as previously proposed for the iron-dependent regulation (13).

X. Flagella assembly and type IV pili are strongly regulated in the exponential growth phase by PerR

During the exponential growth phase the regulation of genes involved in flagella assembly (Table 34) was negatively correlated in the *perR* mutant to genes involved in type IV pili formation (Table 35). While the large operon of the flagella assembly (CD630DERM_02450-CD630DERM_02720) was strongly upregulated, genes of the type IV pili operon (CD630DERM_35070-CD630DERM_35130) were downregulated. Similar observations were made for a *C. difficile fur* mutant. A predicted Fur binding site upstream of several genes involved in flagella assembly, namely *flgC, fliF, flgD, fliL, fliZ, fliP, flhB* and CD630DERM_02670 (13), as we well as the downregulation of *fur* in this study during the exponential growth phase support the proposed Fur-dependent regulation. Furthermore, a co-regulation by PerR is possible due to the presence of the predicted PerR binding box upstream of *flgB* and *flgG1*. Within the operon of the type IV pili formation a potential Fur-box was not predicted (13, 201). Instead, a PerR binding motif could be determined upstream of the genes CD630DERM_35070 and CD630DERM_23050 indicating a direct PerR-dependent regulation. In agreement with the upregulation of *fur* in the stationary phase, some flagella genes were downregulated, but only two genes of them, *fliZ* and CD630DERM_02670, displayed a Fur binding motif.

The formation of type IV pili, however, remains largely unregulated by PerR in the stationary phase.

Table 34 Gene expression profiles associated with changes in flagella assembly between wild type and *perR* mutant.

The relative ratios of gene expression values as log_2FC are shown.

++: Probability is very high. Base T at position 3 and base A at position 23-23 of the predicted binding motif are conserved.

(+): Probability is moderate. Base T at position 3 and base A at position 23-23 of the predicted binding motif are not conserved.

-: No binding motif detected.

locus tag	gene name	function	log_2FC Δ*perR* vs wt exp. phase	log_2FC Δ*perR* vs wt stat. phase	putative PerR-box
Flagella assembly					
CD630DERM_02450	*flgB*	Flagellar basal-body rod protein FlgB	1.12	-0.34*	++
CD630DERM_02460	*flgC*	Flagellar basal-body rod protein FlgC	1.17*	-0.07	-
CD630DERM_02470	*fliE*	Flagellar hook-basal body complex protein FliE	1.18	-0.40	(+)
CD630DERM_02480	*fliF*	Flagellar M-ring protein FliF	1.09*	0.49	(+)
CD630DERM_02490	*fliG*	Flagellar motor switch protein FliG	1.28	-0.49*	-
CD630DERM_02500	*fliH*	Flagellar assembly protein FliH	1.47	-1.36*	-
CD630DERM_02510	*fliI*	ATP synthase subunit beta FliI	1.38	-0.64*	-
CD630DERM_02520	*fliJ*	Flagellar protein FliJ	2.11	-1.60*	-
CD630DERM_02530	*fliK*	Flagellar hook-length control protein FliK	2.06	-1.38*	(+)
CD630DERM_02540	*flgD*	Basal-body rod modification protein FlgD	1.51	0.09*	-
CD630DERM_02550	*flgE*	Flagellar hook protein FlgE (Distal rod protein)	1.63	-0.41*	(+)
CD630DERM_02551	*flbD*	Flagellar protein FlbD	1.31	-1.42*	-
CD630DERM_02560	*motA*	Flagellar motor rotation protein MotA	1.19	-0.59*	-
CD630DERM_02570	*motB*	Flagellar motor rotation protein MotB (Chemotaxis protein MotB)	1.09	-0.52*	(+)
CD630DERM_02580	*fliL*	Flagellar basal body-associated protein FliL	1.01	-0.88*	(+)
CD630DERM_02590	*fliZ*	Flagellar protein FliZ	1.22	-1.50*	-
CD630DERM_02600	*fliP*	Flagellar biosynthesis protein FliP	1.30	-0.25	-
CD630DERM_02610	*fliQ*	Flagellar biosynthetic protein FliQ	1.41	-0.67	-
CD630DERM_02620	*flhB*	Bifunctional flagellar biosynthesis protein FliR/FlhB	1.43	-0.18	-
CD630DERM_02630	*flhA*	Flagellar biosynthesis protein FlhA	1.84	-0.49*	-
CD630DERM_02640	*flhF*	Flagellar biosynthesis regulator FlhF (Flagella-associated GTP-binding protein)	1.66	-0.63	-
CD630DERM_02650	*flhG*	Flagellar number regulator FlhG	1.08	-0.42	(+)
CD630DERM_02660	*fliA*	RNA polymerase sigma-28 factor for flagellar operon	1.11	-0.72*	-
CD630DERM_02670		putative flagellar protein	0.93	-1.15*	(+)
CD630DERM_02671		putative flagellar protein	0.76	-0.68*	-
CD630DERM_02680	*flgG1*	Flagellar hook-basal body complex protein FlgG1	1.05	-0.42*	++
CD630DERM_02690	*flgG*	Flagellar basal body rod protein FlgG	0.93	-0.15	-
CD630DERM_02700	*fliM*	Flagellar motor switch protein FliM	0.64	-0.27	-
CD630DERM_02710	*fliN1*	Flagellar motor switch phosphatase FliN1	0.60	-0.60*	-
CD630DERM_02720		conserved hypothetical protein	0.67	-0.40	-

Table 35 Gene expression profiles associated with changes in type IV pili between wild type and *perR* mutant.

The relative ratios of gene expression values as log_2FC are shown.

++: Probability is very high. Base T at position 3 and base A at position 23-23 of the predicted binding motif are conserved.

(+): Probability is moderate. Base T at position 3 and base A at position 23-23 of the predicted binding motif are not conserved.

-: No binding motif detected.

locus tag	gene name	function	log_2FC Δ*perR* vs wt exp. phase	log_2FC Δ*perR* vs wt stat. phase	putative PerR-box
Type IV pili					
CD630DERM_35070		putative type IV pilin	-1.03	-0.33*	++
CD630DERM_35080		putative type IV pilin	-1.06	-0.16	(+)
CD630DERM_35090		putative type IV pilus assembly protein	-1.25	-0.10	(+)
CD630DERM_35100		putative membrane protein	-1.49	-0.10	-
CD630DERM_35110		putative type IV pilus secretion protein	-1.69	0.46	-
CD630DERM_35120		putative type IV pilus transportersystem,ATP-binding	-2.09	0.51*	-
CD630DERM_35130		putative pilin protein	-2.46	1.02*	(+)
CD630DERM_23050		putative pilin protein	-0.39*	-0.93*	++

XI. Cell wall biosynthesis is upregulated in the exponential growth phase

During the exponential growth phase, the expression of genes involved in the cell wall biosynthesis, namely *mraY, murF* and *murE* was increased in the *perR* mutant, while a differential downregulation was only observed for *murE* at the stationary phase (Table 36).

Table 36 Gene expression profiles associated with changes in cell wall biosynthesis between wild type and *perR* mutant.

The relative ratios of gene expression values as log_2FC are shown.

(+): Probability is moderate. Base T at position 3 and base A at position 23-23 of the predicted binding motif are not conserved.

-: No binding motif detected.

locus tag	gene name	function	log_2FC Δ*perR* vs wt exp. phase	log_2FC Δ*perR* vs wt stat. phase	putative PerR-box
Cell wall biosynthesis					
CD630DERM_26510	*murG*	UDP-N-acetylglucosamine--N-acetylmuramyl-(pentap eptide)pyrophosphoryl-undecaprenol N-acetylglucosaminetransferase	0.62	-0.12	(+)
CD630DERM_26520	*spoVE*	Cell division/stage V sporulation protein	0.72	0.06	(+)
CD630DERM_26530	*murD*	UDP-N-acetylmuramoylalanine--D-glutamate Ligase(UDP-N-acetylmuramoyl-L-alanyl-D-glutamate synthetase)(D-glutamic acid-adding enzyme)	0.77	-0.17	-
CD630DERM_26540	*mraY*	Phospho-N-acetylmuramoyl-pentapeptide-transferase (UDP-MurNAc-pentapeptide phosphotransferase)	1.04	-0.01	(+)
CD630DERM_26550	*murF*	UDP-N-acetylmuramoyl-tripeptide--D-alanyl-D-alan ineligase (UDP-MurNAc-pentapeptide synthetase)(D-alanyl-D-alanine-adding enzyme)	1.21	-0.16	-
CD630DERM_26640	*murE*	UDP-N-acetylmuramyl-tripeptide synthetase	1.56	-2.92	(+)

The predicted PerR binding motif showed only a partial sequence identity for upstream regions of *murG, spoVE, mraY* and *murE*. Consequently, an indirect PerR regulation is more likely than a direct regulation.

XII. Schematic overview of alterations between *C. difficile* wild type and the corresponding *perR* mutant during exponential and stationary phase

The above-mentioned results showed profound divergences between the *C. difficile* wild type and the isogenic *perR* mutant on the metabolomic and transcriptomic level in terms of amino acid fermentation pathways and the central metabolism. A schematic overview is given in Figure 40 and Figure 41.

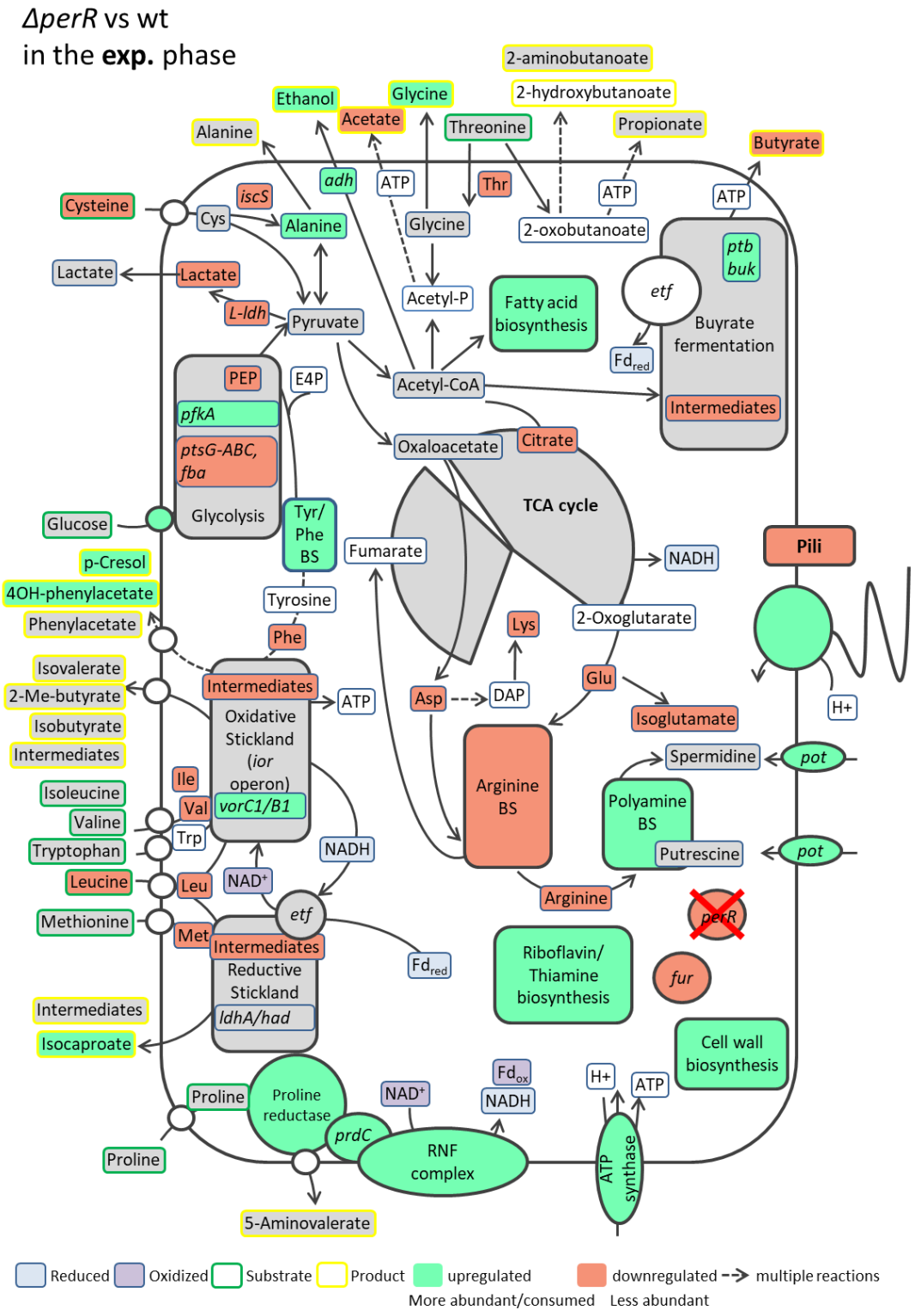

Figure 40 Schematic overview of metabolic and transcriptomic changes in *C. difficile perR* mutant in comparison to the wild type in the exponential phase.

Schematic overview of affected metabolic pathways during the exponential growth phase. An increase in metabolic compounds or gene expression in the *perR* mutant (Δ*perR*) compared to the wild type (wt) is displayed in green, while a decrease/downregulation is shown in red and no significant changes in grey. The illustration was developed in collaboration with Dr. Meina Neumann-Schaal.

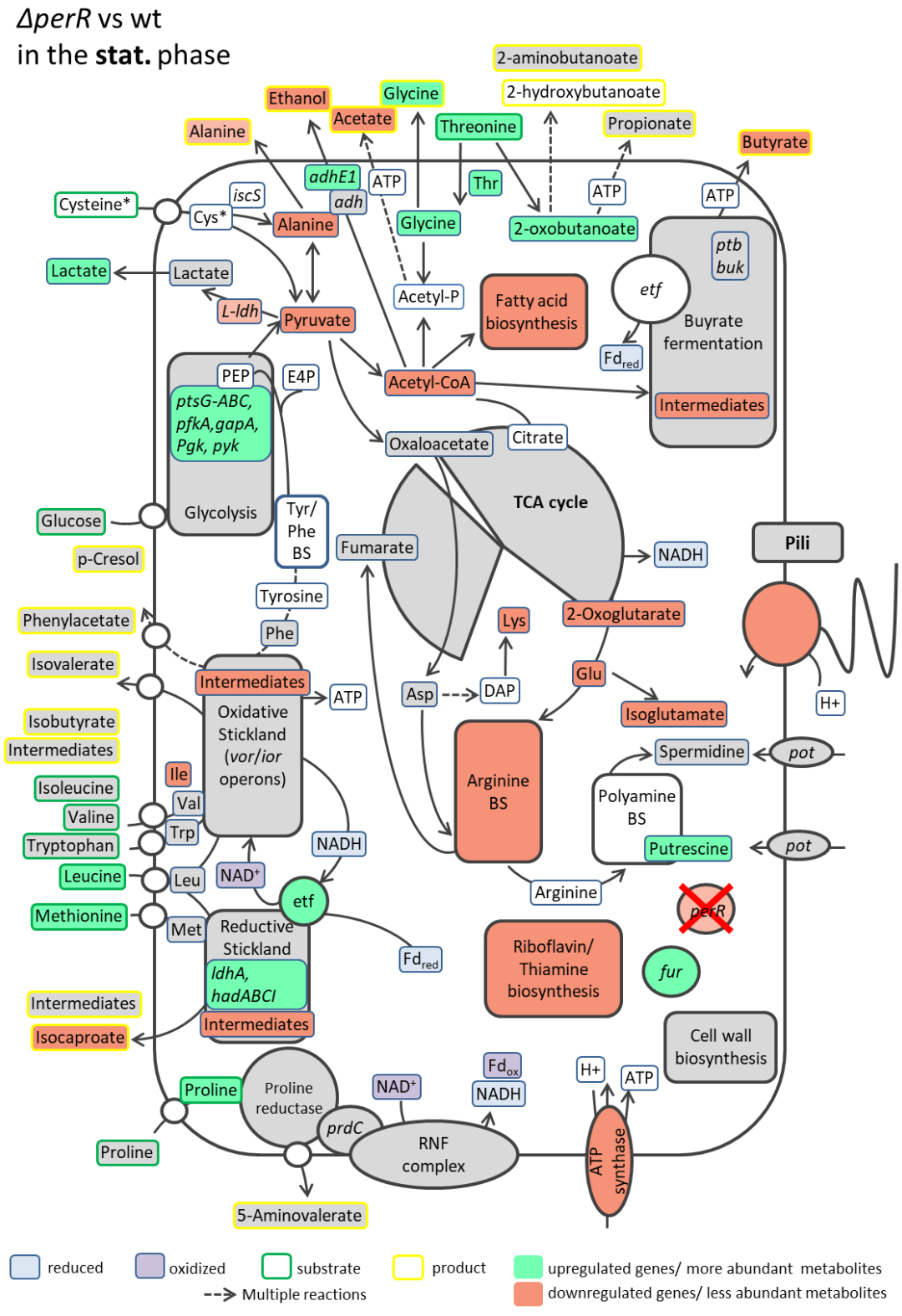

Figure 41 Schematic overview of metabolic and transcriptomic changes in *C. difficile perR* mutant in comparison to the wild type in the stationary phase.

Schematic overview of metabolic pathways changed in the stationary phase. An increase in metabolic compounds or gene expression in the *perR* mutant (Δ*perR*) compared to the wild type (wt) is displayed in green, while a decrease/downregulation is shown in red and no significant changes in grey. The illustration was developed in collaboration with Dr. Meina Neumann-Schaal.

3.3 The iron-regulator Fur and its role in motility and resistance

An earlier PhD thesis of our laboratory was focused on the investigation of the iron regulation in *C. difficile* by the ferric-uptake regulator Fur (13). For that purpose, a *fur*-deficient mutant was generated and tested together with the wild type for its ability to consume different iron sources in CDM medium. A follow-up study was herein pursued. Differential growth behavior was observed when iron sulfate was present in both strains. Consequently, $FeSO_4$ was used to compare changes on the phenotypic, transcriptomic, proteomic and metabolomic level under high (15 µM) or low (0.2 µM) iron conditions (13, 201). Although iron is an essential metal for growth and metabolism of bacteria, freely available ("unbound") iron is limited also in the colon lumen (140). Accordingly, low iron conditions resemble better the pathogen´s natural environment. Growth experiments showed reduced growth of the mutant strain under both high iron and low iron conditions compared to the wild type, whereby both strains showed arrested growth in iron-limited medium. Omics data provided a global overview of the Fur-dependent as well as independent iron regulation. Besides the initial response to low available iron, which includes the induced expression of iron and other metal-uptake systems the expression of ferredoxin-dependent pathways such as phenylalanine, leucine, glycine degradation and butyrate fermentation was significantly reduced. In contrast, proline-reductase and RNF-complex related operons were induced. Further studies showed that not only the energy metabolism depends on the availability of iron and Fur. Flagella and pili formation were also affected. Finally, the enzymatic system involved in the resistance to the collection antimicrobial peptides (CAMPs) appeared to be impacted as well (201).

3.3.1 Fur and its role in motility

Transcriptome studies and field emission scanning microscopy (FESM) imaging showed a reduced expression of flagella genes (*fliC* operon; CDIF630erm_00348 - 00361). Impaired flagella formation in the *fur* mutant was also observed, even if the cells were exposed to high iron concentrations (13, 201). The loss of flagella is naturally accompanied by a reduction in motility. In this study, previous observations suggesting an impact on motility were attempted to be confirmed by motility assays. For this purpose, glass tubes filled with medium containing 0.175 % agar and high or low levels of iron were inoculated with wild type *C. difficile* and the corresponding *fur* mutant (Figure 42).

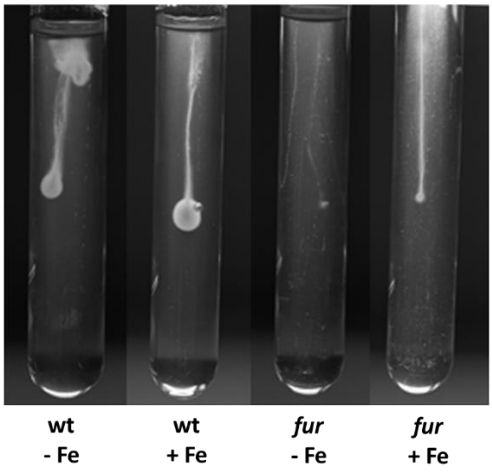

Figure 42 Motility assays of *C. difficile* wild type and the corresponding *fur* mutant.

Glass tubes were filled with CDMM agar containing low (-) or high (+) iron concentrations and were inoculated with wild type (wt) and the corresponding *fur* mutant strain. Incubation was performed anaerobically for 24 h (201).

After 24 hours of anaerobic incubation, the *fur* mutant showed a narrower inoculation halo than the wild type under high iron conditions indicating reduced motility and confirming previous results. Similar observations were made for low iron concentrations. Furthermore, the assay showed that decreased iron amounts led to a reduced flagellar formation. In many bacteria of the GI tract, flagella contribute to virulence due to their multiple functions. In *Yersinia enterolitica*, flagella can serve as a secretion apparatus for virulence factors (244, 245), in *E. coli* flagella are used as adhesins to attach to epithelia cells regardless of their motility (244, 246). In contrast, flagella-associated motility plays a crucial role in the colonization of the stomach of *Helicobacter pylori* (244, 247). Similar function

was monitored in *L. monocytogenes*, which used flagella not as adhesins but rather for motility to invade the host (244). Baban *et al.* studied the flagellation of *C. difficile* 630Δ*erm* and corresponding flagella mutants and proposed that *C. difficile* 630Δ*erm* does not depend on flagella for adherence and colonization, but that flagella-associated motility contribute to general fitness (248). These findings may be an indicative that the reduction of flagella assembly under low iron conditions or even the complete loss of flagella in the *fur* mutant (low iron) has no negative effect on virulence for *C. difficile*.

3.3.2 Fur and its role to CAMPs and vancomycin

Transcriptome analyses comparing gene expression at low iron content versus high iron amounts revealed induction of the *dlt* operon (*dtlCBAD*, CDIF630erm_03118 - 03122) in the first scenario. In addition, the operon was higher expressed in the *fur* mutant than in the wild type (201). The *dlt* operon is an enzymatic battery consisting of four proteins: DltA, a D-alanine: D-alanyl carrier protein ligase; DltB, a D-alanyl transfer protein; DltC, the D-alanyl carrier protein; and DltD, a D-alanine esterase. It is involved in the resistance to the collection antimicrobial peptides (CAMP) that are innate immune factors produced by the host to defend against invasive pathogens. The induction of this enzymatic system enables the integration of D-alanine into the teichoic acids of the bacterial cell wall, thus reducing the efficacy of CAMPs such as polymyxin B and vancomycin (249). In this study, growth experiments with the *C. difficile* wild type (wt) and the *fur* mutant should show in the first instance whether resistance to CAMPs under high iron conditions (15 µM iron sulfate) can also be confirmed at the phenotypic level. For this purpose, the bacterial strains were grown in CDMM exposed to MIC_{50} amounts of vancomycin (0.3 mg/L; 0.75 mg/L), polymyxin B (75 mg/L; 150 mg/L) and nisin (20 mg/L; 50 mg/L) (Figure 43 and Suppl. Figure 9) as described before (249, 250, 251).

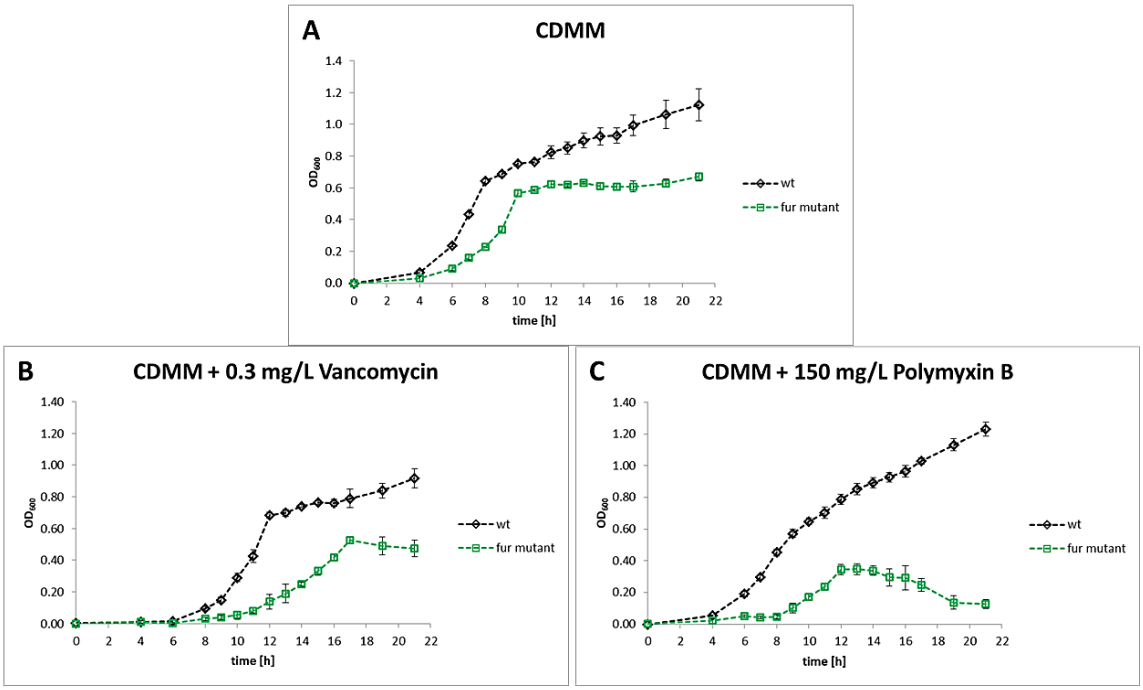

Figure 43 Phenotypical growth behavior of *C. difficile* 630Δ*erm* and *fur* mutant under high iron conditions in the presence of vancomycin and polymyxin B.

C. difficile 630Δ*erm* (black; wt) and the corresponding *fur* mutant (green) were grown in CDMM supplemented with 15 µM iron sulfate (A) in the presence of 0.3 mg/l vancomycin (B) and 150 mg/l polymyxin B (C). Growth was monitored in quadruplicates. Standard deviations are indicated (201).

The previously observed increased expression of the *dlt* operon in wild type under iron-depleted in comparison to high iron conditions indicates iron-dependent expression. Furthermore, due to the induced expression of the *dlt* operon in the *fur* mutant it can be concluded that Fur acts as repressor for the *dlt* operon. Under high iron conditions, Fur binds Fe^{2+} and forms a dimer hat can bind to Fur-boxes, thereby suppressing the transcription of Fur-regulated genes. Depression of these genes is induced when Fur dissociates from the DNA by conformational changes brought about by low iron levels (138, 158). Growth experiments in the presence of 75 mg/L and 150 mg/l polymyxin B under high iron conditions resulted in normal growth for the wild type (Figure 43C and Suppl. Figure 9B). Under these conditions, Fur might act as a suppressor resulting in reduced resistance and thus reduced growth of *C. difficile*. Nevertheless, the wild type displayed a resistance to polymyxin B even under high iron conditions suggesting that this resistance is related also to the presence of polymyxin B itself. The mutant, on the other hand, showed strongly inhibited growth under the same conditions (Figure 43C), indicating that a functional protein is needed for a

potential Fur-dependent regulation. The treatment with 0.3 mg/L vancomycin led to delayed growth for both strains *C. difficile* wild type and its isogenic *fur* mutant showing increased sensitivity after 18 h in the mutant (Figure 43B). A concentration of 75 mg/L yielded no detectable growth (Suppl. Figure 9A). These results showed that *C. difficile* is more sensitive against vancomycin than for polymyxin B, but it can also withstand vancomycin in low concentrations under high iron conditions. Induction of the *dlt* operon under low iron conditions should lead to increased resistance in both tested CAMPs, which should be tested in subsequent studies by phenotypical characterization. In contrast, the *dlt* operon does not confer resistance to nisin under high iron conditions (Suppl. Figure 9C/D).

3.4 *In vivo* testing of various *C. difficile* mutants using mouse model

C. difficile is a human pathogen, which is transmitted via the fecal-oral route in form of spores (12). Across the GI tract the germination of spores is stimulated by bile acids allowing the colonization of the intestine and colon by vegetative cells (16). The antibiotic medication and the associated suppression of the intestinal microbiota further promotes the proliferation of vegetative cells that can produce the exotoxins TcdA and TcdB (11, 16, 18) stimulating the disruption of the cytoskeleton of the intestinal mucosa and the release of pro-inflammatory cytokines (11, 12, 20). Symptoms of *C. difficile*-associated diseases (CDAD) vary from mild diarrhea to toxic megacolon and can lead to death (11, 12). In this study, investigation of the infectivity of different *C. difficile* insertional mutant strains was tested using mice as infection models. The mutants contained disrupted genes encoding the osmoprotective uptake transporter OpuC, the proline transporter PutP, the peroxide sensor regulator PerR and a riboflavin synthesis associated enzyme (*ribBA*). To simulate a natural course of infection the mice were treated with clindamycin beforehand. Afterwards, spores were administered orally to the mice. Two days after infection, the mice were tested for weight loss (Figure 44), colonization (Figure 45) and infiltration by immune cells (Figure 46).

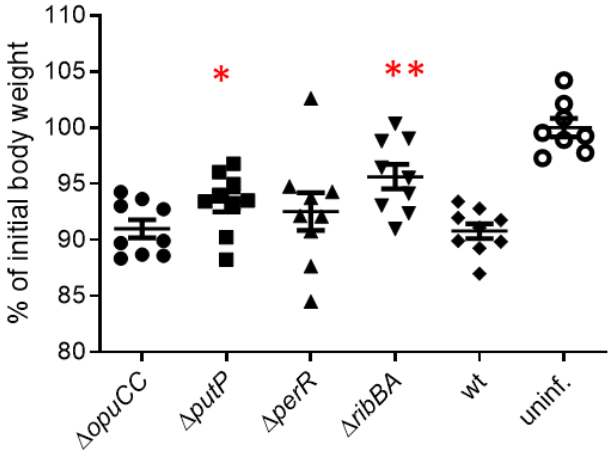

Figure 44 Body weight changes mice infected with *C. difficile* wild type and various knock out strains after two days.

Body weight was determined two days after infection of mice with spores of *C. difficile* 630Δ*erm* wild type (wt) and indicated corresponding insertional mutants. Uninfected mice were used as control. „*" indicates significance (Student´s t-test) compared to wild type: *p < 0.05, **p < 0.01, ***p < 0.001. Data were pooled from two independent experiments with five mice per experimental group. Infections were carried out by Dr. Matthias Lochner and colleagues at the TWINCORE, Hannover, Germany. The illustration was developed by Dr. Matthias Lochner.

Two days after infection, mice were first tested for weight loss (Figure 44). While the non-infected control mice retained their initial weight, mice infected with the *C. difficile* wild type strain (wt) lost about 10 % of their initial weight within the incubation period. Chen and colleagues also showed that infected mice lose substantial weight on day two and reached the lowest value of about 80 % weight loss on day three. Experiments with different *C. difficile* strains showed that the degree of weight loss was strain-specific (252). In this work, similar observations were made in the mice infected with the *opuCC* (90.98 %) and *perR* (92.5 %) mutants as those found in wild type infected mice. Equal body weight rates of the mutant-infected mice in comparison to the wild type-infected mice suggested that these mutations had no impact on the infection fitness. Although mice infected with the *putP* mutant reached 93.38 % of their original body weight, which is comparable to the *perR* mutant infected mice these values were more significant. In this case, the inactivated proline transporter may have led to reduced infectivity. The observations for the mice infected with the *ribBA* mutant led to the same conclusion. These mice reached the highest weight (95.62 %) of all tested mice with highly significant values. Another measurement that reflects colonization efficiency is the colony forming units (CFU). Here, bacteria from the

cecum and colon were isolated and then plated on agar plates to quantify the CFUs (Figure 45).

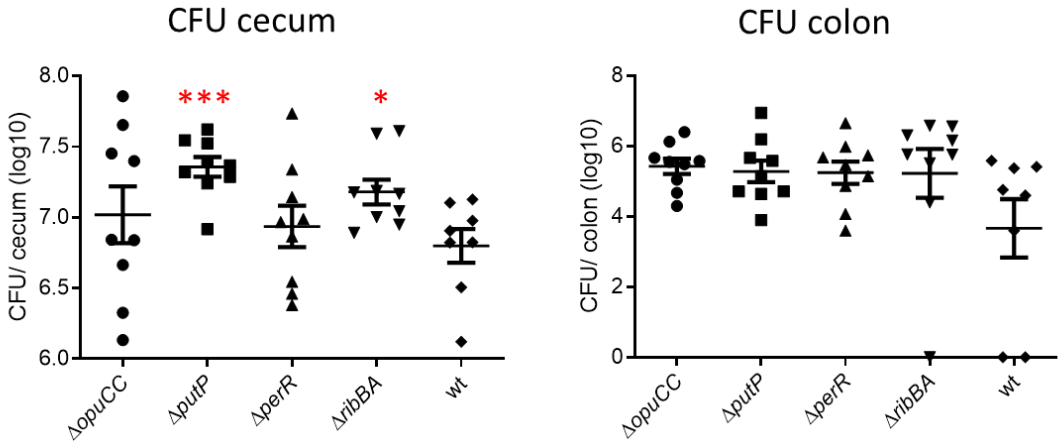

Figure 45 Colony forming units resulting from the cecum and colon of mice infected with *C. difficile* wild type and various corresponding knock out mutant strains.

Colony forming units (CFU) were quantified from the cecum and colon of infected mice by *C. difficile* 630Δ*erm* wild type (wt) and indicated corresponding insertional mutants. Uninfected mice were used as control. „*" indicates significance (Student´s t-test) compared to wild type: *p < 0.05, **p < 0.01, ***p < 0.001. Data were pooled from two independent experiments with five mice per experimental group. Infections were carried out by Dr. Matthias Lochner and colleagues at the TWINCORE, Hannover, Germany. The illustration was developed by Dr. Matthias Lochner.

The lowest CFUs were determined from both the cecum and colon of the wild type (log10 of 6.8 and 3.7, respectively). Similar amounts of colonies were quantified on average for the *perR* (log10 of 6.9) and for the *opuCC* mutant (log10 of 7.0) in the cecum. However, the replicates among themselves showed large fluctuations. A higher colonization rate was achieved by the *ribBA* (log10 of 7.2) and *putP* mutant (log10 of 7.35). The colon was colonized by all mutants at similar rates (log10 of 5.23 to 5.28), whereas the *opuCC* mutant displayed the highest CFUs with log10 of 5.43 values. In conclusion, the quantification of CFUs resulted in higher cell amounts in the cecum than in the colon for all tested *C. difficile* strains indicating enhanced colonization of the cecum. In humans, CDI usually causes intestinal lesions in the descending colon. However, CDI-affected intestinal segments are species-specific and thus an increased colonization of the cecum with a slight extension in the colon is typically observed in mice but also in hamsters (252, 253). After colonization, vegetative cells can produce the exotoxins TcdA and TcdB, catalyzing the transfer of glycosyl residues to small Rho GTPases, which leads to inactivation of Rho and disruption of the

cytoskeleton of the intestinal mucosa (11, 20). Furthermore, the toxins stimulate an inflammatory response involving neutrophil infiltration and trigger an inflammatory cascade of cytokines, when they come in contact with macrophages, monocytes and dendritic cells (254). The inflammatory response, indicated by the frequency of neutrophils, macrophages and dendritic cells in response to wild type infection as well as to the different mutants was studied below (Figure 46).

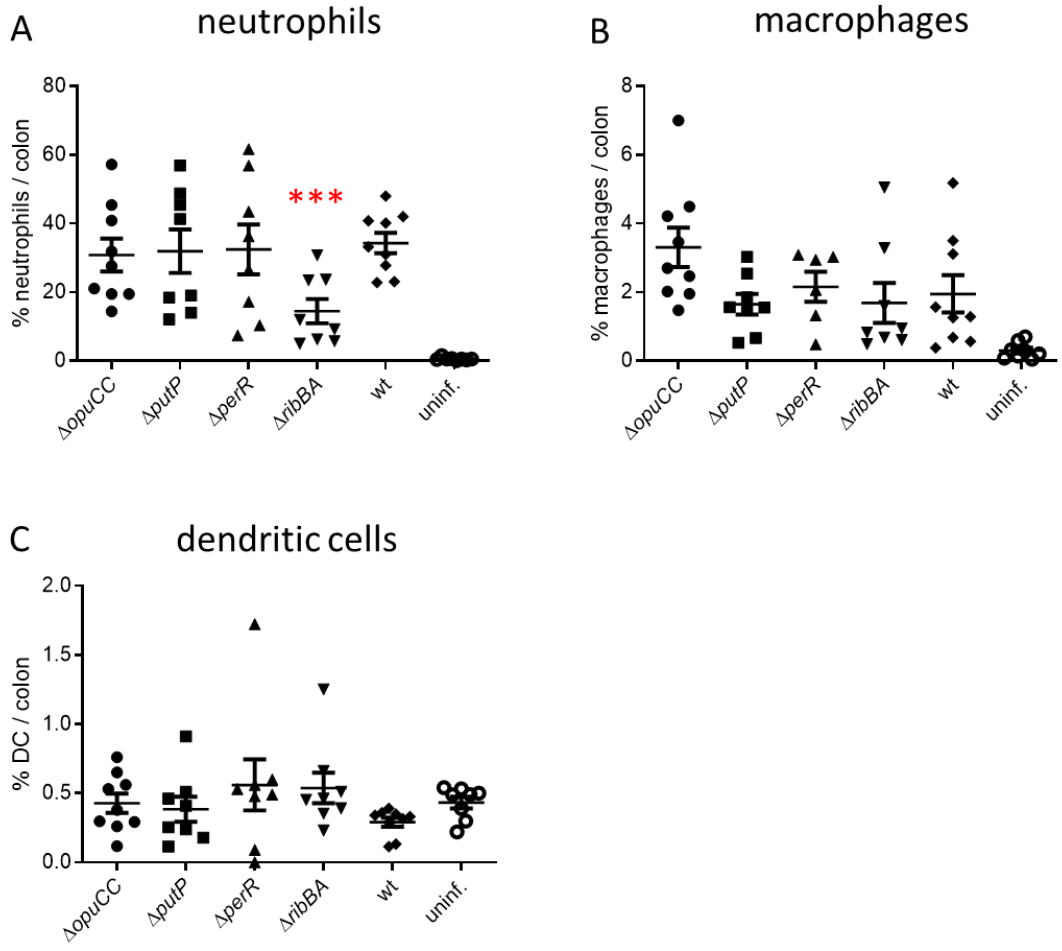

Figure 46 Infiltration of immune cells into the colon in response to infection with *C. difficile* wild type and mutant strains.

Frequency (%) of A) neutrophils, B) macrophages and C) dendritic cells (DC) analyzed from the colon of mice after infection with *C. difficile* 630Δ*erm* wild type (wt) and outlined corresponding insertional mutants. Uninfected mice were used as control. „*" indicates significance (Student´s t-test) compared to the wild type: *p < 0.05, **p < 0.01, ***p < 0.001. Data were pooled from two independent experiments with five mice per experimental group. Infections were carried out by Dr. Matthias Lochner and colleagues at the TWINCORE, Hannover, Germany. Illustrations were developed by Dr. Matthias Lochner.

All tested *C. difficile* strains led to an infiltration of all analyzed immune cells. The infiltration of neutrophils yielded a frequency of 34.3 % of living immune cells when mice were infected with the *C. difficile* wild type (Figure 46A). Similar frequencies but with larger deviations were found in mice infected with the mutants (30.8 % to 32.5 %), except those infected with *ribBA* mutants. In the latter, the frequency of neutrophils was reduced by half (14.5 %). Neutrophils are the most abundant leukocytes that proliferate dramatically during infection due to the key chemokine and activator Il-8 produced by the host (255). Neutrophils play a key role within the immune response, since they are not only capable of phagocytosis, but also further activate immune cells such as macrophages or dendritic cells (255). Our investigations yielded macrophage frequencies of 1.95 % in mice infected with the wild type (Figure 46B). The *putP*- and *ribBA*-mutant infected mice produced macrophages with slightly decreased frequencies of 1.65 % and 1.69 %, while frequencies in *perR* and *opuCC* mutant infected mice were detected at higher values (2.16 % and 3.31 %). Proliferation of dendritic cells (DC) resulted in the same frequencies in mutant infected mice as in uninfected mice, whereas a slightly low number of DC was measured in wild type infected mice (Figure 46C).

These investigations on the infectivity of different *C. difficile* insertion mutants resulted in a consistent phenotype for the *ribBA* mutant. Despite the higher colonization rate in the cecum and colon in comparison to the wild type, the reduced weight loss and reduced neutrophil frequency indicates a decreased inflammatory response, probably caused by reduced infectivity of the *ribBA* mutant. The reduced amount of neutrophils also leads to less tissue damage by the immune cells themselves (255). The gene *ribBA* (CDIF630erm_01883) encodes for a bifunctional enzyme (3,4-dihydroxy-2-butanone 4-phosphate synthase / GTP cyclohydrolase-2) involved in the biosynthesis of riboflavin. Riboflavin (vitamin B_2) is essential in all organism and acts as precursor of flavin mononucleotides (FMN) and flavin adenine dinucleotides (FAD), which are cofactors for several redox enzymes (240, 241). Growth experiments of the *C. difficile ribBA* mutant in comparison to the wild type cultivated in medium without riboflavin resulted in an inhibited growth (Suppl. Figure 10A). However, colonization was detected in the cecum and colon (Figure 45), which could be explained by an uptake of extracellular riboflavin. *C. difficile* contains a riboflavin

transporter RibU (CDIF630erm_00266), which is still active in the *ribBA* mutant. The supplementation of riboflavin to the growth medium prompted to an improved growth of both *C. difficile* wild type and *ribBA* mutant (Suppl. Figure 10B). Nevertheless, the inactivation of the corresponding enzyme reduces the inflammatory response. The infection with the *putP* mutant led also to significant changes regarding body weight and colonization of the cecum. The gene *putP* (CDIF630erm_03896) encodes for the proline transporter PutP. Proline belongs to the essential amino acids in *C. difficile* playing an important role in the colonization (256). Battaglioli and colleagues showed that a proline-deficient diet of dysbiotic mice lead to a decreased colonization. In addition, a *prdB* mutant, which lacks an essential enzyme in the Stickland fermentation of proline, causes decreased colonization and toxin B formation (256). The results of this work led to an increased colonization of the *putP* mutant. The inactivation of the transporter would imply that proline cannot be transferred into the cell and thus is not available as an energy source that would imply a reduced spread of the mutant. Further investigations are necessary to verify the impact of the PutP deficiency on *C. difficile*. In contrast, the mice infected with the other mutants showed no differences to that infected with the *C. difficile* wild type. Previous studies with the *opuCC* mutant already showed that the growth behavior (see 3.1.4) as well as the toxin production (see 3.1.8) does not differ significantly from that of the wild type, as long as unstressed conditions prevail. Only increased salt concentrations led to different observations. Further infection studies may be necessary, in which the animals ingest salt-rich nutrients in order to generate the stress stimuli and obtain a phenotype on an immunological level.

The *perR* mutant displayed, as shown above (see 3.2.2VII), a reduced butanoate formation. Butanoate, in higher concentrations, improve the inflammatory host response and reduce tissue damage. It was shown, that the restoration of intestinal concentrations of butyrate attenuated CDI in mice (238). Consequently, the PerR mutation could have led to a reduced inflammatory response and more pronounced CDI symptoms, such as significant weight loss, but this requires further investigations.

4. CONCLUSION AND PERSPECTIVES

C. difficile is a human pathogen of the gastrointestinal tract and the leading cause of severe nosocomial diarrhea and pseudomembranous colitis, which can ultimately lead to death. During infection, this strictly anaerobic and spore-forming pathogen is exposed to varying osmolarities, oxygen concentrations and iron availability. In the present study, the adaptative responses to high salinity conditions and the regulatory network of the peroxide sensor PerR were characterized. Furthermore, former observations of the Fur-dependent iron regulation were further inspected by phenotypical profiling.

4.1 Response of *C. difficile* to high osmolarity

Bioinformatic mining via structural comparisons of *C. difficile* transport systems with known osmolyte transporters identified two proteins, the already annotated OpuC (CDIF630erm_01020/ CDIF630erm_01021) and the unknown transporter system "UtS" (CDIF630erm_03509/ CDIF630erm_03510). Both transporters are each encoded by two genes and thus reveal a similar genetic architecture as the genes encoding the OpuF transporter of *B. infantis*. The $OpuC_{Cdiff}$ transporter was recombinantly produced in the osmolyte transporter-deficient *B. subtilis* strain TMB118 to determine its substrate spectrum. A transport spectrum consisting of carnitine, glycine betaine, choline, γ-butyrobetaine, homobetaine, proline betaine, crotonobetaine, dimethyl sulfoniopropionate (DMSP) and ectoine was found comparable to that of OpuC from *B. subtilis* when the organism was exposed to high osmolarity. In contrary, the UtS showed no compatible solute transport capacities under identical test conditions. Subsequently, the osmotic stress tolerance of *C. difficile* and the corresponding *opuCC* mutant was evaluated by the addition of increasing NaCl amounts. Upon 350 mM NaCl, significantly reduced growth was observed for the wild type strain, whereas growth of the mutant strain was nearly abolished. Addition of the compatible solutes carnitine, glycine betaine, γ-butyrobetaine, crotonobetaine, homobetaine, proline betaine, and DMSP restored bacterial growth in the wild type but not in the *opuCC* mutant. Choline did not appear to display any osmo-protective function. Additionally, changes in phenotypic growth behavior in response to osmotic stress correlated with drastic morphological changes were revealed by electron microscopy. The commonly rod-shaped organism switched to a coccoid cell form under salt stress

and reverted to its natural morphology in the presence of 1 mM carnitine. Interestingly, salt addition led to reduced Toxin A production being only partially restored by carnitine supplementation. Finally, metabolome analyses showed diminished amounts of the archetypical fermentation products involved in the oxidative and reductive Stickland reactions, such as butanoate and isocaproate. While acetate, propanoate and isobutanoate were substantially reduced, the alcoholic fermentation products remained unaffected. The addition of carnitine restored almost entirely the metabolic fingerprints of the wild type to the levels of the control. In contrast, the metabolic profile of the *opuCC* mutant was not rescued by the addition of carnitine. *In vivo* analyses with the *opuCC* mutant and with the wild type strain in mouse model revealed no significant differences. Further infection studies may be required, in which the animals ingest salt-rich nutrients to generate the stress stimuli necessary to obtain a visual infection phenotype.

4.2 The non-oxygen stress regulation mediated by H_2O_2-responsive regulator PerR in *C. difficile*

The regulator PerR is described in many bacteria as a peroxide sensor, which is involved in the response to oxidative stress acting as a H_2O_2-response repressor of gene expression. In this thesis the H_2O_2-independent PerR regulation was defined using a holistic systems biology approach encompassing transcriptome and metabolome analyses. The phenotypic growth behavior of a *perR*-deficient mutant showed a significant growth deficit in the stationary phase compared to the wild type. A closer look into the network of PerR-dependent regulation in the absence of H_2O_2 revealed that PerR is involved in the repression of genes of fatty acid and riboflavin/thiamine biosynthesis as well as flagellar assembly in the exponential phase. The same processes were strongly de-repressed in the stationary phase. Similarly, threonine and phenylalanine biosynthesis, tyrosine fermentation, polyamine biosynthesis, proline reductase, the associated RNF complex, and cell wall synthesis were repressed by PerR in the exponential phase. However, in the stationary phase, gene expression and metabolism were found almost identical to the wild type. Interestingly, PerR-regulated pathways correlated highly with the Fur-dependent regulation which was previously

investigated (13, 201). This observation combined with the identification of a potential Fur binding box upstream of the *perR*-operon and the up-regulation of Fur in the absence of PerR suggests a co-regulation of the regulators Fur and PerR. Further studies, such as EMSAs are necessary to define Fur- and PerR-DNA binding sites and to confirm the direct or indirect regulation of these regulators. *In vivo* analyses of the *perR* mutant in mouse model showed no differences to the *C. difficile* wild type strain.

4.3 Experiments for the characterization of the iron-regulator Fur

Previous transcriptome results indicated a reduction of flagella formation under low iron conditions in the *C. difficile* wild type strain and in the *fur* mutant. In this work, strongly impaired motility was shown under low iron conditions for the wild type and for the *fur* mutant. It was also shown that *C. difficile* wild type exhibits resistance to CAMPs such as polymyxin B and vancomycin at high iron concentrations, while the *fur* mutant remained strongly inhibited in its growth under the identical conditions.

In summary, this work contributed to our overall understanding of the molecular mechanism underlying the adaptive responses elicited by *C. difficile* under stress conditions, laying the groundwork for future investigations of this prominent human pathogen.

5. ZUSAMMENFASSUNG UND AUSSICHT

C. difficile ist ein humanpathogener Erreger des Gastrointestinaltrakts und die Hauptursache für schwere Diarrhöe und pseudomembranöse Kolitis, die letztlich zum Tod führen können. Während der Infektion ist dieser streng anaerobe und sporenbildende Erreger schwankenden Osmolaritäten, Sauerstoffkonzentrationen und Eisenverfügbarkeiten ausgesetzt. In der vorliegenden Studie wurden die adaptiven Reaktionen auf Bedingungen mit hohem Salzgehalt und das regulatorische Netzwerk des Peroxidsensors PerR charakterisiert. Darüber hinaus wurden frühere Beobachtungen der Fur-abhängigen Eisenregulation durch phänotypische Profilierung weiter untersucht.

Durch bioinformatische Strukturvergleiche von *C. difficile*-Transportsystemen mit bekannten Osmolyt-Transportern wurden zwei Proteine identifiziert, einerseits der bereits annotierte OpuC Transporter (CDIF630erm_01020/ CDIF630erm_01021) und andererseits das unbekannte Transportsystem "UtS" (CDIF630erm_03509/ CDIF630erm_03510). Beide Transporter werden jeweils von zwei Genen kodiert und weisen damit eine ähnliche genetische Architektur auf wie die Gene, die den OpuF-Transporter von *B. infantis* kodieren. Der $OpuC_{Cdiff}$-Transporter wurde rekombinant in dem Osmolyt-Transporter-defizienten *B. subtilis*-Stamm TMB118 produziert, um sein Substratspektrum zu bestimmen. Carnitin, Glycinbetain, Cholin, γ-Butyrobetain, Homobetain, Prolinbetain, Crotonobetain, Dimethylsulfoniopropionat (DMSP) und Ectoin wurden durch $OpuC_{Cdiff}$ transportiert, vergleichbar mit OpuC aus *B. subtilis*. Im Gegensatz dazu zeigte das UtS unter identischen Versuchsbedingungen keine Transportkapazitäten für die kompatiblen Solute. Anschließend wurde die osmotische Stresstoleranz von *C. difficile* und der entsprechenden *opuCC*-Mutante durch die Zugabe steigender NaCl-Mengen untersucht. Bei 350 mM NaCl wurde beim Wildtyp-Stamm ein signifikant reduziertes Wachstum beobachtet, während das Wachstum des mutierten Stammes nahezu aufgehoben war. Durch die Zugabe der kompatiblen Solute Carnitin, Glycinbetain, γ-Butyrobetain, Crotonobetain, Homobetain, Prolinbetain und DMSP konnte das bakterielle Wachstum des Wildtyps wiederhergestellt werden, nicht aber das Wachstum der *opuCC*-Mutante. Cholin schien keine osmoprotektive Funktion zu haben. Zusätzlich korrelierten Veränderungen im

phänotypischen Wachstumsverhalten als Reaktion auf osmotischen Stress mit drastischen morphologischen Veränderungen, wie sie in der Elektronenmikroskopie sichtbar wurden. Der üblicherweise stäbchenförmige Organismus wechselte unter Salzstress in eine kokkoide Zellform und kehrte in Gegenwart von 1 mM Carnitin zu seiner natürlichen Morphologie zurück. Interessanterweise führte die Salzzugabe zu einer verminderten Toxin A-Produktion, die durch Carnitin-Supplementierung nur teilweise wiederhergestellt wurde. Schließlich zeigten Metabolomanalysen verminderte Mengen der archetypischen Fermentationsprodukte, die an den oxidativen und reduktiven Stickland-Reaktionen beteiligt sind, wie Butanoat und Isocaproat. Während weiterhin Acetat, Propanoat und Isobutanoat deutlich reduziert waren, blieben die alkoholischen Gärungsprodukte unbeeinflusst. Die Zugabe von Carnitin stellte den metabolischen Fingerabdruck des Wildtyps fast vollständig auf das Niveau der Kontrolle wieder her. Im Gegensatz dazu wurde das metabolische Profil der *opuCC*-Mutante nicht durch die Zugabe von Carnitin gerettet. *In vivo*-Analysen mit der *opuCC*-Mutante und mit dem Wildtyp-Stamm im Mausmodell zeigten keine signifikanten Unterschiede. Möglicherweise sind weitere Infektionsstudien erforderlich, bei denen die Tiere salzreiche Nährstoffe aufnehmen, um die notwendigen Stressreize zu erzeugen, um einen visuellen Phänotyp und eine entsprechende immunologische Reaktion zu erhalten.

5.1 Die Nicht-Sauerstoff-Stress-Regulation, vermittelt durch den H_2O_2-sensitiven Regulator PerR in *C. difficile*

Der Regulator PerR ist in vielen Bakterien als Peroxid-Sensor beschrieben, der als H_2O_2-abhängiger Repressor der Genexpression an der Antwort auf oxidativen Stress beteiligt ist. In dieser Arbeit wurde die H_2O_2-unabhängige PerR-Regulation mit einem ganzheitlichen systembiologischen Ansatz, der Transkriptom- und Metabolomanalysen umfasst, definiert. Das phänotypische Wachstumsverhalten einer *perR*-defizienten Mutante zeigte ein signifikantes Wachstumsdefizit in der stationären Phase im Vergleich zum Wildtyp. Eine genauere Betrachtung des Netzwerks der PerR-abhängigen Regulation in Abwesenheit von H_2O_2 zeigte, dass PerR an der Repression von Genen der Fettsäure- und Riboflavin/Thiamin-Biosynthese sowie der Flagellenassemblierung in der exponentiellen Phase

beteiligt ist. Die gleichen Prozesse waren in der stationären Phase stark de-reprimiert. Ebenso wurden die Threonin- und Phenylalanin-Biosynthese, die Tyrosin-Fermentation, die Polyamin-Biosynthese, die Prolin-Reduktase Reaktion, wie die des dazugehörigen RNF-Komplexes und die Zellwandbiosynthese in der exponentiellen Phase durch PerR unterdrückt. In der stationären Phase wurde jedoch eine fast identische Genexpression und ein fast identischer Metabolismus wie beim Wildtyp vorgefunden. Interessanterweise korrelierten die PerR-regulierten Stoffwechselwege stark mit der Fur-abhängigen Regulation, die bereits zuvor untersucht wurde (201). Diese Beobachtung in Kombination mit der Identifizierung einer potentiellen Fur-Bindungsstelle stromaufwärts des PerR-Operons und der Hochregulierung von Fur in Abwesenheit von PerR legen eine Co-Regulation der Regulatoren Fur und PerR nahe. Weitere Studien, wie z. B. EMSAs, sind notwendig, um Fur- und PerR-DNA-Bindungsstellen zu definieren und die direkte oder indirekte Regulation dieser Regulatoren zu bestätigen. *In vivo*-Analysen der *perR*-Mutante im Mausmodell zeigten keine Unterschiede zum *C. difficile*-Wildtyp-Stamm.

5.2 Experimente zur Charakterisierung des Eisen-Regulators Fur

Frühere Transkriptom-Ergebnisse deuteten auf eine reduzierte Flagellenbildung unter eisenarmen Bedingungen im *C. difficile* Wildtypstamm und in der Fur-Mutante hin. In dieser Arbeit wurde eine stark beeinträchtigte Motilität unter eisenarmen Bedingungen für den Wildtyp und für die *fur*-Mutante gezeigt. Außerdem wurde gezeigt, dass der *C. difficile* Wildtyp bei hohen Eisenkonzentrationen eine Resistenz gegen CAMPs wie Polymyxin B und Vancomycin aufweist, während die *fur*-Mutante unter den identischen Bedingungen in ihrem Wachstum stark gehemmt blieb.

Zusammenfassend hat diese Arbeit zum Gesamtverständnis der molekularen Mechanismen beigetragen, der den von *C. difficile* unter Stressbedingungen ausgelösten adaptiven Reaktionen zugrunde liegen, und damit weitere Grundlage für zukünftige Untersuchungen dieses prominenten Humanpathogens gelegt.

6. REFERENCES

1. Vos PD, Garrity GM, Jones D, Krieg NR, Ludwig W, Rainey FA, Schleifer KH, & Whitman WB. Bergey's Manual® of Systematic Bacteriology. In *Systematic Bacteriology*, edn 2, Eds Vos PD, Garrity GM, Jones D, Krieg NR, Ludwig W, Rainey FA, Schleifer KH, & Whitman WB. Springer New York,2009.

2. Michel AMD. Oxidative Stressantwort von *Clostridium difficile*. 2016.

3. Collins MD, Lawson PA, Willems A, Cordoba JJ, Fernandez-Garayzabal J, Garcia P, Cai J, Hippe H, & Farrow JAE. The Phylogeny of the Genus *Clostridium*: Proposal of Five New Genera and Eleven New Species Combinations. *International Journal of Systematic Bacteriology* 1994 **44** 812–826. (doi:10.1099/00207713-44-4-812)

4. Hall IC & O'Toole E. INTESTINAL FLORA IN NEW-BORN INFANTS: WITH A DESCRIPTION OF A NEW PATHOGENIC ANAEROBE, BACILLUS DIFFICILIS. *American Journal of Diseases of Children* 1935 **49** 390–402. (doi:10.1001/archpedi.1935.01970020105010)

5. SNEATH PHA, McGOWAN V, & SKERMAN VBD. Approved Lists of Bacterial Names. *International Journal of Systematic and Evolutionary Microbiology* 1980 **30** 225–420. (doi:10.1099/00207713-30-1-225)

6. Yutin N & Galperin MY. A genomic update on clostridial phylogeny: Gram-negative spore formers and other misplaced clostridia. *Environmental Microbiology* 2013 **15** 2631–2641. (doi:10.1111/1462-2920.12173)

7. Lawson PA, Citron DM, Tyrrell KL, & Finegold SM. Reclassification of *Clostridium difficile* as *Clostridioides difficile* (Hall and O'Toole 1935) Prévot 1938. *Anaerobe* 2016 **40** 95–99. (doi:10.1016/j.anaerobe.2016.06.008)

8. Kochan TJ, Foley MH, Shoshiev MS, Somers MJ, Carlson PE, & Hanna PC. Updates to *Clostridium difficile* Spore Germination. *Journal of Bacteriology* 2018 **200** 1–12. (doi:10.1128/JB.00218-18)

9. Hatheway CL. Toxigenic Clostridia. *Clinical Microbiology Reviews* 1990 **3** 66–98. (doi:10.1128/cmr.3.1.66)

10. Bartlett JG. *Clostridium difficile*: History of Its Role as an Enteric Pathogen and the Current State of Knowledge About the Organism. *Clinical Infectious Diseases* 1994 **18** S265–S272. (doi:10.1093/clinids/18.Supplement_4.S265)

11. Kelly CP & Lamont JT. *CLOSTRIDIUM DIFFICILE* INFECTION. *Annu. Rev. Med.* 1998 **49** 375–390. (doi:10.1146/annurev.med.49.1.375)

12. Martin JSH, Monaghan TM, & Wilcox MH. *Clostridium difficile* infection: epidemiology, diagnosis and understanding transmission. *Nature Reviews Gastroenterology and Hepatology* 2016 **13** 206–216. (doi:10.1038/nrgastro.2016.25)

13. Berges MP. Transcriptional , proteomic and metabolic networks of the Fur-regulated iron metabolism of *Clostridium difficile*. 2017.

14. Lessa FC, Mu Y, Bamberg WM, Beldavs ZG, Dumyati GK, Dunn JR, Farley MM, Holzbauer SM, Meek JI, Phipps EC, Wilson LE, Winston LG, Cohen JA, Limbago BM, Fridkin SK, Gerding DN, & Mcdonald LC. Burden of *Clostridium difficile* Infection in the United States. *The New England Journal of Medicine* 2015 **372** 825–834. (doi:10.1056/NEJMoa1408913)

15. Miller BA, Chen LF, Sexton DJ, & Anderson DJ. Comparison of the Burdens of Hospital-Onset, Healthcare Facility-Associated *Clostridium difficile* Infection and of Healthcare-Associated Infection due to Methicillin-Resistant *Staphylococcus aureus* in Community Hospitals. *Infection Control & Hospital Epidemiology* 2011 **32** 387–390. (doi:10.1086/659156)

16. Sorg JA & Sonenshein AL. Inhibiting the Initiation of *Clostridium difficile* Spore Germination using Analogs of Chenodeoxycholic Acid, a Bile Acid. *JOURNAL OF BACTERIOLOGY* 2010 **192** 4983–4990. (doi:10.1128/JB.00610-10)

17. Kochan TJ, Shoshiev MS, Hastie JL, Somers MJ, Plotnick YM, Gutierrez-Munoz DF, Foss ED, Schubert AM, Smith AD, Zimmerman SK, Carlson PE, & Hanna PC. Germinant Synergy Facilitates *Clostridium difficile* Spore Germination under Physiological Conditions. *mSphere* 2018 **3** e00335-18. (doi:10.1128/MSPHERE.00335-18)

18. Furuya-Kanamori L, Marquess J, Yakob L, Riley T V., Paterson DL, Foster NF, Huber CA, & Clements ACA. Asymptomatic *Clostridium difficile* colonization: Epidemiology and clinical implications. *BMC Infectious Diseases* 2015 **15** 516. (doi:10.1186/s12879-015-1258-4)

19. Aktories K, Schwan C, & Jank T. *Clostridium difficile* Toxin Biology. *Annual Review of Microbiology* 2017 **71** 281–307. (doi:10.1146/annurev-micro-090816)

20. Shen A. *Clostridium difficile* Toxins: Mediators of Inflammation. *Journal of Innate Immunity* 2012 **4** 149–158. (doi:10.1159/000332946)

21. Chandrasekaran R & Borden Lacy D. The role of toxins in *Clostridium difficile* infection. *FEMS Microbiology Reviews* 2017 **41** 723–750. (doi:10.1093/femsre/fux048)

22. Dingle KE, Elliott B, Robinson E, Griffiths D, Eyre DW, Stoesser N, Vaughan A, Golubchik T, Fawley WN, Wilcox MH, Peto TE, Walker AS, Riley T V., Crook DW, & Didelot X. Evolutionary History of the *Clostridium difficile* Pathogenicity Locus. *Genome Biology and Evolution* 2014 **6** 36–52. (doi:10.1093/GBE/EVT204)

23. Hundsberger T, Braun V, Weidmann M, Leukel P, Sauerborn M, & Eichel-Streiber C. Transcription analysis of the genes *tcdA-E* of the pathogenicity locus of *Clostridium difficile*. *European Journal of Biochemistry* 1997 **244** 735–742. (doi:10.1111/j.1432-1033.1997.t01-1-00735.x)

24. Dupuy B & Sonenshein AL. Regulated transcription of *Clostridium difficile* toxin genes. *Molecular Microbiology* 1998 **27** 107–120. (doi:10.1046/j.1365-2958.1998.00663.x)

25. Darkoh C, Dupont HL, Norris SJ, & Kaplan HB. Toxin Synthesis by *Clostridium difficile* Is Regulated through Quorum Signaling. *mBio* 2015 **6** e02569-14. (doi:10.1128/mBio.02569-14)

26. Hofmann JD, Otto A, Berges M, Biedendieck R, Michel AM, Becher D, Jahn D, & Neumann-Schaal M. Metabolic Reprogramming of *Clostridioides difficile* During the Stationary Phase With the Induction of Toxin Production. *Frontiers in Microbiology* 2018 **9** 1970. (doi:10.3389/fmicb.2018.01970)

27. Neumann-Schaal M, Hofmann JD, Will SE, & Schomburg D. Time-resolved amino acid uptake of *Clostridium difficile* 630Δerm and concomitant fermentation product and toxin formation. *BMC Microbiology* 2015 **15** 281. (doi:10.1186/s12866-015-0614-2)

28. Yamakawa K, Karasawa T, Ikoma S, & Nakamura S. Enhancement of *Clostridium difficile* toxin production in biotin-limited conditions. *J. Med Microbiol.* 1996 **44** 111–114. (doi:10.1099/00222615-44-2-111)

29. Karlsson S, Lindberg A, Norin E, Burman LG, & Akerlund T. Toxins, Butyric Acid, and Other Short-Chain Fatty Acids Are Coordinately Expressed and Down-Regulated by Cysteine in *Clostridium difficile*. *Infection and Immunity* 2000 **68** 5881–5888. (doi:10.1128/IAI.68.10.5881-5888.2000)

30. Karlsson S, Burman LG, & Akerlund T. Suppression of toxin production in *Clostridium difficile* VPI 10463 by amino acids. *Microbiology* 1999 **145** 1683–1693. (doi:10.1099/13500872-145-7-1683)

31. Jurtshuk PJ. Bacterial metabolism. In *Medical Microbiology*,ch. 4, Ed Baron S. University of Texas Medical Branch at Galveston,1996.

32. Neumann-Schaal M, Jahn D, & Schmidt-Hohagen K. Metabolism the Difficile Way: The Key to the Success of the Pathogen *Clostridioides difficile*. *Frontiers in Microbiology* 2019 **10** 219. (doi:10.3389/fmicb.2019.00219)

33. MEAD GC. The Amino Acid-fermenting Clostridia. *Journal of General Microbiology* 1971 **67** 47–56. (doi:10.1099/00221287-67-1-47)

34. Jackson S, Calos M, Myers A, & Self WT. Analysis of Proline Reduction in the Nosocomial Pathogen *Clostridium difficile*. *Journal of Bacteriology* 2006 **188** 8487–8495. (doi:10.1128/JB.01370-06)

35. Elsden SR, Hilton MG, & Waller JM. The End Products of the Metabolism of Aromatic Amino Acids by Clostridia. *Arch. Microbiol.* 1976 **107** 283–288. (doi:10.1007/BF00425340)

36. Elsden SR & Hilton MG. Volatile Acid Production from Threonine, Valine, Leucine and Isoleucine by Clostridia. *Arch. Microbiol.* 1978 **117** 165–172. (doi:10.1007/BF00402304)

37. Stickland LH. STUDIES IN THE METABOLISM OF THE STRICT ANAEROBES (GENUS *CLOSTRIDIUM*): THE CHEMICAL REACTIONS BY WHICH *CL. SPOROGENES* OBTAINS ITS ENERGY. *Biochemical Journal* 1934 **28** 1746–1759. (doi:10.1042/bj0281746)

38. Elsden SR & Hilton MG. Amino Acid Utilization Patterns in Clostridial Taxonomy. *Arch. Microbiol.* 1979 **123** 137–141. (doi:10.1007/BF00446812)

39. Tremblay PL, Zhang T, Dar SA, Leang C, & Lovley DR. The Rnf Complex of *Clostridium ljungdahlii* Is a Proton-Translocating Ferredoxin: NAD+ Oxidoreductase Essential for Autotrophic Growth. *mBio* 2013 **4** e00406-12. (doi:10.1128/mBio.00406-12)

40. Roeßler M & Müller V. Osmoadaptation in bacteria and archaea: Common principles and differences. *Environmental Microbiology* 2001 **3** 743–754. (doi:10.1046/j.1462-2920.2001.00252.x)

41. Wood JM. Osmosensing by Bacteria: Signals and Membrane-Based Sensors. *Microbiology and Molecular Biology Reviews* 1999 **63** 230–262. (doi:10.1128/mmbr.63.1.230-262.1999)

42. Overduin J, Tylee TS, Frayo RS, & Cummings DE. Hyperosmolarity in the Small Intestine Contributes to Postprandial Ghrelin Suppression. *American Journal of Physiology Gastrointestinal and Liver Physiology* 2014 **306** G1108–G1116. (doi:10.1152/ajpgi.00072.2014)

43. Morbach S & Krämer R. Body Shaping under Water Stress: Osmosensing and Osmoregulation of Solute Transport in Bacteria. *ChemBioChem* 2002 **3** 384. (doi:10.1002/1439-7633(20020503)3:5<384::AID-CBIC384>3.0.CO;2-H)

44. Csonka LN & Hanson AD. PROKARYOTIC OSMOREGULATION: Genetics and Physiology. *Annual Review of Microbiology* 1991 **45** 569–606. (doi:10.1146/annurev.mi.45.100191.003033)

45. Boch J, Kempf B, & Bremer E. Osmoregulation in *Bacillus subtilis*: Synthesis of the Osmoprotectant Glycine Betaine from Exogenously Provided Choline. *Journal of Bacteriology* 1994 **176** 5364–5371. (doi:10.1128/jb.176.17.5364-5371.1994)

46. Csonka LN. Physiological and Genetic Responses of Bacteria to Osmotic Stress. *Microbiological Reviews* 1989 **53** 121–147. (doi:10.1128/mmbr.53.1.121-147.1989)

47. Hoffmann T, Boiangiu C, Moses S, & Bremer E. Responses of *Bacillus subtilis* to Hypotonic Challenges: Physiological Contributions of Mechanosensitive Channels to Cellular Survival. *Applied and Environmental Microbiology* 2008 **74** 2454–2460. (doi:10.1128/AEM.01573-07)

48. Wilson ME, Maksaev G, & Haswell ES. MscS-like Mechanosensitive Channels in Plants and Microbes. *Biochemistry* 2013 **52** 5708–5722. (doi:10.1021/bi400804z)

49. Booth IR, Edwards MD, Black S, Schumann U, & Miller S. Mechanosensitive channels in bacteria: signs of closure? *Nature Reviews Microbiology*2007. pp 431–440. . (doi:10.1038/nrmicro1659)

50. Lucht JM & Bremer E. Adaptation of *Escherichia coli* to high osmolarity environments: Osmoregulation of the high-affinity glycine betaine transport system ProU. *FEMS Microbiology Reviews* 1994 **14** 3–20. (doi:10.1111/j.1574-6976.1994.tb00067.x)

51. Weinisch L, Kühner S, Roth R, Grimm M, Roth T, Netz DJA, Pierik AJ, & Filker S. Identification of osmoadaptive strategies in the halophile, heterotrophic ciliate *Schmidingerothrix salinarum*. *PLOS Biology* 2018 **16** e2003892. (doi:10.1371/journal.pbio.2003892)

52. Sleator RD & Hill C. Bacterial osmoadaptation: the role of osmolytes in bacterial stress and virulence. *FEMS Microbiology Reviews* 2001 **26** 49–71. (doi:10.1111/j.1574-6976.2002.tb00598.x)

53. Siglioccolo A, Paiardini A, Piscitelli M, & Pascarella S. Structural adaptation of extreme halophilic proteins through decrease of conserved hydrophobic contact surface. *BMC Structural Biology* 2011 **11** . (doi:10.1186/1472-6807-11-50)

54. Gunde-Cimerman N, Plemenitaš A, & Oren A. Strategies of adaptation of microorganisms of the three domains of life to high salt concentrations. *FEMS Microbiology Reviews* 2018 **42** 353–375. (doi:10.1093/femsre/fuy009)

55. Holtmann G, Bakker EP, Uozumi N, & Bremer E. KtrAB and KtrCD: Two K+ uptake systems in *Bacillus subtilis* and their role in adaptation to hypertonicity. *Journal of Bacteriology* 2003 **185** 1289–1298. (doi:10.1128/JB.185.4.1289-1298.2003)

56. Epstein W. Osmoregulation by potassium transport in *Escherichia coli*. *FEMS Microbiology Letters* 1986 **39** 73–78. (doi:10.1111/j.1574-6968.1986.tb01845.x)

57. Voelkner P, Puppe W, & Altendorf K. Characterization of the KdpD protein, the sensor kinase of the K+-translocating Kdp system of *Escherichia coli*. *European Journal of Biochemistry* 1993 **217** 1019–1026. (doi:10.1111/j.1432-1033.1993.tb18333.x)

58. Laimins LA, Rhoads DB, & Epstein W. Osmotic control of *kdp* operon expression in *Escherichia coli*. *Proceedings of the National Academy of Sciences of the United States of America* 1981 **78** 464–468. (doi:10.1073/pnas.78.1.464)

59. Roe AJ, McLaggan D, O'Byrne CP, & Booth IR. Rapid inactivation of the *Escherichia coli* Kdp K+ uptake system by high potassium concentrations. *Molecular Microbiology* 2000 **35** 1235–1243. (doi:10.1046/j.1365-2958.2000.01793.x)

60. Asha H & Gowrishankar J. Regulation of *kdp* Operon Expression in *Escherichia coli*: Evidence against Turgor as Signal for Transcriptional Control. *Journal of Bacteriology* 1993 **175** 4528–4537. (doi:10.1128/jb.175.14.4528-4537.1993)

61. Galinski EA. Compatible solutes of halophilic eubacteria: molecular principles, water-solute interaction, stress protection. *Experientia* 1993 **49** 487–496. (doi:10.1007/BF01955150)

62. Holtmann G & Bremer E. Thermoprotection of *Bacillus subtilis* by Exogenously Provided Glycine Betaine and Structurally Related Compatible Solutes: Involvement of Opu Transporters. *Journal of Bacteriology* 2004 **186** 1683–1693. (doi:10.1128/JB.186.6.1683-1693.2004)

63. Hoffmann T & Bremer E. Protection of *Bacillus subtilis* against Cold Stress via Compatible-Solute Acquisition. *Journal of Bacteriology* 2011 **193** 1552–1562. (doi:10.1128/JB.01319-10)

64. Bashir A, Hoffmann T, Kempf B, Xie X, Smits SHJ, & Bremer E. Plant-derived compatible solutes proline betaine and betonicine confer enhanced osmotic and temperature stress tolerance to *Bacillus subtilis*. *Microbiology (United Kingdom)* 2014 **160** 2283–2294. (doi:10.1099/mic.0.079665-0)

65. Hoffmann T & Bremer E. Guardians in a stressful world: the Opu family of compatible solute transporters from *Bacillus subtilis*. *Biological Chemistry* 2017 **398** 193–214. (doi:10.1515/hsz-2016-0265)

66. Diamant S, Eliahu N, Rosenthal D, & Goloubinoff P. Chemical Chaperones Regulate Molecular Chaperones *in Vitro* and in Cells under Combined Salt and Heat Stresses. *Journal of Biological Chemistry* 2001 **276** 39586–39591. (doi:10.1074/jbc.M103081200)

67. Kempf B & Bremer E. Uptake and synthesis of compatible solutes as microbial stress responses to high-osmolality environments. *Archives of Microbiology* 1998 **170** 319–330. (doi:10.1007/s002030050649)

68. Yancey PH. Organic osmolytes as compatible, metabolic and counteracting cytoprotectants in high osmolarity and other stresses. *Journal of Experimental Biology* 2005 **208** 2819–2830. (doi:10.1242/jeb.01730)

69. Flowers TJ & Colmer TD. Salinity tolerance in halophytes*. *New Phytologist* 2008 **179** 945–963. (doi:10.1111/j.1469-8137.2008.02531.x)

70. Dijksterhuis J & Vries RP De. Compatible solutes and fungal development. *Biochem. J* 2006 **399** e3–e5. (doi:10.1042/BJ20061229)

71. Alfieri RR, Cavazzoni A, Petronini PG, Bonelli MA, Caccamo AE, Borghetti AF, & Wheeler KP. Compatible osmolytes modulate the response of porcine endothelial cells to hypertonicity and protect them from apoptosis. *Journal of Physiology* 2002 **540** 499–508. (doi:10.1113/jphysiol.2001.013395)

72. Burg MB & Ferraris JD. Intracellular Organic Osmolytes: Function and Regulation*. *Journal of Biological Chemistry* 2008 **283** 7309–7313. (doi:10.1074/jbc.R700042200)

73. Kempf B & Bremer E. Stress responses of *Bacillus subtilis* to high osmolarity environments: Uptake and synthesis of osmoprotectants. *Journal of Biosciences* 1998 **23** 447–455. (doi:10.1007/BF02936138)

74. Boch J, Kempf B, Schmid R, & Bremer E. Synthesis of the Osmoprotectant Glycine Betaine in *Bacillus subtilis*: Characterization of the *gbsAB* genes. *Journal of Bacteriology* 1996 **178** 5121–5129. (doi:10.1128/jb.178.17.5121-5129.1996)

75. Landfald B & Strom AR. Choline-Glycine Betaine Pathway Confers a High Level of Osmotic Tolerance in *Escherichia coli*. *Journal of Bacteriology* 1986 **165** 849–855. (doi:10.1128/jb.165.3.849-855.1986)

76. Meadows JA & Wargo MJ. Carnitine in bacterial physiology and metabolism. *Microbiology* 2015 **161** 1161–1174. (doi:10.1099/mic.0.000080)

77. Kleber HP. Bacterial carnitine metabolism. *FEMS Microbiology Letters* 2006 **147** 1–9. (doi:10.1111/j.1574-6968.1997.tb10212.x)

78. Rebouche CJ & Seim H. CARNITINE METABOLISM AND ITS REGULATION IN MICROORGANISMS AND MAMMALS. *Annu. Rev. Nutr.* 1998 **18** 39–61. (doi:doi: 10.1146/annurev.nutr.18.1.39)

79. Kappes RM, Kempf B, Kneip S, Boch J, Gade J, Meier-Wagner J, & Bremer E. Two evolutionarily closely related ABC transporters mediate the uptake of choline for synthesis of the osmoprotectant glycine betaine in *Bacillus subtilis*. *Molecular Microbiology* 1999 **32** 203–216. (doi:10.1046/j.1365-2958.1999.01354.x)

80. Kempf B & Bremer E. OpuA, an Osmotically Regulated Binding Protein-dependent Transport System for the Osmoprotectant Glycine Betaine in *Bacillus subtilis*. *Journal of Biological Chemistry* 1995 **270** 16701–16713. (doi:10.1074/jbc.270.28.16701)

81. Teichmann L, Chen C, Hoffmann T, Smits SHJ, Schmitt L, & Bremer E. From substrate specificity to promiscuity: hybrid ABC transporters for osmoprotectants. *Molecular Microbiology* 2017 **104** 761–780. (doi:10.1111/mmi.13660)

82. Horn C, Jenewein S, Sohn-Bösser L, Bremer E, & Schmitt L. Biochemical and Structural Analysis of the *Bacillus subtilis* ABC Transporter OpuA and Its Isolated Subunits. *J ournal of Molecular Microbiology Biotechnology* 2005 **10** 76–91. (doi:10.1159/000091556)

83. Blohn C von, Kempf B, Kappes RM, & Bremer E. Osmostress response in *Bacillus subtilis*: characterization of a proline uptake system (OpuE) regulated by high osmolarity and the alternative transcription factor sigma B. *Molecular Microbiology* 1997 **25** 175–187. (doi:10.1046/j.1365-2958.1997.4441809.x)

84. Kappes RM, Kempf B, & Bremer E. Three Transport Systems for the Osmoprotectant Glycine Betaine Operate in *Bacillus subtilis*: Characterization of OpuD. *Journal of Bacteriology* 1996 **178** 5071–5079. (doi:10.1128/jb.178.17.5071-5079.1996)

85. Wood JM, Bremer E, Csonka LN, Kraemer R, Poolman B, Heide T van der, & Smith LT. Osmosensing and osmoregulatory compatible solute accumulation by bacteria. *Comparative Biochemistry and Physiology - A Molecular and Integrative Physiology* 2001 **130** 437–460. (doi:10.1016/S1095-6433(01)00442-1)

86. Teichmann L, Kümmel H, Warmbold B, & Bremer E. OpuF, a New *Bacillus* Compatible Solute ABC Transporter with a Substrate-Binding Protein Fused to the Transmembrane Domain. *Applied and Environmental Microbiology* 2018 **84** e01728-18. (doi:10.1128/AEM.01728-18)

87. Rice AJ, Park A, & Pinkett HW. Diversity in ABC transporters: Type I, II and III importers. *Critical Reviews in Biochemistry and Molecular Biology* 2014 **49** 426–437. (doi:10.3109/10409238.2014.953626)

88. Beis K. Structural basis for the mechanism of ABC transporters. *Biochem. Soc. Trans.* 2015 **43** 889–893. (doi:10.1042/BST20150047)

89. Cui J & Davidson AL. ABC solute importers in bacteria. *Essays in Biochemistry* 2011 **50** 85–99. (doi:10.1042/BSE0500085)

90. Saurin W, Hofnung M, & Dassa E. Getting In or Out: Early Segregation Between Importers and Exporters in the Evolution of ATP-Binding Cassette (ABC) Transporters. *Journal of Molecular Evolution* 1999 **48** 22–41. (doi:https://doi.org/10.1007/PL00006442)

91. Schneider E & Hunke S. ATP-binding-cassette (ABC) transport systems: Functional and structural aspects of the ATP-hydrolyzing subunits/domains. *FEMS Microbiology Reviews* 1998 **22** 1–20. (doi:10.1111/j.1574-6976.1998.tb00358.x)

92. Beek J ter, Guskov A, & Slotboom DJ. Structural diversity of ABC transporters. *Journal of General Physiology* 2014 **143** 419–435. (doi:10.1085/jgp.201411164)

93. Lewis VG, Ween MP, & McDevitt CA. The role of ATP-binding cassette transporters in bacterial pathogenicity. *Protoplasma* 2012 **249** 919–942. (doi:10.1007/s00709-011-0360-8)

94. Lewinson O & Livnat-Levanon N. Mechanism of Action of ABC Importers: Conservation, Divergence, and Physiological Adaptations. *Journal of Molecular Biology* 2017 **429** 606–619. (doi:10.1016/j.jmb.2017.01.010)

95. Biemans-Oldehinkel E, Doeven MK, & Poolman B. ABC transporter architecture and regulatory roles of accessory domains. *FEBS Letters* 2006 **580** 1023–1035. (doi:10.1016/j.febslet.2005.11.079)

96. Gottesman MM, Fojo T, & Bates SE. MULTIDRUG RESISTANCE IN CANCER: ROLE OF ATP-DEPENDENT TRANSPORTERS. *Nature Reviews Cancer* 2002 **2** 48–58. (doi:10.1038/nrc706)

97. Patel NH & Rothenberg ML. Multidrug resistance in cancer chemotherapy. *Investigational*

New Drugs 1994 **12** 1–13. (doi:10.1007/BF00873229)

98. Lankat-Buttgereit B & Tampé R. The transporter associated with antigen processing TAP: structure and function. *FEBS Letters* 1999 **464** 108–112. (doi:10.1016/S0014-5793(99)01676-2)

99. Koch J, Guntrum R, Heintke S, Kyritsis C, & Tampé R. Functional Dissection of the Transmembrane Domains of the Transporter Associated with Antigen Processing (TAP). *Journal of Biological Chemistry* 2004 **279** 10142–10147. (doi:10.1074/jbc.M312816200)

100. Procko E, O'Mara ML, Bennett WFD, Tieleman DP, & Gaudet R. The mechanism of ABC transporters: general lessons from structural and functional studies of an antigenic peptide transporter. *The FASEB Journal* 2009 **23** 1287–1302. (doi:10.1096/fj.08-121855)

101. Berger HA, Travis SM, & Welsh MJ. Regulation of the Cystic Fibrosis Transmembrane Conductance Regulator Cl- Channel by Specific Protein Kinases and Protein Phosphatases. *Journal of Biological Chemistry* 1993 **268** 2037–2047. (doi:10.1016/S0021-9258(18)53959-4)

102. Collins FS. Cystic Fibrosis: Molecular Biology and Therapeutic Implications. *Science* 1992 **256** 774–779. (doi:10.1126/science.1375392)

103. Linton KJ. Structure and Function of ABC Transporters. *Physiology* 2007 **22** 122–130. (doi:10.1152/physiol.00046.2006)

104. Jones PM & George AM. Mechanism of ABC transporters: A molecular dynamics simulation of a well characterized nucleotide-binding subunit. *Proceedings of the National Academy of Sciences of the United States of America* 2002 **99** 12639–12644. (doi:10.1073/pnas.152439599)

105. Kadaba NS, Kaiser JT, Johnson E, Lee A, & Rees DC. The High-Affinity *E. coli* Methionine ABC Transporter: Structure and Allosteric Regulation. *Science*2008. (doi:10.1126/science.1157987)

106. Dawson RJP & Locher KP. Structure of a bacterial multidrug ABC transporter. *Nature* 2006 **443** 180–185. (doi:10.1038/nature05155)

107. Ward A, Reyes CL, Yu J, Roth CB, & Chang G. Flexibility in the ABC transporter MsbA: Alternating access with a twist. *Proceedings of the National Academy of Sciences of the United States of America* 2007 **104** 19005–19010. (doi:10.1073/pnas.0709388104)

108. Walker JE, Saraste M, Runswick MJ, & Gay NJ. Distantly related sequences in the alpha- and beta-subunits of ATP synthase, myosin, kinases and other ATP-requiring enzymes and a common nucleotide binding fold. *The EMBO Journal* 1982 **1** 945–951. (doi:10.1002/j.1460-2075.1982.tb01276.x)

109. Hyde SC, Emsley P, Hartshorn MJ, Mimmack MM, Gileadi U, Pearce SR, Gallagher MP, Gill DR, Hubbard RE, & Higgins CF. Structural model of ATP-binding proteing associated

with cystic fibrosis, multidrug resistance and bacterial transport. *Nature* 1990 **346** 362–365. (doi:10.1038/346362a0)

110. Fetsch EE & Davidson AL. Vanadate-catalyzed photocleavage of the signature motif of an ATP-binding cassette (ABC) transporter. *PNAS* 2002 **99** 9685–9690. (doi:10.1073/pnas.152204499)

111. Hopfner KP, Karcher A, Shin DS, Craig L, Arthur LM, Carney JP, & Tainer JA. Structural Biology of Rad50 ATPase: ATP-Driven Conformational Control in DNA Double-Strand Break Repair and the ABC-ATPase Superfamily. *Cell* 2000 **101** 789–800. (doi:10.1016/S0092-8674(00)80890-9)

112. Wen PC & Tajkhorshid E. Dimer Opening of the Nucleotide Binding Domains of ABC Transporters after ATP Hydrolysis. *Biophysical Journal* 2008 **95** 5100–5110. (doi:10.1529/biophysj.108.139444)

113. Davidson AL, Dassa E, Orelle C, & Chen J. Structure, Function, and Evolution of Bacterial ATP-Binding Cassette Systems. *Microbiology and Molecular Biology Reviews* 2008 **72** 317–364. (doi:10.1128/mmbr.00031-07)

114. Berntsson RPA, Beek J ter, Majsnerowska M, Duurkens RH, Puri P, Poolman B, & Slotboom DJ. Structural divergence of paralogous S components from ECF-type ABC transporters. *Proceedings of the National Academy of Sciences of the United States of America* 2012 **109** 13990–13995. (doi:10.1073/pnas.1203219109)

115. Zhang P, Wang J, & Shi Y. Structure and mechanism of the S component of a bacterial ECF transporter. *Nature* 2010 **468** 717–720. (doi:10.1038/nature09488)

116. Tirado-Lee L, Lee A, Rees DC, & Pinkett HW. Article Classification of a *Haemophilus influenzae* ABC Transporter HI1470/71 through Its Cognate Molybdate Periplasmic Binding Protein, MolA. *Structure* 2011 **19** 1701–1710. (doi:10.1016/j.str.2011.10.004)

117. Soriano E V., Rajashankar KR, Hanes JW, Bale S, Begley TP, & Ealick SE. Structural Similarities between Thiamin-Binding Protein and Thiaminase-I Suggest a Common Ancestor. *Biochemistry* 2008 **47** 1346–1357. (doi:10.1021/bi7018282)

118. Heide T van der & Poolman B. ABC transporters: one, two or four extracytoplasmic substrate-binding sites? *EMBO reports* 2002 **3** 938–943. (doi:10.1093/embo-reports/kvf201)

119. Berntsson RPA, Smits SHJ, Schmitt L, Slotboom DJ, & Poolman B. A structural classification of substrate-binding proteins. *FEBS Letters* 2010 **584** 2606–2617. (doi:10.1016/j.febslet.2010.04.043)

120. Russell RRB, Opoku JA, Sutcliffe IC, Tao L, & Ferretti JJ. A Binding Protein-dependent Transport System in *Streptococcus mutans* Responsible for Multiple Sugar Metabolism. *Journal of Biological Chemistry* 1992 **267** 4631–4637. (doi:https://doi.org/10.1016/S0021-

9258(18)42880-3)

121. Higgins CF & Ferro-Luzzi Ames G. Two periplasmic transport proteins which interact with a common membrane receptor show extensive homology: Complete nucleotide sequences. *Proceedings of the National Academy of Sciences of the United States of America* 1981 **78** 6038–6042. (doi:10.1073/pnas.78.10.6038)

122. Daus ML, Berendt S, Wuttge S, & Schneider E. Maltose binding protein (MalE) interacts with periplasmic loops P2 and P1 respectively of the MalFG subunits of the maltose ATP binding cassette transporter (MalFGK 2) from *Escherichia coli/Salmonella* during the transport cycle. *Molecular Microbiology* 2007 **66** 1107–1122. (doi:10.1111/j.1365-2958.2007.05982.x)

123. Mächtel R, Narducci A, Griffith DA, Cordes T, & Orelle C. An integrated transport mechanism of the maltose ABC importer. *Research in Microbiology* 2019 **170** 321–337. (doi:10.1016/j.resmic.2019.09.004)

124. Ehrmann M, Ehrle R, Hofmann E, Boos W, & Schlösser A. The ABC maltose transporter. *Molecular Microbiology* 1998 **29** 685–694. (doi:10.1046/j.1365-2958.1998.00915.x)

125. Oldham ML, Khare D, Quiocho FA, Davidson AL, & Chen J. Crystal structure of a catalytic intermediate of the maltose transporter. *Nature* 2007 **450** 515–521. (doi:10.1038/nature06264)

126. Bordignon E, Grote M, & Schneider E. The maltose ATP-binding cassette transporter in the 21st century - towards a structural dynamic perspective on its mode of action. *Molecular Microbiology* 2010 **77** 1354–1366. (doi:10.1111/j.1365-2958.2010.07319.x)

127. Cui J, Qasim S, & Davidson AL. Uncoupling Substrate Transport from ATP Hydrolysis in the *Escherichia coli* Maltose Transporter. *The Journal of Biological Chemistry* 2010 **285** 39986–39993. (doi:10.1074/jbc.M110.147819)

128. Locher KP & Borths E. ABC transporter architecture and mechanism: Implications from the crystal structures of BtuCD and BtuF. *FEBS Letters* 2004 **564** 264–268. (doi:10.1016/S0014-5793(04)00289-3)

129. Korkhov VM, Mireku SA, & Locher KP. Structure of AMP-PNP-bound vitamin B12 transporter BtuCD-F. *Nature* 2012 **490** 367–372. (doi:10.1038/nature11442)

130. Felder CB, Graul RC, Lee AY, Merkle HP, & Sadee W. The Venus Flytrap of Periplasmic Binding Proteins: An Ancient Protein Module Present in Multiple Drug Receptors. *AAPS PharmSci* 1999 **1** E2. (doi:10.1208/ps010202)

131. Wilkens S. Structure and mechanism of ABC transporters. *F1000Prime Reports* 2015 **7** . (doi:10.12703/P7-14)

132. Zhang XC, Han L, & Zhao Y. Thermodynamics of ABC transporters. *Protein and Cell* 2016 **7** 17–27. (doi:10.1007/s13238-015-0211-z)

133. Shilton BH. The dynamics of the MBP-MalFGK2 interaction: A prototype for binding protein dependent ABC-transporter systems. *Biochimica et Biophysica Acta* 2008 **1778** 1772–1780. (doi:10.1016/j.bbamem.2007.09.005)

134. Kappes RM & Bremer E. Response of *Bacillus subtilis* to high osmolarity: uptake of carnitine, crotonobetaine and γ-butyrobetaine via the ABC transport system OpuC. *Microbiology* 1998 **144** 83–90. (doi:10.1099/00221287-144-1-83)

135. Rath H, Reder A, Hoffmann T, Hammer E, Seubert A, Bremer E, Völker U, & Mäder U. Management of Osmoprotectant Uptake Hierarchy in *Bacillus subtilis* via a SigB-Dependent Antisense RNA. *Frontiers in Microbiology* 2020 **11** 622. (doi:10.3389/fmicb.2020.00622)

136. Du Y, Shi WW, He YX, Yang YH, Zhou CZ, & Chen Y. Structures of the substrate-binding protein provide insights into the multiple compatible solute binding specificities of the *Bacillus subtilis* ABC transporter OpuC. *Biochemical Journal* 2011 **436** 283–289. (doi:10.1042/BJ20102097)

137. Pittelkow M, Tschapek B, Smits SHJ, Schmitt L, & Bremer E. The Crystal Structure of the Substrate-Binding Protein OpuBC from Bacillus subtilis in Complex with Choline. *Journal of Molecular Biology* 2011 **411** 53–67. (doi:10.1016/j.jmb.2011.05.037)

138. Pinochet-Barros A & Helmann JD. Redox Sensing by Fe2+ in Bacterial Fur Family Metalloregulators. *Antioxidants and Redox Signaling* 2018 **29** 1858–1871. (doi:10.1089/ars.2017.7359)

139. Troxell B & Hassan HM. Transcriptional regulation by Ferric Uptake Regulator (Fur) in pathogenic bacteria. *Frontiers in Cellular and Infection Microbiology* 2013 **3** . (doi:10.3389/fcimb.2013.00059)

140. Kortman GAM, Raffatellu M, Swinkels DW, & Tjalsma H. Nutritional iron turned inside out: intestinal stress from a gut microbial perspective. *FEMS Microbiology Reviews* 2014 **38** 1202–1234. (doi:10.1111/1574-6976.12086)

141. Herbig AF & Helmann JD. Roles of metal ions and hydrogen peroxide in modulating the interaction of the *Bacillus subtilis* PerR peroxide regulon repressor with operator DNA. *Molecular Microbiology* 2002 **41** 849–859. (doi:10.1046/j.1365-2958.2001.02543.x)

142. Mongkolsuk S & Helmann JD. Regulation of inducible peroxide stress responses. *Molecular Microbiology* 2002 **45** 9–15. (doi:10.1046/j.1365-2958.2002.03015.x)

143. Hillmann F, Fischer RJ, Saint-Prix F, Girbal L, & Bahl H. PerR acts as a switch for oxygen tolerance in the strict anaerobe *Clostridium acetobutylicum*. *Molecular Microbiology* 2008 **68** 848–860. (doi:10.1111/j.1365-2958.2008.06192.x)

144. Lee JW & Helmann JD. The PerR transcription factor senses H2O2 by metal-catalysed histidine oxidation. *Nature* 2006 **440** 363–367. (doi:10.1038/nature04537)

145. Dubbs JM & Mongkolsuk S. Peroxide-sensing transcriptional regulators in bacteria. *Journal of Bacteriology* 2012 **194** 5495–5503. (doi:10.1128/JB.00304-12)

146. Henningham A, Döhrmann S, Nizet V, & Cole JN. Mechanisms of group A *Streptococcus* resistance to reactive oxygen species. *FEMS Microbiology Reviews* 2015 **39** 488–508. (doi:10.1093/femsre/fuu009)

147. Jacquamet L, Traoré DAK, Ferrer JL, Proux O, Testemale D, Hazemann JL, Nazarenko E, Ghazouani A El, Caux-Thang C, Duarte V, & Latour JM. Structural characterization of the active form of PerR: insights into the metal-induced activation of PerR and Fur proteins for DNA binding. *Molecular Microbiology* 2009 **73** 20–31. (doi:10.1111/j.1365-2958.2009.06753.x)

148. Traoré DAK, Ghazouani A El, Jacquamet L, Borel F, Ferrer JL, Lascoux D, Ravanat JL, Jaquinod M, Blondin G, Caux-Thang C, Duarte V, & Latour JM. Structural and functional characterization of 2-oxo-histidine in oxidized PerR protein. *Nature Chemical Biology* 2009 **5** 53–59. (doi:10.1038/nchembio.133)

149. Marinho HS, Real C, Cyrne L, Soares H, & Antunes F. Hydrogen peroxide sensing, signaling and regulation of transcription factors. *Redox Biology* 2014 **2** 535–562. (doi:10.1016/j.redox.2014.02.006)

150. Fuangthong M, Herbig AF, Bsat N, & Helmann JD. Regulation of the *Bacillus subtilis fur* and *perR* Genes by PerR: Not All Members of the PerR Regulon are Peroxide Inducible. *Journal of Bacteriology* 2002 **184** 3276–3286. (doi:10.1128/JB.184.12.3276-3286.2002)

151. Hillmann F, Döring C, Riebe O, Ehrenreich A, Fischer RJ, & Bahl H. The role of PerR in O2-affected gene expression of *Clostridium acetobutylicum*. *Journal of Bacteriology* 2009 **191** 6082–6093. (doi:10.1128/JB.00351-09)

152. Vliet AHM van, Stoof J, Vlasblom R, Wainwright SA, Hughes NJ, Kelly DJ, Bereswill S, Bijlsma JJE, Hoogenboezem T, Vandenbroucke-Grauls CMJE, Kist M, Kuipers EJ, & Kusters JG. The Role of the Ferric Uptake Regulator (Fur) in Regulation of *Helicobacter pylori* Iron Uptake. *Helicobacter* 2002 **7** 237–244. (doi:10.1046/j.1523-5378.2002.00088.x)

153. Pi H & Helmann JD. Sequential induction of Fur-regulated genes in response to iron limitation in *Bacillus subtilis*. *PNAS* 2017 **114** 12785–12790. (doi:10.1073/pnas.1713008114)

154. Da JF, Neto S, Braz NS, Italiani CS, & Marques M V. Fur controls iron homeostasis and oxidative stress defense in the oligotrophic alpha-proteobacterium *Caulobacter crescentus*. *Nucleic Acids Research* 2009 **37** 4812–4825. (doi:10.1093/nar/gkp509)

155. Yu C & Genco CA. Fur-Mediated Global Regulatory Circuits in Pathogenic *Neisseria* Species. *Journal of Bacteriology* 2012 **194** 6372–6381. (doi:10.1128/JB.00262-12)

156. Foster JW & Hall HK. Effect of *Salmonella typhimurium* Ferric uptake Regulator (*fur*)

Mutations on Iron- and pH-Regulated Protein Synthesis. *Journal of Bacteriology* 1992 **174** 4317–4323. (doi:10.1128/jb.174.13.4317-4323.1992)

157. Oglesby AG, Farrow Iii JM, Lee JH, Tomaras AP, Greenberg EP, Pesci EC, & Vasil ML. The Influence of Iron on Pseudomonas aeruginosa Physiology A REGULATORY LINK BETWEEN IRON AND QUORUM SENSING. *The Journal of Biological Chemistry* 2008 **283** 15558–15567. (doi:10.1074/jbc.M707840200)

158. Santander J, Golden G, Wanda SY, & Curtiss III R. Fur-Regulated Iron Uptake System of *Edwardsiella ictaluri* and Its Influence on Pathogenesis and Immunogenicity in the Catfish Host. *Infect Immun.* 2012 **80** 2689–2703. (doi:10.1128/IAI.00013-12)

159. Heap JT, Kuehne SA, Ehsaan M, Cartman ST, Cooksley CM, Scott JC, & Minton NP. The ClosTron: Mutagenesis in *Clostridium* refined and streamlined. *Journal of Microbiological Methods* 2010 **80** 49–55. (doi:10.1016/j.mimet.2009.10.018)

160. Heap JT, Pennington OJ, Cartman ST, & Minton NP. A modular system for *Clostridium* shuttle plasmids. *Journal of Microbiological Methods* 2009 **78** 79–85. (doi:10.1016/j.mimet.2009.05.004)

161. Fagan RP & Fairweather NF. *Clostridium difficile* Has Two Parallel and Essential Sec Secretion Systems. *The Journal of Biological Chemistry* 2011 **286** 27483–27493. (doi:10.1074/jbc.M111.263889)

162. Truthe S. Charakterisierung eines oxidativen Stress Regulators in *Clostridioides difficile*. 2019.

163. Schrader M. Charakterisierung von *Clostridioides difficile* unter Umweltstress. 2018.

164. Kim L, Mogk A, & Schumann W. A xylose-inducible *Bacillus subtilis* integration vector and its application. *Gene* 1996 **181** 71–76. (doi:10.1016/S0378-1119(96)00466-0)

165. Hanahan D, Jessee J, & Bloom FR. Plasmid transformation of *Escherichia coli* and other bacteria. *Methods in Enzymology* 1991 **204** 63–113. (doi:10.1016/0076-6879(91)04006-A)

166. Brehm SP, Staal SP, & Hoch JA. Phenotypes of Pleiotropic-Negative Sporulation Mutants of *Bacillus subtilis*. *Journal of Bacteriology* 1973 **115** 1063–1070. (doi:10.1128/jb.115.3.1063-1070.1973)

167. Hussain HA, Roberts AP, & Mullany P. Generation of an erythromycin-sensitive derivative of *Clostridium difficile* strain 630 (630Δ*erm*) and demonstration that the conjugative transposon Tn*916*ΔE enters the genome of this strain at multiple sites. *Journal of Medical Microbiology* 2005 **54** 137–141. (doi:10.1099/jmm.0.45790-0)

168. Derksen E. Phänotypische Charakterisierung von *Clostridium difficile* unter Salzstress und Generierung einer *opuC* – Mutante. 2018.

169. Heap JT, Pennington OJ, Cartman ST, Carter GP, & Minton NP. The ClosTron: A universal

gene knock-out system for the genus *Clostridium*. *Journal of Microbiological Methods* 2007 **70** 452–464. (doi:10.1016/j.mimet.2007.05.021)

170. Cartman ST & Minton NP. A *mariner*-Based Transposon System for *In Vivo* Random Mutagenesis of *Clostridium difficile*. *Applied and Environmental Microbiology* 2010 **76** 1103–1109. (doi:10.1128/AEM.02525-09)

171. Karlsson S, Burman LG, & Akerlund T. *Clostridium difficile* VPI 10463 by amino acids. *Microbiology* 1999 **145** 1683–1693. (doi:10.1099/13500872-145-7-1683)

172. Purdy D, O'Keeffe TAT, Elmore M, Herbert M, McLeod A, Bokori-Brown M, Ostrowski A, & Minton NP. Conjugative transfer of clostridial shuttle vectors from *Escherichia coli* to *Clostridium difficile* through circumvention of the restriction barrier. *Molecular Microbiology* 2002 **46** 439–452. (doi:10.1046/j.1365-2958.2002.03134.x)

173. Perutka J, Wang W, Goerlitz D, & Lambowitz AM. Use of Computer-designed Group II Introns to Disrupt *Escherichia coli* DExH/D-box Protein and DNA Helicase Genes. *Journal of Molecular Biology* 2004 **336** 421–439. (doi:10.1016/J.JMB.2003.12.009)

174. Will SE, Henke P, Boedeker C, Huang S, Brinkmann H, Rohde M, Jarek M, Friedl T, Seufert S, Schumacher M, Overmann J, Neumann-Schaal M, & Petersen J. Day and Night: Metabolic Profiles and Evolutionary Relationships of Six Axenic Non-Marine Cyanobacteria. *Genome Biology and Evolution* 2019 **11** 270–294. (doi:10.1093/gbe/evy275)

175. Wolf J, Stark H, Fafenrot K, Albersmeier A, Pham TK, Müller KB, Meyer BH, Hoffmann L, Shen L, Albaum SP, Kouril T, Schmidt-Hohagen K, Neumann-Schaal M, Bräsen C, Kalinowski J, Wright PC, Albers SV, Schomburg D, & Siebers B. A systems biology approach reveals major metabolic changes in the thermoacidophilic archaeon *Sulfolobus solfataricus* in response to the carbon source L-fucose versus D-glucose. *Molecular Microbiology* 2016 **102** 882–908. (doi:10.1111/mmi.13498)

176. Mamareli P, Kruse F, Friedrich C, Smit N, Strowig T, Sparwasser T, & Lochner M. Epithelium-specific MyD88 signaling, but not DCs or macrophages, control acute intestinal infection with *Clostridium difficile*. *European Journal of Immunology* 2019 **49** 747–757. (doi:10.1002/eji.201848022)

177. Madeira F, Park YM, Lee J, Buso N, Gur T, Madhusoodanan N, Basutkar P, Tivey ARN, Potter SC, Finn RD, & Lopez R. The EMBL-EBI search and sequence analysis tools APIs in 2019. *Nucleic Acids Research* 2019 **47** W636–W641. (doi:10.1093/nar/gkz268)

178. Kelley LA, Mezulis S, Yates CM, Wass MN, & Sternberg MJE. The Phyre2 web portal for protein modeling, prediction and analysis. *Nature Protocols* 2015 **10** 845–858. (doi:10.1038/nprot.2015.053)

179. Sonnhammer ELL, Heijne G Von, & Krogh A. A hidden Markov model for predicting transmembrane helices in protein sequences. *Proc Int Conf Intell Syst Mol Biol.*1998. pp

175–182. .

180. Krogh A, Larsson B, Heijne G von, & Sonnhammer ELL. Predicting Transmembrane Protein Topology with a Hidden Markov Model: Application to Complete Genomes. *J. Mol. Biol.* 2001 **305** 567–580. (doi:10.1006/jmbi.2000.4315)

181. Tsirigos KD, Peters C, Shu N, Käll L, & Elofsson A. The TOPCONS web server for consensus prediction of membrane protein topology and signal peptides. *Nucleic Acids Research* 2015 **43** W401–W407. (doi:10.1093/nar/gkv485)

182. Wang H, Roberts AP, Lyras D, Rood JI, Wilks M, & Mullany P. Characterization of the Ends and Target Sites of the Novel Conjugative Transposon Tn5397 from *Clostridium difficile*: Excision and Circularization Is Mediated by the Large Resolvase, TndX. *Journal of Bacteriology* 2000 **182** 3775–3783. (doi:10.1128/JB.182.13.3775-3783.2000)

183. Ritchie ME, Phipson B, Wu D, Hu Y, Law CW, Shi W, & Smyth GK. *limma* powers differential expression analyses for RNA-sequencing and microarray studies. *Nucleic Acids Research* 2015 **43** e47. (doi:10.1093/nar/gkv007)

184. Yee Hwa (Jean) Yang, Paquet A, & Dudoit S. marray: Exploratory analysis for two-color spotted microarray data. R package version 1.66.0. 2020.

185. Ritchie ME, Silver J, Oshlack A, Holmes M, Diyagama D, Holloway A, & Smyth GK. A comparison of background correction methods for two-colour microarrays. *Bioinformatics* 2007 **23** 2700–2707. (doi:10.1093/bioinformatics/btm412)

186. Yang YH, Dudoit S, Luu P, Lin DM, Peng V, Ngai J, & Speed TP. Normalization for cDNA microarray data: a robust composite method addressing single and multiple slide systematic variation. *Nucleic acids research* 2002 **30** e15. (doi:10.1093/nar/30.4.e15)

187. Yang YH & Thorne NP. Normalization for Two-color cDNA Microarray Data. In *Institute of Mathematical Statistics Lecture Notes - Monograph Series*,ch. Statistics, pp 403–418. 2003.

188. Benjamini Y & Hochberg Y. Controlling the False Discovery Rate: A Practical and Powerful Approach to Multiple Testing. *Journal of the Royal Statistical Society* 1995 **57** 289–300. (doi:10.2307/2346101)

189. Bailey TL, Boden M, Buske FA, Frith M, Grant CE, Clementi L, Ren J, Li WW, & Noble WS. MEME Suite: Tools for motif discovery and searching. *Nucleic Acids Research* 2009 **37** W202–W208. (doi:10.1093/nar/gkp335)

190. Hennequin C, Collignon A, & Karjalainen T. Analysis of expression of GroEL (Hsp60) of *Clostridium difficile* in response to stress. *Microbial Pathogenesis* 2001 **31** 255–260. (doi:10.1006/mpat.2001.0468)

191. Wolf C, Hochgräfe F, Kusch H, Albrecht D, Hecker M, & Engelmann S. Proteomic analysis of antioxidant strategies of *Staphylococcus aureus*: Diverse responses to different

oxidants. *Proteomics* 2008 **8** 3139–3153. (doi:10.1002/pmic.200701062)

192. Ternan NG, Jain S, Srivastava M, & McMullan G. Comparative Transcriptional Analysis of Clinically Relevant Heat Stress Response in *Clostridium difficile* Strain 630. *PLoS ONE* 2012 **7** e42410. (doi:10.1371/journal.pone.0042410)

193. Godard T, Zühlke D, Richter G, Wall M, Rohde M, Riedel K, Poblete-Castro I, Krull R, & Biedendieck R. Metabolic Rearrangements Causing Elevated Proline and Polyhydroxybutyrate Accumulation During the Osmotic Adaptation Response of *Bacillus megaterium*. *Frontiers in Bioengineering and Biotechnology* 2020 **8** 47. (doi:10.3389/fbioe.2020.00047)

194. Fraser KR, Harvie D, Coote PJ, & O'Byrne CP. Identification and Characterization of an ATP Binding Cassette l-Carnitine Transporter in *Listeria monocytogenes*. *Applied and Environmental Microbiology* 2000 **66** 4696–4704. (doi:10.1128/AEM.66.11.4696-4704.2000)

195. Ruiz SJ, Schuurman-Wolters GK, & Poolman B. Crystal Structure of the Substrate-Binding Domain from *Listeria monocytogenes* Bile-Resistance Determinant BilE. *Crystals* 2016 **6** 162. (doi:10.3390/cryst6120162)

196. Bouvier J, Bordes P, Romeo Y, Fourçans A, Bouvier I, & Gutierrez C. Characterization of OpuA, a Glycine-Betaine Uptake System of *Lactococcus lactis*. *Journal of Molecular Microbiology and Biotechnology* 2000 **2** 199–205.

197. Sleator RD, Wemekamp-Kamphuis HH, Gahan CGM, Abee T, & Hill C. A PrfA-regulated bile exclusion system (BilE) is a novel virulence factor in *Listeria monocytogenes*. *Molecular Microbiology* 2005 **55** 1183–1195. (doi:10.1111/j.1365-2958.2004.04454.x)

198. Kagawa M, Fujimoto Z, Momma M, Takase K, & Mizuno H. Crystal Structure of *Bacillus subtilis* α-Amylase in Complex with Acarbose. *Journal of Bacteriology* 2003 **185** 6981–6984. (doi:10.1128/JB.185.23.6981-6984.2003)

199. Smith JL, Goldberg JM, & Grossman AD. Complete Genome Sequences of *Bacillus subtilis* subsp. *subtilis* Laboratory Strains JH642 (AG174) and AG1839. *Genome Announcements* 2014 **2** e00663-14. (doi:10.1128/genomeA.00663-14.Copyright)

200. Scaria J, Mao C, Chen JW, McDonough SP, Sobral B, & Chang YF. Differential Stress Transcriptome Landscape of Historic and Recently Emerged Hypervirulent Strains of *Clostridium difficile* Strains Determined Using RNA-seq. *PLoS ONE* 2013 **8** e78489. (doi:10.1371/journal.pone.0078489)

201. Berges M, Michel AM, Lassek C, Nuss AM, Beckstette M, Dersch P, Riedel K, Sievers S, Becher D, Otto A, Maaß S, Rohde M, Eckweiler D, Borrero-de Acuña JM, Jahn M, Neumann-Schaal M, & Jahn D. Iron Regulation in *Clostridioides difficile*. *Frontiers in Microbiology* 2018 **9** 3183. (doi:10.3389/fmicb.2018.03183)

202. Kuehne SA & Minton NP. ClosTron-mediated engineering of Clostridium. *Bioengineered* 2012 **3** 247–254. (doi:10.4161/bioe.21004)

203. Dapa T, Leuzzi R, Ng YK, Baban ST, Adamo R, Kuehne SA, Scarselli M, Minton NP, Serruto D, & Unnikrishnan M. Multiple Factors Modulate Biofilm Formation by the Anaerobic Pathogen *Clostridium difficile*. *Journal of Bacteriology* 2013 **195** 545–555. (doi:10.1128/JB.01980-12)

204. Schroeter R, Hoffmann T, Voigt B, Meyer H, Bleisteiner M, Muntel J, Jürgen B, Albrecht D, Becher D, Lalk M, Evers S, Bongaerts J, Maurer KH, Putzer H, Hecker M, Schweder T, & Bremer E. Stress Responses of the Industrial Workhorse *Bacillus licheniformis* to Osmotic Challenges. *PLoS ONE* 2013 **8** e80956. (doi:10.1371/journal.pone.0080956)

205. Vijaranakul U, Nadakavukaren MJ, Jonge BLM De, Wilkinson BJ, & Jayaswal RK. Increased Cell Size and Shortened Peptidoglycan Interpeptide Bridge of NaCl-Stressed *Staphylococcus aureus* and Their Reversal by Glycine Betaine. *Journal of Bacteriology* 1995 **177** 5116–5121. (doi:10.1128/jb.177.17.5116-5121.1995)

206. Rudulier D Le & Bouillard L. Glycine Betaine, an Osmotic Effector in *Klebsiella pneumoniae* and Other Members of the *Enterobacteriaceae*. *Applied and Environmental Microbiology* 1983 **46** 152–159. (doi:10.1128/aem.46.1.152-159.1983)

207. Chowdhury R, Sahu GK, & Das J. Stress response in pathogenic bacteria. *Journal of Biosciences* 1996 **21** 149–160. (doi:10.1007/BF02703105)

208. Fordtran JS & Locklear TW. Ionic Constituents and Osmolality of Gastric and Small-Intestinal Fluids after Eating. *The American Journal of Digestive Diseases* 1966 **11** 503–521. (doi:10.1007/BF02233563)

209. Nau-Wagner G, Opper D, Rolbetzki A, Boch J, Kempf B, Hoffmann T, & Bremer E. Genetic Control of Osmoadaptive Glycine Betaine Synthesis in *Bacillus subtilis* through the Choline-Sensing and Glycine Betaine-Responsive GbsR Repressor. *Journal of Bacteriology* 2012 **194** 2703–2714. (doi:10.1128/JB.06642-11)

210. Jameson E, Fu T, Brown IR, Paszkiewicz K, Purdy KJ, Frank S, & Chen Y. Anaerobic choline metabolism in microcompartments promotes growth and swarming of *Proteus mirabilis*. *Environmental Microbiologycrobiology* 2016 **18** 2886–2898. (doi:10.1111/1462-2920.13059)

211. Möller B, Hippe H, & Gottschalk G. Degradation of various amine compounds by mesophilic clostridia. *Arch Microbiol* 1986 **145** 85–90. (doi:10.1007/BF00413032)

212. Craciun S & Balskus EP. Microbial conversion of choline to trimethylamine requires a glycyl radical enzyme. *Proceedings of the National Academy of Sciences of the United States of America* 2012 **109** 21307–21312. (doi:10.1073/pnas.1215689109)

213. Bradbeer C. The Clostridial Fermentations of Choline Ethanolamine. *Journal of*

Bacteriological Chemistry 1965 **240** 4669–4674.

214. Martínez-del Campo A, Bodea S, Hamer HA, Marks JA, Haiser HJ, Turnbaugh PJ, & Balskusa EP. Characterization and Detection of a Widely Distributed Gene Cluster That Predicts Anaerobic Choline Utilization by Human Gut Bacteria. *mBio* 2015 **6** e00042-15. (doi:10.1128/mBio.00042-15)

215. Wang Z & Zhao Y. Gut microbiota derived metabolites in cardiovascular health and disease. *Protein and Cell*2018. pp 416–431. . (doi:10.1007/s13238-018-0549-0)

216. Bae S, Ulrich CM, Neuhouser ML, Malysheva O, Bailey LB, Xiao L, Brown EC, Cushing-Haugen KL, Zheng Y, David Cheng TY, Miller JW, Green R, Lane DS, Beresford SAA, & Caudill MA. Plasma Choline Metabolites and Colorectal Cancer Risk in the Women's Health Initiative Observational Study. *Cancer Research* 2014 **74** 7442–7452. (doi:10.1158/0008-5472.CAN-14-1835)

217. Zhu Y, Jameson E, Crosatti M, Schäfer H, Rajakumar K, Bugg TDH, & Chen Y. Carnitine metabolism to trimethylamine by an unusual Rieske-type oxygenase from human microbiota. *PNAS* 2014 **111** 4268–4273. (doi:10.1073/pnas.1316569111)

218. Romano KA, Vivas EI, Amador-Noguez D, & Rey FE. Intestinal Microbiota Composition Modulates Choline Bioavailability from Diet and Accumulation of the Proatherogenic Metabolite Trimethylamine-*N*-Oxide. *mBio* 2015 **6** e02481-14. (doi:10.1128/mBio.02481-14)

219. Seim H, Ezold R, Kleber HP, Strack E, & Seim H. Stoffwechsel des L-Carnitins bei Enterobakterien. *Zeitschrift für allgemeine Mikrobiologie* 1980 **20** 591–594. (doi:10.1002/jobm.19800200909)

220. Seim H, Löster H, Claus R, Kleber HP, & Strack E. Stimulation of the Anaerobic Growth of *Salmonella typhimurium* by Reduction of L-Carnitine, Carnitine Derivatives and Structure-Related Trimethylammonium Compounds. *Arch Microbiol* 1982 **132** 91–95. (doi:10.1007/BF00690825)

221. Seim H, Löster H, Claus R, Kleber HP, & Strack E. Formation of γ-butyrobetaine and trimethylamine from quaternary ammonium compounds structure-related to L-carnitine and choline by *Proteus vulgaris*. *FEMS Microbiology Letters* 1982 **13** 201–205. (doi:10.1111/j.1574-6968.1982.tb08256.x)

222. Waligora AJ, Barc MC, Bourlioux P, Collignon A, & Karjalainen T. *Clostridium difficile* Cell Attachment Is Modified by Environmental Factors. *Applied and Environmental Microbiology* 1999 **65** 4234–4238. (doi:10.1128/aem.65.9.4234-4238.1999)

223. Philips J, Rabaey K, Lovley DR, & Vargas M. Biofilm Formation by *Clostridium ljungdahlii* Is Induced by Sodium Chloride Stress: Experimental Evaluation and Transcriptome Analysis. *PLoS ONE* 2017 **12** e0170406. (doi:10.1371/journal.pone.0170406)

224. Bouillaut L, Self WT, & Sonenshein AL. Proline-Dependent Regulation of *Clostridium difficile* Stickland Metabolism. *Journal of Bacteriology* 2013 **195** 844–854. (doi:10.1128/JB.01492-12)

225. Zaprasis A, Brill J, Thüring M, Wünsche G, Heun M, Barzantny H, Hoffmann T, & Bremer E. Osmoprotection of *Bacillus subtilis* through Import and Proteolysis of Proline-Containing Peptides. *Applied and Environmental Microbiology* 2013 **79** 576–587. (doi:10.1128/AEM.01934-12)

226. Moses S, Sinner T, Zaprasis A, Stöveken N, Hoffmann T, Belitsky BR, Sonenshein AL, & Bremer E. Proline Utilization by *Bacillus subtilis*: Uptake and Catabolism. *Journal of Bacteriology* 2012 **194** 745–758. (doi:10.1128/JB.06380-11)

227. Fonknechten N, Chaussonnerie S, Tricot S, Lajus A, Andreesen JR, Perchat N, Pelletier E, Gouyvenoux M, Barbe V, Salanoubat M, Paslier D Le, Weissenbach J, Cohen GN, & Kreimeyer A. *Clostridium sticklandii*, a specialist in amino acid degradation:revisiting its metabolism through its genome sequence. *BMC Genomics* 2010 **11** 555. (doi:10.1186/1471-2164-11-555)

228. Sévin DC, Stählin JN, Pollak GR, Kuehne A, & Sauer U. Global Metabolic Responses to Salt Stress in Fifteen Species. *PLoS ONE* 2016 **11** e0148888. (doi:10.1371/journal.pone.0148888)

229. Dannheim H, Will SE, Schomburg D, & Neumann-Schaal M. *Clostridioides difficile* 630Δ*erm in silico* and *in vivo* – quantitative growth and extensive polysaccharide secretion. *FEBS Open Bio* 2017 **7** 602–615. (doi:10.1002/2211-5463.12208)

230. Karlsson S, Burman LG, & Akerlund T. Induction of toxins in *Clostridium difficile* is associated with dramatic changes of its metabolism. *Microbiology* 2008 **154** 3430–3436. (doi:10.1099/mic.0.2008/019778-0)

231. Dubois T, Dancer-Thibonnier M, Monot M, Hamiot A, Bouillaut L, Soutourina O, Martin-Verstraete I, & Dupuy B. Control of *Clostridium difficile* Physiopathology in Response to Cysteine Availability. *Infection and Immunity* 2016 **84** 2389–2405. (doi:10.1128/IAI.00121-16)

232. Troitzsch D, Zhang H, Dittmann S, Düsterhöft D, Michel AM, Jänsch L, Riedel K, Borrero-de Acuña JM, Jahn D, & Sievers S. Work horse strain *Clostridioides difficile* 630Δ*erm* is oblivious to its anaerobic lifestyle. *bioRxiv* 2020 . (doi:10.1101/2020.01.07.897181)

233. Kim M, Hwang S, Ryu S, & Jeon B. Regulation of *perR* Expression by Iron and PerR in *Campylobacter jejuni*. *Journal of Bacteriology* 2011 **193** 6171–6178. (doi:10.1128/JB.05493-11)

234. Lumppio HL, Shenvi N V., Summers AO, Voordouw G, & Kurtz DMJ. Rubrerythrin and Rubredoxin Oxidoreductase in *Desulfovibrio vulgaris*: a Novel Oxidative Stress Protection System. *Journal of Bacteriology* 2001 **183** 101–108. (doi:10.1128/JB.183.1.101-108.2001)

235. Lumppio HL, Shenvi N V., Garg RP, Summers AO, & Kurtz DMJ. A Rubrerythrin Operon and Nigerythrin Gene in *Desulfovibrio vulgaris* (Hildenborough). *Journal of Bacteriology* 1997 **179** 4607–4615. (doi:10.1128/jb.179.14.4607-4615.1997)

236. Louis P & Flint HJ. Diversity, metabolism and microbial ecology of butyrate-producing bacteria from the human large intestine. *FEMS Microbiology Letters* 2009 **294** 1–8. (doi:10.1111/j.1574-6968.2009.01514.x)

237. Theriot CM & Young VB. Microbial and metabolic interactions between the gastrointestinal tract and Clostridium difficile infection. *Gut Microbes* 2014 **5** 86. (doi:10.4161/GMIC.27131)

238. Fachi JL, Felipe J de S, Pral LP, Silva BK da, Corrêa RO, Andrade MCP de, Fonseca DM da, Basso PJ, Câmara NOS, Sales e Souza ÉL de, Santos Martins F dos, Guima SES, Thomas AM, Setubal JC, Magalhães YT, Forti FL, Candreva T, Rodrigues HG, Jesus MB de, Consonni SR, Farias A dos S, Varga-Weisz P, & Vinolo MAR. Butyrate Protects Mice from *Clostridium difficile*-Induced Colitis through an HIF-1-Dependent Mechanism. *Cell Reports* 2019 **27** 750-761.e7. (doi:10.1016/j.celrep.2019.03.054)

239. Yuan Y, Sachdeva M, Leeds JA, & Meredith TC. Fatty Acid Biosynthesis in Pseudomonas aeruginosa Is Initiated by the FabY Class of β-Ketoacyl Acyl Carrier Protein Synthases. *Journal of Bacteriology* 2012 **194** 5171–5184. (doi:10.1128/JB.00792-12)

240. Cai X & Bennett GN. Improving the *Clostridium acetobutylicum* butanol fermentation by engineering the strain for co-production of riboflavin. *Journal of Industrial Microbiology and Biotechnology* 2011 **38** 1013–1025. (doi:10.1007/s10295-010-0875-6)

241. Gutiérrez-Preciado A, Torres AG, Merino E, Bonomi HR, Goldbaum FA, & García-Angulo VA. Extensive Identification of Bacterial Riboflavin Transporters and Their Distribution across Bacterial Species. *PLOS ONE* 2015 **10** e0126124. (doi:10.1371/journal.pone.0126124)

242. Sepúlveda Cisternas I, Salazar JC, & García-Angulo VA. Overview on the Bacterial Iron-Riboflavin Metabolic Axis. *Frontiers in Microbiology* 2018 **9** 1478. (doi:10.3389/fmicb.2018.01478)

243. Du Q, Wang H, & Xie J. Thiamin (Vitamin B1) Biosynthesis and Regulation: A Rich Source of Anti- microbial Drug Targets? *International Journal of Biological Sciences*2011. pp 41–52. . (doi:10.7150/ijbs.7.41)

244. O'Neil HS & Marquis H. *Listeria monocytogenes* Flagella Are Used for Motility, Not as Adhesins, To Increase Host Cell Invasion. *Infection and Immunity* 2006 **74** 6675–6681. (doi:10.1128/IAI.00886-06)

245. Young GM, Schmiel DH, & Miller VL. A new pathway for the secretion of virulence factors by bacteria: The flagellar export apparatus functions as a protein-secretion system. *PNAS* 1999 **96** 6456–6461. (doi:10.1073/pnas.96.11.6456)

246. Girón JA, Torres AG, Freer E, & Kaper JB. The flagella of enteropathogenic *Escherichia coli* mediate adherence to epithelial cells. *Molecular Microbiology* 2002 **44** 361–379. (doi:10.1046/j.1365-2958.2002.02899.x)

247. Schreiber S, Konradt M, Groll C, Scheid P, Hanauer G, Werling HO, Josenhans C, & Suerbaum S. The spatial orientation of *Helicobacter pylori* in the gastric mucus. *PNAS* 2004 **101** 5024–5029. (doi:10.1073/pnas.0308386101)

248. Baban ST, Kuehne SA, Barketi-Klai A, Cartman ST, Kelly ML, Hardie KR, Kansau I, Collignon A, & Minton NP. The Role of Flagella in *Clostridium difficile* Pathogenesis: Comparison between a Non-Epidemic and an Epidemic Strain. *PLoS ONE* 2013 **8** e73026. (doi:10.1371/journal.pone.0073026)

249. McBride SM & Sonenshein AL. The *dlt* operon confers resistance to cationic antimicrobial peptides in *Clostridium difficile*. *Microbiology* 2011 **157** 1457–1465. (doi:10.1099/mic.0.045997-0)

250. Ammam F, Meziane-cherif D, Mengin-Lecreulx D, Blanot D, Patin D, Boneca IG, Courvalin P, Lambert T, & Candela T. The functional *vanGCd* cluster of *Clostridium difficile* does not confer vancomycin resistance. *Molecular Microbiology* 2013 **89** 612–625. (doi:10.1111/mmi.12299)

251. Peltier J, Courtin P, Meouche I El, Catel-Ferreira M, Chapot-Chartier MP, Lemée L, & Pons JL. Genomic and expression analysis of the *vanG*-like gene cluster of *Clostridium difficile*. *Microbiology* 2013 **159** 1510–1520. (doi:10.1099/mic.0.065060-0)

252. Chen X, Katchar K, Goldsmith JD, Nanthakumar N, Cheknis A, Gerding DN, & Kelly CP. A Mouse Model of *Clostridium difficile*-Associated Disease. *Gastroenterology* 2008 **135** 1984–1992. (doi:10.1053/j.gastro.2008.09.002)

253. Keel MK & Songer JG. The comparative pathology of *Clostridium difficile*-associated disease. *Veterinary Pathology* 2006 **43** 225–240. (doi:10.1354/vp.43-3-225)

254. Solomon K. The host immune response to *Clostridium difficile* infection. *Therapeutic Advances in Infectious Disease* 2013 **1** 19–35. (doi:10.1177/2049936112472173)

255. Amulic B, Cazalet C, Hayes GL, Metzler KD, & Zychlinsky A. Neutrophil Function: From Mechanisms to Disease. *Annu. Rev. Immunol.* 2012 **30** 459–489. (doi:10.1146/annurev-immunol-020711-074942)

256. Battaglioli EJ, Hale VL, Chen J, Jeraldo P, Ruiz-Mojica C, Schmidt BA, Rekdal VM, Till LM, Huq L, Smits SA, Moor WJ, Jones-Hall Y, Smyrk T, Khanna S, Pardi DS, Grover M, Patel R, Chia N, Nelson H, Sonnenburg JL, Farrugia G, & Kashyap PC. *Clostridioides difficile* uses amino acids associated with gut microbial dysbiosis in a subset of patients with diarrhea. *Science Translational Medicine* 2018 **10** eaam7019. (doi:10.1126/scitranslmed.aam7019)

7. APPENDIX

List of figures

List of supplemental figures

List of tables

List of supplemental tables

Abbreviations

BHI	Brain Heart Infusion
bp	base pair
ca.	circa
CDAD	*Clostridium difficile* associated diarrhea
CDI	*Clostridium difficile* Infection
CDMM	*Clostridium difficile* Minimal Medium
CFU	colony forming units
dH_2O	deionized water
ddH_2O	double deionized water
DNA	deoxyribonucleic acid
e.g.	exempli gratia (lat.)
EtOH	ethanol
h	hour
min	minute
mRNA	messenger RNA
OD_x	optical density at x nanometer
PBS	phosphatgepufferte Salzlösung (engl. *phosphate buffered saline*)
PCR	polymerase chain reaction
pH	decimal logarithm of the reciprocal of the hydrogen ion activity
Tm	melting temperature at °C
U	Unit
%	percent
µl	microliter
µm	micrometer
°C	degree Celsius
M	molar concentration/molarity
mg	milligram
v/v	volume per volume
w/v	per volume
x g	acceleration of gravity

8. SUPPLEMENTAL MATERIAL

8.1 Homologous recombination of *B. subtilis* TMB118

Shown are the generated transporter sequences including RBS and promotor sequences of OpuC$_{Bsub}$ for the homologous recombination in *B. subtilis* TMB118.

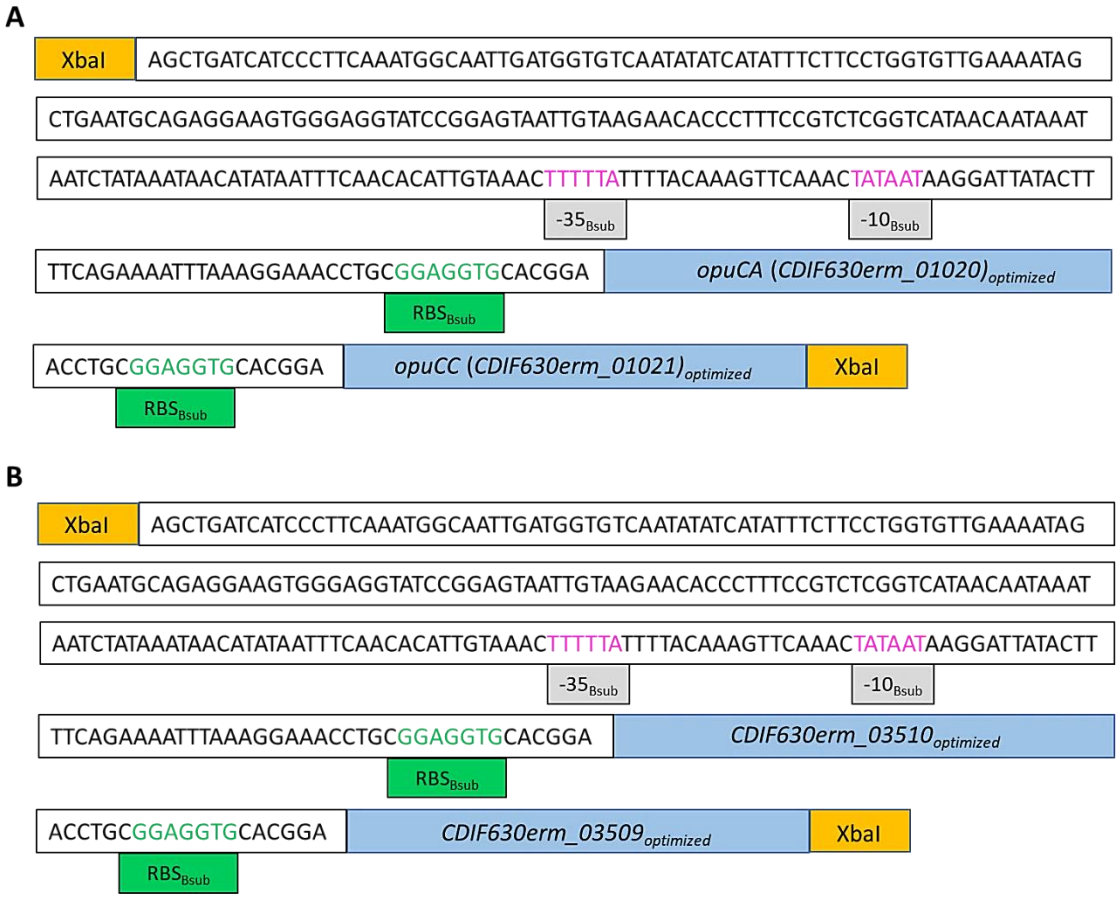

Suppl. Figure 1 Optimized insertion sequence for homologous recombination in *B. subtilis*.

Sequences of *C. difficile* transport systems, A) OpuC and B) UtS, were optimized for *B. subtilis* codon usage using the GeneArt Gene Synthesis tool of Thermo Fisher Scientific. Each transport system consisting of two genes between which the *Bacillus* RBS was cloned. Additionally, the promotor sequence of OpuC$_{Bsub}$ was used. Insertion sequences were flanked by the enzyme restriction site XbaI.

8.2 Characterization of osmolyte transport

Shown are the growth curves of *B. subtilis* AM01 (Suppl. Figure 2), AM02 (Suppl. Figure 3), TMB118 (Suppl. Figure 4) and JH642 (Suppl. Figure 5) cultivated in SMM, SMM supplemented with 1 M NaCl in the presence or absence of several compatible solutes with a final concentration of 1 mM.

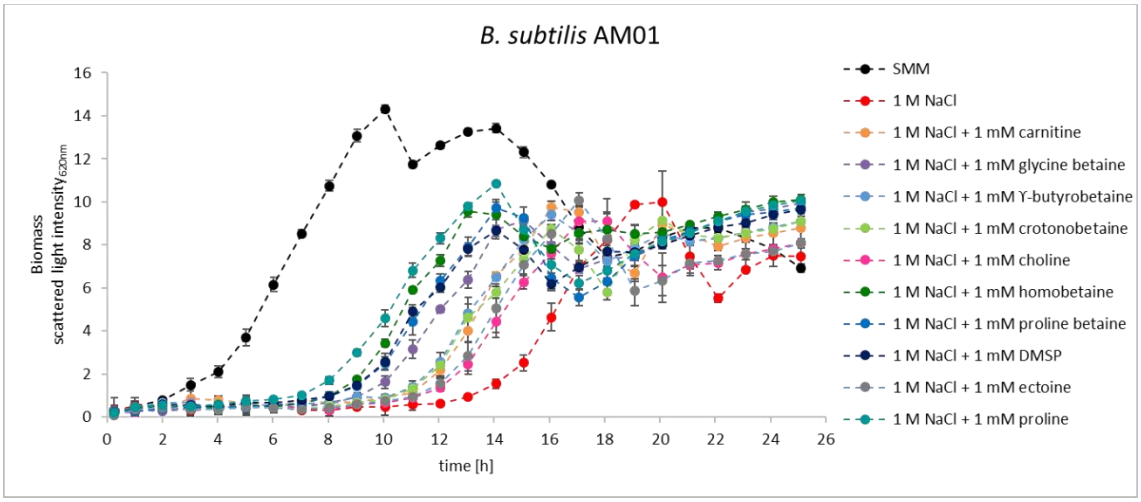

Suppl. Figure 2 Compatible solute transport of *C. difficile* OpuC expressed in *B. subtilis* AM01.

B. subtilis AM01 was cultivated in SMM as reference medium and under salt stressed conditions triggered by 1.0 M NaCl in the absence or presence of various compatible solutes using a concentration of 1 mM. Cultures were grown in three biological replicates in 48-well FlowerPlates in a BioLector system for 25 h at 37 °C, 1,400 rpm under humidity control. The mean and standard deviation values of biomass measured by scattered light at 620nm are shown. The strain AM01 is based on TMB118 which expresses the *C. difficile* 630Δ*erm opuC* operon inserted into the chromosomal *amyE* gene.

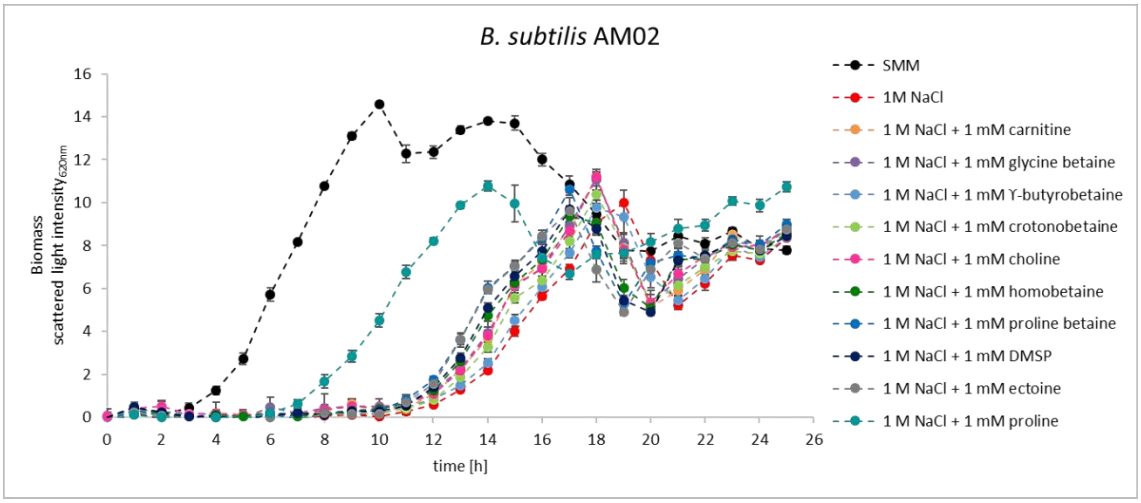

Suppl. Figure 3 Compatible solute transport of *C. difficile* UtS expressed in *B. subtilis* AM02.

B. subtilis AM02 was cultivated in SMM as reference medium and under salt stressed conditions triggered by 1.0 M NaCl in the absence or presence of various compatible solutes using a concentration of 1 mM. Cultures were grown in three biological replicates in 48-well FlowerPlates in a BioLector system for 25 h at 37 °C, 1,400 rpm under humidity control. The mean and standard deviation values of biomass measured by scattered light at 620nm are shown. The strain AM02 is based on TMB118 which expresses the *C. difficile* 630Δ*erm* operon of the UtS inserted into the chromosomal *amyE* gene.

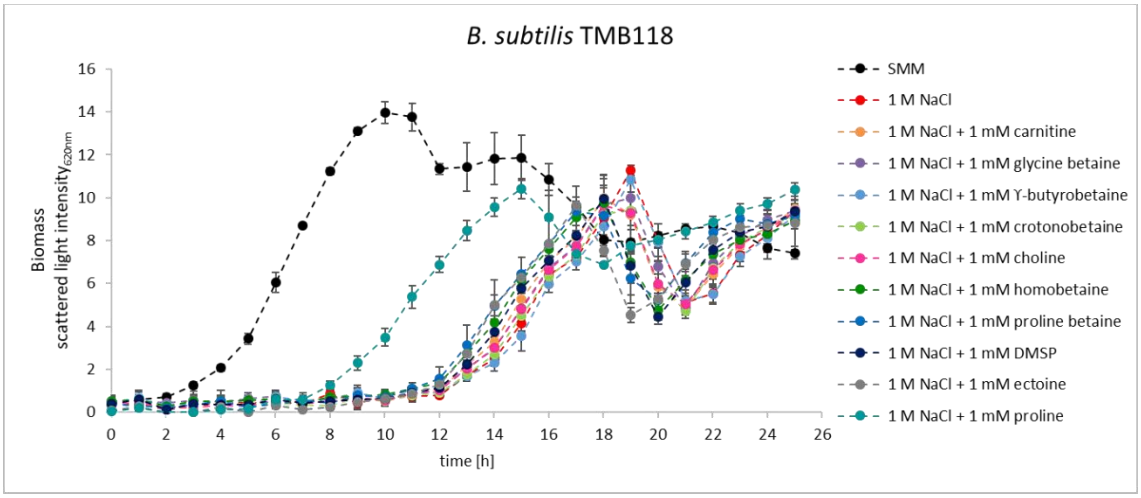

Suppl. Figure 4 Compatible solute transport in *B. subtilis* TMB118.

B. subtilis TMB was cultivated in SMM as reference medium and under salt stressed conditions triggered by 1.0 M NaCl in the absence or presence of various compatible solutes using a concentration of 1 mM. Cultures were grown in three biological replicates in 48-well FlowerPlates in a BioLector system for 25 h at 37 °C, 1,400 rpm under humidity control. The mean and standard deviation values of biomass measured by scattered light at 620nm are shown. The strain TMB is deficient for the Opu transporter OpuA/B/C/D and harbors only the OpuE transporter. For this purpose, TMB 118 was used as control strain for the new strains AM01 and AM02.

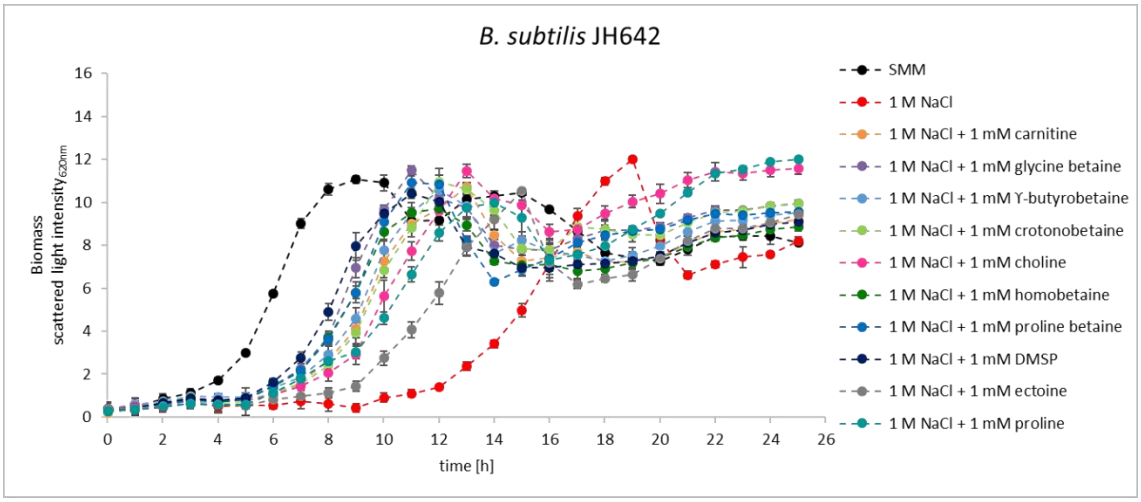

Suppl. Figure 5 Compatible solute transport in *B. subtilis* JH642.

B. subtilis JH642 was cultivated in SMM as reference medium and under salt stressed conditions triggered by 1.0 M NaCl in the absence or presence of various compatible solutes using a concentration of 1 mM. Cultures were grown in three biological replicates in 48-well FlowerPlates in a BioLector system for 25 h at 37 °C, 1,400 rpm under humidity control. The mean and standard deviation values of biomass measured by scattered light at 620nm are shown. The strain JH642 harbors all OpuC transporters and was used as control strain.

8.3 Characterization of osmo protective osmolytes in *C. difficile*

Shown are the growth curves of *C. difficile* 630Δ*erm* wild type and the corresponding *opuCC* mutant cultivated in MDM, MDM supplemented with 350 mM NaCl in the presence or absence of several compatible solutes with a final concentration of 1 mM.

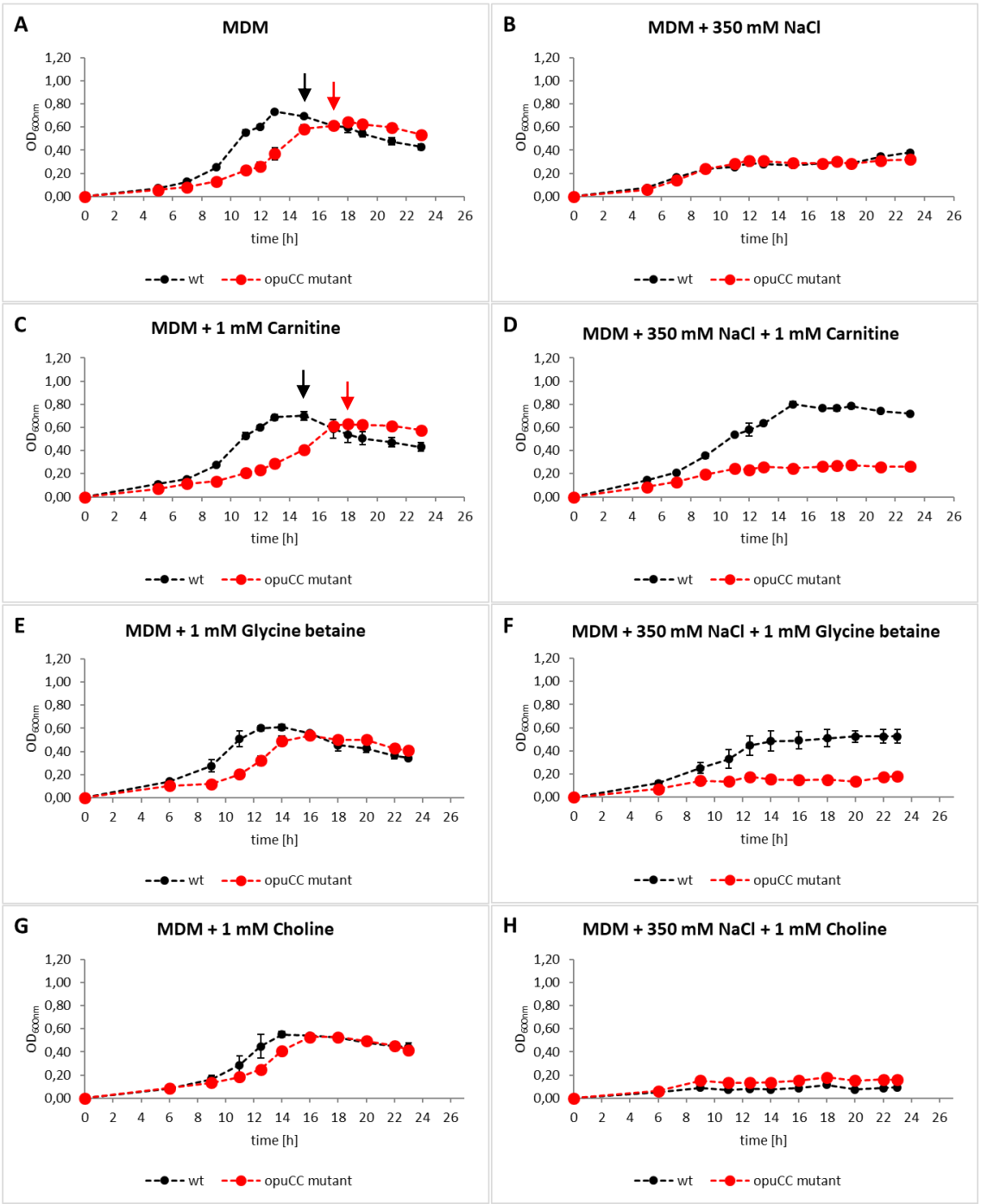

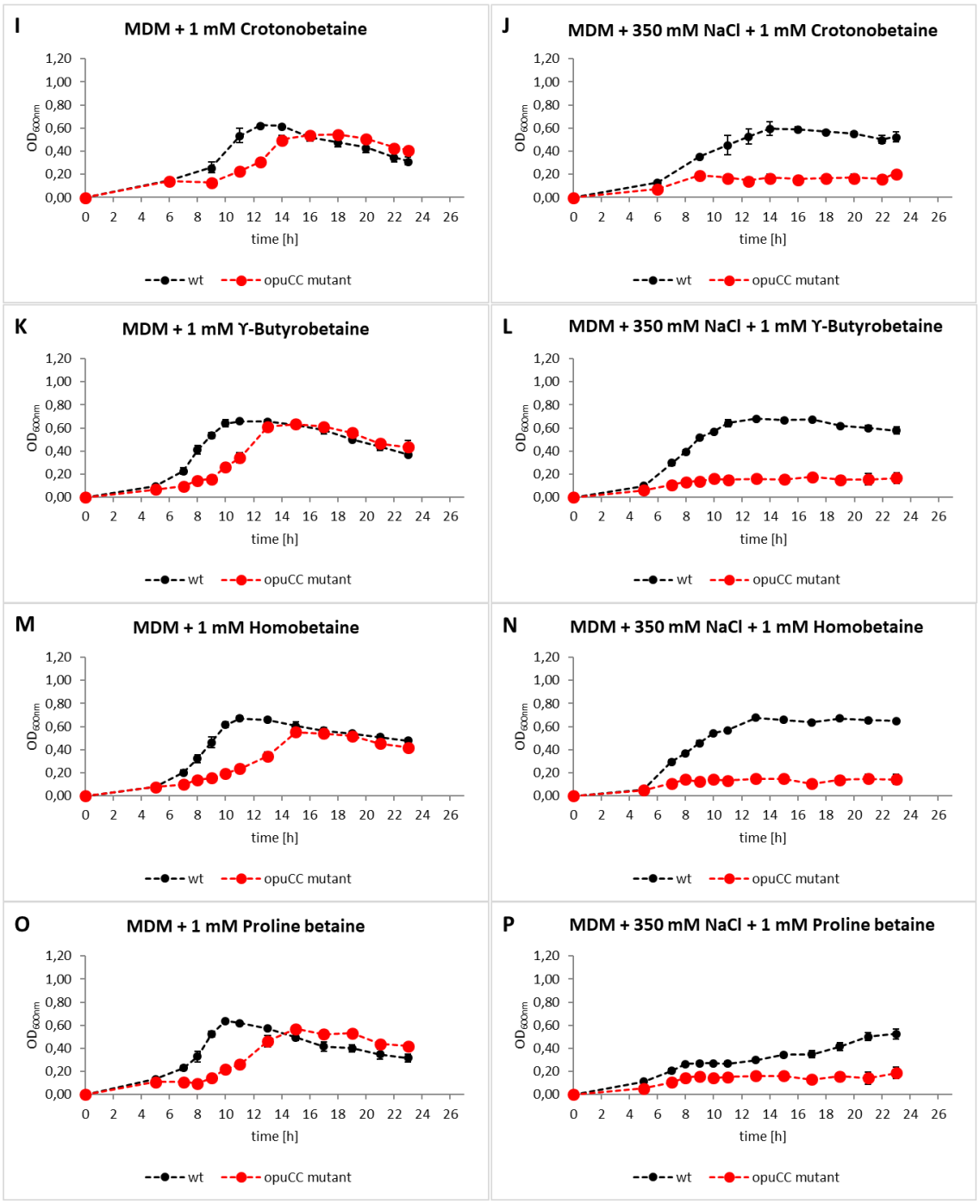
I
MDM + 1 mM Crotonobetaine
J
MDM + 350 mM NaCl + 1 mM Crotonobetaine
K
MDM + 1 mM Y-Butyrobetaine
L
MDM + 350 mM NaCl + 1 mM Y-Butyrobetaine
M
MDM + 1 mM Homobetaine
N
MDM + 350 mM NaCl + 1 mM Homobetaine
O
MDM + 1 mM Proline betaine
P
MDM + 350 mM NaCl + 1 mM Proline betaine
OD600nm
time [h]
wt
opuCC mutant

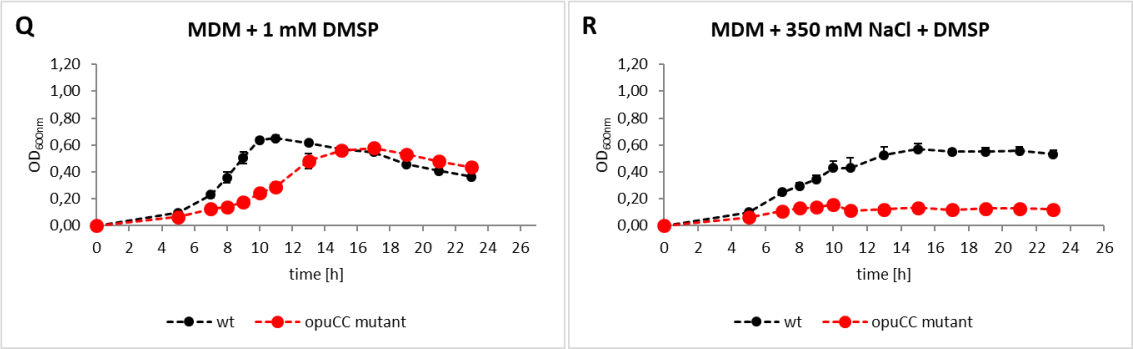

Suppl. Figure 6 Saltstress growth assays assessing the osmo protective substrate profile of the OpuC transport system in *C. difficile* 630Δ*erm*.

C. difficile 630Δ*erm* (wt; ●) and the corresponding *opuCC* mutant (●) were grown in MDM as reference medium and under salt stress conditions induced by 350 mM NaCl in the absence or presence of various compatible solute using a concentration of 1 mM. All measurements were made in quintuplicate. The mean and standard deviation of the growth yield measured at OD_{600nm} are indicated. Arrows indicating sample timepoints for fermentation profile analysis.

Suppl. Table 1 Relative ratios of volatile metabolites as log_2FC of *C. difficile* wild type (wt) and the corresponding *opuCC* mutant in MDM supplemented with carnitine in comparison to the untreated control in MDM.

Metabolites	WT in MDM + carnitine	*opuCC* mutant in MDM + carnitine
4-methylpentanoate	0.02	0.34
2-methylbutanoate	0.00	-0.05
3-methylbutanoate	0.12	0.23
ethanol	-0.20	-0.17
1-hexanol	-0.13	0.16
3-methyl-1-butanol	-0.88	-0.72
butanoate	-0.15	-0.04
1-pentanol	-0.11	-0.09
1-butanol	0.09	0.02
2-methyl-1-propanol	-0.13	-0.27
2-methylpropanoate	-0.19	-0.03
acetate	0.01	-0.11
propanoate	-0.44	-0.22
pentanoate	0.07	0.61
p-cresol	0.08	-0.20

8.3.1 Phenotypical adaptation of *C. difficile* 630Δ*erm* to osmotic changes

Displayed are transmission electron microscopy (TEM) measurements of *C. difficile* 630Δ*erm* wild type cultivated in MDM (Suppl. Figure 7A and B), supplemented with 350 mM NaCl (C and D) as well as under salt stress conditions protected by 1 mM carnitine (E and F).

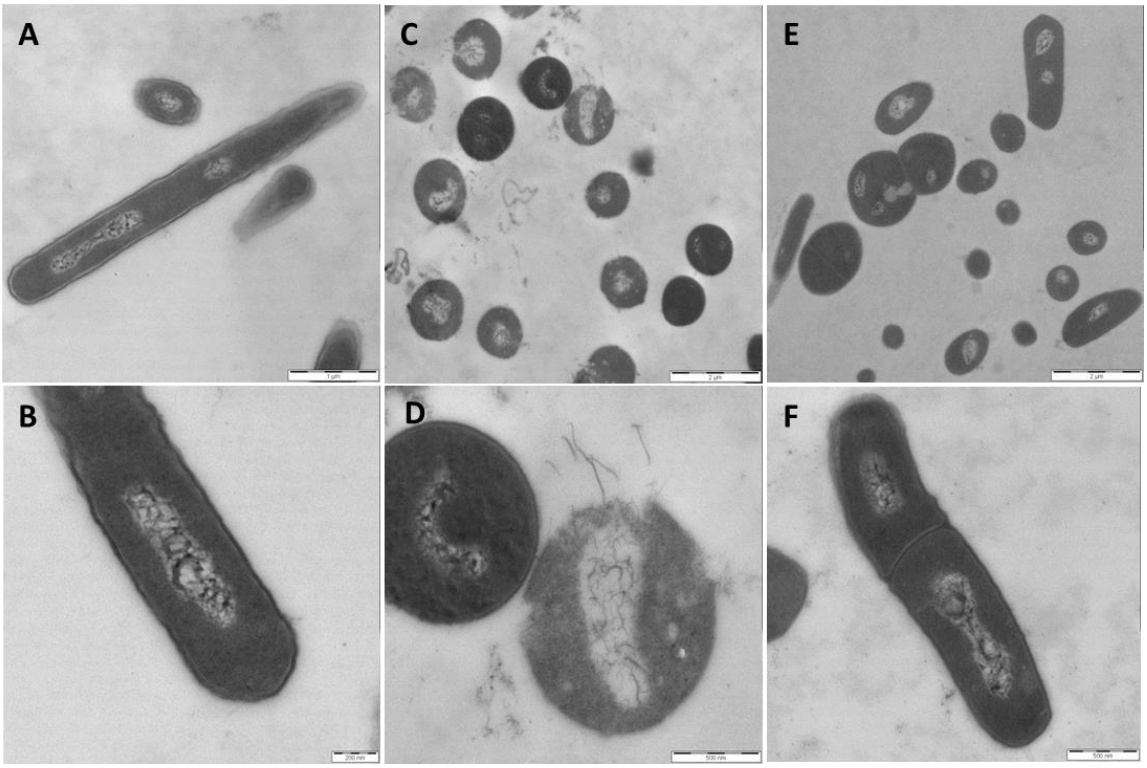

Suppl. Figure 7 Transmission electron microscopy overview of *C. difficile* wild type displaying morphological adaptation to high osmolarity.

Cells were grown in MDM as reference medium (A and B) and under salt stress conditions induced by 350 mM NaCl in the absence (C and D) or presence of 1 mM carnitine (E and F) as osmo protectant. For microscopy analysis cells were harvested during the mid-exponential phase in triplicates. Electron microscopic images were taken by Prof. Dr. Manfred Rohde, HZI, Braunschweig.

8.4 Metabolic consequences of salt stress in *C. difficile* wild type strain

The relative ratios of metabolites as log_2FC are displayed.

Suppl. Table 2 Relative ratios of metabolites as log_2FC of *C. difficile* under salt stress and supplemented with carnitine in comparison to the untreated control in MDM.

A) Relative ratios of intracellular amino acids B) Relative ratios of metabolites involved in reductive Stickland reactions C) Relative ratios of metabolites involved in oxidative Stickland reactions D) Relative ratios of metabolites involved in threonine-associated metabolic pathways E) Relative ratios of metabolites involved in glycolysis F) Relative ratios of metabolites involved in pyruvate related pathways G) Relative ratios of metabolites involved in TCA cycle H) Relative ratios of metabolites involved in butanoate fermentation. Extracellular detected metabolites are indicated by “e”.

A

Intracellular amino acids	WT in MDM + salt	WT in MDM + salt + carnitine
proline	1.30	0.68
methionine	0.14	-0.38
leucine	1.45	-0.79
phenylalanine	-0.12	0.05
isoleucine	1.42	-1.52
valine	1.62	-0.30
threonine	0.86	-0.01
alanine	-3.09	-0.06

B

Metabolites of reductive Stickland reactions	WT in MDM + salt	WT in MDM + salt + carnitine
proline[e]	1.83	0.26
proline	1.30	0.68
5-aminovalerate	-0.40	0.05
5-aminovalerate[e]	-1.57	0.00
leucine	1.45	-0.79
2-oxoisocaproate	0.96	1.54
2-isocaprenoyl-CoA	0.29	-0.51
isocaproyl-CoA	1.32	0.16
isocaproate	0.07	-0.21

C

Metabolites of oxidative Stickland reactions	WT in MDM + salt	WT in MDM + salt + carnitine
leucine	1.45	-0.79
2-oxoisocaproate	0.96	1.54
isovaleryl-CoA	-0.21	0.45
2-oxo-isocaproate[e]	2.17	4.94
isovalerate[e]	-0.30	0.00
isoleucine	1.42	-1.52
(S)-2-methylbutanoyl-CoA	-0.01	0.63
2-methylbutanoate[e]	-1.46	0.33
valine	1.62	-0.30
2-oxoisovalerate[e]	MDM[zz]	MDM[zz]
isobutanoyl-CoA	-0.72	0.50
isobutanoate[e]	-2.05	0.53
phenylalanine	-0.12	0.05
phenylpyruvate	0.30	-3.12
phenylacetyl-CoA	0.70	1.18
phenylacetate	0.58	-0.01
phenylacetate[e]	-1.17	-0.85

D

Metabolites	WT in MDM + salt	WT in MDM + salt + carnitine
threonine[e]	0.64	0.16
threonine	0.86	-0.01
glycine	-1.19	-0.66
acetate	-1.51	0.31
threonine	0.86	-0.01
2-oxobutanoate	-0.42	4.43
2-aminobutanoate	0.59	0.88
2-aminobutanoate[e]	-2.16	0.62
threonine	0.86	-0.01
2-oxobutanoate	-0.42	4.43
propanoyl-CoA	-0.07	0.32
propanoate	-2.23	0.19

E

Metabolites	WT in MDM + salt	WT in MDM + salt + carnitine
glucose[e]	0.00	0.00
glucose	0.20	-0.14
glucose-6-phosphate	-0.10	-0.75
fructose-6-phosphate	0.39	0.83
fructose-1,6-bisphosphate	0.29	1.05
3-phosphoglycerate	0.56	0.69
phosphoenolpyruvate	0.41	0.19
pyruvate	-0.03	-0.57
pyruvate[e]	3.09	1.43

F

Metabolites	WT in MDM + salt	WT in MDM + salt + carnitine
pyruvate	-0.03	-0.57
lactate	0.32	0.29
lactate[e]	1.26	0.82
pyruvate	-0.03	-0.57
alanine	-3.09	-0.06
alanine[e]	-0.64	0.15

G

Metabolites	WT in MDM + salt	WT in MDM + salt + carnitine
pyruvate	-0.03	-0.57
acetyl-CoA	-1.57	-0.04
oxaloacetate	0.48	-0.10
2-oxoglutarate	-1.39	-1.28
glutamate	0.18	-0.20
isoglutamate	-1.29	-0.31
aspartate	0.01	-0.12
arginine	3.99	0.38
fumarate	-0.55	-0.85
malate	3.03	-0.06
succinate	1.26	0.15
succinyl-CoA	0.70	1.37
arginine	3.99	0.38
putrescine	MDM[zz]	MDM[zz]
N-acetyl-putrescine	0.88	-0.54

H

Metabolites	WT in MDM + salt	WT in MDM + salt + carnitine
acetyl-CoA	-1.57	-0.04
acetoacetyl-CoA	nd	nd
3-OH-butanoyl-CoA	3.66	2.08
crotonoyl-CoA	-2.01	-4.42
butanoyl-CoA	nd in MDM	nd in MDM
butanoate[e]	-0.26	0.41

Suppl. Table 3 Relative ratios of volatile metabolites as log_2FC of *C. difficile* wild type (wt) and the corresponding *opuCC* mutant under salt stress and supplemented with carnitine in comparison to the untreated control in MDM.

Metabolites	WT in MDM + salt	WT in MDM + salt + carnitine	*opuCC* mutant in MDM + salt	*opuCC* mutant in MDM + salt + carnitine
4-methylpentanoate	-0.44	0.40	-0.47	-0.61
2-methylbutanoate	-0.75	0.05	-0.73	-1.03
isovalerate	-0.19	0.12	0.03	0.07
ethanol	-0.54	-0.12	-0.69	-0.64
1-hexanol	-0.01	0.13	0.14	0.11
3-methyl-1-butanol	-1.30	0.82	-1.42	-1.25
butanoate	-0.45	0.03	-0.73	-0.64
1-pentanol	-0.01	-0.29	0.10	0.11
1-butanol	-0.10	-0.11	-0.03	0.18
2-methyl-1-propanol	0.57	0.25	0.24	-0.22
2-methylpropanoate	-1.74	0.12	-1.68	-2.13
acetate	-1.43	-0.08	-1.37	-2.23
propanoate	-2.97	-0.23	-2.90	-3.52
pentanoate	-0.12	0.15	-0.23	-0.28
p-cresol	-0.09	0.20	-0.25	-0.43

8.5 Growth state dependent PerR-regulation

Illustrated is the sequence alignment of the predicted Fur binding motif with 250 nucleotides upstream of the *C. difficile* 630Δ*erm* gene *rbr* located in the *perR* operon. Furthermore, the expression profile of genes involved in several pathways is displayed comparing *perR* mutant with *C. difficile* wild type in the exponential as well as stationary phase.

Suppl. Figure 8 Sequence alignment of the predicted Fur binding motif with 250 nucleotides upstream of the *C. difficile* gene *rbr* located in the *perR* operon.

Suppl. Table 4 Relative ratios of intracellular amino acids as log_2FC of the *C. difficile perR* mutant in comparison to the wild type (wt) in the exponential and stationary phase. Completely consumed nutrients in the wild type are indicated by "wt^z", in both strains by "zz". "Z" stands for "zero".

intracellular amino acids	wt vs *perR* mutant exp. phase	wt vs *perR* mutant stat. phase
proline	-0.52	1.05
methionine	-0.73	0.39
leucine	-1.24	0.42
isoleucine	-1.53	-2.96
valine	-0.84	-0.52
threonine	-0.72	wt^Z
tryptophan	-0.02	-0.07
cysteine	0.18	ZZ
glucose	-0.05	-0.28

Suppl. Table 5 Gene expression values of reductive Stickland fermentation related pathways.

locus tag	gene name	function	log_2FC Δ*perR* vs wt exp. phase	log_2FC Δ*perR* vs wt stat. phase
Proline metabolism				
CD630DERM_32370	*prdF*	Proline racemase	1.30	0.03
CD630DERM_32380	*prdE2*	Proline reductase prdE-like	1.50	-0.43*
CD630DERM_32390	*prdE*	Proline reductase PrdE	1.68	-0.42
CD630DERM_32400	*prdD*	Proline reductase PrdD	1.67	0.15*
CD630DERM_32410	*prdB*	Proline reductase (selenocysteine)	1.35	-0.53
CD630DERM_32430		conserved hypothetical protein	2.14	-1.39*
CD630DERM_32440	*prdA*	D-Proline reductase proprotein prdA	2.38*	-0.14
CD630DERM_32460		putative surface protein	-0.99*	0.31
CD630DERM_32450	*prdR*	Transcriptional regulator, sigma-54-dependent	-0.24	-0.66
CD630DERM_32470	*prdC*	putative electron transfer protein	2.79*	0.01
Leucine and phenylalanine metabolism				
CD630DERM_24240		putative pyridoxal phosphate-dependenttransferase	-0.27	0.12
CD630DERM_03940	*ldhA*	D-Lactate dehydrogenase	0.18	0.92*
CD630DERM_03950	*hadA*	Isocaprenoyl-CoA:2-hydroxyisocaproateCoA-transfe rase	-0.16	2.11*
CD630DERM_03960	*hadI*	Activator of 2-hydroxyisocaproyl-CoAdehydratase	-0.16	2.06*
CD630DERM_03970	*hadB*	Subunit of oxygen-sensitive2-hydroxyisocaproyl-CoA dehydratase B	0.08	2.06*
CD630DERM_03980	*hadC*	Subunit of oxygen-sensitive2-hydroxyisocaproyl-CoA dehydratase C	-0.22	1.94*
CD630DERM_03990	*acdB*	Acyl-CoA dehydrogenase, short-chain specific	0.18	2.29*
CD630DERM_04000	*etfB1*	Beta-subunit of electron transfer flavoprotein	0.05	2.31*
CD630DERM_04010	*etfA1*	Alpha-subunit of electron transfer flavoprotein	0.05	2.34*

Suppl. Table 6 Gene expression values of oxidative Stickland fermentation related pathways.

locus tag	gene name	function	log_2FC Δ*perR* vs wt exp. phase	log_2FC Δ*perR* vs wt stat. phase
Leucine, isoleucine and valine metabolism				
CD630DERM_24240		putative pyridoxal phosphate-dependenttransferase	-0.27	0.12
CD630DERM_01120	*ptb*	Phosphate butyryltransferase	2.97*	0.12
CD630DERM_01130	*buk*	Butyrate kinase (BK) (Branched-chain carboxylicacid kinase)	2.83*	0.03
CD630DERM_01140		putative atp/gtp-binding protein	2.36*	-0.25
CD630DERM_01150	*(vorC1)*	putative 4Fe-4S ferredoxin, iron-sulfur bindingdomain protein, delta subunit	1.73*	-0.42*
CD630DERM_01160	*(vorB1)*	putative ferredoxin/flavodoxinoxidoreductase,alpha subunit	1.51*	-0.03*
CD630DERM_01170	*(vorA1)*	putative ferredoxin/flavodoxinoxidoreductase,beta subunit	0.92	-0.38
CD630DERM_01180	*(vorA´1)*	putative ferredoxin/flavodoxinoxidoreductase,gamma subunit	0.62	-0.50

8.6 Fur and its role to CAMPs and vancomycin

Shown is the growth behavior of *C. difficile* 630Δ*erm* wild type and its corresponding *fur* mutant grown in CDMM supplemented with vancomycin, polymyxin B or nisin.

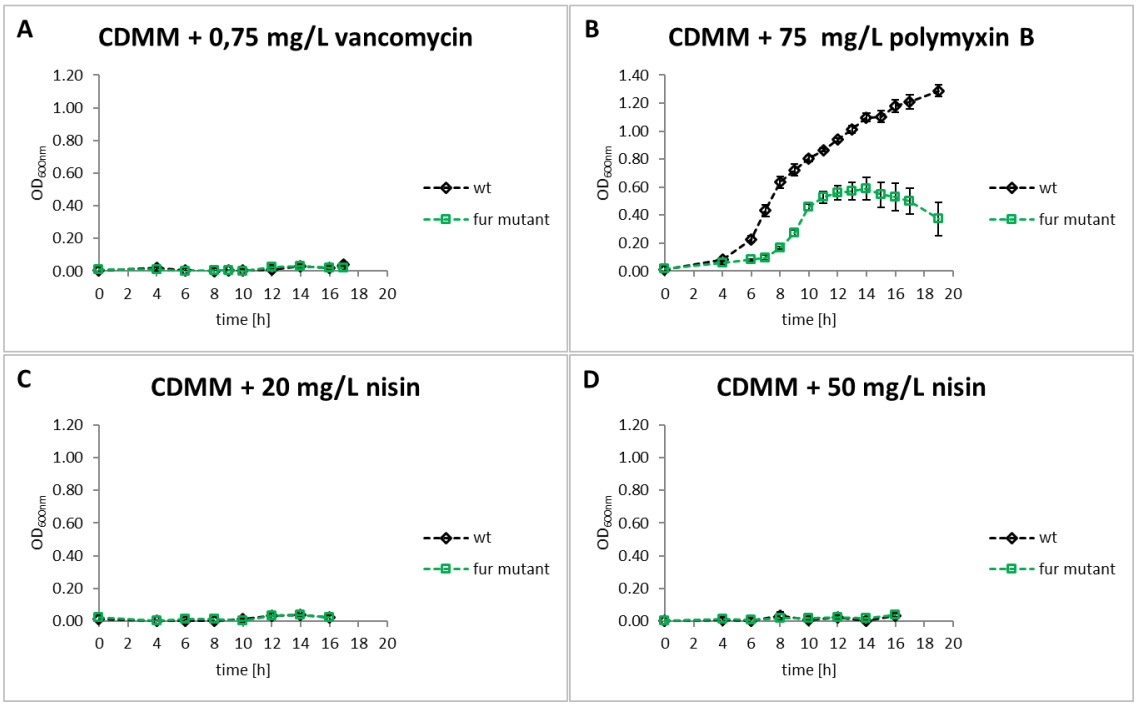

Suppl. Figure 9 Phenotypical growth behavior of *C. difficile* 630Δ*erm* and *fur* mutant under high iron conditions in the presence of vancomycin, polymyxin B and nisin.

C. difficile 630Δ*erm* (black; wt) and the corresponding *fur* mutant (green) were grown in CDMM supplemented with 15 µM iron sulfate in the presence of 0.75 mg/l vancomycin (A), 75 mg/l polymyxin B (B) and 20 mg/L (C) or 50 mg/L (D) nisin. Growth was monitored in quadruplicates. Standard deviations are indicated.

8.7 *In vivo* testings of various *C. difficile* mutants using mouse model

Shown is the growth behavior of *C. difficile* 630Δ*erm* wild type and its corresponding *ribBA* mutant grown in CDMM and supplemented with riboflavin.

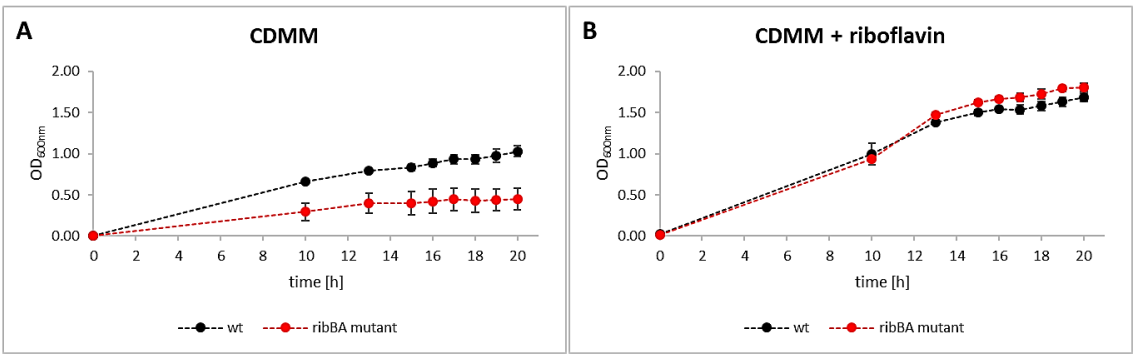

Suppl. Figure 10 Phenotypical growth behavior of *C. difficile ribBA* mutant in absence and presence of riboflavin.

C. difficile 630Δ*erm* (wt; ●) and the corresponding *ribBA* mutant (●) were grown in A) CDMM without riboflavin as well as B) in presence of riboflavin with a final concentration of 500 µM. All measurements were made in quintuplicate. The mean and standard deviation values of the growth yield measured at OD_{600nm} are indicated.

9. ACKNOWLEDGEMENTS

Ein ganz besonderer Dank gilt meinem Doktorvater Prof. Dr. Dieter Jahn, der es mir ermöglicht hat, in seiner Arbeitsgruppe meine Doktorarbeit auf diesem spannenden Thema anzufertigen. Danke für deine stetige Unterstützung und Mut machenden Worte, nicht nur wenn Cdiff seinem Namen wieder alle Ehre machte und mich ab und an zum Verzweifeln brachte. Weiterhin möchte ich mich ganz besonders dafür bedanken, dass du mir die Möglichkeit gegeben hast, nicht nur auf vielen nationalen, sondern auch internationalen Konferenzen meine Daten zu präsentieren. Diese Erfahrung darf nicht jeder machen. Zu Guter letzt möchte ich mich für die überaus schnelle Korrektur dieser Arbeit bedanken.

Prof. Dr. Michael Steinert möchte ich zum einen für die Übernahme des Zweitgutachtens dieser Dissertation danken und zum anderen für eine lockere Atmosphäre in den Mittwochs-Seminaren.

Bei Prof. Dr. Michael Hust möchte ich mich für die freundliche Übernahme des Vorsitzes der Prüfungskommission bedanken.

Ein riesen Dank geht an Dr. José M. Borrero de Acuña, bei dem meine Zeit in der Mibi als Bachelorstudentin begonnen und nun als fertige Doktorandin zu Ende geht. Ich danke dir für deine Unterstützung und dein Verständnis in allen Bereichen. Danke, für die hilfreichen Anmerkungen zu dieser Arbeit sowie für deine Hilfe beim Verfassen der dazugehörigen Publikation. Insbesondere möchte ich mich bei dir dafür bedanken, dass ich (wieder) Teil deiner Arbeitsgruppe sein durfte, mit der wir tolle Betriebsausflüge und Feierabend-Treffen hatten.

Weiterhin möchte ich Dr. Can Ünal für seine hilfreichen Ratschläge rund um Cdiff danken sowie für seine tolle Unterstützung beim Verfassen unserer Publikation.

Ein großes Dankeschön geht an meine Kooperationspartner, mit deren Hilfe viele spannende Ergebnisse generiert wurden. Hier möchte ich allen voran Dr. Meina Neumann-Schaal für ihre Hilfe bei den Metabolom-Analysen danken. Bei Dr. Sabine Will und Dr. Julia Hoffmann möchte ich mich für ihre Unterstützung bei den systembiologischen Experimenten bedanken. Dr. Denitsa Eckweiler danke ich für die bioinformatische Auswertung meiner Daten, sowie Dr. Christian Dudek für die Optimierung zur bioinformatischen Auswertung der Arraydaten. Dr. Matthias Lochner und seinem Team danke ich für die Mausexperimente und

dessen Auwertung. Weiterhin bedanke ich mich bei Prof. Dr. Manfred Rohde und seinem Team für die tollen mikroskopischen Cdiff-Aufnahmen.

Ein riesen Dank gilt vor allem den BRICS-Mibis. Danke Dr. Rebekka (Rebi) Biedendieck, dass du unsere Cdiff-Gruppe im BRICS aufgenommen hast und immer geholfen hast, wenn es nötig war. Ganz besonders möchte ich Dr. Mareike Berges danken. Danke für deine Unterstützung und unsere kleinen Lab-Meetings. Ein großes Danke geht auch an Gabi Günther, Simone Thiel, Janine Mayer und Dr. Sarah Wienecke für die ganz tolle Zeit im BRICS. Die Zeit mit euch allen hat wahnsinnig viel Spaß gemacht, egal ob beim Mittagessen, beim jährlichen Plätzchen backen oder auf dem Weihnachtsmarkt.

Außerdem Danke ich meiner Arbeitsgruppe aus dem Biozentrum mit José, Kim Rennhack, Ilka Pusch, Viktoria Otto, Ayten Mustafayeva und Dr. Hao Zhang für die gemeinsamen Unternehmungen, schönen Betriebsausflüge und kulinarischen Treffen.

Ebenfalls danke ich Dr. Matthias Ebert, der mich auf meinem gesamten Weg im Institut begleitet und unterstützt hat.

Weiterhin danke ich allen meinen Studenten, die ich in den letzten Jahren betreut habe und die wesentliche Ergebnisse zu dieser Arbeit beigetragen haben: Elisabeth Derksen, Sina Wiechers, Michel Schrader, Johanna Vogler, Sarah Truthe, Mihriban Somar und Veronika Martin.

Dem gesamten Institut für Mikrobiologie möchte ich für die tolle Arbeitsatmosphäre bedanken.

Der größte Dank gilt meiner Familie: meinen Eltern und meinem Bruder. Danke Mama und Papa, dass ihr mich immer in all meinen Entscheidungen unterstützt habt. Danke für euren Zuspruch und euer Vertrauen. Ohne euch wäre das das alles nicht möglich gewesen.